

Spring 5-2001

# The Partition/Adsorption Model for the Description of the Retention Mechanism in Reversed Phase Liquid Chromatography

Tarun S. Patel  
*Seton Hall University*

Follow this and additional works at: <https://scholarship.shu.edu/dissertations>

 Part of the [Chemistry Commons](#)

---

## Recommended Citation

Patel, Tarun S., "The Partition/Adsorption Model for the Description of the Retention Mechanism in Reversed Phase Liquid Chromatography" (2001). *Seton Hall University Dissertations and Theses (ETDs)*. 1259.  
<https://scholarship.shu.edu/dissertations/1259>

**The Partition/ Adsorption Model for the  
Description of the Retention Mechanism in  
Reversed Phase Liquid Chromatography**

By:

Tarun S. Patel

Dissertation submitted to the  
Department of Chemistry & Biochemistry of  
Seton Hall University  
in partial fulfillment of the requirements for the degree of

DOCTOR OF PHILOSOPHY

in

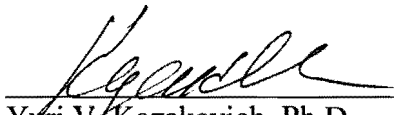
Chemistry

May 2001

South Orange, New Jersey

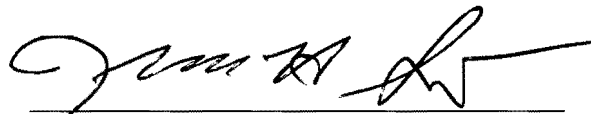
We certify that we have read this dissertation and that, in our opinion, it is adequate in scientific scope and quality as a dissertation for the degree of Doctor of Philosophy.

APPROVED



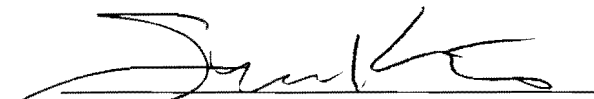
---

Yuri V. Kazakevich, Ph.D.  
Research Mentor




---

Nicholas H. Snow, Ph.D.  
Member of Dissertation Committee



---

Stephen Kelty, Ph.D.  
Member of Dissertation Committee



---

Richard Sheardy, Ph.D.  
Chairperson, Department of Chemistry and Biochemistry

## The Partition/ Adsorption Model for the Description of the Retention Mechanism in Reversed Phase Liquid Chromatography

### Abstract

The adsorption-partitioning model based on the formation of the adsorbed organic layer on the top of reversed-phase adsorbent surface was verified using two different homologue series as analytes (alkyl benzenes and ketones) and five different HPLC reversed-phase columns (C<sub>18</sub>, C<sub>12</sub>, C<sub>8</sub>, C<sub>4</sub> and C<sub>1</sub>). Adsorbents used were based on the same silica support with the surface modified by alkylsilanes of different chain length.

The model describes the analyte RPLC retention as a sum of two processes: partitioning into the organic adsorbed layer followed by analyte adsorption on the hydrophobic surface. The following equation was derived using the proposed model.

$$V_r = V_o + (K_p - 1)V_s + SK_p \frac{d\Gamma(c_s)}{dc_s}$$

where  $V_r$  = retention volume of an analyte,  
 $V_o$  = total liquid volume inside the column,  
 $K_p$  = distribution coefficient of an analyte between the mobile phase and the adsorbed layer,  
 $V_s$  = total adsorbed layer volume,  
 $S$  = the total surface area of the adsorbent per column and  
 $d\Gamma(c_s)/dc_s = K_H$  = Henry adsorption constant.

The main goal was to test the applicability of the proposed model and verify the possibility of independent determination of individual parameters of the equation written above. Four independent variables ( $V_o$ ,  $K_p$ ,  $V_s$  and  $K_H$ ) to predict the retention were measured independently in a binary system (acetonitrile-water or acetonitrile-analyte) while the experimentally obtained retention was measured in a ternary system (acetonitrile-water-analyte).

The model works well throughout the concentration range studied (acetonitrile-water as the mobile phase) on three columns ( $C_{18}$ ,  $C_{12}$  and  $C_8$ ). For mobile phase composition below 40% (v/v) acetonitrile-water, the correction of the volume of the adsorbed acetonitrile is required. This is because the formation of a stable adsorbed layer was found when the mobile phase composition exceeded 40% (v/v) acetonitrile-water. The predicted retention volume was found to be much higher than experimentally obtained retention volume when columns having shorter alkyl chains ( $C_4$  and  $C_1$ ) were used. This was attributed to the polarity of the solvated-bonded ligand. The derived equation does not have polarity of the solvated-bonded ligand as one of the variables since it was derived based on distribution.

## **Dedication**

To my family

## **Acknowledgments**

I would like to give special thanks to my advisor Dr. Kazakevich for his leadership, encouragement, time, expertise and most of all his friendship.

I would also like to acknowledge the Kazakevich/ Snow research group at Seton Hall University and several faculty members who helped me throughout the doctoral process. The faculty members to whom I would like to give special appreciation for all their help during my graduate degree include Dr. Snow, Dr. Kelty, and Dr. Sheardy. The research group members I would especially like to thank for all their help with the experimental work and for being good friends are Rosario LoBrutto and Fred Chan.

I would like to thank the Novartis Pharmaceutical Corporation for their financial support. The Novartis colleagues I would like to especially thank include Ray Hofmeister, LayChoo Tan, Thomas Fink, Patrick Drumm and Yatindra Joshi for their encouragement throughout the Ph.D. process and allowing flexibility in my work schedule to finish my degree.

On the non-academic side I would like to express my thanks to all my family members (Suryakant, Shakuntala, Parul, Heenal, Aarsh, Pintu, Sujal and Dhruvi). I would like to give special thanks to my brother, Pintu, for his help to take care of house and cars during my years in school. I also would like to thank my parents for all their support and encouragement over the many years that I have spent in school. Most of all, I would like to thank my wife, Parul, for all her patience, understanding and taking care of children while I was obtaining my Ph.D.

## Table of Contents

	Page
Dedication	ii
Acknowledgments	iii
Table of Contents	iv
List of Tables	ix
List of Figures	x
Thesis Structure	xvi
Chapter I: Historical	1
Summary	1
Introduction	1
Proposed Retention Mechanisms in RPLC	2
Mobile Phase Driven vs. Stationary Phase Driven Retention Mechanisms	2
Partitioning vs. Adsorption Mechanisms	9
Stationary Phase Models in RPLC	13
Liquid Hydrocarbon Partition Model or Lochmuller & Wilder Model	15
Liquid-Crystalline Hydrocarbon Partition Model or Martire-Boehm Model	17
Adsorptive Hydrocarbon Monolayer Model or Dill's Model	18
Amorphous-Crystalline Hydrocarbon Partition Model or Dill-Dorsey Model	21
Bohmer-Koopal-Tijssen Model	23
Liquid/Liquid Partitioning vs. RPLC	23



Chain Flexibility	26
Silica Surface	28
Evidence Supporting Solvent Adsorption on the Bonded Phase	28
Thermal/Chromatographic Evidence of Solvent Adsorption	29
Spectroscopic Evidence of Solvent Adsorption	31
The Effect of Mobile Phase Composition, Bonded Alkyl Chain Length and Solvent Adsorption on the Structure of Bonded Alkyl Phase Under RPLC Conditions.	34
Conclusions	50
Chapter II: Introduction of the Partition/ Adsorption Model	51
Summary	51
Background	51
The Concept of Excess Adsorption	53
The Relationship between Excess Adsorption and HPLC Retention	56
The Partition/ Adsorption Retention Model	68
Conclusions	76
Chapter III: Results - RPLC	78
Summary	78
Dead Volume, $V_0$	78
Definition of $V_0$	80
Experimental	82
Adsorbents and Columns	82
HPLC Systems	82
Solvents and Chemicals	84
Dead Volume Measurement by Minor Disturbance Method	84

Results and Discussion	85
The Adsorbed Layer Volume, $V_s$	89
Experimentally Measured Retention Volumes	96
Introduction	96
Effect of Bonded Alkyl Chain Length on RPLC Retention	101
Effect of Mobile Phase Composition on RPLC Retention	104
Experimental	108
Adsorbents and Columns	108
Solvents and Chemicals	108
HPLC System and Conditions	108
Results and Discussion	110
Henry Constant, $K_H$	127
Conclusions	130
Chapter IV: Measurement of $K_P$ by Headspace Gas Chromatography (HS-GC)	131
Summary	131
Introduction	131
Experimental (for Isochoric Headspace System)	139
Principles of Isochoric Headspace System	146
Vapor Transfer and Measurement Processes	147
Isochoric Vapor Extraction Method	148
The Experimental Procedure	148
Theory of Sequential (discontinuous) Withdrawal of the Analyte Vapor in the Isochoric System	156
Isochoric Vapor Loading Method	158

Theory of Isochoric Vapor Transfer where the Analyte is Not Added to the Solvent before the 1st Loading	171
Theory of Isochoric Vapor Transfer where the Analyte is Added to the Solvent in the Beginning	176
Calibration of System Volumes	178
The Speed of the Syringe Piston	180
Experimental (for the Measurement of $K_P$ )	184
Step by Step Calculation of Gas-Liquid Distribution Constant Using the Isochoric Vapor Loading Method.	190
Precision and Accuracy of the Measured Gas-Liquid Distribution Constant(s) by the Isochoric Vapor Loading Method	195
Evaluation on the Obtained Data for the Gas-Liquid Distribution Constant(s) by the Isochoric Vapor Loading Method	205
Results and Discussion: Gas-Liquid Distribution Constants	209
Results and Discussion: Liquid-Liquid Partition Coefficients ( $K_P$ )	221
Conclusions	229
Chapter V: Comparison of Calculated Retention Volumes ( $V_R$ ) versus Experimentally Measured Retention Volumes ( $V_r$ ) of all Analytes.	230
Summary	230
Introduction	230
Results	231
Comparison of $V_R$ versus $V_r$	232
Discussion	248
Comparison of $V_R$ versus $V_r$ Using Statistics	250
Conclusions	251
Chapter VI: Overall Conclusions	254
Appendix I – Derivation of the mass-balance equation for a two component system.	258



## List of Tables

Table		Page(s)
1-I	Proposed Retention Mechanisms and Models in RPLC.	3-4
1-II	Geometric Parameters of Bare Porous Silica and Alkylsililated Gels Measured by LTNA.	48
3-I	Geometric Parameters of Bare Porous Silica and Alkylsililated Gels.	83
3-II	Acetonitrile/Water Minor Disturbance Retention Volumes, in mL, for Five Columns.	86
3-III	Void Volume Values Measured by Minor Disturbance Method with Acetonitrile-Water for Five Columns.	88
3-IV	Excess Adsorption of Acetonitrile on a C <sub>18</sub> Column (in Terms of Volume).	93
3-V	Excess Adsorption of Acetonitrile on a C <sub>12</sub> Column (in Terms of Volume).	97
3-VI	Excess Adsorption of Acetonitrile on a C <sub>8</sub> Column (in Terms of Volume).	98
3-VII	Excess Adsorption of Acetonitrile on a C <sub>4</sub> Column (in Terms of Volume).	99
3-VIII	Excess Adsorption of Acetonitrile on a C <sub>1</sub> Column (in Terms of Volume).	100
3-IX	The Largest Standard Deviation ( $\sigma$ ), in mL, Found for the Retention Volume From the Five Columns Studied for Each Analyte at Given Mobile Phase Composition.	111
3-X	Experimentally Measured Retention Volume, in mL, (Corrected for System Volume) of Each Analyte, on a C <sub>18</sub> Column, at a Given Acetonitrile-Water Composition.	112
3-XI	Experimentally Measured Retention Volume, in mL, (Corrected for System Volume) of Each Analyte, on a C <sub>12</sub> Column, at a Given Acetonitrile-Water Composition.	113
3-XII	Experimentally Measured Retention Volume, in mL, (Corrected for System Volume) of Each Analyte, on a C <sub>8</sub> Column, at a Given Acetonitrile-Water Composition.	114
3-XIII	Experimentally Measured Retention Volume, in mL, (Corrected for System Volume) of Each Analyte, on a C <sub>4</sub> Column, at a Given Acetonitrile-Water Composition.	115

3-XIV	Experimentally Measured Retention Volume, in mL, (Corrected for System Volume) of Each Analyte, on a C <sub>1</sub> Column, at a Given Acetonitrile-Water Composition.	116
3-XV	Measured Henry Constant, K <sub>H</sub> , (in mL) for all Analytes Studied on Every Column.	128
4-I	Dependence of The Pressure Drop on the Gas Flow Rate.	182
4-II	List of GC Conditions Used for all Analytes in Order to Separate Acetonitrile (Solvent) and the Analyte.	185
4-III	The Number of Syringe Strokes Required, for Each Analyte, for The Listed Steps of the Vapor Loading Method to Determine the K.	188
4-IV	An Excel Spreadsheet Showing the Step-By-Step Calculation of the Gas-Liquid Distribution Constant of Benzene in Acetonitrile: Water Mixture (90:10, V/V) as a Solvent at 30°C.	194
4-V	Peak Area of Benzene During Equilibration Process with the Solvent (Acetonitrile: Water, 90:10, V/V).	198
4-VI	Precision and Accuracy of the Measured Gas-Liquid Distribution Constants at 30 ± 1°C.	203
4-VII	Measured Gas-Liquid Distribution Constants of Acetone, Butanone and Pentanone in Given Acetonitrile: Water Mixtures at 30°C.	211
4-VIII	Measured Gas-Liquid Distribution Constants of Hexanone in Given Acetonitrile: Water Mixtures at Three Different Temperatures and Then the Calculated Value at 30°C From the Three Measured Values.	213
4-IX	Step-By-Step Calculation of the Gas-Liquid Distribution Constant, K, of Hexanone at 30.0°C in Given Acetonitrile: Water Mixtures.	214
4-X	Measured Gas-Liquid Distribution Constants of Heptanone in Given Acetonitrile: Water Mixtures at Three Different Temperatures and Then the Calculated Value at 30°C From the Three Measured Values.	215
4-XI	Step-By-Step Calculation of the Gas-Liquid Distribution Constant, K, of Heptanone at 30.0°C in Given Acetonitrile: Water Mixtures.	216
4-XII	Measured Gas-Liquid Distribution Constants of Four Alkyl Benzenes in Given Acetonitrile: Water Mixtures at 30°C.	219
4-XIII	Calculated Liquid-Liquid Partition Coefficients of Five Ketones in Given Acetonitrile: Water Mixtures at 30°C.	223

4-XIV	Calculated Liquid-Liquid Partition Coefficients of Four Alkyl Benzenes in Given Acetonitrile: Water Mixtures at 30°C	225
4-XV	The Transfer of Methylene Groups From the Studied Ketones From the Mobile Phase to the Adsorbed Layer.	227
4-XVI	The Transfer of Methylene Groups From the Studied Alkyl Benzenes From the Mobile Phase to the Adsorbed Layer.	228
5-I	Calculated Retention Volumes (in mL), $V_R$ , of All Analytes on a C <sub>18</sub> Column.	233
5-II	Calculated Retention Volumes (in mL), $V_R$ , of All Analytes on a C <sub>12</sub> Column.	234
5-III	Calculated Retention Volumes (in mL), $V_R$ , of All Analytes on a C <sub>8</sub> Column.	235
5-IV	Calculated Retention Volumes (in mL), $V_R$ , of All Analytes on a C <sub>4</sub> Column.	236
5-V	Calculated Retention Volumes (in mL), $V_R$ , of All Analytes on a C <sub>1</sub> Column.	237
5-VI	Calculation of Propagation of Error.	252

## List of Figures

Figure		Page
1-1	Plot of Log K (Gas to Liquid Partition Coefficients) vs Volume Fraction of Acetonitrile.	7
1-2	Schematic Drawing Illustrating a Partition Mechanism and an Adsorption Mechanism.	11
1-3	Schematics Drawing Illustrating Early Models of Molecular Organization of Bonded Phase Chains in RPLC: (A) Brush Model and (B) Blanket Model.	14
1-4	Schematics Drawing Illustrating the Early Models of Molecular Organization of Bonded Phase Chains in RPLC: (A) Liquid-Droplet Model and (B) Picket Fence Model.	16
1-5	Schematic Drawing Illustrating the Definitions of (A) Interphase and (B) Interface as applied to the RPLC Bonded Phase.	19
1-6	Schematic Illustration (A) and Lattice Model (B) of the Retention in RPLC According to the Adsorption Mechanism.	20
1-7	Schematic Drawing Illustrating A Monomolecular Layer Thick of Solvent Layer Adsorbed on the Bonded Alkyl Chains and Analyte Molecules Interact with the Solvent Layer Instead of with the Bonded Chains.	30
1-8	Schematic Representation of the Postulated Solvation-Layer Polarity Gradient in the ODS-Bonded Silica Stationary Phase.	41
1-9	Comparison of the Molecular Volumes of Bonded Ligands with That Calculated From the Density of Corresponding Liquid.	45
1-10	Molecular Model Showing the Silica Surface Modified with (A) Trichlorosilane - C <sub>1</sub> , (B) Octadecylsilane in All Trans Conformation - C <sub>18</sub> , and (C) Same as B Except with Minimized Energy.	47
2-1	Schematic Drawing Illustrating the Concept of Excess Adsorption.	54
2-2	Acetonitrile Excess Adsorption Isotherms on C <sub>1</sub> , C <sub>2</sub> , C <sub>3</sub> , C <sub>4</sub> , C <sub>5</sub> , C <sub>6</sub> , C <sub>8</sub> , C <sub>10</sub> , C <sub>12</sub> , and C <sub>18</sub> Modified Adsorbents.	61
2-3	Estimation of the Maximum Adsorbed Amount on the Basis of the Model of Finite Thickness Adsorbed Layer.	63
2-4	Adsorbed Layer Thickness For THF, Acetonitrile, and Methanol on the Surface of Silica-Based Adsorbents Modified with Alkylsilanes of Different Chain Length	65



2-5	Comparison of the Bonded Layer and Adsorbed Layer Thickness Versus Carbon Number of the Alkyl Chain Bonded to the Silica Surface.	66
2-6	The Dependence of the Acetonitrile Adsorbed Layer and Collapsed Bonded Layer Thickness on the Length of the Bonded Chains.	67
2-7	A Schematic Representation of the Bonded Layer, the Adsorbed Layer and the Mobile Phase.	69
2-8	Schematic Representation of the Analyte Distribution According to the Described Partitioning-Adsorption Model For RPLC.	70
3-1	Dependencies of the Minor Disturbance Peaks on Different Columns.	87
3-2	Determination of the Molecular Area of Adsorbed Molecule From the Excess Adsorption Isotherm Using Everett's Approach.	91
3-3	Excess Adsorption of Acetonitrile From Water on Different Bonded Alkyl Chains.	94
3-4	Estimation of the Maximum Adsorbed Volume of Acetonitrile on a C <sub>18</sub> Column.	95
3-5	Experimentally Measured Retention Data For Acetone on All Five Columns.	117
3-6	Experimentally Measured Retention Data For Butanone on All Five Columns.	118
3-7	Experimentally Measured Retention Data For Pentanone on All Five Columns.	119
3-8	Experimentally Measured Retention Data For Hexanone on All Five Columns.	120
3-9	Experimentally Measured Retention Data For Heptanone on All Five Columns.	121
3-10	Experimentally Measured Retention Data For Benzene on All Five Columns.	122
3-11	Experimentally Measured Retention Data For Toluene on All Five Columns.	123
3-12	Experimentally Measured Retention Data For Ethyl Benzene on All Five Columns.	124
3-13	Experimentally Measured Retention Data For Propyl Benzene on All Five Columns.	125

3-14	Measured Henry Constant (in mL), $K_H$ , of All Analytes (A-Ketones and B-Alkyl Benzenes) Versus Carbon Number of Bonded Alkyl Chain Length for All Five Columns.	129
4-1	Principle Schematic of the Isochoric Headspace System.	140
4-2	Same as Figure 4-1 Except Showing Movement of Syringes in the Opposite Direction.	141
4-3	Photograph of the Isochoric Headspace System Installed on Top of HP 5890 GC.	142
4-4	Photograph of the Syringe Assembly Inside the Isochoric Headspace System.	143
4-5	Photograph of the Valves Inside the Isochoric Headspace System.	144
4-6	Photograph of the Backside of the Isochoric Headspace System Where All of the Electronic Connections Are Located.	145
4-7 to 4-12	Schematics of an Isochoric Headspace System Showing the Step-By-Step Procedure For the Vapor Extraction Method.	150 to 155
4-13 to 4-22	Schematics of an Isochoric Headspace System Showing the Step-By-Step Procedure For the Vapor Loading Method.	160 to 169
4-23	Vapor Composition Equilibration Between the Analyte Bottle and the Syringe Assembly Measured at Different Syringe Piston Speeds.	183
4-24	Linear Regression Using Found Concentrations of Benzene, at Equilibrium For Each Cycle, in the Liquid Phase Versus the Gas Phase.	196
4-25	An Example of the Temperature Readings Found From Within the HS System During Typical HS Experiment.	200
4-26	An illustration of the Accumulation of the Error on the Extrapolated Point From the Linear Regression.	206
4-27	The Graph Representing the Liquid Phase Concentration Versus the Gas Phase Concentration of an Analyte, at Equilibrium with Some Solvent at Temperature T.	210
4-28	Plot of log K of Measured Gas-Liquid Distribution Constants at 30°C Versus Volume Fraction of Acetonitrile For All Five Ketones.	217
4-29	Plot of log K of Measured Gas-Liquid Distribution Constants at 30°C Versus Volume Fraction of Acetonitrile For All Five Alkyl Benzenes.	220

4-30	Plot of $\log K_p$ of Calculated Liquid-Liquid Partition Coefficients at 30°C Versus Mobile Phase Composition (in Acetonitrile-Water) For All Five Ketones Studied.	224
4-31	Plot of $\log K_p$ of Calculated Liquid-Liquid Partition Coefficients at 30°C Versus Mobile Phase Composition (in Acetonitrile-Water) for All Four Alkyl Benzenes Studied.	226
5-1	Comparison of Theoretical versus Experimentally Measured Values for All Studied Ketones on a $C_{18}$ Column.	238
5-2	Comparison of Theoretical versus Experimentally Measured Values for All Studied Ketones on a $C_{12}$ Column.	239
5-3	Comparison of Theoretical versus Experimentally Measured Values for All Studied Ketones on a $C_8$ Column.	240
5-4	Comparison of Theoretical versus Experimentally Measured Values for All Studied Ketones on a $C_4$ Column.	241
5-5	Comparison of Theoretical versus Experimentally Measured Values for All Studied Ketones on a $C_1$ Column.	242
5-6	Comparison of Theoretical versus Experimentally Measured Values for All Studied Alkyl Benzenes on a $C_{18}$ Column.	243
5-7	Comparison of Theoretical versus Experimentally Measured Values for All Studied Alkyl Benzenes on a $C_{12}$ Column.	244
5-8	Comparison of Theoretical versus Experimentally Measured Values for All Studied Alkyl Benzenes on a $C_8$ Column.	245
5-9	Comparison of Theoretical versus Experimentally Measured Values for All Studied Alkyl Benzenes on a $C_4$ Column.	246
5-10	Comparison of Theoretical versus Experimentally Measured Values for All Studied Alkyl Benzenes on a $C_1$ Column.	247

## Thesis Structure

The work described in this thesis contains studies performed to support the partition/adsorption model presented here. This section is provided for the reader to understand how different aspects of the work are related to each other.

Chapter I is dedicated to the different retention models presented over the years of exploration of retention mechanism of reversed-phase liquid chromatography (RPLC). The emphasis is placed on the partition versus the adsorption process. An overview of the current understanding of the bonded layer is presented with chromatographic and spectroscopic evidence stating that the organic modifier of the mobile phase is adsorbed on the bonded phase. The chapter ends with the results generated in our laboratory indicating that the bonded layer under the chromatographic conditions is in its least energy state or collapsed.

Chapter II describes the adsorbed layer in terms of composition and volume. Interpretation of the excess adsorption isotherms leads to the conclusion that the adsorbed layer is a multilayer when acetonitrile is used as the organic modifier. It is also shown that this multilayer adsorption lies on top of the collapsed bonded layer. Then, a model is presented which describes the RPLC retention as a sum of two processes: partitioning into the organic adsorbed layer followed by analyte adsorption on the hydrophobic surface. A mathematical relationship was derived which can predict the retention of an analyte under given set of experimental conditions based on the presented model. This equation has four unknowns: dead volume, adsorbed layer volume, liquid-liquid partition coefficient and Henry's constant.

Chapter III summarizes the data obtained using RPLC for the measurement of three of the four unknowns (void volume, adsorbed layer volume and Henry's constant). A brief

literature review is given on the effect of mobile phase composition and the effect of bonded alkyl chain length on RPLC retention.

Chapter IV describes measurement of the gas-liquid distribution constant using headspace gas chromatography. A literature review on current methods and instrumentation used to measure the gas-liquid distribution constants is given. An isochoric headspace system is introduced which was used for the measurement of gas-liquid distribution constants at atmospheric pressure. The calculation of liquid-liquid partition coefficients on the basis of the measured gas-liquid distribution constants is discussed.

In Chapter V, the comparison of the predicted retention volumes with experimentally measured retention volumes for all analytes studied at different experimental conditions (acetonitrile-water composition and alkyl chain length) are discussed. Based on the comparison, some conclusions and limitations of the proposed partition/ adsorption model are discussed.

Chapter VI highlights the important conclusions of the current study.

## **Chapter I: Historical**

### **Summary**

The mobile phase driven retention mechanism (solvophobic theory) that is widely referenced in the literature and the experimental evidence that challenges its validity is addressed since stationary phase is a passive receptor in this model. Studies that support the concept that the stationary phase drives retention will then be presented. The partitioning mechanism is compared with the adsorption mechanism in discussing the relative importance of the stationary phase to the mobile phase. Early models and more advanced statistical models of bonded chain organization are discussed with the goal of highlighting the influence of chain organization on retention. In addition, adsorption of mobile phase components onto the bonded phase and its effect on the chemical and structural nature of the stationary phase will be discussed through several representative chromatographic and spectroscopic studies. Lastly, the effect of solvent adsorption on the conformation and the structures of the stationary phase are discussed in terms of the effect of mobile phase composition and bonded alkyl chain length. All of the discussions on the RPLC stationary phase are restricted to alkyl bonded phase, with an emphasis on monomeric type phases.

### **Introduction**

Reversed phase liquid chromatography (RPLC) has been the most widely used branch of high-performance liquid chromatography (HPLC) for the analysis and purification of a wide variety of substances [1]. Most commonly, RPLC employs porous silica chemically modified with alkylsilanes of various alkyl chain length [2], such as octadecylated silica,

which offer high separation efficiency combined with versatility and reproducibility. The use of bonded hydrocarbon stationary phases of different provenance and a variety of hydro-organic eluents to modulate retention offers a wide range of operating conditions to separate mixtures containing small or large molecules of different polarity [3]. As a result, RPLC is employed in science and technology for numerous applications such as pollution control, food, clinical and pharmaceutical analysis, and separation of peptides, proteins and nucleic acids.

### **Proposed Retention Mechanisms in RPLC**

Despite its importance, there is still considerable uncertainty as to the mechanism of the overall retention process [4-41]. Retention in RPLC has received extensive theoretical treatment over the past thirty years [4-41]. The major question asked by many chromatographers is what is the mechanism of HPLC retention [4, 30, 31]. There have been many retention mechanisms proposed (refer to Table 1-I) on the basis of experimental results [5-42], but not all of the obtained data can be applied to one of the proposed mechanism. Three major retention mechanisms widely discussed in the literature are adsorption [9-12], partitioning [13-14] and solvophobic theory [15].

### **Mobile Phase Driven vs. Stationary Phase Driven Retention Mechanisms**

Most of the early retention models emphasized the role of the mobile phase as the sole governing factor in determining analyte retention in RPLC. This concept of mobile phase driven retention mechanism traces back to Horvath et al's solvophobic theory [15], adapted from the work of Sinanoglu [42, 43]. This model emphasizes the exclusion of the

**Table 1-I:** Proposed retention mechanisms and models in RPLC.

Major driving force of retention and/or the name of the model	Reference(s)
Scott-Kucera model – solvent-solute and dispersion interactions – based on adsorption of organic molecules on the surface	5
Snyder-Soczewinski model – displacement mechanism	6-8
Adsorption	9-12
Partition	13-14
Solvophobic theory	15
Solubility parameter is used to predict retention in RP-HPLC	16-17
Model based on molecular connectivity	18
Based on adsorption of organic solvent molecules on the surface	19
Interfacial aggregation – microscopic micro-droplet model	20
Two-site adsorption model	21
“Penetration and close contact” mechanism	22
Dual mechanism – solvophobic (hydrophobic) and silanophilic (participation of silanols) interactions	23
Aggregation/deaggregation model to explain wetting (reordering/resolution) of immobilized chains	24
Model based on interaction indices	25-27
Breathing model – Lattice model	28
Distribution theory (between two phases)	29
Partitioning through Lattice models	30-31
Lattice theory	32



**Table 1-I (continued)**

Major driving force of retention and/or the name of the model	Reference(s)
Partition-Displacement model	4, 33
Retardation coefficient ( $R_F = t_m / \{t_m + t_s\}$ ) is used to explain retention in RP-HPLC	34
Model based on bonding density: High bonding density is partitioning and Low bonding density is adsorption	35
Intermolecular interactions between solute and mobile phase	36
UNIFAC model – functional group-oriented method	37
Linear solvent strength theory	38
Organization and formation of clusters in hydro-organic (acetonitrile) mixtures	39
LSERs to predict retention – Linear Solvation Energy Relationships	40
Adsorption/partition model	41

less polar analyte molecules from the polar mobile phase with subsequent sorption by the stationary phase. According to this model, the analytes are “driven” towards the stationary phase because of their “fear” of the aqueous mobile phase, rather than any intrinsic affinity between the analyte and the stationary phase. The stationary phase is considered as a passive receptor.

The solvophobic theory focuses on the closing of an analyte size cavity in the mobile phase after the transfer of a analyte molecule from the mobile phase to the stationary phase. The theory models the analyte retention based on the free energy obtained in closing a analyte-size cavity in a single phase, i.e., the mobile phase in this case. The transfer process of analyte from the mobile phase to the stationary phase and the interactions of analyte with the stationary phase bonded ligands are neglected. In summary, the solvophobic theory considers the RPLC retention as a solubility process in a single phase rather than as a transfer process between two chromatographic phases. Although the model gives fairly good predictions on the retention of nonpolar analytes, it does not provide a sufficiently detailed explanation of the dependence of analyte retention and selectivity on the stationary phase variables.

Nonetheless, the solvophobic theory has influenced many research groups in interpreting their experimental data and in making conclusions about the retention mechanism in RPLC [24-26, 48-50]. Cheong and Carr [48] found that the retention factors for a series of alkylbenzenes were highly correlated with their activity coefficients in the mobile phase. Thus, they concluded that most of the free energy of transfer in RPLC arises from processes taking place in the mobile phase. Alvarez-Zepeda et al. [49] reached a similar conclusion based on studies of molar excess enthalpies and entropies of transfer.

Jandera and coworkers [25-27, 50] developed a retention model based on “interaction indexes” of mobile phase and analyte molecules, and neglected the effects of stationary phase. Two possible reasons have led to a biased opinion about the role of stationary phase in analyte retention. First, technical limitations in the early days hindered direct investigation on the role of the stationary phase. Second, many results were deduced from chromatographic measurements that were largely based on variations in mobile phase composition. The relative changes in the free energy terms as the mobile phase was varied have been mistaken as the analyte contribution in a retention term [25-27, 50].

Nevertheless, there are many chromatographic studies that pointed to the fact that the stationary phase is not a passive partner in the retention process [28, 51-68]. These studies showed that chromatographic retention and/or selectivity are greatly influenced by the nature of the bonded phase, such as the length of the bonded chains [53-57], the chemical properties of the bonded chains [58] and surface coverage [59]. The stationary phase also shows functional group selectivity that could not be explained by the solvophobic theory [51-52, 60-63]. In addition, according to the solvophobic theory, analyte transfer from water is accompanied by a large negative change in heat capacity, being entropy-driven around room temperature and being enthalpy-driven at higher temperatures. However, these temperature dependencies were not observed in the chromatographic retention of many nonpolar analytes [28, 64-68].

In a study of gas-liquid partitioning of a series of alkylbenzenes in aqueous organic mixtures, Carr et al. [45] found that there is a very narrow range in the solvent compositions (around 20% acetonitrile in water) at which the partition coefficients, and thus the free energies of transfer, of the alkylbenzenes are the same. Figure 1-1 shows the gas-liquid partitioning

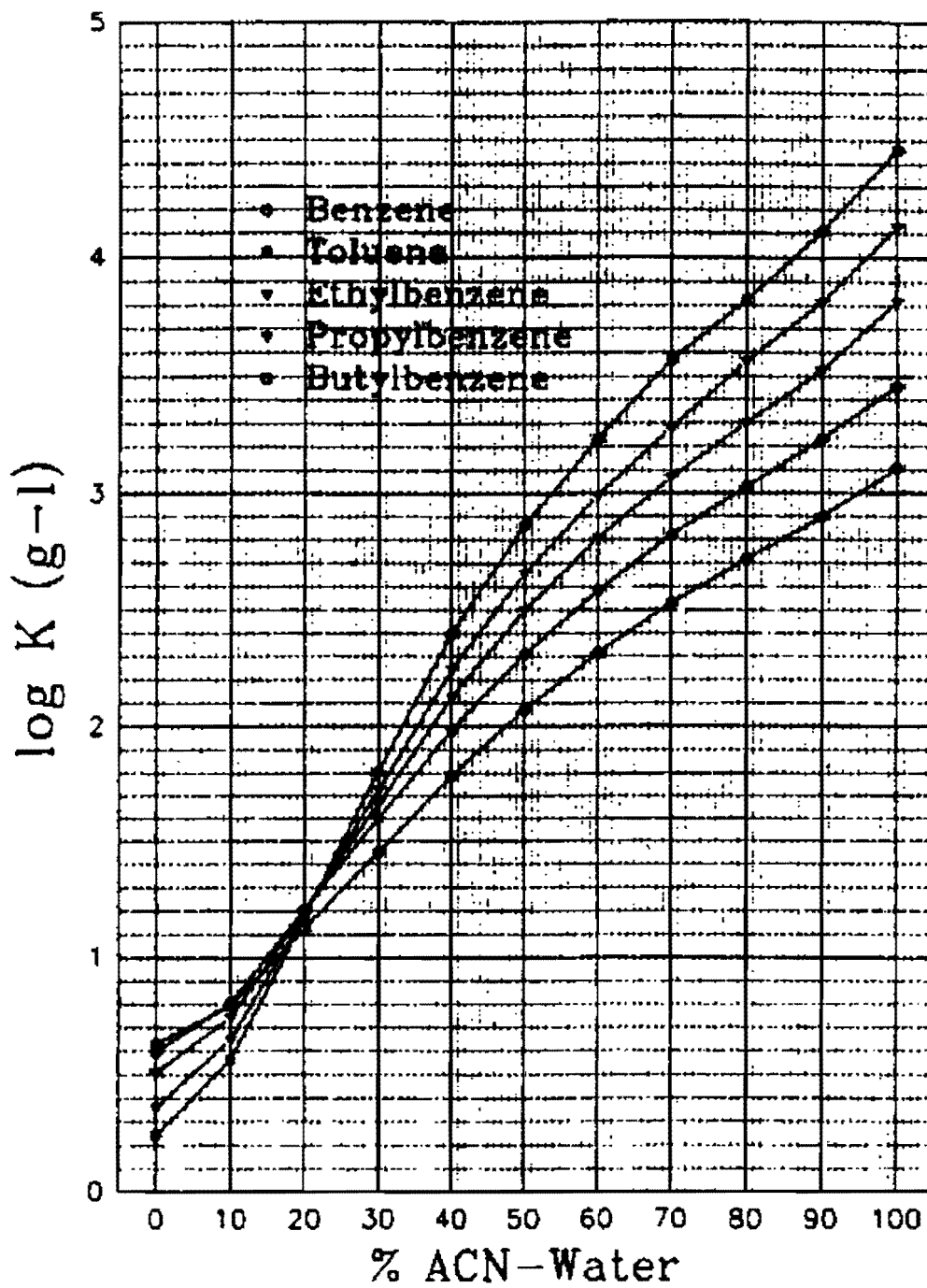


**Figure 1-1:** Plots of log K (gas to liquid partition coefficients) vs volume fraction of acetonitrile. O = Benzene; • = Toluene; ∇ = n-Ethylbenzene; Δ = n-Propylbenzene; □ = n-Butylbenzene. The figure is taken from reference [45], figure 2.

results for aqueous acetonitrile mixtures. Similar results were obtained for aqueous mixtures of methanol, tetrahydrofuran and 2-propanol. However, alkylbenzenes can be separated with excellent selectivity in RPLC using the same aqueous mixtures as mobile phase. This result strongly implies that at those mobile phase compositions, a great deal of the non-polar functional group selectivity observed in RPLC is due to the net free energy of the analyte in the stationary phase. Besides, in the same study, the pure organic solvents were found to better discriminate the alkylbenzenes, in terms of gas-liquid partition coefficients, than does water. This is in stark contrast to RPLC practice where mobile phase of higher water content leads to greater methylene group selectivity [69]. Unless one considers the stationary phase to dominate the analyte retention, the above findings cannot be reconciled with practical experience in RPLC.

In order to investigate whether the mobile phase or stationary phase drives the retention process in RPLC, one has to compare the free energy of the analyte in the mobile phase and stationary phase, separately. Carr et al. [45] showed that the free energy of transfer of a methylene group from gas to hexadecane is larger than that from gas to water or to organic aqueous mixtures. The free energy term here indicates the net free energy resulting from the endergic cavity formation process and the exoergic analyte-solvent interaction.

On the premise that bulk hexadecane is justified as a good model for RPLC bonded phase, at least for nonpolar analytes, Carr et al. [45] concluded that most of the energy of retention arises from the net attractive (exoergic) processes in the bonded phases (shorter than eight carbons), and not from net repulsive (endoergic) processes in the mobile phase. In other words, they conclude that retention mechanism of nonpolar analytes is stationary

phase-driven (for bonded length less than eight carbons), not mobile phase-driven, which is in contrast to the solvophobic theory. This result was found to hold for at least four organic modifiers; methanol, acetonitrile, tetrahydrofuran and 2-propanol.

Hence, for at least nonpolar analytes, the retention mechanism is not mobile phase-driven (when using bonded chain less than eight carbons), as predicted by the solvophobic theory, instead it is stationary phase-driven. The retention mechanism of polar analytes is predicted to be strongly dependent on the nature of the mobile phase in view of the substantial polar interactions (dipole-dipole, dipole-induced dipole and hydrogen bonding) between the analytes and mobile phase. However, this does not mean that the solvophobic theory will be able to explain the retention mechanism of polar analytes, since it was initially adapted to explain mainly the retention of nonpolar analytes only.

### **Partitioning vs. Adsorption Mechanisms**

Whether an analyte physically partitions into the layer of the bonded phase or adsorbs at the interface between the bonded phase and the adjacent freely moving milieu is a long-standing debate among chromatographers [12, 37, 38, 40]. Knowledge of the physical location of analyte molecules is important in predicting retention and in designing chromatographic phases. Many retention models involving both partitioning and adsorption have been proposed [6, 28, 31, 70-73], and even the definitions of partitioning and adsorption have varied. Here, the partitioning vs. adsorption mechanism in terms of the definitions given by Dill and Dorsey are addressed [31]. In a partitioning mechanism, an analyte molecule is approximately fully embedded within the stationary phase; while in an adsorption mechanism, the analyte is in contact with surface with the stationary phase and is

not fully embedded [31]. A representative schematic of these two definitions is shown in Figure 1-2. According to Dill and Dorsey, the main driving force for analyte retention by either mechanism is the differential chemical affinity of the analyte for the mobile- and stationary- phase molecules. Under the partitioning mechanism, all the analyte-mobile phase interactions are replaced by analyte-stationary phase interactions; while only a fraction of the analyte-mobile phase interactions are replaced under the adsorption mechanism. Thus, based on the number of intermolecular contacts, the driving force for adsorption mechanism can only be a fraction of that for the partitioning process. In addition, the chain organization imposed by the interfacial constraints will influence the partitioning mechanism, but has no effect on the adsorption mechanism as the analyte is not immersed within the bonded chains.

Based on the Dill and Dorsey definitions of the partitioning and adsorption processes, a great deal of experimental evidence leads to the conclusion that the retention mechanism in RPLC resembles partitioning rather than adsorption. First, retention in RPLC was found to be proportional to the oil/mobile phase partition coefficients [3, 74-82], i.e. the slope of the dependence is close to unity. A slope of  $1/z$  ( $z$  is the lattice coordination number) would have been expected if analytes were retained via the adsorption mechanism. Tan and Carr [40] compared the free energy of transfer of a methylene group from the mobile phase to RPLC bonded phase to that from the same mobile phase to bulk hexadecane. They found that the energetics of the transfer of alkylbenzenes from hydroorganic liquid phase to bulk hexadecane was similar to that RPLC retention in the organic modifier range from 0-70%. They concluded that the retention of small nonpolar analytes in RPLC is governed by the partition mechanism with bulk liquid hexadecane serving as a good representative of the stationary phase characteristics for describing the retention behavior in the above range of

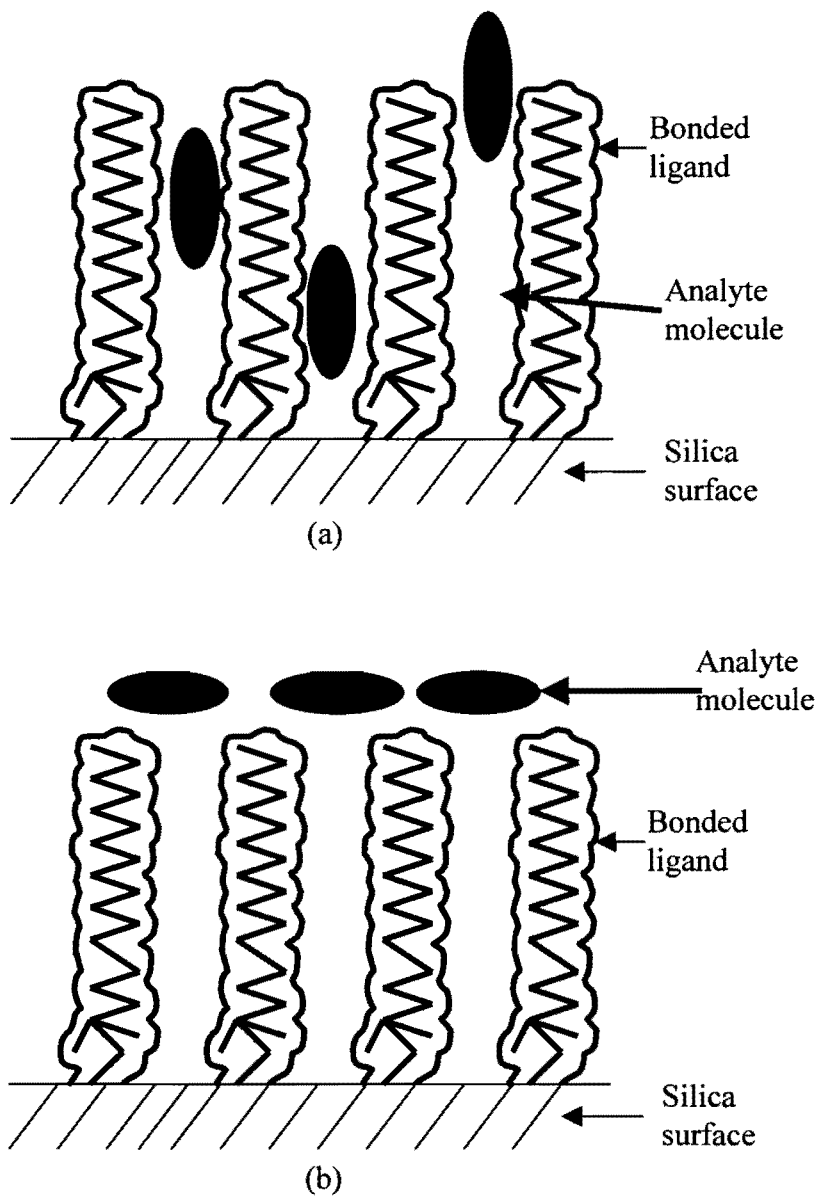


**Figure 1-2:** Schematic drawing illustrating a partition mechanism and an adsorption mechanism. An analyte molecule is fully embedded within the stationary phase in a partitioning mechanism (a) and only in surface contact with the stationary phase in an adsorption mechanism (b).



organic modifier concentrations. At higher organic modifier concentrations, retention behavior in RPLC deviated from partition like behavior and this was attributed to a shift to adsorption mechanism, to the adsorption of organic modifier on the stationary phase. By examining the methylene group selectivity for the ratio of equilibrium constants of two homologous differing by a single methylene unit (for the transfer from the mobile phase to the gas phase as well as from the gas phase to bulk liquid hexadecane), the authors further concluded that the contribution of the stationary phase to methylene selectivity in RPLC is significantly greater than that of the mobile phase.

Second, RPLC retention of nonpolar analytes depends on the surface density of the bonded phase [59, 83]. If analyte molecules adsorb onto the bonded phase, the dependence on the surface density would be insignificant. Third, Tchaplal et al. [84] showed the existence of a very subtle but real discontinuity in plots of  $\log k'$  (retention factor) vs. the number of methylene groups in a side chain of an analyte for a given homologous series. The discontinuity in the plot was shown where the number of methylene groups in a side chain of an analyte for a given homologous series was nearly equal to the number of methylene groups attached to the bonded alkyl chain of the bonded ligand as the stationary phase. This suggests the analyte alkyl chain insert itself within the bonded phase, in other words, the analyte partitions as per Dill and Dorsey's definition. Fourth, RPLC retention coefficients (of nonpolar analytes) were shown to depend approximately linearly on analyte size and the surface tension of mobile phase, as predicted for distribution coefficients in a pure partition system [15, 72, 75, 85, 86].

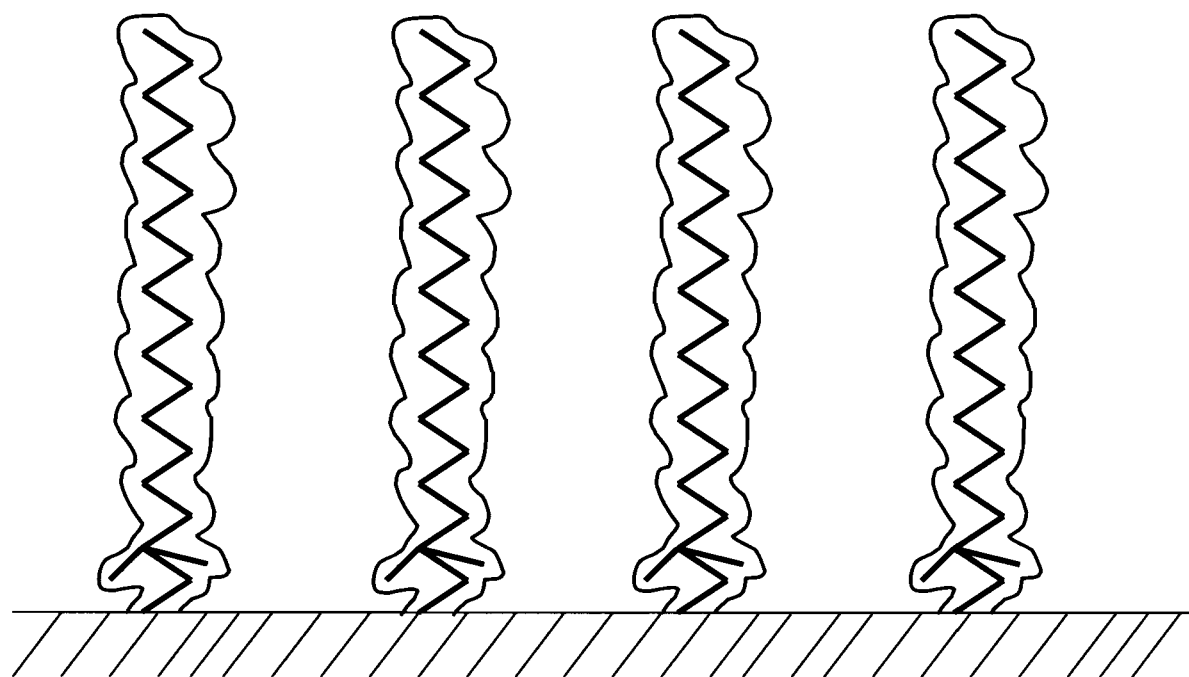
Despite the fact that many studies have shown that RPLC retention is partition-like, analyte molecules are not homogeneously distributed throughout the bonded phase upon

retention. Statistical models [4, 30, 87] suggest that most analyte molecules reside in the boundary region between the mobile phase and the stationary phase.

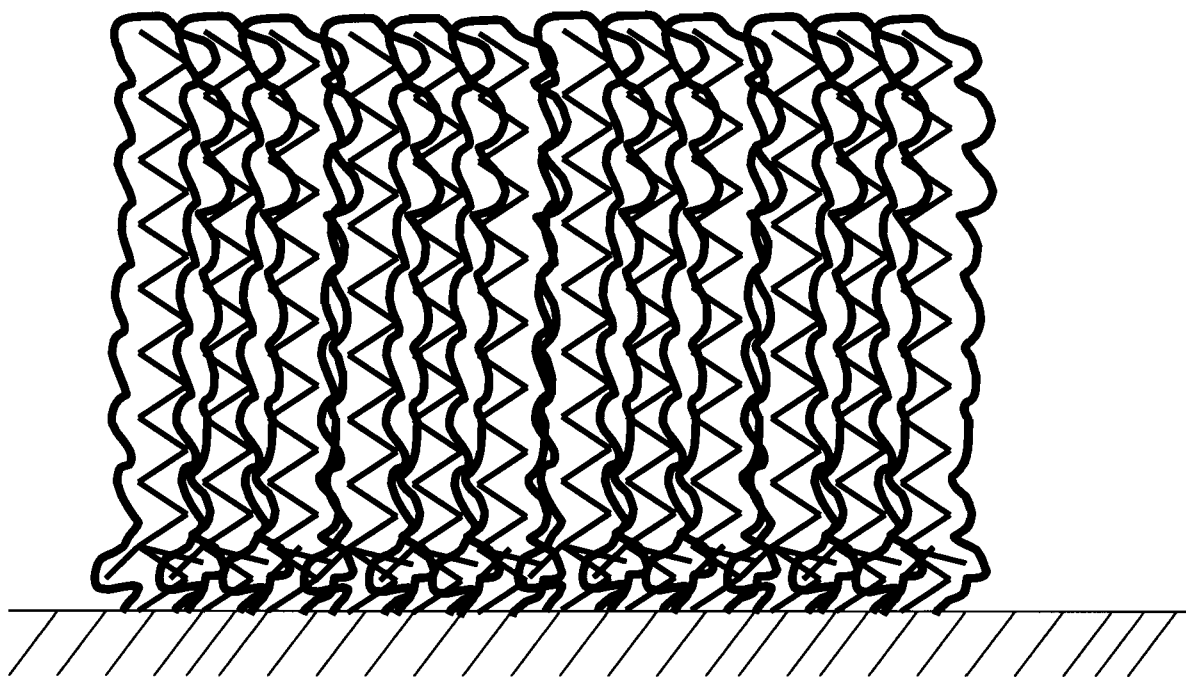
### **Stationary Phase Models in RPLC**

The structure and composition of bonded phases in the presence of different eluents have been the subject of many studies [3, 6, 30, 37, 44-45, 88-90]. In the literature, there have been about five stationary phase models that have been proposed to describe retention in RPLC. A review given below describes the characteristic features of some of these models.

Early models of the organization of bonded alkyl chains were derived from chromatographic results. Bonded phases were pictured as an alkyl “brush” (refer to Figure 1-3a), whose individual bristles extend away from the silica surface [88]. The “brush” or “bristle” model is also referred as the “fur” model. The model predicts that the extended bristles are fully exposed to the mobile phase molecules and made up of rather rigid matrix with which analyte molecules in the mobile phase interacted. However, the concept of fully extended configuration of the bonded chains contradicts the solvophobic theory that implies aggregation of nonpolar moieties upon contact with polar environment. The free energy will be prohibitively high in order for the bonded chains to configure themselves to allow for such a high degree of exposure. In view of the solvophobic effects, Hemetsberger proposed the blanket model (refer to Figure 1-3b), where bonded phase is depicted as a hydrocarbonaceous sheath made up of recumbent alkyl chains [91]. The alkyl chains lie close to the surface to minimize the solvophobic surface area in contact with the polar mobile phase. However, the blanket model failed to explain the liquid-like nature observed on the bonded phase.



(a)



(b)

**Figure 1-3:** Schematics drawing illustrating early models of molecular organization of bonded phase chains in RPLC: (a) brush model and (b) blanket model.

### **Liquid Hydrocarbon Partition Model or Lochmuller & Wilder Model**

Lochmuller and Wilder [20] were the first ones to propose the liquid hydrocarbon layer model to describe the sorptive behavior of alkyl-silica bonded stationary phases in RPLC.

They proposed that bonded alkyl chains in methanol-water mobile phases might associate with each other due to hydrophobic interactions to form “liquid-droplet” like clusters. Such clusters could afford a bulk liquid-like environment for the partitioning of small analytes. They were the first ones to propose a liquid-droplet model where the collapsed alkyl chains form “patches” of alkyl droplets that permit three-dimensional interactions with analyte molecules (refer to Figure 1-4a). The “patches” model is more realistic in view of the heterogeneity in surface coverage of alkyl chains, as a result of the amorphous nature of silica supports and configuration constraints on derivatized chains. In summary, according to the liquid hydrocarbon model, the partition-like behavior of RPLC is observed only with the retention of small nonpolar analyte molecules by stationary phases employing alkyl-bonded chains longer than 12 carbon atoms.

Another liquid hydrocarbon layer model depicts the bonded alkyl chains as “picket fence” of rigid rods with no internal degrees of freedom [3] (refer to Figure 1-4b). According to the model, the bonded alkyl chains are grafted close to one another and none of the mobile phase or analyte molecules can essentially fit in between the “fence posts”. This “picket fence” model is not realistic from two practical perspectives. First, within the temperature range for practical chromatography, alkane molecules are highly disordered [92]. A significant population of the bonded alkyl chains in RPLC has been shown

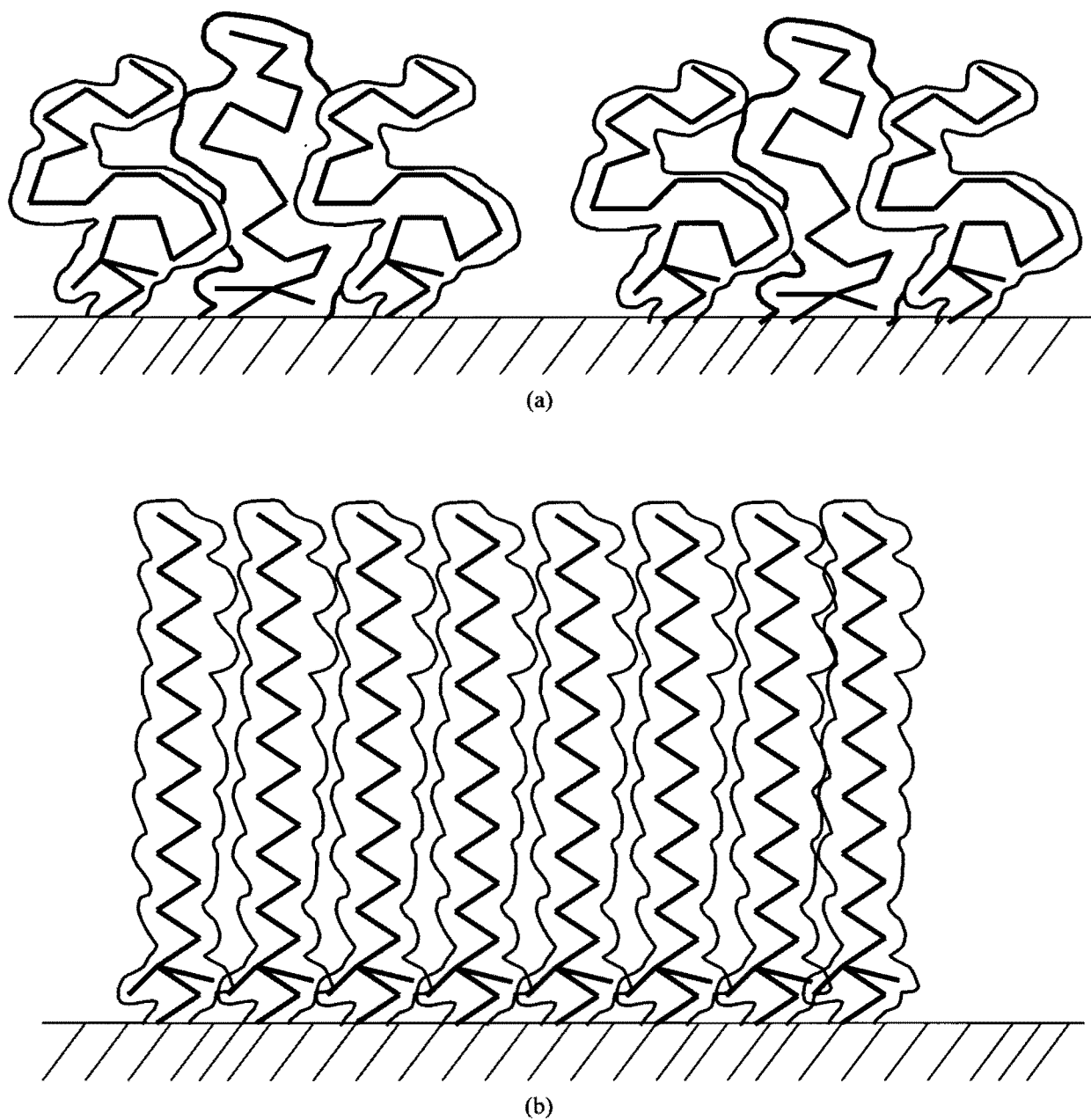


**Figure 1-4:** Schematics drawing illustrating the early models of molecular organization of bonded phase chains in RPLC: (a) liquid-droplet model and (b) picket fence model.

to assume gauche conformation [92]. Second, the model represents only the limiting case of maximum possible surface coverage, a situation prohibited by the interchain constraints that is extremely expensive entropically. In practice, the surface coverage of bonded alkyl chains ranges from 1.5 to 4.0  $\mu\text{mol}/\text{m}^2$  for silica surface of 8.0  $\mu\text{mol}/\text{m}^2$  silanol bonding sites.

### **Liquid-Crystalline Hydrocarbon Partition Model or Martire-Boehm Model**

Recently, the Flory-Huggins lattice theory for polymer in solution was applied to model bonded alkyl chains. Based on an extension of mean field statistical thermodynamic adsorption theory, Martire and Boehm proposed the first statistical mechanical model that addressed the effects of bonded chain organization in RPLC [28]. They considered the changes in the properties of the stationary phases under different mobile phase conditions, and their influence on the retention behavior in RPLC. Two regimes of the eluent composition were identified in which the stationary phase chains were believed to assume different geometric configurations. At high organic modifier concentration, the bonded chains are expected to be extended and oriented more or less normal to the surface, thus giving it a brush-like appearance and allowing complete penetration by the solvent and analyte molecules. In contradiction, the authors found that with water-rich mobile phases, the stationary phase behaves as a quasi-liquid layer of recumbent alkyl chains that hinder solvent penetration but do not preclude analyte penetration. They provided theoretical support for the latter geometric configuration under typical conditions in RPLC with commonly used hydro-organic eluents and concluded that the retention process approaches that of classical liquid-liquid partitioning. According to the model, the bonded phase is

comprised of chemically homogeneous, semi-flexible chains randomly bonded to an inert surface, with mobile phase components intercalated within the bonded chains. The first segment of the bonded chains is fixed to the solid surface while the last segment is fixed in the layer adjacent to the mobile phase. The bonded phase is assumed to be uniform in chemical composition, density and chain organization. It resembles a liquid crystal. Although chain organization is considered in this model, the ordering of the stationary phase was overestimated. Nonetheless, Martire and Boehm introduced the important idea of a “breathing model” for the stationary phase, where the interphase volume changes upon sorption of mobile phase component [28]. We need to define the term interphase, as it is different from the term interface. An interphase denotes the whole volume of the body comprised of the bonded alkyl chains, the sorbed mobile phase components, and the mobile phase components subjected to influence of the potential (refer to Figure 1-5a). An interface denotes the surface area between the mobile phase and the bonded phase (refer to Figure 1-5b). Martire and Boehm [28] predicted an increase in solvent sorption into the bonded phase as the compatibility between solvent molecules and bonded chain increases and as the stiffness of the bonded chains. This dependence has been observed in many RPLC experiments [3, 20, 91, 93-94].

### **Adsorptive Hydrocarbon Monolayer Model or Dill's Model**

Dill considered adsorption as an alternative mechanism of retention in RPLC [30]. A schematic of the analyte retention in RPLC according to the adsorption mechanism is illustrated in figure 1-6a. Retention in RPLC is believed to be governed solely by the adsorption mechanism when the density of bonded nonpolar functions is high enough for the

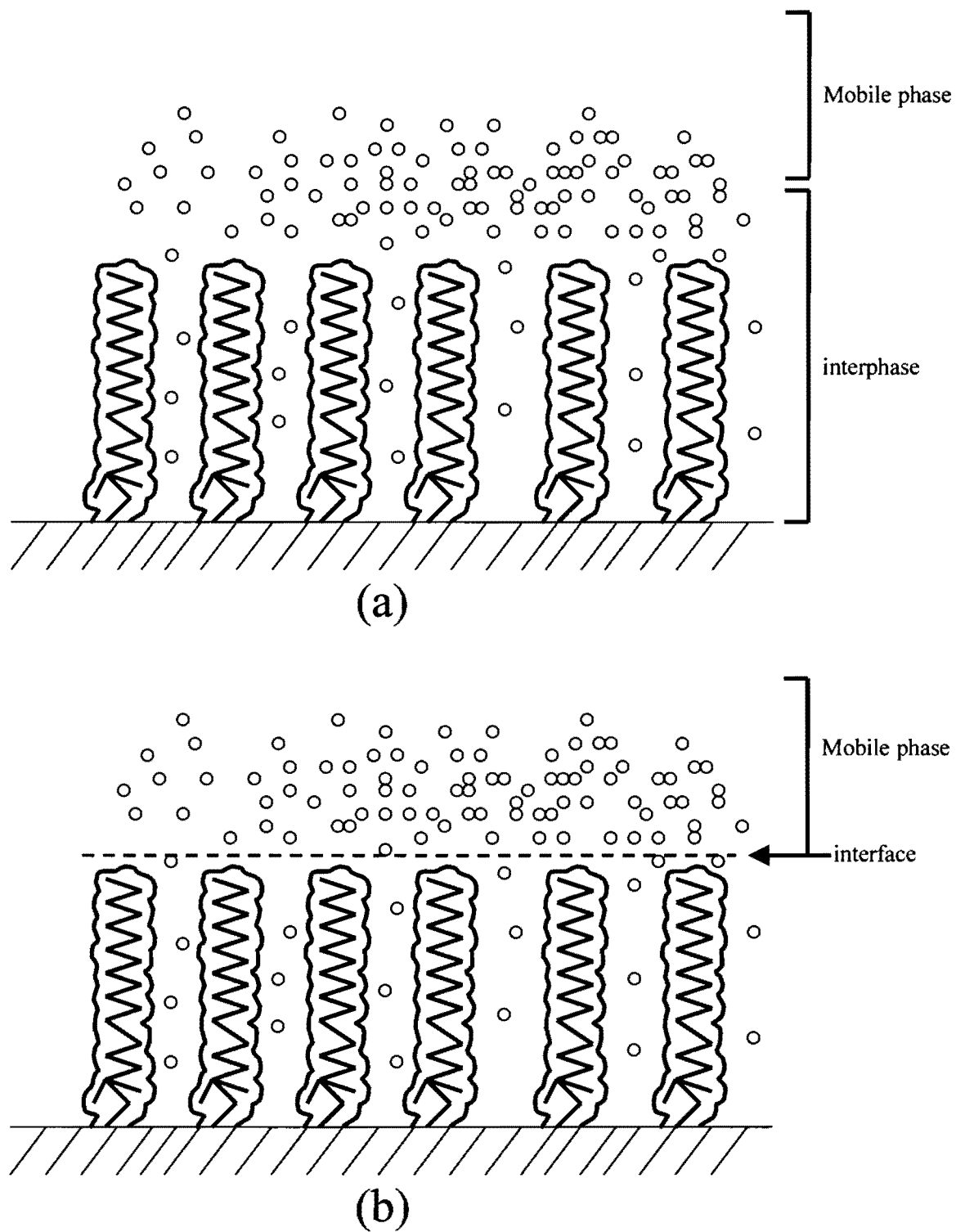


**Figure 1-5:** Schematic drawing illustrating the definitions of (a) interphase and (b) interface as applied to the RPLC bonded phase.



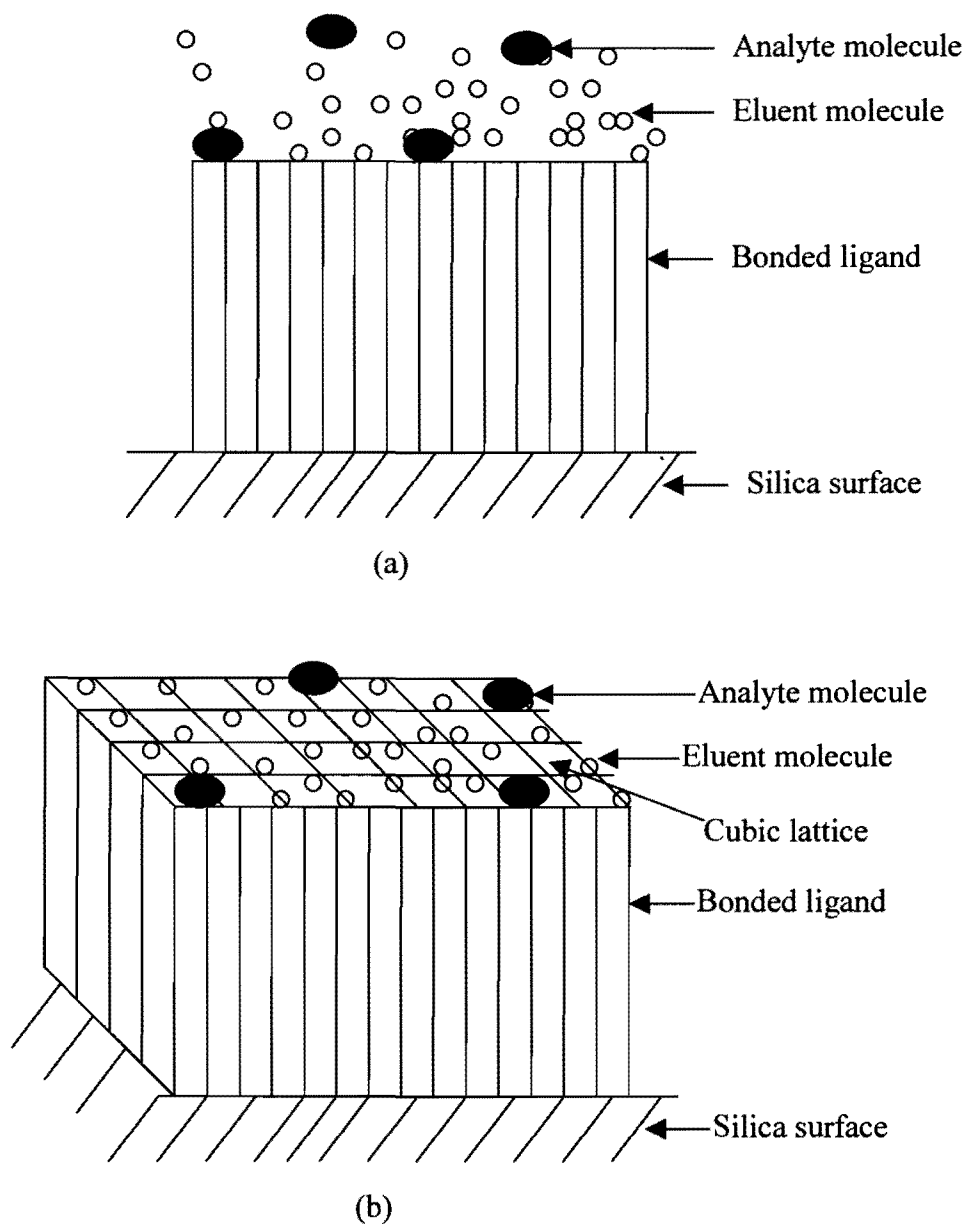


**Figure 1-6:** Schematic illustration (a) and lattice model (b) of the retention in RPLC according to the adsorption mechanism. The tips of the alkyl-bonded silica form a hydrocarbonaceous adsorptive monolayer serving as the chromatographic surface for analyte binding.

chains to interact laterally among themselves and to disallow penetration of analyte molecules into the amorphous-crystalline hydrocarbon layer at the chromatographic surface. In this case, the tips of the alkyl-bonded-silica chains offer a hydrocarbonaceous surface for the adsorption of the sample components.

Lattice monolayer approximation was employed [30] to treat adsorption in RPLC. Assuming a cubic lattice as shown in figure 1-6b, the theory predicts that logarithmic retention factors in RPLC depend linearly on the logarithmic equilibrium coefficients of the appropriate liquid-liquid partition system with a proportionality factor of  $1/6$  ( $1$ =adsorption,  $6$ =partition). Only one cubic face of the analyte surface is supposed to be in contact with the stationary phase in adsorption while all 6 sides of the cube are in contact with the stationary phase in partitioning. On the other hand, the lattice theory based on the amorphous-crystalline hydrocarbon layer model predicts a similar linear dependence but with a proportionality factor of 1. Upon analyzing the experimental RPLC data obtained with hydrocarbonaceous analytes, Dill observed a value of unity for the proportionality factor and concluded that partition is the primary mechanism of retention in RPLC in a wide range of mobile phase conditions [30]. Again, the major weakness of this model is it neglects the adsorption of mobile phase components onto the bonded phase.

#### **Amorphous-Crystalline Hydrocarbon Partition Model or Dill-Dorsey Model**

Dill and Dorsey [31] proposed the so-called “interphase” model for the description of retention behavior in RPLC. They argued that the molecular organization of the bonded phase resembles neither the all-trans crystalline state of n-alkane chains nor the randomly structured liquid state nor even a liquid-crystalline state of intermediate order. Instead, the

chromatographic surface in RPLC may be likened to the interphase between lamellar crystalline and adjoining amorphous regions in a semicrystalline polymer [95]. The “interphase” model is referenced here as the “amorphous-crystalline hydrocarbon layer model”, in order to differentiate it from the liquid-crystalline hydrocarbon layer model proposed by Martire and Boehm.

Based on a mean-field lattice statistical mechanics theory, Dill and Dorsey describe the bonded layer as small, flexible chain molecules organized in different conformations [30, 31]. In contrast to the Martire-Boehm model, Dill and Dorsey predict a “density gradient” and “chain disorder gradient” normal to the grafted surface. The bonded phase density and chain configuration constraints are predicted to decrease with depth from the grafting surface. The concept of a “disorder gradient” is more consistent with spectroscopic observations on chain mobility [96]. Nonetheless, within an individual lattice layer parallel to the grafting surface, the chain density and configuration constraints are homogeneous. The Dill-Dorsey model predicts an increase in bonded chain extension and order upon insertion of a analyte into the partially ordered interphase. In view of the induced ordering, the analyte concentration profile is predicted to be the greatest near the chain terminal and diminishes as the grafting surface is approached. Nonetheless, the density profile and configurations of bonded chains are prefixed in Dill-Dorsey model, and only the distribution profile of analytes in the grafted layer is obtained from statistical thermodynamics. One great weakness of the Dill-Dorsey model is that it neglects the adsorption of mobile phase components onto the bonded phase. This neglect is contradicted by a multitude of chromatographic and spectroscopic studies that indicate extensive solvent adsorption [15, 97-

101]. In the Dill-Dorsey model, the bonded phase is thus chemically much less polar than it actually is, and its volume is virtually constant.

### **Bohmer-Koopal-Tijssen Model**

To allow for a more realistic description of the alkyl bonded phase, Bohmer-Koopal-Tijssen model extended the self-consistent field theory of adsorption (SCFA) to accommodate RPLC conditions [87]. In contrast to the above models, the SCFA theory does not make a priori assumptions about the conformations of the bonded chains, or the distributions of the sorbed solvent and analyte molecules in the bonded phase. Instead, the equilibrium distribution of each participating molecule-chain, solvent and analyte is obtained from the self-consistent minimization of the free energy of the system. The bonded chain configurations, solvent adsorption and analyte distribution can thus be studied in a wide variety of conditions and as functions of solvent quality, surface coverage, bonded chain length, analyte polarity, etc. The thickness of the bonded phase was shown to be functions of solvent quality, surface coverage and the length of the bonded chain. It agrees with the “breathing model” proposed by Martire and Boehm [28].

### **Liquid/Liquid Partitioning vs. RPLC**

A strong correlation between retention in RPLC and liquid/liquid partitioning were predicted using the Martire-Boehm and Dill-Dorsey models [102]. This implies that the main driving force for analyte transfer in RPLC is the relative chemical affinity of analyte molecules for the mobile- and stationary phases. Bohmer et al. [46] concluded that, if the bonded chains are not too short (c.a. octyl chain) and the surface coverage is moderate (c.a.

30% surface coverage), analyte distribution in RPLC resembles liquid/liquid partitioning closer than it does adsorption on a surface. However, this does not mean that the analyte molecules are homogeneously distributed throughout the bonded phase. The Bohmer-Koopal-Tijssen model strongly suggests that analyte molecules, regardless of polarity, accumulate near the boundary between the bonded chains and mobile phase [103]. For amphiphilic analyte molecules, the polar head group generally lies close to the mobile phase than does the nonpolar moiety of the analyte. The specified accumulation profiles of analyte molecules are largely due to the effects of entropic packing, being lowest in the boundary region and increasing as the grafting surface is approached. The simulation results also stress the importance of the boundary region in analyte retention, as has been suggested by previous study [48]. However, this boundary accumulation profile is not consistent with the work of Tchaplal et al. [84] that proposes insertion of linear analyte molecules aligned with the bonded alkyl chains. In Bohmer et al.'s simulation, analytes with chain length equivalent to five methylene units accumulate mostly on the boundary instead of being inserted within the bonded alkyl chains. However, Bohmer et al.'s model is more consistent with the entropic requirement imposed on the chain configuration. The Martire-Boehm, and Dill-Dorsey models also suggest a strong correlation between liquid/liquid partitioning and retention in RPLC, but their description of the boundary region are over simplified. Martire and Boehm totally ignore the boundary region in their model, while Dill and Dorsey treat it as a simple planar interface.

As mentioned earlier, the main driving force for analyte transfer in either RPLC retention or liquid/liquid partitioning, is the analyte's relative chemical affinity for mobile- and stationary phase molecules [31]. However, two types of chain constraints complicate

analyte distribution in a bonded phase: the boundary constraint imposed by the interface, and the packing constraint resulting from the lateral interactions among neighboring chains [31]. Both constraints cause the bonded chains to be more “ordered” than on amorphous bulk alkane liquid, and thus partitioning of analyte into the bonded phase is less favorable than into an amorphous phase. In addition, the interfacial constraints, imposed by the grafting surface and the bonded chains-mobile phase boundary, greatly limit the volume of the interphase. In contrast, the bulk phase in liquid/liquid partitioning is macroscopic in scale and the interfacial region has little influence on the partition coefficient.

The following lines of evidence demonstrate the effects of chain organization on retention. First, isomers with nearly identical hexadecane/water partition coefficients can be well separated in RPLC [52]. This clearly shows that the anisotropy of the bonded chains gives rise to functional group selectivity among the isomers. Second, functional group selectivity of RPLC bonded phase was shown to increase with increasing surface coverage density [59]. Third, the selectivity of a series of polycyclic aromatic hydrocarbons (PAHs) were found to be dependent on the type of the bonded phase, whether monomeric, oligomeric or polymeric [6].

The Martire-Boehm and Bohmer-Koopal-Tijssen models can be extended to analyte molecules of different size, shape and flexibility; thus permitting the study of functional group selectivity. Both models show that rigid-rod analytes are more retained than the flexible-chain analytes and that functional group selectivity increase with surface coverage [31, 80, 87]. The rod-like analyte and alkyl chains of the bonded layer can align, and thus do not have much consequence for the entropy of the analytes. Flexible chains will loose more entropy on alignment and hence lead to weaker retention. The Dill-Dorsey model requires

the analyte and mobile phase components to be monomeric, and thus does not allow the study of functional group selectivity.

The statistical mechanical models presented before have greatly improve the description of bonded phase chains in RPLC, compared to the bristle, blanket, picket fence or liquid-droplet models. The chain configurations were considered, as well as the interactions between bonded chains and solvents. However, all three models consider the mobile phase as a homogeneous medium, neglecting microheterogeneity that has been observed in acetonitrile-water and tetrahydrofuran-water mixtures and preferential adsorption observed in almost all organic-water mixtures [103-106]. In addition, all three models consider that the bonding surfaces as approximately planar and are sufficiently separated that chains emanating from one surface do not interact with those of another. However, in practice, surface curvature can be significant and can limit the coverage of the alkyl bonded phase. Given a fully extended (all trans) octadecyl chains measures about 22Å, the extending bonded chains may easily interact with one another in a 60Å pore. These interacting alkyl chains can affect the mass transfer of mobile phase and analyte molecules. Because silica supports always show significant degrees of polydispersity in pore size distribution, the curvature effects must be considered as being substantial.

### **Chain Flexibility**

Although chain flexibility is seldom mentioned in chromatographic practice, simulation of semiflexible, anchored alkyl chains in lattice models pose a real challenge. In the Martire-Boehm model, a “chain stiffness” parameter was introduced to account for the energy required for a bond to bend in a direction parallel to the grafting surface [107]. The

bonded phase thickness was shown to increase with increasing chain stiffness. However, the Martire-Boehm model does not prevent backtracking of a chain segment on its predecessor and thus, it underestimates the stretching power of the bonded chains into the mobile phase. Dill and Dorsey preclude back folding of chain segment in their model [30, 31]. In Bohmer-Koopal-Tijssen model [88], chain flexibility is moderated such that back folding is forbidden for five subsequent segments and trans bonds are energetically favored over gauche bonds [107, 108]. The trans bonds become increasingly favored over gauche bonds as the surface coverage increases, so as to reduce the packing entropy of bonded chains.

Fadeev and Staroverov [109] showed that the conformation structure of long alkyl bonded chain layers depends on the pore structure support. Reduction in average pore diameter produces a bonded layer of “rigid structure” in contrast to the “flexible structure” found in wide-pore modified silicas. Later, Fadeev et al. [110] studied pyrene lateral diffusion in the bonded layer of n-alkylsilane-modified silicas and emphasis was placed on the effect of the bonded alkyl chain length and average pore diameter. Their results indicated that the bonded alkyl layers have markedly higher viscosity than the corresponding liquid alkanes. This was attributed to the reduction in the degree of freedom after alkyl chain fixation on the silica surface. The viscosity of the bonded hexadecyl layer reduced as the average pore diameter of the silica support decreased. This was explained through the concept of a “rigid structure” of the bonded layer [109]. In summary, they found that the smaller the average support pore diameter, the greater the rigid structure.



## **Silica surface**

In actual chromatographic practice, the residual silanol groups on the silica supports are found to affect the solvent adsorption process (discussed later), and exhibit specific affinities for basic compounds. The active role of the silica support is neglected in Martire and Boehm's model [91]. In Dill's model, the silanol effects were indirectly addressed by assigning a different interaction parameter to analyte molecules adjacent to the underlying surface [30, 31]. Bohmer et al. addressed the issues in detail. Properties of the underlying surface can be varied by adjusting its relative compatibility with other molecules, i.e. the bonded chains, the mobile phase components and analyte molecules, in the system [87]. When the underlying surface is simulated as silica, i.e. having great affinity towards polar components (e.g. water), Bohmer et al. [46] showed that a layer of water molecules was formed on the underlying surface. Their simulation results are consistent with some experimental reports that suggest physisorb of water molecules on the silica surface [111-112]. Thus, Bohmer et al.'s model is considered quite successful in predicting the active roles of the silica-bonding surface in interacting with the polar components of the mobile phase.

Although participation of silanols and metal impurities on the silica support generate problems in RPLC, details of these topics will not be discussed here. Review articles on the topics have been presented elsewhere [113-115].

## **Evidence Supporting Solvent Adsorption on the Bonded Phases in RPLC**

This section only focuses on the evidence supporting the solvent adsorption on the bonded phase. The thermal/chromatographic and spectroscopic evidence of solvent

adsorption are presented. The next section will focus on the effects of solvent adsorption on the structure of the bonded alkyl chains.

### **Thermal/Chromatographic Evidence of Solvent Adsorption**

Significant amounts of mobile phase components – the organic modifier and water – are adsorbed on the bonded phase [14, 102-106]. The organic modifier is preferentially adsorbed compared to water [103-105, 116], i.e., the composition of the adsorbed layer is always richer in organic content than the bulk mobile phase. In reversed phase conditions, the adsorbed organic solvent has found to be monomolecular [14]. Scott and Kucera [14] assumed that upon retention, analyte molecules with  $k'$  values less than 10 will not be able to displace the adsorbed solvent. Preferential adsorption of mobile phase constituents will affect the functional group selectivity of the analyte. The more favorable solvent environment that the organic modifier represents to the analyte compared to that of the binary hydro-organic mobile phase, the analyte will spend more or less time in the organic rich adsorbed layer compare to the mobile phase depending on the nature of the organic modifier. The difference in polarity between the hydro-organic mobile phase and the solvent modified stationary phase ligands is also less than that between the bulk mobile-phase and alkyl ligands alone, and this should allow for a lower energy of analyte transfer under these conditions. Thus, analyte molecules are thought to interact more with this adsorbed organic layer and less with the alkyl chains (refer to Figure 1-7).

The formation of the adsorbed layer is a dynamic process controlled by the mobile phase composition, the length of the bonded alkyl chains, the bonding density and the residual silanol activity [15, 102-105, 117]. Adsorption of organic modifier on the bonded

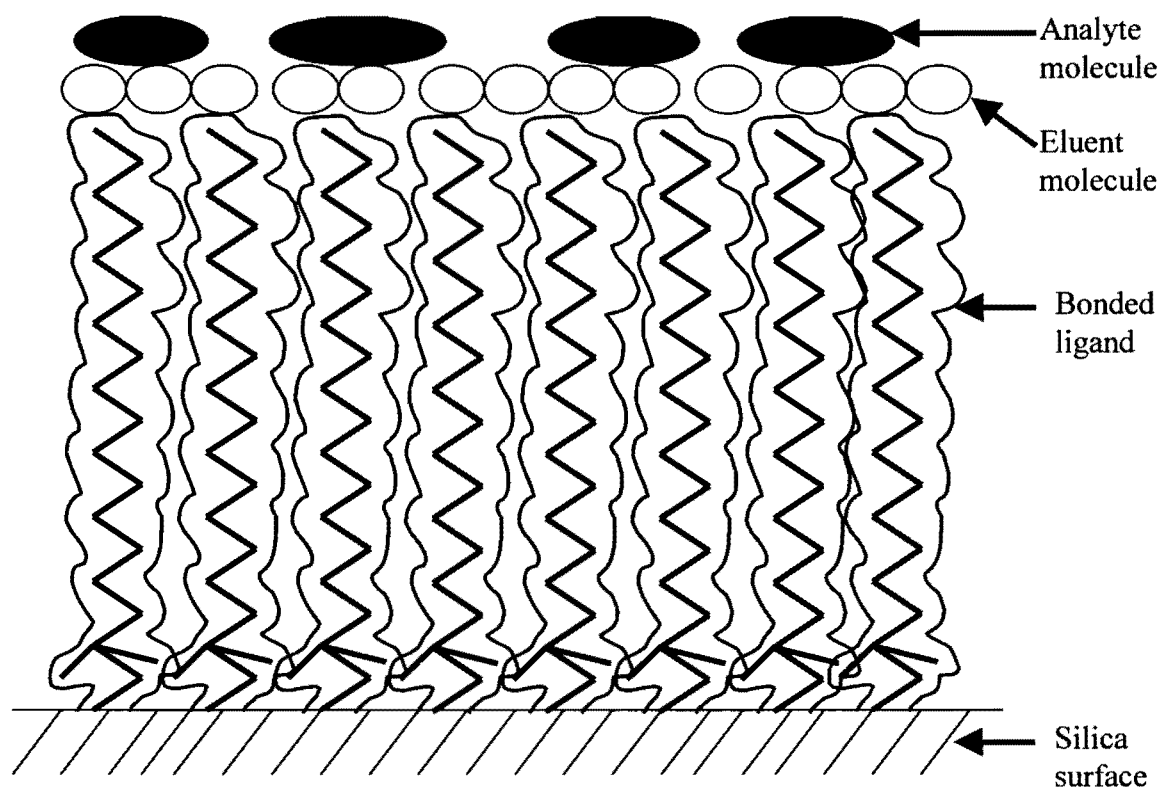


**Figure 1-7:** Schematic drawing illustrating a monomolecular layer thick of solvent layer adsorbed on the bonded alkyl chains and analyte molecules interact with the adsorbed layer instead of with the bonded chains.

phase is governed primarily by dispersive interactions between the organic solvent and the bonded chains. Thus, the amount of organic modifier adsorbed increases in the order of RPLC solvent strength as follows: tetrahydrofuran > 2-propanol > acetonitrile > methanol [15, 102, 104, 105]. The enrichment of water molecules in the stationary phase is controlled by hydrogen bonding of water with the adsorbed organic modifier molecules and residual silanol groups [106, 118]. Thus, the amount of adsorbed water depends on the relative hydrogen bonding strength of the organic modifier, and has been shown to vary in the following order: tetrahydrofuran >> 2-propanol > methanol > acetonitrile [104, 105]. The adsorption of organic solvent and water on the surface of the bonded phase varies significantly with the organic content of the mobile phase. The incorporation of organic modifier increases nonlinearly with the organic concentration of the mobile phase [15, 103, 105]. The trend of water adsorption is more complicated [104, 105].

### **Spectroscopic Evidence of Solvent Adsorption**

Spectroscopic techniques provide a more direct means of obtaining bonded phase structural information, compared to the thermal approach which infers the information from chromatographic results. In addition, information deduced from spectroscopic techniques is independent of and complimentary to chromatographic studies. Electronic spectroscopy is a powerful tool for assessing the nature of the local environment of the bonded phase. This is because the changes in the characteristic electronic state of an indicator dye result from changes in its cybotactic region. A great body of experimental evidence from fluorescence and UV-visible absorption spectroscopies shows that typical C<sub>18</sub> reversed phases in contact with mobile phases are significantly more “polar” than either a dry C<sub>18</sub> phase or the analogous bulk alkane [119-124]. The results are consistent with chromatographic isotherm

studies [15, 102, 104, 105] that show the adsorption of significant amount of organic solvents on the bonded phase. The “polarity” of a C<sub>18</sub> surface in contact with water has been reported to be similar to bulk octanol [120]. “Polarity” here refers to the overall measure of a solvent’s ability to interact with an analyte, comprised of dispersion, induction, orientation, and hydrogen bonding interaction [125].

Fluorescence studies show that the “polarity” of the bonded phase greatly depends on the type and concentration of organic modifier in contact with the bonded phase [119]. This is consistent with thermal studies that show variation of adsorption properties with the nature of the mobile phase. However, the trend of dependence is complicated. Carr and Harris found that the effective polarity of a C<sub>18</sub> phase decreased with increasing organic concentration in the mobile phase over the range of 0-50% methanol, but then increased with the organic concentration over the range of 50-80% methanol [121-122]. On the other hand, the bonded phase polarity increased non-linearity with organic concentration for 20-70% acetonitrile and 25-45% tetrahydrofuran. These complex adsorption trends suggest that the measured polarity depends not only on the type and amount of organic modifier adsorbed, but the amount of water adsorbed, which in turn is controlled by the residual silanol groups [104, 105].

Spectroscopic studies also suggest that the alkyl-bonded phase is in fact an anisotropic medium. <sup>13</sup>C NMR chemical shift studies suggest that the surface coverage of bonded alkyl chains is heterogeneous, even at high coverage density [125]. The heterogeneity in bonded chain distribution was largely due to the complex chemical and structural properties of the base silica [127] and the variability in silanol activity [128]. Gangoda et al. showed that bonded alkyl chains exhibit a mobility gradient along the axis

normal to the silica surface [101, 129]. The bonded chains exhibit lowest mobility at the methylene group next to the silica supports and highest mobility at the terminal group. The observation is in accord with Dill's lattice model that suggests a chain-ordering gradient along the chain backbone [30, 31, 130]. Gilpin and Gangoda [131] observed that the terminal end rotation of a bonded chain is significantly reduced once a particular bonded density was attained. At lower surface coverage than the critical bonded density, the mobility of bonded chains is relatively constant. The results suggest that chain ordering is influenced by the alkyl chain surface coverage. Thus, the overall structure of the RPLC adsorbed layer is a function of the bonded alkyl chain, the degree of alkyl derivatization of the silica surface, the system temperature and pressure, the number and types of residual silanols remaining on the silica surface following derivatization.

NMR studies have also shown that the addition of neat organic solvents to a dry bonded phase drastically increases the mobility of the chain segments. However, as water concentration is increased in the organic-aqueous mobile phase, random motion in bonded alkyl chains decreases [132-135]. In predominantly aqueous mobile phase, the hydrophobic alkyl chains are thought to assume a highly collapsed or folded configuration in order to minimize their surface contact with the polar mobile phase [91, 136, 137]. This "hydrophobic clustering" phenomenon is thought to cause entrapment of mobile phase components within the collapsed stationary phase structure, especially within narrow-necked silica pores [136]. The bonded phase was also reported to lose its liquid like nature as the water content in the mobile phase increases [138].

### **The Effect of Mobile Phase Composition, Bonded Alkyl Chain Length and Solvent Adsorption on the Structure of Bonded Alkyl Phase under RPLC Conditions.**

The detailed models of chemical interactions on the adsorbed layer on octadecylsilane bonded silica which have been developed are an attempt to represent the average interactions which are available [4]. These refinements of the RPLC stationary phase model provide a more detailed and accurate description of the intermolecular interactions responsible for retention and selectivity than was previously available. However, it must be remembered that, when a highly porous silica surface is chemically modified with an alkyl silane, a surface which is heterogeneous in both physical structure and chemical activity is obtained, so that any average picture of the system is not complete in itself. Further considerations such as the nature of the original surface, the intermolecular interactions of the solvent components of the contacting mobile phase and the chemical nature of the bonded species must be taken into account in order to understand the behavior of widely varying systems. The major focus of this section is to describe the effects of bonded alkyl chain length, mobile phase composition and solvent adsorption on the bonded phase structure.

Adsorption of the mobile phase components has an immense impact on the physical/chemical properties of the bonded phase and the structural organization of the bonded alkyl chains. The current understanding of the composition of RPLC stationary phase and its interactions with analyte species are based upon three important parameters [128]. The adsorption of solvent components on the bonded alkyl chains plus the bonded alkyl chains together represents a dynamic layer on the silica whose structure is determined by (i) the length and type of the bonded hydrocarbon alkyl chains, (ii) the surface density of the bonded alkyl chains, and (iii) the type of intermolecular interactions provided by the solvent component(s) adsorbed on the stationary phase. All three of these parameters have an impact

on the structure of bonded alkyl chains under RPLC conditions. Only the effect of linear hydrocarbon chains bonded to the surface will be considered in the current discussions.

The alkyl chain length and the surface density primarily determine the volume of the stationary phases in a column. Here, we will discuss the definition of phase ratio. In classical terms, the phase ratio is defined as the volume of the stationary phase divided by the volume of the mobile phase. The main problem with this definition is that it is too general. It is now known that the components of the mobile phase are adsorbed on the stationary phase and the degree of adsorption depends on alkyl chain length, surface density and silanols present on the silica surface. So, what is the volume of the stationary phase? Is it just the bonded alkyl chain layer volume or does it also include with it the adsorbed solvent molecules? Determining the volume of the stationary phase is a practical problem. It is for this reason, in the literature, researchers have avoided defining what actually is the phase ratio, in particular, the volume of the stationary phase.

In classical terms, once the phase ratio is defined, the simple understanding of the retention process (the partitioning of analytes between the mobile phase and the bonded ligand chains containing organic solvents extracted from the mobile phase) can explain the effects of mobile phase composition and stationary phase structure. The theory developed by Jaroniec [4] represents the currently most comprehensive explanation. According to the model, one should distinguish between two stages of the process of RPLC: (i) the formation of a combined solvent-surface stationary phase and (ii) the partitioning of the analyte between the mobile phase and this stationary phase. According to this model, the stationary phase is made up of bonded ligand chains and adsorbed solvent molecules. This model is very similar to the classical partitioning, except the stationary phase contains the adsorbed



solvent molecules. The analyte distribution, thus the retention, occurs via a partition mechanism only, according to the model. The model, however, does not take adsorption into account. As indicated earlier, a pure partitioning mechanism cannot explain the retention in RPLC. In summary, this model takes solvent adsorption into effect, but fails to explain the retention in RPLC, since the prediction of the model is that only process via the retention occurs is partitioning.

RPLC retention cannot be described as a purely adsorptive process either because the surface-bonded groups do not represent a classical surface [139]. Neither do these groups comprise a liquid phase because of their surface anchoring and sparse population relative to a pure liquid hydrocarbon [31]. It has been shown that solute molecules intercalate themselves between the hydrocarbon chains and that once the entire molecule further increase in bonded chain length has a diminished effect on retention [84]. A plateau in length, as well as a dependence of the critical chain length on the size of the solute molecule has also been observed [57].

Surface coverage of the bonded hydrocarbon moieties has a two-fold effect. As the number of hydrocarbon groups on the surface is increased, the retentive capacity of the material through non-polar interactions increases. However, past a certain point determined by the packing density of the bonded chains, the solute distribution coefficient decreases as a result of restricted access between the bonded hydrocarbon chains [31, 140]. A complementary consideration is that, as an increasing number of hydrocarbon groups are bonded to the silica surface through siloxane bonds, the amount of polar silica sites is decreased in both concentration [141] and accessibility [31, 142]. The effect of these sites is primarily seen on sparsely derivatized silica in the asymmetric elution band shape of polar

solute species. The interactions at these polar sites are usually attributed to silanol groups [24] and accompanying adsorbed water [97, 143, 144].

The chemical and structural heterogeneity of the base silica [128] can also affect the bonding density and distribution of alkyl moieties. Surface chemical heterogeneity can produce non-uniformity in the distribution of alkyl moieties during bonded phase synthesis based on the variability in silanol reactivity. The highly complex porous structure of the silica can produce bonding heterogeneity based on both size exclusion of bonding reagent, as well as cooperativity of densely packed alkyl moieties. The resultant heterogeneity in bonded moiety distribution can effect solute and solvent interactions with the stationary phase particularly for polar species, which participate in hydrogen-bonding interactions.

Retention of non-polar solute species is accompanied by intercalation of the solute molecule into the solvated stationary phase [30-31, 59, 140]. A statistical mechanical lattice model developed by Martire and Boehm [28] described chain organization in the stationary phase as similar to a liquid crystalline material. Dorsey and Dill [30, 31] presented refinements to the lattice-interphase model in terms of the surface-anchored chains and their configuration entropy. The bonding density studies of Sentell and Dorsey [59] experimentally supported the model presented by Dorsey and Dill. Evidence that molecular shape selectivity is related to hydrocarbon bonding density, especially on polymeric bonded phases, has been presented by Sander and Wise [145, 146] and Sentell and Henderson [147].

The third factor controlling the behavior of the stationary phase is the type of organic solvent(s) used as the mobile phase modifier(s). The saturated hydrocarbon moieties participate in interactions based upon the relatively weak Van der Waals and dipole-induced dipole forces. However, additional forces (dipole-dipole, hydrogen bonding) may play a role

in the solvent-solvent, solvent-solute [148], and solvent-silica surface interactions. Because of the strength of the specific hydrogen-bonding interactions between the silica surface and water, as evidenced by the difficulty in drying the silica by thermal means [128], it is expected that accessible silica surface is covered by at least one monolayer of adsorbed water [97, 143]. The organic-water solutions have been found to possess a positive surface excess of organic solvent component of the mobile phase and this enrichment increases as the chromatographic strength of the solvent increases [Methanol<Acetonitrile<Ethanol<THF]. In addition, the incorporation of water into the adsorbed layer has been shown to vary significantly with organic solvent component in the order Acetonitrile<Methanol<Ethanol<<THF [102, 149].

At this point, it is necessary to add a forth consideration to the structure and interactions of the stationary phase, namely, the conformational shape and mobility of the bonded hydrocarbon chains. Karch et al. [150] suggested that the bonded hydrocarbon chains be described as bristles sticking out from the silica surface like a brush. Further research added refinements to this model and Riedo et al. [93] showed a phase transition in hydrocarbon bonded to acid-etched silica as detected by a sharp change in wetting angle as a function of temperature and chain length. In comparing liquid-liquid extraction data with RPLC bonded phase selectivity, Lochmuller and Wilder [20] proposed that the hydrocarbon moieties preferentially associate with one another to form pseudo-liquid droplets on the surface. Gilpin and coworkers [24, 151] further showed that for intermediate length ( $C_8$ - $C_{10}$ ) bonded hydrocarbon materials with pure water mobile phases, an irreversible transition involving the release of surface organic solvent could be effected as a function of temperature. This transition was shown to be a function of the bonded-alkyl chain length and

the type of organic conditioning solvent, but not the type of bonding chemistry [152]. Based upon these data, they proposed that hydrocarbon chains held trapped organic solvent until sufficient thermal energy was supplied to extend the chains in pure water and release the trapped solvent. Complementary observations on the kinetics of exchange of stationary phase-entrapped solvent have been presented for gradient elution equilibria [153]. Another type of surface transition was observed by Morel et al. [139, 154] using both GC and LC retention data in which they found a non-linear change in retention as a function of temperature. Similar conformational transitions of octadecyl-bonded phases were observed with RPLC on densely bonded materials with non-polar solutes [147, 155]. Morel et al. [154] suggested that it is unfortunate that RPLC phases were not historically developed using C<sub>16</sub> or shorter bonded hydrocarbons because octadecyl chains form a thermodynamically unstable system over the usual operating temperature range.

The molecular mobility of bonded hydrocarbon chains has also been investigated spectroscopically. Using <sup>13</sup>C NMR, Zwier [156] showed that the liquid-like mobility of the chains increased as a function of chain length and solvation, but only minor changes occurred as a function of temperature over the range studied. By selective positional <sup>13</sup>C enrichment of hydrocarbon bonding reagents, Gilpin and Gangoda [129] showed with NMR that mobility increases rapidly with distance from the anchoring surface bond along the carbon chain. This is also consistent with the lattice model predictions of Dorsey and Dill [30, 31]. FTIR spectrometry was employed by Sander et al. [92] to show that for dry bonded-phase silica, a phase transition similar to that of a pure liquid hydrocarbon can be thermally induced on long-chain bonded-phases (C<sub>18</sub>-C<sub>22</sub>). For well-solvated materials FTIR measurements

indicated a decrease in the number of gauche C-C bonds of the hydrocarbon moieties relative to unsolvated conditions.

Adsorption of mobile phase components on the bonded phase can greatly alter the chemical properties of the bonded phase, and thus affect the interactions with solute molecules. A growing body of spectroscopic and thermodynamic evidence suggests that bonded phase with the adsorbed layer have higher polarity and hydrogen bonding ability than bulk alkanes [48, 119-123, 157-159]. The proposed polarity profile of the bonded phase with adsorbed layer is shown schematically in Figure 1-8 as a function of distance from the silica surface and interchain distance. It is seen from the schematic drawing that the polarity of shorter alkyl chains, when adsorbed by the organic modifier, are more polar than longer alkyl chains when they are adsorbed by the organic modifier.

Direct experiments with pyrene as a fluorescent probe demonstrated that the diffusion of solute molecules within the bonded layer is markedly increased in the presence of solvent [58]. It was shown that the environment of pyrene adsorbed on an ODS (Octadecylsilane) support in the absence of a solvent is very non-polar and it corresponds to that in liquid hydrocarbons. In the presence of solvent the environment of pyrene depends both on the eluent composition and on the properties of the ODS support.

Upon application of binary mixtures, e.g., alcohol-water, acetonitrile-water, THF-water, the organic molecules having a high affinity to get adsorbed on the bonded hydrocarbon chains. However, in relation to the structure of the bonded layer (rigid, flexible), the nature of the modifier and the method of modification, the resulting effect of the solvent on the bonded layer can be different. Two papers [120, 121] dealing with the effect of the eluent composition on the polarity of the bonded layer as studied by analysis of

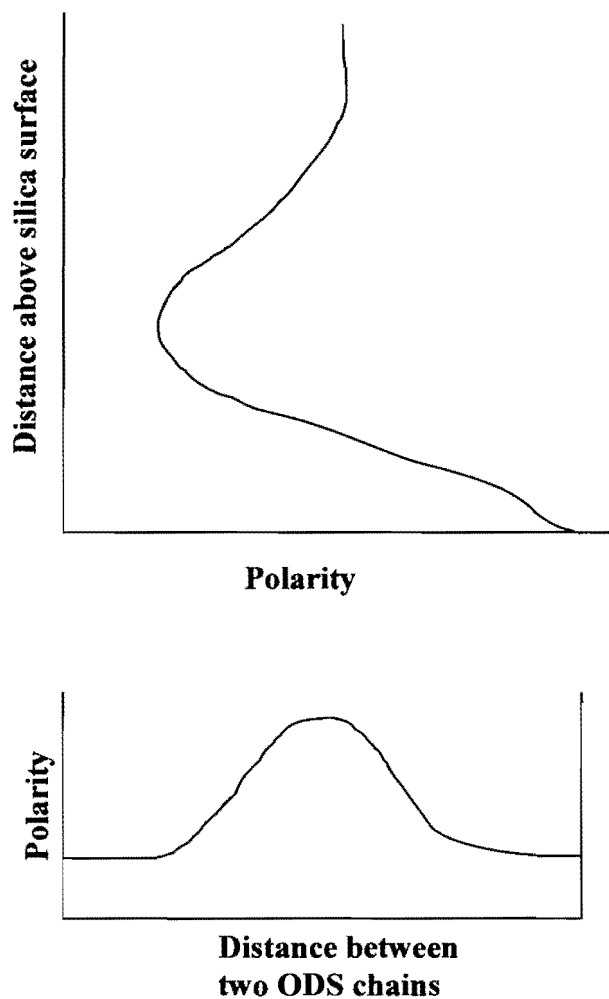


**Figure 1-8:** Schematic representation of the postulated adsorbed-layer polarity gradient in the ODS-bonded silica stationary phase.  
Figure taken from Reference 159.

the fine structure of the fluorescence spectra of pyrene sorbed on reversed stationary phases are considered as an example. In these papers, LiChrosorb C<sub>18</sub> based on silica with a pore diameter of 10nm modified by octadecylmethyldichlorosilane [120] and Partisil C<sub>18</sub> [121] based on silica with a pore diameter of 5nm modified by octadecyltrichlorosilane and end-capped with were studied.

It was demonstrated [120] that when the content of organic modifier in the mobile phase is increased (up to 30% with methanol and up to 14% with acetonitrile), the polarity of the environment of sorbed pyrene is decreased in comparison with an aqueous eluent. Penetration of organic components of the eluent into the bonded layer and blocking of accessible silanol groups may cause this. A further increase of the content of, e.g., acetonitrile (from 14 to 28%) leads to an increase in the polarity of the pyrene environment owing to saturation of the bonded layer by the molecules of the organic component.

In contrast, an increase in the polarity of the environment was observed [60] at a low content of organic component in the eluent in comparison with an eluent containing a high concentration of organic component (methanol). This effect was explained by “displacement” of pyrene from the bonded layer at low contents of methanol in the eluent.

These apparently contradictory results [60, 120, 121] may be explained by the effect of the pore structure on the state of the bonded layer. Thus, the stationary phase [121] consists in a 100% rigid structure and the penetration of pyrene into the bonded layer is hampered. This is related first to eluent containing a small amount of organic component, which hardly wet the bonded phase. An increase in the organic component content favors wetting of the bonded layer and the partial penetration of pyrene into the layer of attached hydrocarbons. Thus the polarity of the pyrene environment is decreased. The rigid bonded

layer causes a low accessibility of silanol groups for both pyrene and methanol. The difficulties in penetration of methanol into the rigid bonded layer were confirmed [160].

According to the models considered above, part of the bonded layer in case of a support based on LiChrosorb 100Å-silica [120] has a flexible structure. It is difficult to estimate the proportion of flexible structure as some batches of LiChrosorb 100Å-silica may have an average pore diameter of even 16-17 nm, i.e., may contain about 100% flexible structure in bonded layer.

Hence, the variations in the structure of the bonded layer of ODS stationary phases may lead to basically different mechanisms of interaction between the support and a solute and the support and a mobile phase.

Recently, Dorsey et al. [161] employed a direct, noninvasive, on-column approach to examine the solvent-dependent conformational behavior of bonded C<sub>18</sub> ligands under flowing conditions by Raman spectroscopy. In addition, the bonded chain rigidity was also investigated by examining two stationary phases differing only in ligand density: a 2.34 and a 3.52 μmol/m<sup>2</sup> Microporasil C<sub>18</sub> stationary phase. Their results indicated that the drastic solvent-induced conformational changes of the bonded C<sub>18</sub> ligands, from a collapsed state in the presence of the polar aqueous mobile phase to an extended “brushlike” state in less polar organic mobile phases, was not observed by Raman spectroscopy. Such conformational changes would have been indicated by significant spectral changes in the carbon-carbon-stretching region for the bonded phase ligands. No dramatic changes in the carbon-carbon stretching region were observed with mobile phase changes, although, as was shown in their other paper [162], the temperature effects on the C<sub>18</sub> bonded ligand spectral features in this region are significant. Nonetheless, more subtle solvent-induced conformational changes



were observed, as evidenced by the difference in methylene stretching of the bonded C<sub>18</sub> ligands in aqueous and chloroform mobile phase environments. Bonded ligand methylene stretching was observed to be more prominent in chloroform than in water, and was observed to be more prominent for the lower bonding density stationary phase upon exposure to chloroform.

Their interpretation of the effects of acetonitrile and methanol on the conformational behavior of the bonded C<sub>18</sub> ligands was complicated by the incomplete subtraction of the solvent features [161]. The C<sub>18</sub> ligand spectral features obtained from acetonitrile and methanol, as with those obtained from water and chloroform, do not support the hypothesis that the stationary phase ligands collapse and elongate with changes in mobile phase composition. However, more subtle solvent-induced changes were not readily discernable in acetonitrile and methanol, due to the overlapping of bonded ligand and solvent spectral features. They indicated that the use of deuterated acetonitrile and methanol solvents would provide more information about the effects of these solvents on the orientation of the C<sub>18</sub> ligands.

A more direct approach was taken in our laboratory to see the effect of bonded alkyl chain length on the bonded phase structure under RPLC conditions [163-164]. First, the molecular volumes of bonded ligands was calculated experimentally (refer to Figure 1-9) under LTNA (Low Temperature Nitrogen Adsorption) conditions (77°K under vacuum). When compared to the liquid n-alkanes (most dense conformation of the chains), the values found for each bonded ligand is approximately the same between the two (refer to Figure 1-9). Silica modified with trimethylchlorosilane (C<sub>1</sub>) has bonding density of 3.12 μmol/m<sup>2</sup>, C<sub>18</sub> bonded phase had bonding density of 2.12 μmol/m<sup>2</sup>. These values are translated to the

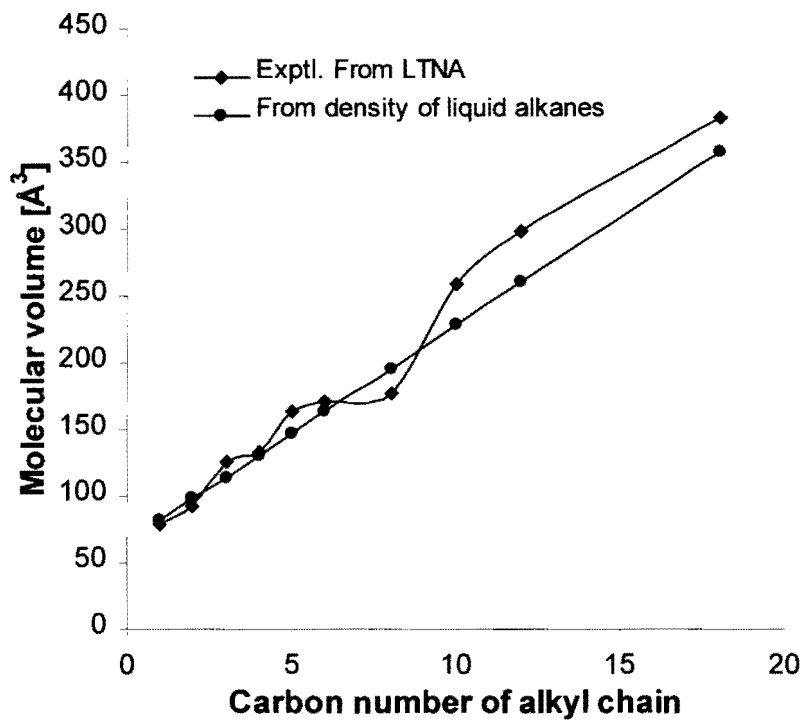


**Figure 1-9:** Comparison of the molecular volumes of bonded ligands with that calculated from the density of corresponding liquid.

approximate linear distance between anchoring points of 4.3Å for C<sub>1</sub> and 7Å for C<sub>18</sub> on the surface. Figure 1.10 shows molecular model of silica surface (assuming cylindrical pore model) with C<sub>1</sub> (A) and C<sub>18</sub> (B) chains attached on the surface with mentioned average distance. The C<sub>1</sub> layer is dense and does not have any “gaps” between bonded chains. The C<sub>18</sub> bonded layer, on the other hand, has significant space between bonded chains shown in all-trans conformation, which in further discussion is denoted as “free” volume. Model C in Figure 1-10 represents the same C<sub>18</sub> bonded phase in a “collapsed” state. The energy of these chains has been minimized using MM2 minimization with HyperChem software. The density of this phase with minimized energy is the same as the density of the corresponding liquid n-alkanes. .

The shortest ligand (C<sub>1</sub>) has a very high bonding density. Its effective volume is mainly determined by bonding density and not by its conformational freedom, which is minimal. However, longer ligands (C<sub>8</sub> - C<sub>18</sub>) have lower bonding density values (Table 1-II, column 6) and greater conformational freedom (Figure 1-6, B and C). Thus, not only their bonding density determines their effective volumes but also by their conformation. The correspondence of the effective molecular volume assessed from LTNA data with that volume of liquid n-alkanes (Figure 1-9) indicates that this flexible chains most probably in the most dense conformation (Figure 1-10, C) and may fill “gaps” in the surface. Since adsorbent samples were vacuumed first at elevated temperature and then submerged to liquid nitrogen temperature (77°K), that restricts the chain mobility, the experimental dependencies represent the molecular arrangement of alkyl chains in vacuum. However, the calculation has been made solely by using the surface area of bare silica and the total pore volume of modified adsorbents, without any assumptions in reference to the pore shape,

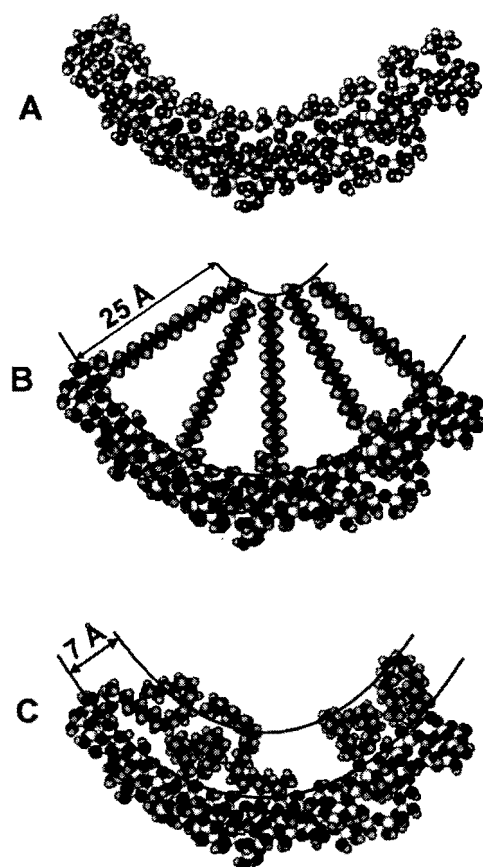


**Figure 1-10:** Molecular model showing the silica surface modified with  
(A) Trichlorosilane -  $C_1$ ,  
(B) octadecylsilane in all trans conformation -  $C_{18}$ , and  
(C) same as B except with minimized energy.  
Figure taken from reference 164, figure 6.

**Table 1-II.** Geometric parameters of bare porous silica and alkylsililated gels measured by LTNA.

1	2	3	4	5	6
Adsorbent	BET surface area [m <sup>2</sup> /g]	Total pore volume [mL/g]	Mean pore diameter [Å]	“Carbon” Load [C% w/w]	Bonding density [μmole/m <sup>2</sup> ]
Silica	374	0.965	97	0	0
C <sub>1</sub>	292	0.804	88.6	4.840	3.121
C <sub>2</sub>	301	0.804	88.2	5.383	2.650
C <sub>3</sub>	295	0.781	87.1	6.010	2.401
C <sub>4</sub>	299	0.778	86.4	6.735	2.272
C <sub>5</sub>	288	0.746	84.8	7.677	2.253
C <sub>6</sub>	288	0.736	83	8.502	2.210
C <sub>8</sub>	287	0.726	81	9.996	2.123
C <sub>10</sub>	264	0.687	80	10.92	2.123
C <sub>12</sub>	236	0.623	78	13.17	2.082
C <sub>18</sub>	182	0.531	79	17.98	2.117

structure and the pore size distribution. This treatment leads to the conclusion that alkyl chains under vacuum are “collapsed” on the surface, so that they occupy minimum possible volume, and surface energy is minimized.

However, after being exposed to mobile phase under HPLC conditions, the conformation (or bulk molecular arrangement) that these ligands are in is another question and this was also addressed as following. If the conformation of the bonded alkyl chains under HPLC condition is same as it is under LTNA condition, then the pore volume from LTNA in reference to silica should be proportional to the total pore volume from HPLC, and the proportionality coefficient should be the same for all adsorbents. Indeed, for  $C_1$  the pore volume should be the same for HPLC and LTNA, due to the lack of conformational freedom of the alkyl group. However, for a  $C_{18}$  modified adsorbent, the situation may be different, since long alkyl chains may have different conformations under LTNA and HPLC conditions, and organic eluents may show preferential solvation of the bonded layer. The ratio of HPLC to LTNA pore volume is very consistent for all columns ( $C_1$  to  $C_{18}$ ), with a 2.5 % RSD. This clearly indicates that prevalent alkyl chain conformation of the bonded phase exposed to HPLC eluent is practically the same (in terms of occupied volume) as it is under LTNA conditions. Therefore, alkyl chains tend to occupy lowest possible volume (“collapsed”; refer to figure 1-10 (C)) since the intermolecular interactions are dominant compared to eluent-alkyl chain interactions.

The conclusion is also supported by the comparison of the void volume ( $V_o$ ) values obtained for three different eluent systems [163, 164]. If there is preferential solvation of the bonded phase the pore volume decreases and hence yield lower pore volume values.  $V_o$

values measured with methanol, acetonitrile, and tetrahydrofuran match for each column and are independent of the eluent used.

## **Conclusions**

The stationary phase in RPLC is definitely not a passive receptor in the retention process. Advanced statistical mechanical models for RPLC bonded chain have shown that analyte distributions and solvent adsorption are greatly influenced by the nature of the bonded phase, such as the length of the bonded chain, surface density and chain flexibility. In addition, adsorption of mobile phase components on the bonded phase was shown to have great effects on the chemical and structural nature of the stationary phase, which in turn affects the retention. The conclusions given by the chromatographic and spectroscopic studies, although varied in small details, all suggest that the RPLC stationary phase is highly heterogeneous, in terms of physical/ chemical properties and structural conformations. The bonded phase is by no means similar to an analogous liquid alkane. Its chemical properties are largely modified by the adsorbed mobile phase components, while its structural conformations are altered by the boundary and packing constraints.

Although many mechanisms have been proposed to account for retention process in RPLC, most of them are based on or can be applied to the retention behavior of a limited range of analyte under limited LC conditions (e.g., mobile phase composition, type of bonded phase, temperature). It is desirable to have a unified understanding of the retention behavior including that provided by the stationary phase effects. In fact, important information can be gained from the stationary phase effects in terms of the retention mechanism, which indicates an active role for the stationary phase.

## **Chapter II: Introduction of the Partition/ Adsorption Model**

### **Summary**

Excess adsorption isotherms can be measured in order to study the adsorbed layer that is residing near a surface, in terms of composition, thickness and volume. First, the concept of excess adsorption is explained. The correlation is made between the excess adsorption and RPLC retention, and then, the partitioning/ adsorption model is introduced. The proposed model describes the RPLC retention as a sum of two processes: analyte partitioning between the mobile phase and the organic rich adsorbed layer followed by its adsorption on the hydrophobic surface. A mathematical equation is derived from the model that can predict analyte retention when certain conditions are given (mobile phase composition, column etc.).

### **Background**

To shed light on the retention mechanism of RPLC, a theory that describes both the mobile- and the stationary phases, and that pays due attention to conformational aspects of retention in a grafted layer is needed. Further, this theory should provide insight into aspects such as the dependence of chain length and mobile phase composition on retention. In order to obtain an accurate description of the retention mechanism in RPLC, the boundary region (preferential adsorption of organic solvent modifier) between bonded chains and the mobile phase cannot be ignored. Experimental evidence presented in Chapter I suggests that a better understanding of the physical location of the solute molecules could certainly improve the development of molecular retention models.



To provide a better model that can describe RPLC retention, it was made clear in Chapter I that stationary phase plays a big role in retention and it is not a passive receptor. So, a discussion of the structure of the bonded phase was made and it was concluded that the bonded alkyl chains are in their least energy state or “collapsed” phase. In addition, it was shown that there is preferential adsorption of the organic solvent molecules on the surface and due to this adsorption, the chemical environment near the surface is changed. In other words, the adsorbed layer is somewhat different in composition than the mobile phase. To learn more about retention theory, the surface must be considered first, in this case, with the adsorbed layer.

The connection of RPLC retention with adsorption phenomena is one of the keys for the interpretation of the retention mechanism. It was shown in Chapter I that in RPLC, when using a binary solvent system (e.g., acetonitrile/water), the organic solvent molecules (e.g., acetonitrile) are preferentially accumulated on the surface. The first question that can be raised is whether this is a monomolecular or a multilayer adsorption? The next question is how are monomolecular or multilayer adsorption on a RPLC column measured? The last question is what is the composition and thickness/volume of this layer? To answer these questions and to obtain more insight into the influence of the organic modifier on the bonded alkyl chain length and the nature and concentration of the adsorbed organic modifier, it is important to study the adsorption isotherms for organic modifiers on reversed-phase materials.

There have been different methods [19, 98, 119, 165-172] used to measure the adsorption of organic eluent components on the surface of reversed-phase packing material. The methods applied for adsorption measurements are frontal chromatography [19, 98, 119,

165-172], retention of deuterated eluent components [19, 98, 119, 165-172], and introduction of a minor disturbance into the equilibrated chromatographic system [98, 119, 170-172]. All of these methods allow the measurement of the excess amount of the component adsorbed on the surface.

### **The Concept of Excess Adsorption**

Adsorption is an accumulation of one component in a close proximity to the adsorbent surface, under the influence of surface forces. In a binary liquid solution, this accumulation is accompanied by the corresponding displacement of another component (solvent) from the surface region into the bulk solution, thus increasing its concentration there. At equilibrium, a certain amount of the solute will be accumulated on the surface in excess of its equilibrium concentration in the bulk solution, as shown in Figure 2-1 [173].

Everett [174, 175] gave a strict definition for the excess adsorption value on the basis of experimentally observable quantities for binary mixtures. Refer to Figure 2-1 for the following discussion.  $n^0$  is the analyte amount in the initial solution of mole fraction  $x_2^0$ , the mass of solid adsorbent is  $m$  that has a specific surface area  $S$ , and the final equilibrium mole fraction in the liquid is  $x_2^e$  at given temperature  $T$  and pressure  $P$ . The system thus contains an amount  $n^0 x_2^0$  of component 2. If, in the final state, the liquid phase were of uniform composition  $x_2^e$  throughout its extent, it would contain an amount  $n^0 x_2^e$ . This latter hypothetical state in which the composition remains uniform up to the solid surface is taken as the reference state. The real system thus contains an

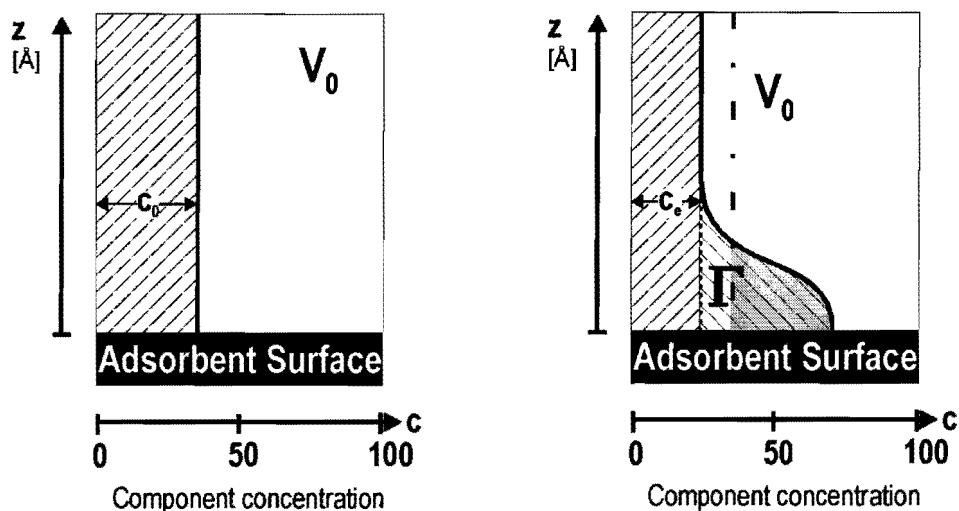


**Figure 2-1:** Schematic drawing illustrating the concept of excess adsorption.  $C$ -axis represents the analyte (component 2) concentration, which is dependent on the distance from the adsorbent surface ( $z$ -axis). The system on the left represents inactive adsorbent surface (original concentration  $c_0$  is uniform throughout the whole volume of the liquid phase). The right system is with active adsorbent surface.  $c_e$  is the equilibrium concentration in bulk solution after adsorption. Shadow areas represent equal amounts of analyte, which was transferred on the surface from bulk solution. An excessively adsorbed amount  $\Gamma$  is represented by right lined area under the distribution curve.

(Figure taken from reference 173, figure 1).

excess of component 2, over and above that was present in the reference system. This is given by

$$n^0(x_2^0 - x_2') = n^0 \Delta x_2' \quad (2-1)$$

and defines one measure of adsorption,  $n_2^{(n)}$ , called the reduced surface excess of component 2 [175]. This may be expressed in terms of the surface excess associated with unit of surface area, the areal (reduced) surface excess,  $\Gamma_2^{(n)}$ ,

$$\Gamma_2^{(n)} = \frac{n^0 \Delta x_2'}{mS} \quad (2-2)$$

This include two assumptions:

1. The liquid is incompressible, or molecular volumes of the solution components are constant.
2. The adsorbent surface is impermeable and represents a physical boundary introducing adsorption forces into the liquid phase adjacent to that surface. [174].

Assumption of a constant molecular volume allows the transition from  $\Gamma_2^{(n)}$  to  $\Gamma_2^{(v)}$ , i.e. from molar excess adsorption to volume based excess adsorption.

$$\Gamma_2^{(v)} = \frac{(c_0 - c_e)V_0}{mS} \quad (2-3)$$

Instead of the total number of moles of component 2, the total volume of the liquid phase in the system,  $V_0$ , and corresponding molar concentrations of component 2 before adsorption,  $c_0$ , and after the equilibrium is established,  $c_e$ , are used.

$c_0V_0/mS$  in the Equation 2-3 is the total amount of preferentially adsorbed component in a binary system (shown on the left pane of Figure 2-1), and  $c_eV_0/mS$  is the amount left in

the hypothetical equilibrated system where, according to Everett, the composition remains uniform up to the solid surface. The difference between these values would represent an excessive amount accumulated on the surface due to adsorption. This definition is shown graphically in Figure 2-1.

After establishing the equilibrium there will be a certain distribution of the analyte along the z-axis due to the stronger attractive effect of the surface in respect to component 2. It should be noted that the profile of the analyte distribution is dependent on the types of the analyte, the solvent, the chemistry of the surface, and the initial analyte concentration. However, the total volume of the liquid phase will not change since the accumulation of the analyte will cause the displacement of the solvent into the bulk liquid far from the surface and constant molecular volume of all components is assumed.

For reversed-phase adsorbents, the concept of the surface area is complex [164]. The only definite surface area, which could be taken into account, is the surface area of the original silica. Any comparison of the adsorption values (usually related to the unit of the surface) should be done relative to the surface area of underlying silica.

### **The Relationship between Excess Adsorption and HPLC Retention**

The connection of HPLC retention with adsorption phenomena is the key for the interpretation of the retention mechanism. The general concept is based on the assumption of instantaneous adsorption equilibrium in a dynamic chromatographic system and the solution of the mass-balance equation for a chromatographic column. General relationships for calculating the surface excess amount from chromatographic retention data was first given by

Wand, Duda and Radke [19] and later generalized, on the basis of adsorption theory, by Riedo and Kovats [176]. Both had introduced the Gibbs dividing plane prior to the application of the excess adsorption concept to the mass-balance in the HPLC column.

It is shown below that while using the excess adsorption concept, the introduction of the Gibbs dividing plane is not necessary for construction and solution of the mass-balance equation. However, the introduction of this plane is necessary for interpretation of the excess adsorption isotherms.

An infinitely small cross-sectional area of the column with thickness  $dx$  is considered.  $F$  is the volumetric flow through the column and  $c_e$  is a concentration of the analyte in the bulk flow. During the time  $dt$ , the amount  $c_e F dt$  of the analyte will move into the selected section. At the same time, the amount  $(c_e + dc_e) F dt$  will leave this section of the column. Total accumulation (positive or negative) in the selected cross-section of the column is  $F dt dc_e$ . Any accumulation in continuous media will form the gradient ( $\nabla$ ).

$$\nabla(c_e) = -\left(\frac{\partial c_e}{\partial x}\right)_t \quad \text{Or} \quad F dt dc_e = -F \left(\frac{\partial c_e}{\partial x}\right)_x dx dt \quad (2-4)$$

The total amount of analyte in a selected cross-section of the column is distributed between the contacting phases and surfaces. If the distribution function is denoted as  $\psi(c_e)$ , a general form of mass balance equation can be written

$$-F \left(\frac{\partial c_e}{\partial x}\right)_t dt dx = \left(\frac{\partial}{\partial t} \psi(c_e)\right)_x dt dx \quad (2-5)$$

where  $\psi(c_e)$  in this equation provides a sense of the number of moles of analyte in the selected area of the column.

To solve this equation, a specific distribution model must be assumed and an exact expression for the analyte distribution must be written. In the equilibrated column with constant flow of binary solution, some excessive amount of one component is adsorbed on the surface and the solution pumped through the column has equilibrium concentration similar to that shown in the right panel of Figure 1. The total amount of the component in the liquid phase in a small cross-section of the column can therefore be written as:

$$\Psi(c_e) = v_0 c_e + s \Gamma^{(v)}(c_e) \quad (2-6)$$

where  $v_0$  is the total volume of the liquid phase in that cross-section,  $c_e$  is the component equilibrium concentration,  $s$  is the adsorbent surface area in selected cross-section, and  $\Gamma^{(v)}$  is the component excess adsorption. The term  $v_0 c_e$  represents the analyte amount in the whole volume,  $v_0$ , of the liquid phase of chosen cross-section, as it was defined by Everett [174]. The rightmost term of Equation 2-6 represents the excessive amount adsorbed on the adsorbent surface,  $s$ .

Equation 2-6 is the basis for the solution of mass-transport equation, which has been discussed before [19, 172, 176] and leads to the following expression (refer to Appendix I for its step-by-step derivation).

$$V_R(c_e) = V_0 + S \frac{d\Gamma^{(v)}(c_e)}{dc} \quad (2-7)$$

where  $V_R$  is the component retention volume,  $V_0$  is the column void volume (the total volume of the liquid phase in the column),  $S$  is the adsorbent surface area, and  $d\Gamma^{(v)}(c_e)/dc$  is the derivative of the component excess adsorption isotherm. Parameter  $V_0$  in this expression represents the total volume of liquid phase in the HPLC column and  $S$  is the total surface of

adsorbent in this column. Note that in this brief description, no model of the adsorbed layer was introduced, nor was the position of the Gibbs dividing plane defined. Use of the excess adsorption concept in HPLC does not require any additional assumptions, but, as stated before, the interpretation of the excess adsorption isotherms does.

Integration of the Equation 2-7 leads to the expression given in the Equation 2-8.

$$\Gamma^{(v)}(c_e) = \int_0^{c_e} \frac{V_R(c_e) - V_0}{S} dc \quad (2-8)$$

There are no restrictions to the use of this equation for the description of two-component systems. The surface area and dead volume are properties of the chromatographic column. Excess adsorption was defined as the difference in the component concentrations (measured far away from the surface) of two systems, one without the influence of the adsorbent surface and another with influence. In this case, the column is equilibrated with a two-component solution and then a small amount of the same solution with a small difference in concentration is injected (introduction of minor disturbance in the system). This minor disturbance peak for each component will have the retention volume corresponding to the Equation 2-8. Measurement of the dependence of the minor disturbance peak retention through the entire concentration range allows the calculation of the excess adsorption of the component using the Equation 2-8.

To calculate the excess adsorption of organic eluent on a RP surface on three different binary solvent systems typically used in RPLC (acetonitrile-water, methanol-water and THF-water), an extensive study was conducted in our laboratory [163, 164, 173] using a minor disturbance method [98, 119, 170-172]. However, for the current study, the focus will be on an acetonitrile-water system, where acetonitrile is preferentially adsorbed on the surface.



Equation 2-8 was then applied to the measured retention volume of acetonitrile for the calculation of the excess adsorption of acetonitrile. The dependence of excess adsorption of acetonitrile was measured on columns having different alkyl chains ( $C_1$  to  $C_{18}$ ), which were bonded to the same silica surface.

Overlay of the excess adsorption isotherms of acetonitrile (refer to Figure 2-2) reveals the similarity of acetonitrile adsorption behavior on different bonded alkyl chains. All of the isotherms show slight negative excess at high organic concentration. This indicates a preferential adsorption of water and is an indication of the presence of accessible residual silanols. Between the region of 8 and 17 mole/L of acetonitrile (refer to Figure 2-2), all of the isotherms have negative slope. This region represents maximum filling of available hydrophobic adsorbent surface with acetonitrile. Essentially this means the formation of an adsorbed layer composed of pure acetonitrile.

The excess amount adsorbed,  $\Gamma$ , is known, but the amount,  $a_e$ , which was already on the surface from the equilibrium solution is not known (only the concentration,  $c_e$ , is known). A model of the adsorbed layer structure is needed for the estimation of that amount. The introduction of an imaginary plane separates the adsorbed layer from the bulk solution. The underlying assumption is that the adsorbed layer concentration throughout the volume of the adsorbed phase is uniform. Measurement and calculation of the excess adsorption is possible without assumption of any specific adsorption model, however, the interpretation of the adsorption isotherm requires the introduction of a model.

The existence of a hypothetical plane parallel to the adsorbent surface with distance  $\tau$  from the adsorbent surface is assumed. Above this plane, component concentrations are equal to the equilibrium concentration. Between this plane and the adsorbent surface, the

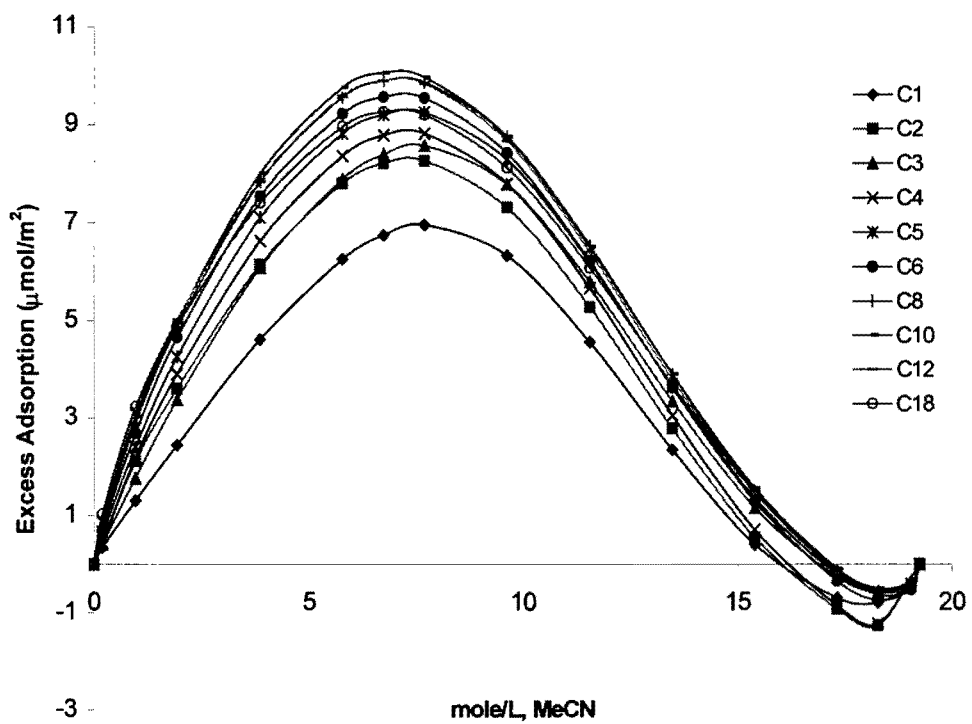


**Figure 2-2:** Acetonitrile excess adsorption isotherms on C<sub>1</sub>, C<sub>2</sub>, C<sub>3</sub>, C<sub>4</sub>, C<sub>5</sub>, C<sub>6</sub>, C<sub>8</sub>, C<sub>10</sub>, C<sub>12</sub>, and C<sub>18</sub> modified adsorbents.  
(Figure taken from reference 173, figure 3).

amount of preferentially adsorbed component per unit of surface area may be expressed as follows

$$n_{ads} = c_e \tau + \Gamma^v(c_e) \quad (2-9)$$

where  $n_{ads}$  is the total amount adsorbed in [mole/m<sup>2</sup>],  $c_e$  is the equilibrium concentration in [mole/mL],  $\tau$  is the adsorbed layer thickness in [Å] multiplied by 10<sup>-4</sup> for unit conversion, and  $\Gamma^v(c_e)$  is the excess adsorption in [mole/m<sup>2</sup>].

Linear decrease of  $\Gamma^v(c_e)$  values with the increase of the acetonitrile concentration in the region between 7 and 18 mole/L (refer to Figure 2-2) indicates complete filling of the adsorbed layer and  $n_{ads}$  is constant in this region. According to Everett [181], extrapolation of the slope of the excess adsorption isotherm in that region to the intercept with the y-axis indicates the maximum adsorbed amount (as shown in Equation 2-9). Estimation of the maximum adsorbed amount from the excess adsorption isotherm, as described by Everett [174], is shown in Figure 2-3.

Since the maximum adsorbed amount represents a complete filling of the adsorbed layer with the corresponding component and since a constant molar volume in the adsorbed and bulk phases is assumed, the volume of adsorbed layer per unit of surface area,  $v_{ads}$ , can be calculated as

$$v_{ads} = n_{max} \cdot v_{mol} \quad (2-10)$$

where  $v_{mol}$  is the adsorbed component molar volume. Value of  $v_{ads}$  has a dimension of [mL/m<sup>2</sup>], which could be transferred into linear dimensions representing the apparent thickness of this adsorbed layer. The thickness of the adsorbed layer for all measured

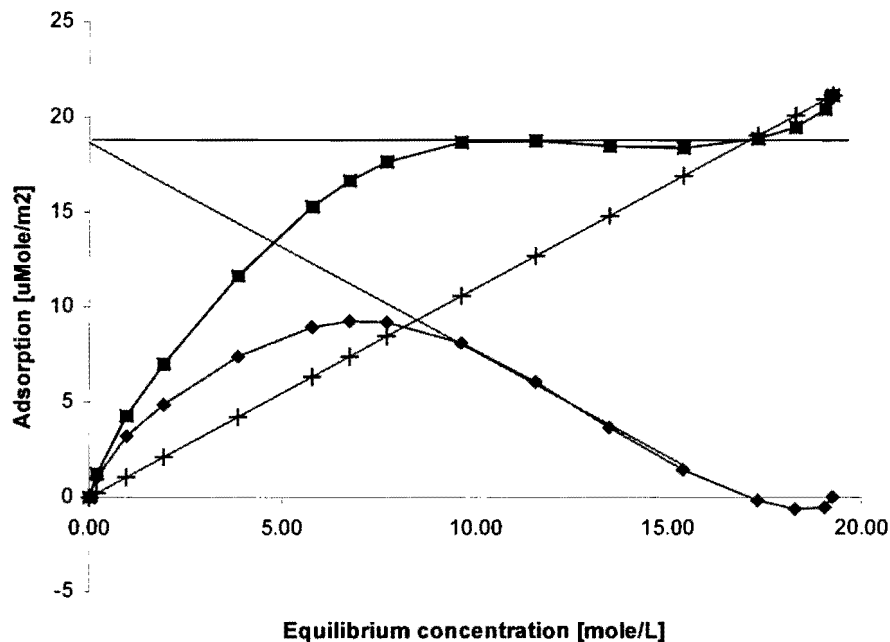
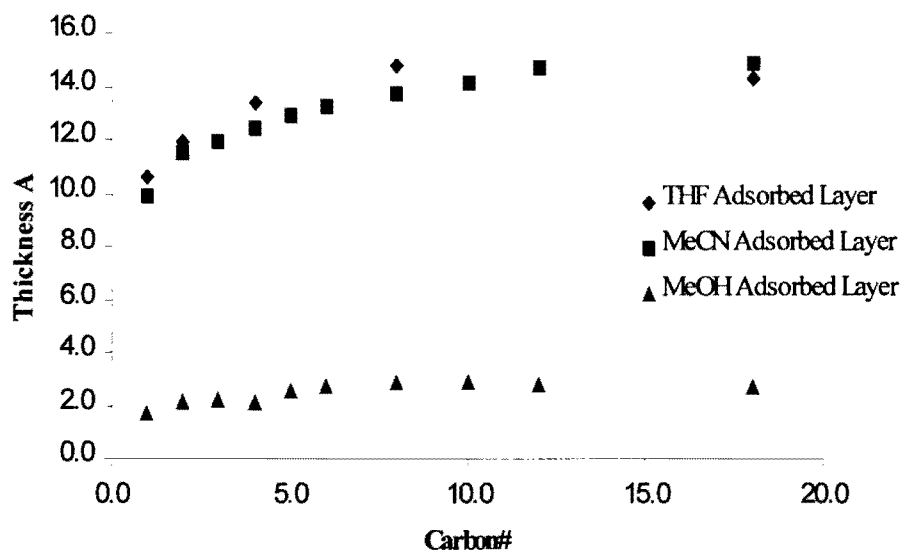


**Figure 2-3.** Estimation of the maximum adsorbed amount on the basis of the model of finite thickness adsorbed layer. Diamonds are the experimental excess adsorption isotherm, crosses are the amount of the adsorbed component in the adsorbed layer from equilibrium concentration, and squares are the total amount of analyte in the adsorbed layer.  
(Figure taken from reference 173, figure 6).

isotherms on all studied adsorbents was calculated. The dependencies of that thickness on the number of carbons of alkyl chains bonded on silica surface are shown in Figure 2-4.

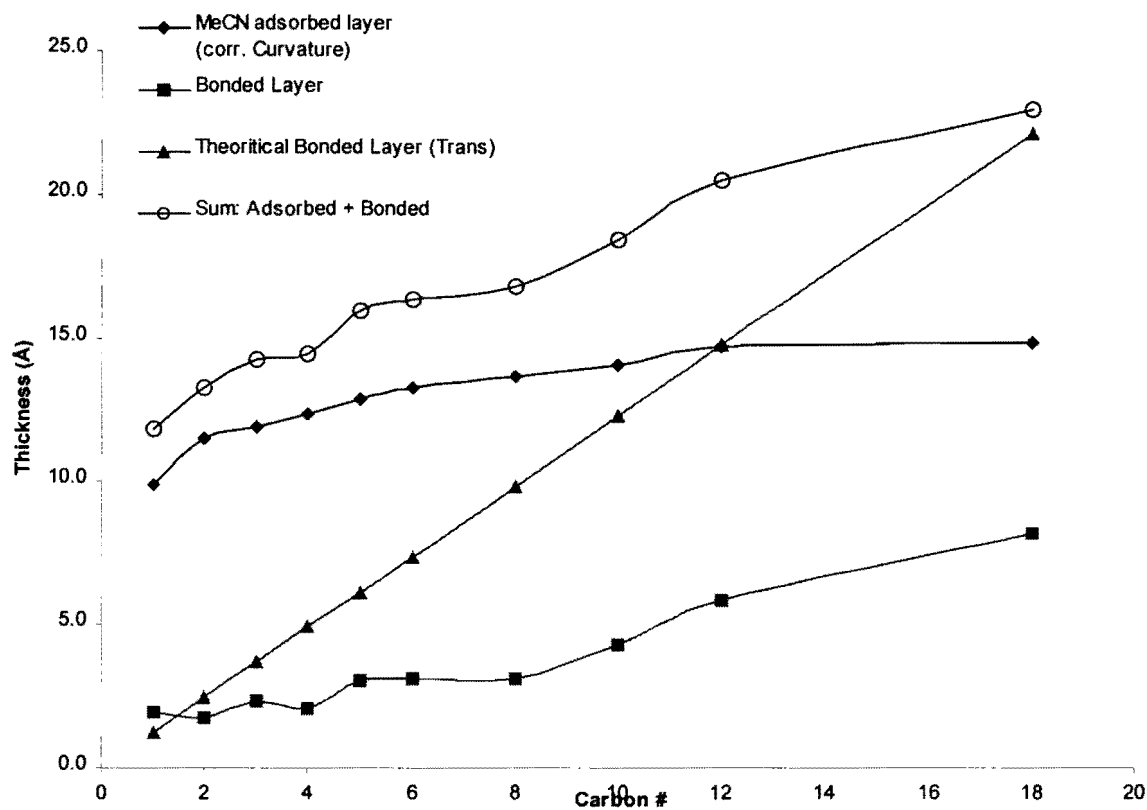
In summary, methanol forms an adsorbed layer of approximately 2.5-Å thickness, which clearly indicates monomolecular character of its adsorption on the surface of the reversed-phase adsorbent. On the other hand, the corresponding thickness for acetonitrile and tetrahydrofuran coincide at about 14 Å. This indicates that these components form multilayer adsorbed phases. As mentioned before, the focus of the current study is on acetonitrile-water as the mobile phase.

The following discussions and conclusions are based on the study performed in our laboratory [163, 173]. If the mobile phase consists of any composition of acetonitrile-water, then acetonitrile molecules could either accumulate on the top of the surface or could get embedded between the alkyl chains. If all acetonitrile molecules are embedded between the alkyl chains of bonded phase, then the increase of the adsorption values should be proportional to the increase of the carbon number of the bonded ligands. Figure 2-5 represents the thickness of the bonded layer and the adsorbed layer of increasing alkyl chain length. It can be seen that at the lower chain lengths there is not enough volume, to accommodate the volume of the adsorbed layer. This confirms that the volume of that adsorbed layer is on top of the bonded layer. However, at higher alkyl chain lengths, C<sub>12</sub> and C<sub>18</sub>, there is room for the acetonitrile molecules to penetrate. However, the adsorbed layer thickness is independent of the alkyl chain length. It can be assumed that since the adsorbed layer is on top of the smaller less hydrophobic alkyl chains that it is still on the top of the longer hydrophobic ligands. These results clearly show that the acetonitrile forms a thick adsorbed layer on the hydrophobic surface of reversed-phase adsorbents (refer to Figure 2-6).



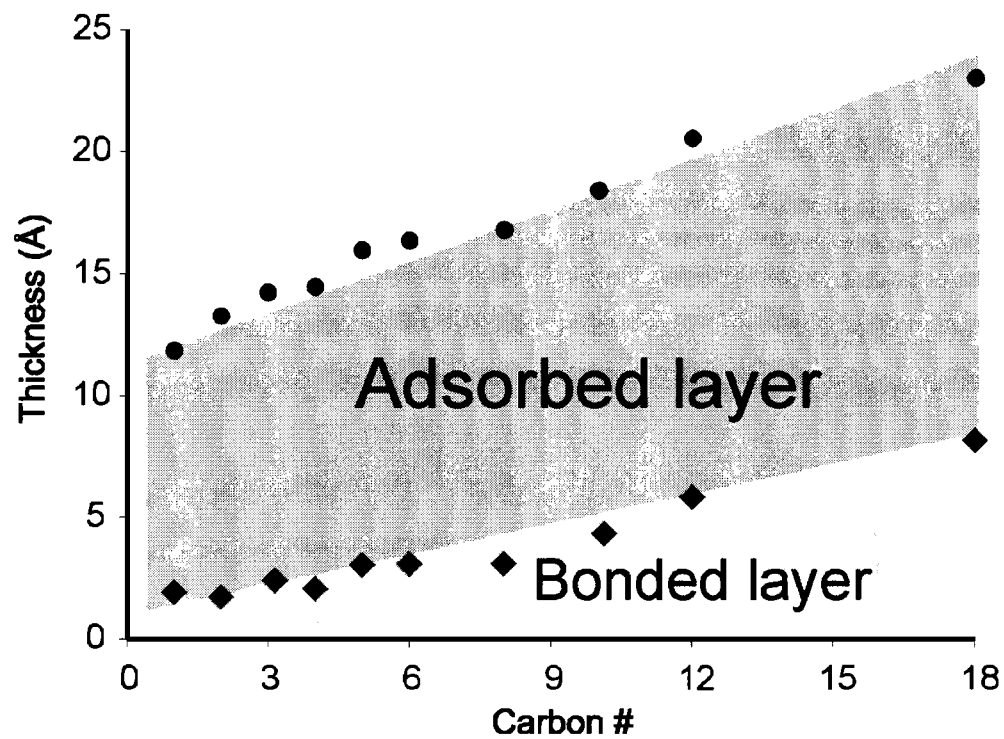
**Figure 2-4:** Adsorbed layer thickness for THF, acetonitrile, and methanol on the surface of silica-based adsorbents modified with alkylsilanes of different chain length.

Figure taken from reference 163, figure 7.



**Figure 2-5:** Comparison of the bonded layer and adsorbed layer thickness versus carbon number of the alkyl chain bonded to the silica surface.

Figure taken from reference 163, figure 5-35.



**Figure 2-6:** The dependence of the acetonitrile adsorbed layer and collapsed bonded layer thickness on the length of the bonded chains.  
Figure taken from reference 173, figure 9.



This layer is shown to be equivalent to about 4 to 5 molecular layers on top of each other. The explanation of this multi-layer formation requires further investigation and out of the scope of the current study, but may be based on the self-association of acetonitrile [176] on the hydrophobic surface. The thickness of this adsorbed layer is independent on the length of underlying bonded alkyl chains. This suggests the prevalent character of dispersive forces in adsorption interactions of the acetonitrile molecules.

From the results obtained in our laboratory [163, 173], a schematic of the surface of the reversed-phase column is shown in Figure 2-7. Majority of the surface in reversed-phase adsorbent is inside the pores of silica. Inside these pores, the bonded alkyl chains are in their most dense configuration, or in “collapsed” state (independent of the bonded alkyl chain length, type of organic modifier and the mobile phase composition). There is preferential adsorption of the organic modifier (e.g., acetonitrile) on top of this collapsed phase, which is different in concentration than the mobile phase (e.g., acetonitrile-water) composition.

### **The Partition/ Adsorption Retention Model**

The adsorbed organic layer on top of the bonded phase may act as a real liquid stationary phase in RPLC and suggest a complex retention mechanism for analytes in the RPLC column. Since there is an adsorbed layer of different composition than the bulk eluent being pumped, an analyte may partition (distribution) from the bulk eluent into the adsorbed layer of a certain thickness. The thickness of this layer is dependent upon the concentration of acetonitrile in the binary eluent system. The overall RPLC retention process most likely consists of two processes (refer to Figure 2-8 for schematic representation of this model): 1) distribution of the analyte between the mobile phase and the adsorbed layer and

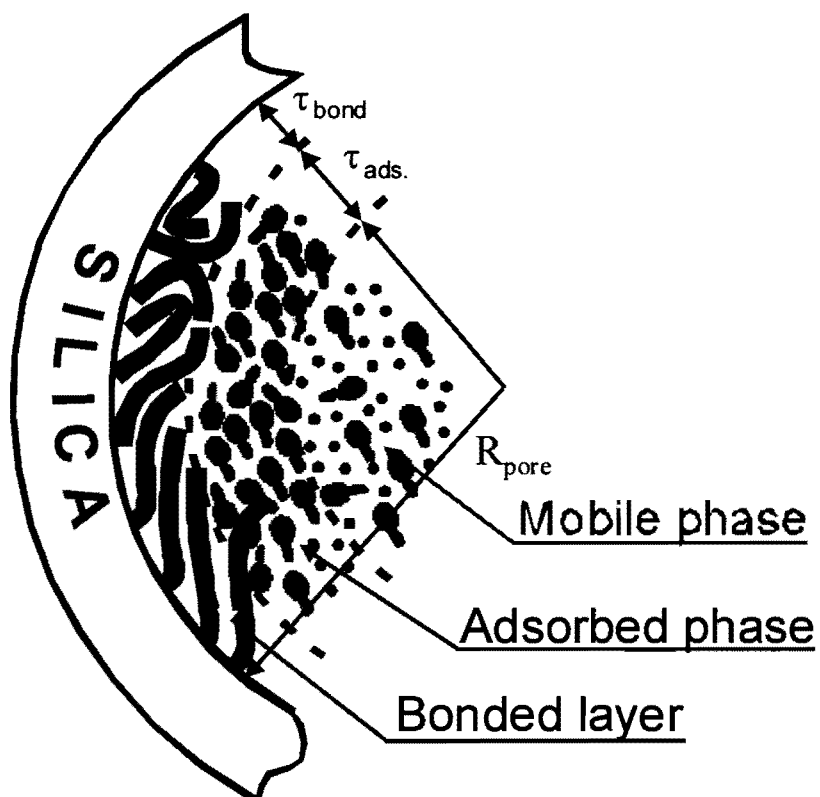


**Figure 2-7:** A schematic representation of the bonded layer, the adsorbed layer and the mobile phase.

Figure taken from reference 163, figure 5-37.

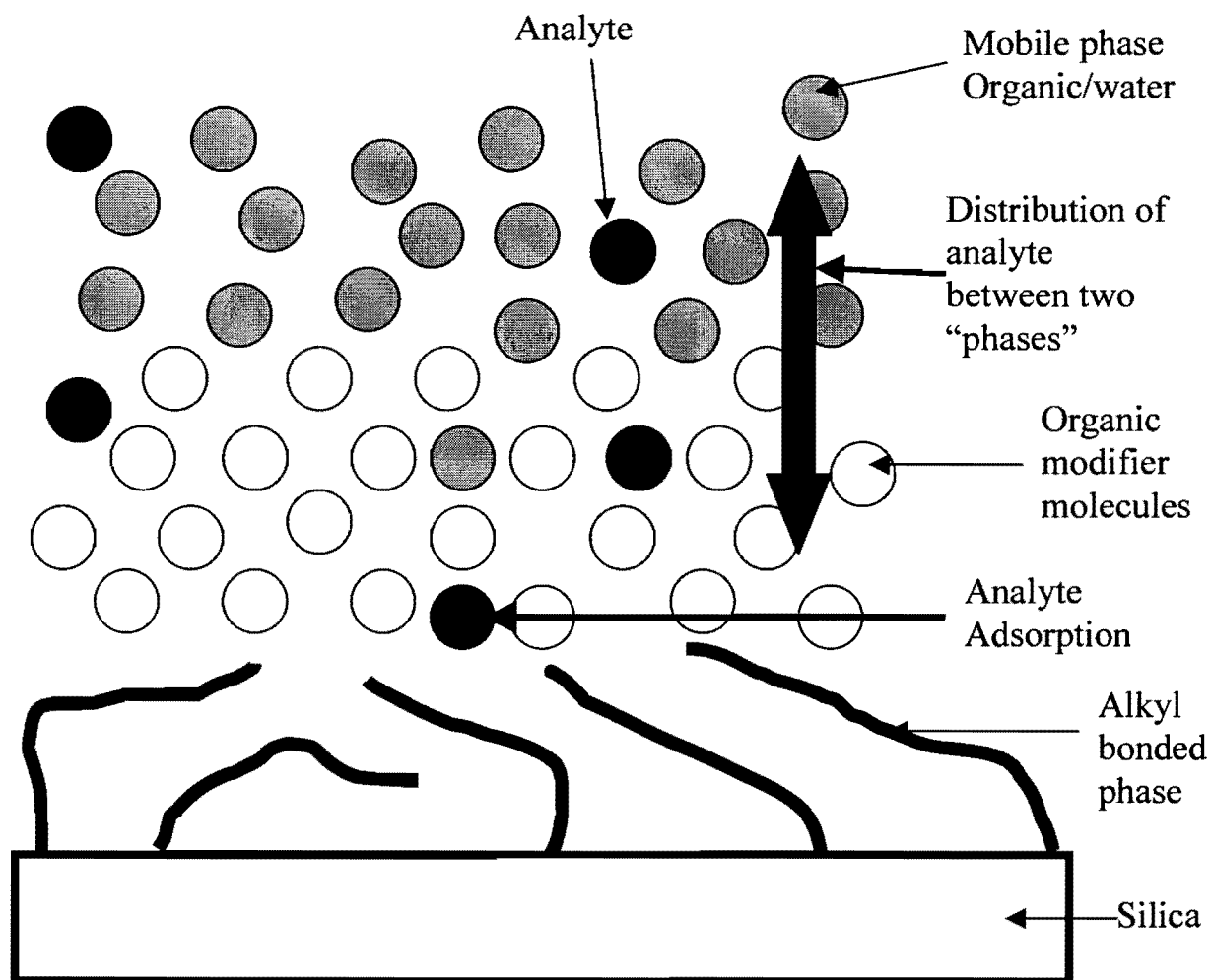


**Figure 2-8:** Schematic representation of the analyte distribution according to the described partitioning-adsorption model for RPLC.

## 2) adsorption of the analyte onto the surface of the reversed phase material

The following assumptions are made: (1) binary mobile phase is pumped through the column at a constant composition long enough to establish equilibrium and to form a stable adsorbed organic layer. (2) Analyte is injected on the column in a small volume of a very dilute solution. (3) Injection of small amount of analyte does not disturb the equilibrium of the binary eluent in the column.

Analyte retention in this system could therefore be described as superposition of two processes: analyte partitioning from the eluent into the adsorbed layer followed by its adsorption from that layer on the surface of the bonded phase. Using the description of the model given, an equation is derived as follows, which can predict analyte retention under given mobile phase composition and a column.

A small section of a column of length  $dx$  that is at the distance  $x$  from the inlet is considered. Analyte concentration,  $c_e$ , in the eluent is a function of both time and length. The volumetric flow rate through the column is  $F$  mL/min, therefore during time  $dt$  the analyte amount of  $c_e F dt$  will move into the layer  $dx$  of the column and the amount  $(c_e + dc_e) F dt$  will move out of this layer. The accumulation (positive or negative) in this layer will be

$$- F dt dc_e = F dt \cdot \nabla(c_e) dx \quad (2-11)$$

where  $\nabla(c_e) = \left( \frac{\partial c_e}{\partial x} \right)_t$  is the gradient of concentration in layer  $dx$  which was formed at time  $t$  for a two-component system. This amount of the analyte is distributed between the mobile phase, the adsorbed layer and the surface.

Analyte concentration in the adsorbed layer is governed by its distribution coefficient between the mobile phase and the liquid that is adsorbed on the bonded alkyl chains. This distribution coefficient,  $K_p$ , is defined as the ratio of the concentrations of the analyte inside the adsorbed layer,  $c_s$  and inside the mobile phase,  $c_e$ .

$$K_p = c_s / c_e \quad (2-12)$$

$K_p$  will depend on the temperature and the mobile phase composition. The total amount,  $n$ , of analyte in the length  $dx$  of our column at a given concentration can be represented as follows:

$$n = (v_0 - v_s)c_e + v_s c_s + s\Gamma(C_s) \quad (2-13)$$

Where  $v_0$  is the total liquid volume per length  $dx$  of the column,  $v_s$  is the total adsorbed layer volume of the organic component of the mobile phase per length  $dx$  of the column,  $s$  is the surface area of the adsorbent per length  $dx$  of the column and  $\Gamma$  is the excess adsorption of the analyte on the surface from the bonded alkyl chains (where the analyte concentration is  $c_s$ ). Equation 2-13 reflects the summation of the amount of analyte present in the different regions of the column. The first term of Equation 2-13 represents the amount of analyte present in the bulk mobile phase (not counting the adsorbed layer volume). The second term represents the amount of analyte present in the adsorbed layer volume and the third term represents the amount of analyte present on top of the bonded alkyl chains.

The change in the amount of the analyte in the cross-sectional area of the column of thickness  $dx$  at the distance  $x$  from the column inlet during the time  $dt$  will be:

$$\left[ \frac{\partial}{\partial t} ((v_0 - v_s)c_e + v_s c_s + s\Gamma(c_s)) \right] dx dt \quad (2-14)$$

According to mass balance conditions, the rate of accumulation of the analyte in the length  $dx$  and the rate of its distribution inside this area, (i.e. partitioning inside adsorbed layer and forming the excess amount) should be equal. Thus,

$$-F \left( \frac{\partial c_e}{\partial x} \right)_t dt dx = \left[ \frac{\partial}{\partial t} ((v_0 - v_s)c_e + v_s c_s + s\Gamma(c_s)) \right]_x dt dx \quad (2-15)$$

or, equating partial derivatives

$$-F \left( \frac{\partial c_e}{\partial x} \right)_t = (v_0 - v_s) \left( \frac{\partial c_e}{\partial t} \right)_x + v_s \left( \frac{\partial c_s}{\partial t} \right)_x + s \left( \frac{\partial \Gamma(c_s)}{\partial t} \right)_x \quad (2-16)$$

Substituting for  $c_s$  from Equation 2-12 and since  $K_P$  does not depend on time we obtain:

$$-F \left( \frac{\partial c_e}{\partial x} \right)_t = (v_0 - v_s) \left( \frac{\partial c_e}{\partial t} \right)_x + v_s K_P \left( \frac{\partial c_e}{\partial t} \right)_x + s \left( \frac{\partial \Gamma(c_s)}{\partial t} \right)_x \quad (2-17)$$

Since the concentration of the analyte is measured by the detection in the liquid phase we have to substitute the surface excess by the concentration in the mobile phase according to the following expression:

$$\left( \frac{\partial \Gamma(c_s)}{\partial t} \right)_x = \left( \frac{\partial \Gamma(c_s)}{\partial c_s} \right)_x \left( \frac{\partial c_s}{\partial t} \right)_x \quad (2-18)$$

The function  $(\partial c_s / \partial t)_x$  can be substituted as follows:

$$\left( \frac{\partial c_s}{\partial t} \right)_x = \left( \frac{\partial c_s}{\partial c_e} \right)_x \left( \frac{\partial c_e}{\partial t} \right)_x \quad (2-19)$$

When equations 2-17, 2-18 and 2-19 are combined and remembering that  $(\partial c_s / \partial c_e)_x = K_P$ , the following equation is obtained.

$$-F \left( \frac{\partial c_e}{\partial x} \right)_t = \left( v_0 - v_s + K_P v_s + s K_P \frac{d\Gamma(c_s)}{dc_s} \right) \left( \frac{\partial c_e}{\partial t} \right)_x \quad (2-20)$$

Since the concentration of the analyte is a function of both  $x$  and  $t$ , its full derivative is

$$dc_e = \left( \frac{\partial c_e}{\partial x} \right) dx + \left( \frac{\partial c_e}{\partial t} \right) dt \quad (2-21)$$

Dividing this expression by  $dt$  at constant  $c_e$  ( $dc_e=0$ ) we obtain an equation relating partial derivatives:

$$\left( \frac{\partial c_e}{\partial t} \right)_x = - \left( \frac{\partial c_e}{\partial x} \right)_t \left( \frac{\partial x}{\partial t} \right)_c \quad (2-22)$$

Substituting into the Equation 2-20, this expression is obtained:

$$-F \left( \frac{\partial c_e}{\partial x} \right)_t = \left( v_0 - v_s + K_p v_s + sK_p \frac{d\Gamma(c_s)}{dc_s} \right) \left( - \frac{\partial c_e}{\partial x} \right)_t \left( \frac{\partial x}{\partial t} \right)_c \quad (2-23)$$

Dividing both parts by  $-\left(\partial c_e / \partial x\right)_t$  the following expression is obtained:

$$F = \left( v_0 - v_s + K_p v_s + sK_p \frac{d\Gamma(c_s)}{dc_s} \right) \left( \frac{\partial x}{\partial t} \right)_c \quad (2-24)$$

Where  $\left(\partial x / \partial t\right)_c = u_c$  (the linear velocity of the chromatographic band at a certain concentration of the analyte) is substituted.

$$F = \left( v_0 - v_s + K_p v_s + sK_p \frac{d\Gamma(c_s)}{dc_s} \right) u_c \quad (2-25)$$

Dividing both parts of the equation by  $u_c$  and substituting for  $F/u_c = v_r$ ,

$$v_r = v_0 + (K_p - 1)v_s + sK_p \frac{d\Gamma(c_s)}{dc_s} \quad (2-26)$$

Now to go from the reduced amounts (area  $dx$ ) to total amounts (column length), both parts of the equation are multiplied by  $L$ , which is the column length.

$$V_R = V_0 + (K_P - 1)V_s + SK_P \frac{dI(c_s)}{dc_s} \quad (2-27)$$

where  $V_R$  is the retention volume of an analyte,  $V_0$  is the total liquid volume inside the column,  $K_P$  is the distribution coefficient of an analyte between the mobile phase and the adsorbed layer,  $V_s$  is total adsorbed layer volume,  $S$  is the total surface area of the adsorbent per column and  $dI(c_s)/dc_s$  can also be referred to as  $K_H$  (Henry adsorption constant). This is because the analyte is injected in very low amount and its adsorption on the surface of the bonded alkyl chains is assumed to be in the Henry region (analyte adsorption is linear with respect to analyte concentration). Equation 2-27 is re-written as the following:

$$V_R = V_0 + (K_P - 1)V_s + SK_P K_H \quad (2-28)$$

$K_H$  is the analyte Henry constant for its adsorption from pure eluent component (adsorbed layer) on the surface of the bonded phase.

According to this model, Equation 2-28 represents the mathematical relationship describing analyte retention in RPLC. Retention volume of an analyte is a function of void volume, adsorbed layer volume, distribution constant of that analyte between the mobile phase and the adsorbed layer, surface area and analyte's Henry constant.  $(K_P - 1)V_s$  term is referred to as the partition term and  $SK_P K_H$  term is referred to as the adsorption term. The analyte must distribute itself between the mobile phase and adsorbed organic layer before it can adsorb on the bonded alkyl chains. Therefore,  $K_P$  is also present in the adsorption term, which indicates that adsorption process depends on the partition process.

$K_P$  is defined as the distribution constant of an analyte between the adsorbed layer (pure organic modifier) and the mobile phase (organic-water mixture). If the mobile phase is pure



organic, then  $K_P$  is equal, by the definition set in this model, to 1. So, for a given column, at pure organic mobile phase, the Equation 2-28 is reduced to the following:

$$V_R^{100} = V_0 + SK_H \quad (2-29)$$

where  $V_R^{100}$  is the retention volume of an analyte in pure organic as the mobile phase.  $V_0$  is measure independently, as we will see in Chapter III, in a binary system (organic-water) and  $S$  does not need to be measured for the following reason. When analyte retention volume is predicted using Equation 2-28, we know two parameters; column and mobile phase composition. The same column is used to measure  $V_R^{100}$ , from which  $K_H$  is derived as shown below.

$$K_H = \frac{V_R^{100} - V_0}{S} \quad (2-30)$$

So, in reality,  $K_H$  depends on the given column since dead volume and surface area will vary from one column to another. When equation 2-30 is combined with equation 2-28, the surface area cancels out (only when  $V_0$ ,  $K_H$  and experimentally measured  $V_r$  are measured on the same column).

## Conclusions

Since all involved parameters can be measured independently, the partition/adsorption model can be experimentally verified. Column's dead volume ( $V_0$ ), and adsorbed layer volume ( $V_s$ ) of the organic modifier are product of a given chromatographic column and can be measured independently in a binary system (organic modifier plus water). The Henry constant of the analyte is the slope of its adsorption from pure organic component

(two component system; organic modifier and analyte). By measuring  $V_o$ ,  $V_s$  and  $K_H$  in a two component system (e.g., acetonitrile-water or acetonitrile-analyte) and  $K_P$  is measured independently by headspace gas chromatography (HS-GC), we can predict the retention of an analyte for a given chromatographic conditions (this is a ternary system – acetonitrile, water and analyte). By comparing the theoretically predicted  $V_R$  of an analyte on a given column and mobile phase composition using Equation 2-27 to the experimentally measured  $V_R$  of that analyte on the same exact column and mobile phase composition, we can find out the validity of the model presented here. This is the main goal of this study.

## Chapter III: Results - RPLC.

### Summary

Results obtained using RPLC are summarized in this chapter. Three of the four independent variables ( $V_o$ ,  $V_s$  and  $K_H$ ) of Equation 2-28 measured using RPLC to predict the retention volumes of all analytes being studied are given here. All of the materials, instrumentation and parameters used for RPLC experiments are also summarized in two separate experimental sections.

The definition of  $V_o$  and the measurement of  $V_o$  using the minor disturbance method are discussed. A procedure to calculate the  $V_s$  is described and results obtained for all five columns are given. Directly measured experimental retention volumes for all analytes at different acetonitrile-water composition on all five columns are given and discussed. The  $K_H$  values measured for all analytes on five columns are also discussed here.

### Dead Volume, $V_o$

The dead volume,  $V_o$ , (also known as the void volume) is one of the most significant parameters in modern liquid chromatography (LC) and it is essential for all HPLC calculations. The primary chromatographic retention parameter  $V_R$  (retention volume) consists of two parts: first, the volume in which the analyte molecules are in the moving phase and second, the volume of the mobile phase passed through the column while the analyte is retained on the surface of the solid phase. The first part depends only on particle porosity, particle shape, packing quality, and other geometrical parameters of the column and the chromatographic system. The second part is concerned with the partition coefficient.

In all chromatographic methods, the contribution of surface interaction to the retention volume must be separated from its geometrical part. The widely used retention factor,  $k'$ , is the most convenient approach to do this.

$$k' = \frac{(V_R - V_o)}{V_o} \quad (3-1)$$

It allows us to eliminate geometrical parameters of the adsorbent, column, system and it also looks like the partition coefficient. Because it resembles the partition coefficient, chromatographers widely use  $k'$  as a thermodynamic parameter (partitioning process is assumed) [13-14]. It is obvious that the accurate, universal, and precise determination of dead volume is very important. There have been at least six methods suggested for the determination of  $V_o$ ; direct weighing methods [84, 97, 99, 178-180], use of unretained compounds [18, 179, 181-187], use of isotopically labeled components of the eluent [77, 83-85, 98, 170, 180, 188], minor disturbance methods [18, 97, 99, 189-191], inorganic salts [99, 179-182, 184, 186, 189, 193] and linearization of homologous series [57, 179, 180, 193-195]. Knox and Kaliszan [170] mentioned that all of these methods neither represent an acceptable definition of  $V_o$  nor provide reliable methods for its determination.

Riedo and Kovats [176] based their description of the liquid chromatographic phenomena on the more widely known partitioning principle common to gas chromatography (GC). This partitioning model is based on the exchange of analyte molecules between two different and well-determined phases (gas- and stationary phase in GC). In LC, however, the adsorption layer is part of the liquid phase and, as pointed out by Gibbs [196], it is very difficult to determine the exact position of a divided plane between a bulk phase and an adsorbed layer.

### Definition of $V_o$

There have been numerous attempts to define  $V_o$  [19, 97, 99, 116, 172, 178, 193, 197]. Mockel and Freyholdt [194] proposed that the dead volume of a LC column is that volume of the mobile phase that passes through the column while the analyte molecules are distributed in it. However, it has been shown by many chromatographers [97, 99] that eluent molecules are adsorbed onto the bonded phase, forming a stationary layer of mobile phase components, and they concluded that this reduces the column dead volume. Most chromatographers base their approach to the LC process on the classical distribution model, which consists of partitioning of the sample molecules between mobile and stationary phases (both liquids) [69]. It is known that for different kinds of molecules, the volume of the adsorbed layer will be different. Hence, different molecules will have different dead volumes. J. H. Knox and co-workers have also considered the molecular exclusion effect and its influence on  $V_o$  [192].

To determine the dead volume of a column, it must be defined. The dead volume,  $V_o$ , can be defined as the total volume of the liquid phase inside the column. This volume is the sum of mobile phase volume ( $V_m$ ) and adsorbed layer volume ( $V_s$ ). Inside the column, we have three different volumes: pore volume ( $V_p$ ), exclusion volume or interstitial volume ( $V_{ex}$ ) and adsorbed layer volume ( $V_s$ ). The following equations can be written:

$$V_m = (V_p - V_s) + V_{ex} \quad (3-2)$$

$$V_o = V_m + V_s \quad (3-3)$$

$$V_o = V_p + V_{ex} \quad (3-4)$$

The  $V_o$  is easily accessible, e.g., by filling the column with two solvents of different density and then weighing it after each filling. This, of course, is contingent on the

assumption that the molar volumes of all components do not change on adsorption, which is a good approximation.

Since liquid is practically incompressible,  $V_m$  could be determined by injection of a compound that is believed not to be adsorbed, that is, it does not enter the adsorbed layer. Multiplication of the retention time of this compound by the flow-rate gives  $V_m$ . It turns out that different neutral " $V_m$  probes" of moderate molecular size (organic compounds) yield different  $V_m$  values, while deviations of the order of 50% occur when ions (inorganic salts) or polymers are used as probes. This uncertainty seems to corrupt the reliability of liquid chromatography experimental data (capacity factor, selectivity and resolution).

Consider a different approach to the definition of dead volume. First, we assume that all processes (adsorption, retention, exclusion, etc.) occur in the liquid phase that is in contact with the adsorbent surface. Gibbs' approach is applicable to this adsorption phenomenon. It should be pointed out that the results are independent of the cause of concentration changes (physical adsorption, exclusion, or ionic attraction).

A basic thermodynamic approach to a description of adsorption processes following Gibbs [196] is based on the comparison of the two systems (refer to Figure 2-1). The first system corresponds to the two-component solution with initial concentration of the solute ( $C_o$ ) and volume ( $V$ ) and without any influence from the adsorbent surface. The second system is essentially the same as the first except the solution is in contact with the adsorbent surface. Excess adsorption (as defined in Chapter II) of the investigated substance is measured as the difference between the  $C_o$  (initial concentration) and  $C_e$  (equilibrium concentration) after achieving equilibrium. The following equation was derived in Chapter II (Equation 2-3).

$$\Gamma_2^{(v)} = \frac{(c_0 - c_e)V_0}{mS} \quad (3-5)$$

The relationship between excess adsorption and chromatographic retention volume was described in Chapter II and the following equation was derived (Equation 2-7).

$$V_R(c_e) = V_0 + S \frac{d\Gamma^{(v)}(c_e)}{dc} \quad (3-6)$$

The given definition of  $V_0$  leads to the consequence that all adsorption processes occur in the liquid phase. It is not necessary to define the position of the dividing plane between bulk solution and adsorbed layer on that stage.

## Experimental

### Adsorbents and Columns

High purity porous silica was used in this study. This silica was chemically modified with alkyldimethylchlorosilanes of different alkyl chain length ( $C_1$ ,  $C_4$ ,  $C_8$ ,  $C_{12}$  and  $C_{18}$ ) [164]. The alkylsilylation procedure has been described elsewhere [198]. Adsorbents were packed into 150 x 4.6 mm stainless steel columns using the slurry packing procedure (Phenomenex Inc., Torrance, CA). Phenomenex also supplied the technical details, geometric parameters of bare porous silica and alkylsilylated gels for all five columns. These are summarized in Table 3-I.

### HPLC Systems

Two different HPLC systems were used for dead volume determination. System I: HP model 1050 pump and autosampler (Agilent Tech, Little Falls, DE) equipped with

**Table 3-I.** Geometric parameters of bare porous silica and alkylsililated gels.

1	2	4	5	6	7
Adsorbent	BET surface area	Total pore volume	Mean pore diameter	“Carbon” Load	Bonding density
	[m <sup>2</sup> /g]	[mL/g]	[Å]	C% w/w	[μmole/m <sup>2</sup> ]
Si	374	0.965	97	0	0
C1	----	0.804	88.6	4.840	3.121
C4	----	0.778	86.4	6.735	2.272
C8	----	0.726	81	9.996	2.123
C12	----	0.623	78	13.17	2.082
C18	----	0.531	79	17.98	2.117



refractive index detector ERC-7510 (Erma, Kingston, MA). System II: PE model 410 pump (Perkin-Elmer, Norwalk, CT); HP model 1050 autosampler (Agilent Tech, Little Falls, DE) and model 401 RI detector (Waters, Millford, MA). The column temperature was set at 25 °C and controlled by a circulating water-bath (Brinkman Model RC6, Lauda-Konigshofen, Germany). All eluents were degassed with a degasser unit (Phenomenex, Torrance, CA).

All HPLC systems were equipped with Turbochrom-4 data acquisition system (Perkin-Elmer, Norwalk, CT).

Extra-column volumes of all systems were determined by direct connection of column inlet and outlet capillaries. The measured extra-column volumes are 53  $\mu\text{L}$  for Waters 401 RI detector (Waters Corp., Millford, MA) and 117  $\mu\text{L}$  for the Erma detector (Erma, Kingston, MA). The average retention volume of a 1  $\mu\text{L}$  injection of 100 ppm benzene solution at 5 different flow rates was used.

### **Solvents and Chemicals**

All solvents and reagents used were high purity HPLC grade (Sigma, Allentown, PA).

### **Dead Volume Measurement by Minor Disturbance Method**

From equation 3-6, a simple method for the determination of dead volume can be derived. If the data for the excess adsorption of the compound of interest on the adsorbent is available, then the dead volume can be calculated using Equation 3-6.

Another method for determining dead volume is based on using the data for the retention of the disturbance peaks (minor disturbance) of a component of the eluent [172,

175]. Excess adsorption for any pure component is always equal to zero because of the assumption of uniformity of the specific molar volume in both the bulk phase and on the surface. If we integrate Equation 3-6 through the entire concentration range

$$\int_{C_{e \min}}^{C_{e \max}} V_R(c_e) = \int_{C_{e \min}}^{C_{e \max}} V_0 dc_e + S \int_{C_{e \min}}^{C_{e \max}} \left( \frac{d\Gamma(c)}{dc} \right) dc_e \quad (3-7)$$

$V_0$  is a constant and by definition,  $\Gamma_{C_{e \min}}(0) = \Gamma_{C_{e \min}}(100) = 0$ , hence

$$V_0 = \frac{\int_{C_{e \min}}^{C_{e \max}} V_R(C_e) dc_e}{C_{\max} - C_{\min}} \quad (3-8)$$

Equation 3-8 gives us a simple method to calculate  $V_0$  from the data generated.

On the basis of this approach, it can be concluded that  $V_0$  should be independent of the type of mobile phase components. Many researchers have confirmed this [97, 163, 172, 195]. For the current study, the minor disturbance method was used to determine the dead volume of five reversed-phase columns using acetonitrile-water as the mobile phase.

## Results and Discussion

The minor disturbance measurements were performed using acetonitrile-water for all five columns studied (refer to Table 3-II). Figure 3-1 represents the retention volume of minor disturbance peak versus the percent acetonitrile in the acetonitrile-water mobile phase. The dead volume measured with the minor disturbance method is actually an integral average (Equation 3-8) of the retention dependence of minor disturbance peaks throughout the entire acetonitrile concentration range. The measured dead volumes for five columns using minor disturbance method are given in Table 3-III. The dead volume values decrease as the alkyl bonded chain length increases since longer alkyl chain occupies more volume.

**Table 3-II.** Acetonitrile/Water minor disturbance retention volumes, in mL, for five columns.

Acetonitrile concentration (% v/v)	C <sub>1</sub>	C <sub>4</sub>	C <sub>8</sub>	C <sub>12</sub>	C <sub>18</sub>
0	2.694	2.817	3.496	4.020	4.258
1	2.373	-----	2.906	3.089	3.125
5	2.309	2.557	2.589	2.530	2.432
10	2.328	2.467	2.438	2.386	2.274
20	2.270	2.297	2.236	2.210	2.122
30	2.131	2.097	2.001	1.964	1.903
35	2.022	1.967	1.865	1.800	1.751
40	1.918	1.807	1.742	1.683	1.628
50	1.636	1.567	1.491	1.410	1.381
60	1.488	1.397	1.352	1.268	1.256
70	1.473	1.387	1.342	1.283	1.244
80	1.589	1.497	1.439	1.376	1.324
90	1.789	1.677	1.609	1.543	1.476
95	1.927	1.797	1.736	1.673	1.597
99	2.227	-----	2.063	1.985	1.921
100	3.027	2.867	2.770	3.224	3.540

----- Not determined.

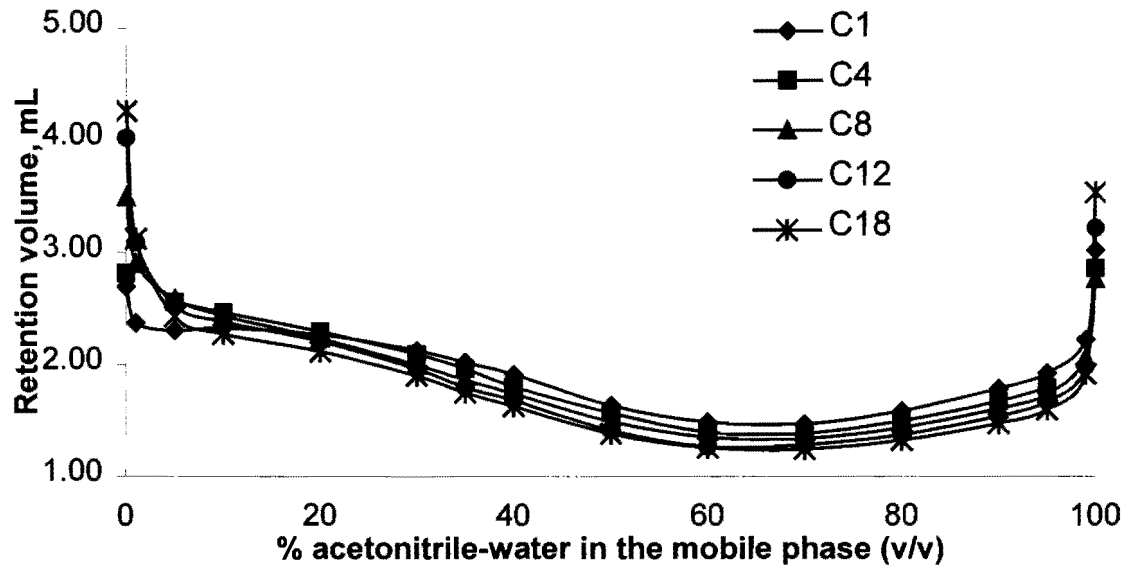


Figure 3-1: Dependencies of the minor disturbance peaks on different columns.

**Table 3-III.** Void volume values measured by minor disturbance method with acetonitrile-water for five columns.

<b>Bonded alkyl chain length</b>	<b><math>V_{md}^*</math> (mL)</b>
C <sub>1</sub>	1.893 ± 0.057
C <sub>4</sub>	1.876 ± 0.020
C <sub>8</sub>	1.814 ± 0.053
C <sub>12</sub>	1.765 ± 0.042
C <sub>18</sub>	1.713 ± 0.036

\* Integral average (using Equation 3-8) of the minor disturbance peak retention dependence (values obtained from Table 3-II) on the eluent concentration.

The standard deviation of the three values obtained, for each column, using three different methods represents the error for the measured dead volume.

The accuracy of the measured dead volume was also studied in our laboratory by three different methods: minor disturbance (three different solvent systems: acetonitrile-, methanol- and tetrahydrofuran-water), isotopically labeled solvents and pycnometry (three different measurements). It was shown [163, 164, 173] that all-different methods give the same value of the volume of liquid phase inside the column – dead volume (2.2% RSD of all measurements).

### **The Adsorbed Layer Volume, $V_s$**

The preferential adsorption of acetonitrile molecules on top of the collapsed bonded phase was discussed in Chapter II. When the thickness of this adsorbed layer is compared using different alkyl bonded chain lengths, it was shown in Chapter II that it does not change much. For the current study, the adsorbed layer volume of acetonitrile at each composition on every column (different bonded alkyl chain length) must be known.

Using the retention volumes obtained from the minor disturbance method for each column, an excess adsorption isotherm was created as described in Chapter II. These isotherms, one for each column, are represented graphically in Figure 2-2 (page 61). For the current study, the isotherm should be represented in terms of adsorbed volume ( $\mu\text{L}/\text{m}^2$ ) for the reasons given below.

Interesting information can be obtained from the adsorption isotherm of acetonitrile and water. Everett [174] had described the interpretation of the excess adsorption isotherm of binary mixtures (e.g., acetonitrile-water). The procedure proposed by Everett [174] allow the estimation of the maximum total amount of organic component that could be accumulated in

the adsorbed layer. As illustrated in Figure 3-2, Everett showed using the monomolecular adsorption model, the crossing of the tangent to the slope of the excess adsorption isotherm in the saturation region (linear portion of the excess adsorption isotherm) with the y-axis represents the reciprocal value of the adsorbate molecular area (if the graph is plotted as  $\mu\text{moles}/\text{m}^2$  versus mole/L). The molecular area of the acetonitrile molecule may be obtained by dividing the reciprocal maximum amount adsorbed by Avogadro's number. Using this technique, it was shown that acetonitrile adsorption has multilayer character [163, 164, 173].

For the current study, the number of layers or the thickness of this layer are not important, but the volume of this layer (one of the four variables needed to predict the retention volume) is of interest. The linear decrease of the excess adsorption with the increase of the equilibrium concentration is associated with the saturation of the adsorbed layer. Extrapolation of this slope towards the y-axis will give the maximum possible (absolute) volume of adsorbed component that could be accumulated in the adsorbed layer. To calculate the adsorbed layer volume, Everett [174] showed that if the excess adsorption isotherm were plotted as  $\mu\text{L}/\text{m}^2$  versus volume fraction of analyte being adsorbed (acetonitrile for the current study), the extrapolation of the linear portion would be the volume of the adsorbed layer per unit area ( $\text{m}^2$ ). Since the surface area of the column is already known, the volume of the saturated adsorbed acetonitrile layer can be obtained.

Excess adsorption isotherms of acetonitrile from water have been measured by means of the minor disturbance method. The following step by step calculation is shown as an example using  $\text{C}_{18}$  column. The calculations on other four columns were performed using identical steps. The retention volume values over the entire composition range are given in Table 3-II (for all five columns). Excess adsorption values [ $\mu\text{L}/\text{m}^2$ ] were calculated using the

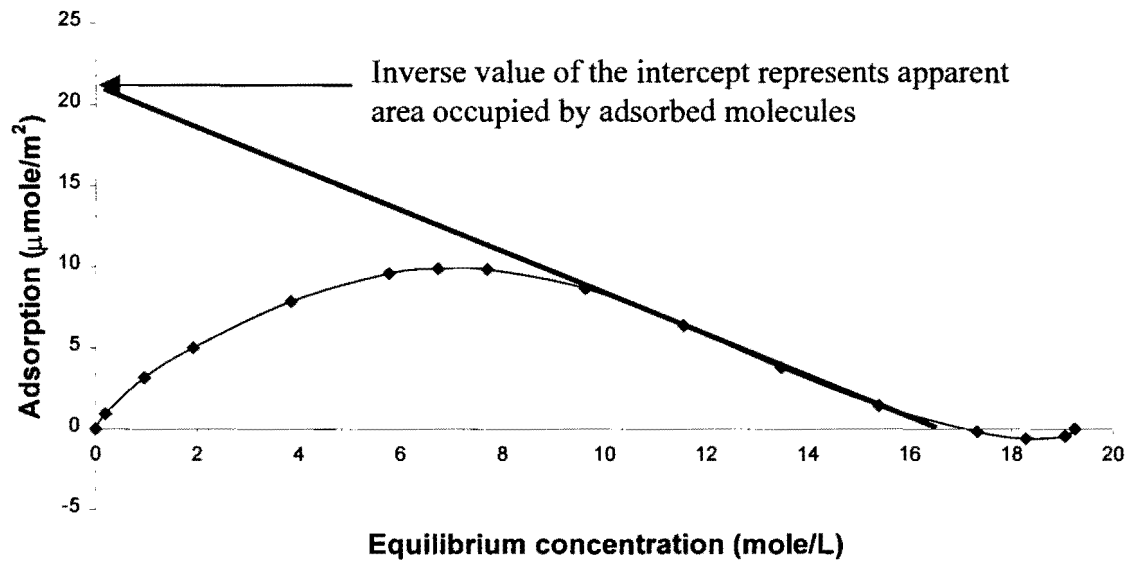


**Figure 3-2.** Determination of the molecular area of adsorbed molecule from the excess adsorption isotherm using Everett's [174] approach.



following equation (derived from Equation 3-6) and using the surface area of the adsorbent in the column.

$$\Gamma^{(v)}(C_e) = \int_{C_e \text{ min}}^{C_e \text{ max}} \left( \frac{V_R(C_e) - V_0}{S} \right) dc \quad (3-9)$$

$V_R(C_e)$  is taken from Table 3-II,  $V_0$  is taken from Table 3-III and  $S$  is taken from Table 3-I. Once the integration is performed, the values found for  $\Gamma^{(v)}(C_e)$  are given in column A of Table 3-IV for each volume fraction of acetonitrile. When column A is plotted versus column B (volume fraction of acetonitrile in the mobile phase), an excess adsorption isotherm is generated in terms of volume, for this case. The excess adsorption isotherms for each column are given in Figure 3-3.

The linear portion of the excess adsorption isotherm is from 0.5 to 0.8 volume fraction of acetonitrile (refer to Figure 3-3 and 3-4). An Y-intercept of extrapolated line of this linear portion was calculated and the value obtained for C<sub>18</sub> column is 1.007  $\mu\text{L}/\text{m}^2$ . This volume represents the maximum saturated adsorbed layer volume of acetonitrile at equilibrium per unit surface area. The adsorbed layer volume is constant under the assumptions described in Chapter II. To determine the adsorbed layer volume at equilibrium at each volume fraction of acetonitrile in the mobile phase, each volume fraction of acetonitrile is multiplied with 1.007  $\mu\text{L}/\text{m}^2$ . The resulting value is denoted as  $a_e$  and is given in column C of Table 3-IV. The difference between  $a_e$  and  $\Gamma$  is shown schematically at the bottom of Figure 3-4. The total saturated adsorbed layer volume at each volume fraction of acetonitrile is determined as the sum of  $a_e$  and  $\Gamma$  and this value is given in column D of Table 3-IV. To get the total volume of acetonitrile adsorbed at each volume fraction of acetonitrile, the sum of  $a_e$  and  $\Gamma$  is multiplied by the surface area of the column and the found values are

**Table 3-IV: Excess adsorption of acetonitrile on a C<sub>18</sub> column (in terms of volume).**

A	B	C	D	E
		$a_c$	$\Gamma + a_c$	
$\Gamma$ (vol)	vol frac (v)	$1.007*v$	$\Gamma + 1.007*v$	Adsorbed layer volume for whole column
$\mu\text{L}/\text{m}^2$		$\mu\text{L}/\text{m}^2$	$\mu\text{L}/\text{m}^2$	(mL)
<b>-2.1014 E-16</b>	1.00	1.007	1.007	0.37
<b>-0.0274</b>	0.99	0.997	0.969	0.36
<b>-0.0324</b>	0.95	0.957	0.924	0.34
<b>-0.0086</b>	0.90	0.906	0.898	0.33
<b>0.0755</b>	0.80	0.806	0.881	0.33
<b>0.1910</b>	0.70	0.705	0.896	0.33
<b>0.3156</b>	0.60	0.604	0.920	0.34
<b>0.4217</b>	0.50	0.503	0.925	0.34
<b>0.4778</b>	0.40	0.403	0.881	0.33
<b>0.4809</b>	0.35	0.352	0.833	0.31
<b>0.4655</b>	0.30	0.302	0.768	0.29
<b>0.3848</b>	0.20	0.201	0.586	0.22
<b>0.2542</b>	0.10	0.101	0.355	0.13
<b>0.1680</b>	0.05	0.050	0.218	0.08
<b>0.0533</b>	0.01	0.010	0.063	0.02
<b>0</b>	0.00	0.000	0.000	0.00

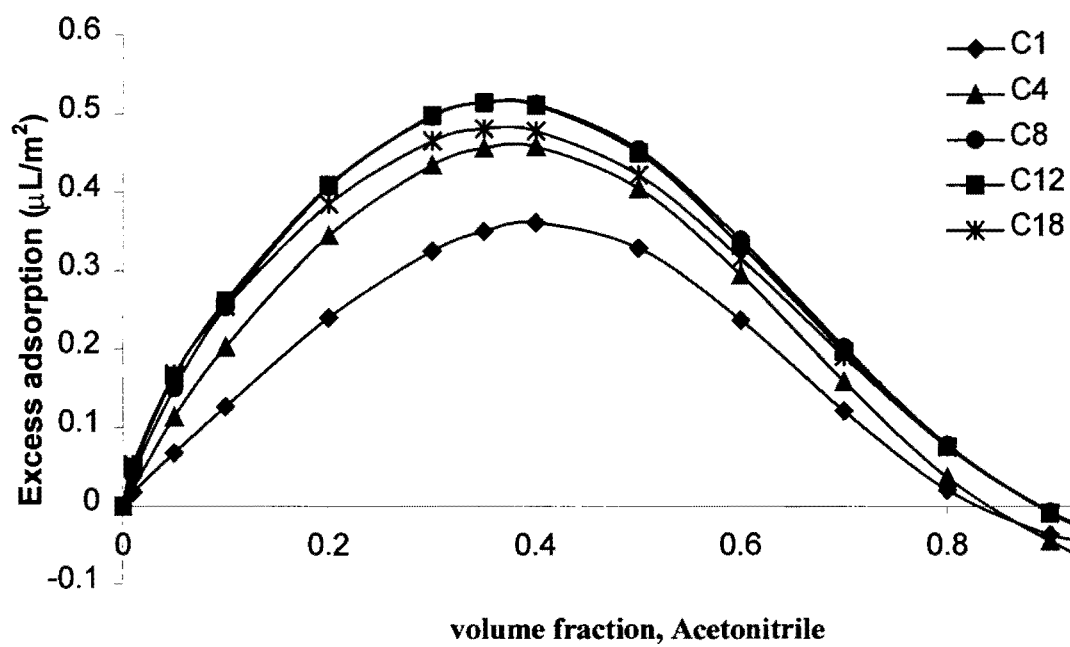
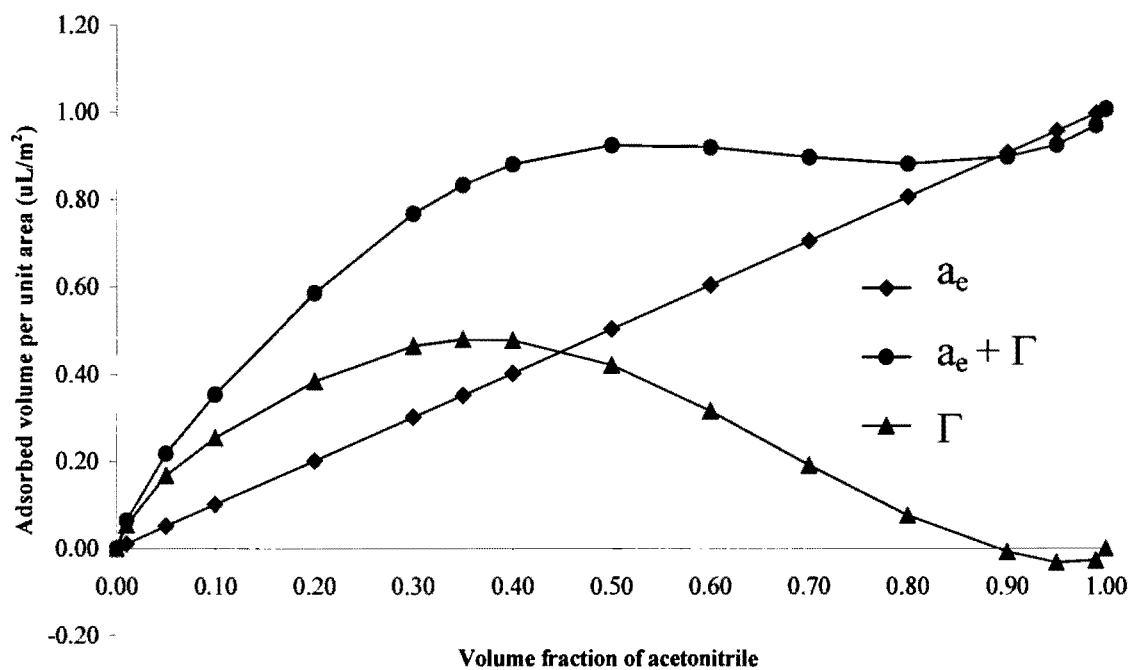
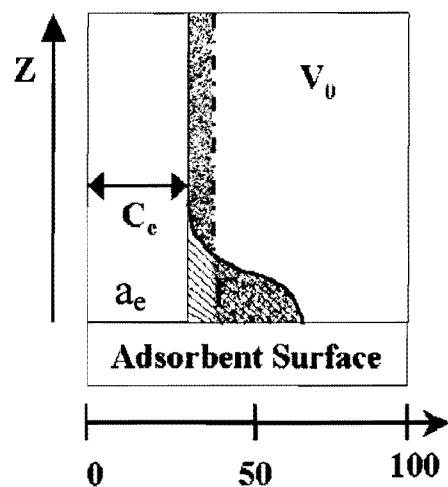


Figure 3-3: Excess adsorption of acetonitrile from water on different bonded alkyl chains.



**Figure 3-4:** Estimation of the maximum adsorbed volume ( $a_e$  and  $\Gamma$ ) of acetonitrile on a C<sub>18</sub> column.



Same as Figure 2-1 except the difference between  $a_e$  and  $\Gamma$  is shown here. See text for details.

given in Column E of Table 3-IV. Graphical representation of  $a_e$ ,  $\Gamma$  and  $a_e + \Gamma$  versus volume fraction of acetonitrile is given in Figure 3-4. It can be seen from the graph that the adsorbed layer is saturated starting at approximately 0.4 volume fraction of acetonitrile. Below this region (<0.40 volume fraction of acetonitrile), the calculated adsorbed layer volume indicated in Column E of Table 3-IV will be used.

Table 3-V to 3-VIII are given for the other four columns. The values in these tables were derived as described above for the C<sub>18</sub> column. The calculated adsorbed acetonitrile layer volume is constant from C<sub>18</sub> to C<sub>4</sub> (different bonded alkyl chain length), except for the C<sub>1</sub> column, which has a lower adsorbed acetonitrile volume.

## Experimentally measured retention volumes ( $V_r$ )

### Introduction

Homologous series are often used as chromatographic solutes to determine the suitability of a particular solvent system of stationary phase to perform high-resolution separations. However, homologous series of compounds, which vary by the number of methylene units in their alkyl group, have also been widely used as solutes for fundamental RPLC studies [199]. Their popularity as test compounds stems from the advantages that they offer in terms of the simple relationship between retention factor ( $k'$ ) and the number of methylene units ( $n$ ) for any given homologue in the series [65]:

$$\ln k'_n = n \ln \alpha + \ln \beta \quad (3-10)$$

where  $k'_n$  is the retention factor of the  $n^{\text{th}}$  homologue,  $\alpha$  is the chromatographic selectivity ( $k'_{n+1}/k'_n$ ), and  $\beta$  is the retention factor of the parent functional group of the homologous series [65]. The selectivity is the difference in the change in free energy ( $\Delta\Delta G$ ) between

**Table 3-V:** Excess adsorption of acetonitrile on a C<sub>12</sub> column (in terms of volume).

A	B	C	D	E
		$a_e$	$\Gamma + a_e$	
$\Gamma$ (vol)	vol frac (v)	$1.082*v$	$\Gamma + 1.082*v$	Adsorbed layer volume for whole column
$\mu\text{L}/\text{m}^2$		$\mu\text{L}/\text{m}^2$	$\mu\text{L}/\text{m}^2$	(mL)
-1.921 E-16	1.00	1.082	1.082	0.39
-0.0232	0.99	1.071	1.047	0.38
-0.0303	0.95	1.027	0.997	0.36
-0.0086	0.90	0.973	0.965	0.35
0.0761	0.80	0.865	0.941	0.34
0.1967	0.70	0.757	0.954	0.34
0.3322	0.60	0.649	0.981	0.35
0.4502	0.50	0.541	0.991	0.36
0.5107	0.40	0.433	0.943	0.34
0.5140	0.35	0.379	0.893	0.32
0.4978	0.30	0.324	0.822	0.30
0.4087	0.20	0.216	0.625	0.23
0.2611	0.10	0.108	0.369	0.13
0.1652	0.05	0.054	0.219	0.08
0.0495	0.01	0.011	0.060	0.02
0	0.00	0.000	0.000	0.00

**Table 3-VI:** Excess adsorption of acetonitrile on a C<sub>8</sub> column (in terms of volume).

A	B	C	D	E
		$a_c$	$\Gamma + a_c$	
$\Gamma$ (vol)	vol frac (v)	$1.092*v$	$\Gamma + 1.092*v$	Adsorbed layer volume for whole column
$\mu\text{L}/\text{m}^2$		$\mu\text{L}/\text{m}^2$	$\mu\text{L}/\text{m}^2$	(mL)
-4.993 E-16	1.00	1.092	1.092	0.37
-0.0177	0.99	1.081	1.063	0.36
-0.0278	0.95	1.037	1.010	0.34
-0.0071	0.90	0.983	0.976	0.33
0.0780	0.80	0.874	0.952	0.32
0.2023	0.70	0.764	0.967	0.33
0.3394	0.60	0.655	0.995	0.34
0.4546	0.50	0.546	1.001	0.34
0.5125	0.40	0.437	0.949	0.32
0.5140	0.35	0.382	0.896	0.31
0.4965	0.30	0.328	0.824	0.28
0.4069	0.20	0.218	0.625	0.21
0.2532	0.10	0.109	0.362	0.12
0.1505	0.05	0.055	0.205	0.07
0.0407	0.01	0.011	0.052	0.02
0	0.00	0.000	0.000	0.00

**Table 3-VII:** Excess adsorption of acetonitrile on a C<sub>4</sub> column (in terms of volume).

A	B	C	D	E
		$a_e$	$\Gamma + a_e$	
$\Gamma$ (vol)	vol frac (v)	$1.030*v$	$\Gamma + 1.030*v$	Adsorbed layer volume for whole column
$\mu\text{L}/\text{m}^2$		$\mu\text{L}/\text{m}^2$	$\mu\text{L}/\text{m}^2$	(mL)
-1.653 E-16	1.00	1.030	1.030	0.37
-0.0639	0.99	1.019	0.955	0.34
-0.0444	0.95	0.978	0.934	0.33
0.0367	0.90	0.927	0.963	0.34
0.1585	0.80	0.824	0.982	0.35
0.2943	0.70	0.721	1.015	0.36
0.4048	0.60	0.618	1.023	0.36
0.4579	0.50	0.515	0.973	0.35
0.4564	0.40	0.412	0.868	0.31
0.4346	0.35	0.360	0.795	0.28
0.3446	0.30	0.309	0.654	0.23
0.2028	0.20	0.206	0.409	0.15
0.1137	0.10	0.103	0.217	0.08
0	0.05	0.051	0.051	0.02
0	0.01	0.010	0.010	0.00
0	0.00	0.000	0.000	0.00



**Table 3-VIII:** Excess adsorption of acetonitrile on a C<sub>1</sub> column (in terms of volume).

A	B	C	D	E
		$a_e$	$\Gamma + a_e$	
$\Gamma$ (vol)	vol frac (v)	$1.007*v$	$\Gamma + 1.007*v$	Adsorbed layer volume for whole column
$\mu\text{L}/\text{m}^2$		$\mu\text{L}/\text{m}^2$	$\mu\text{L}/\text{m}^2$	(mL)
-4.053 E-16	1.00	0.852	0.852	0.31
-0.0204	0.99	0.844	0.823	0.30
-0.0408	0.95	0.809	0.769	0.28
-0.0359	0.90	0.767	0.731	0.26
0.0209	0.80	0.682	0.703	0.25
0.1218	0.70	0.596	0.718	0.26
0.2366	0.60	0.511	0.748	0.27
0.3288	0.50	0.426	0.755	0.27
0.3612	0.40	0.341	0.702	0.25
0.3505	0.35	0.298	0.649	0.23
0.3251	0.30	0.256	0.581	0.21
0.2396	0.20	0.170	0.410	0.15
0.1268	0.10	0.085	0.212	0.08
0.0676	0.05	0.043	0.110	0.04
0.0178	0.01	0.009	0.026	0.01
0	0.00	0.000	0.000	0.00

solutes  $n$  and  $n+1$  for the transfer between the mobile and stationary phase. The magnitude and sign of  $\beta$  are characteristics of the parent functional group, whereas  $\alpha$  is influenced by the homologue unit's chemical properties. It has been shown by many researchers [1, 14, 15, 40, 45-48, 59, 200] that there is a constant contribution to the free energy of retention (and therefore to  $\ln k'$ ) with each methylene increment in the alkyl chain. Since both  $\alpha$  and  $k'$  are thermodynamic quantities, the terms in Equation 3-10 will also depend on the mobile phase and stationary phase composition and the temperature of the chromatographic system [65].

### **Effect of bonded alkyl chain length on RPLC retention**

Numerous studies discussing the effects of changing the length and/or the density of the alkyl chain ligand on the retention behavior in connection with the separation mechanism in RPLC have been published [14, 20, 55, 56, 91, 140, 199, 201-212]. The scientific literature contains contradictory results regarding the influence of the alkyl chain length and/or density on the retention in RPLC [14, 20, 55, 56, 91, 140, 199, 201-212].

Claessens et al. [201] and Scott and Kucera [14] linearly correlated  $k'$  and percent carbon and corrected retention volume and percent carbon, respectively, for various commercial octadecyl and octyl columns. Shaikh and Tomaszewski [202] found a linear relationship between  $k'$  and carbon loading for seven commercial octadecyl packing whereas Engelhardt and Ahr [203] noted linearity between  $\log k'$  and percent carbon for four commercial octadecyl phases. Using stationary phases of varying alkyl chain lengths, Spacek et al. [204] found linear behavior between  $k'$  and percent carbon, whereas Lochmuller and Wilder [20] and Hemetsberger et al. [91] found such plots to be curved. For such stationary phase systems, Hemetsberger et al. [91] and Berendsen and de Galan [205]

obtained linear plots of  $\log k'$  versus percent carbon. Jinno and Kawasaki [55] successfully correlated stationary phase percent carbon and capacity factor for various benzyl-modified phases. Comparison of chromatographic retention behavior of stationary phases prepared with different types of reagents, alkyl chain lengths, and/or silica substrates adds these variables to an already complex situation and may explain the inconsistencies among the conclusions drawn by these different groups. Furthermore, early in the history of bonded phases, Unger et al. [206] pointed out that carbon content is misleading because of differences in the surface area of the original silica which results in different surface densities of the bonded alkyl groups.

Other researchers have synthesized stationary phases from the same batch of base silica by using the same silane reagent on different amounts in order to make bonded phases with various carbon loading, thus eliminating the above variables. Tomellini et al. [207] show, for six non-end-capped monomeric octyl phases,  $\log k'$  first increases as a function of octyl surface coverage and then levels off at higher coverage. Miller et al. [208] observed the same sort of behavior for three monomeric octadecyl bonded phases and noted that the point at which  $\log k'$  begins to plateau is dependent upon solute polarity; polar solutes approach a constant  $\log k'$  value at lower surface coverage than for nonpolar solutes.

Some researchers have examined solute retention as a function of increasing alkyl chain length of the bonded ligands. Colin et al. [209], Jinno [210], Jinno and Kawasaki [55], and Tanaka et al. [56] found that  $\log k'$  increased with increasing bonded chain length. Spacek et al. [204] and Berendsen and de Galan [205] have also noted a general trend of increased retention with increasing chain length of the bonded ligand, but their results were less conclusive than those of Jinno and Kawasaki [55]. Hennion et al. [189], using bonded

phases of constant surface coverage but with bonded chains varying in length from 4 to 18 carbon atoms, found that for nonpolar solutes  $\log k'$  increases linearly with the number of carbon atoms in the bonded ligand; polar solutes exhibited a linear relationship between  $k'$  and bonded chain length. Further, they stated that these results are indicative that the total length of the bonded alkyl chain is available to interact with the solute. Roumeliotis and Unger [211] came to the same conclusion by obtaining a linear relationship between  $\log k'$  normalized to the surface area of the bonded phase (for both polar and nonpolar solutes) and the total hydrocarbonaceous surface area (HAS) of the bonded ligand for C<sub>4</sub>, C<sub>8</sub>, C<sub>12</sub> and C<sub>16</sub> bonded phases. Hennion et al. [212] also observed increasing  $\log k'$  values as a function of HAS for C<sub>4</sub> to C<sub>22</sub> alkyl-bonded phases.

It is not clear from any of these studies that the trends noted are due to actual increased partitioning of the solute into the longer alkyl chains (as many of them have stated). It is also unclear as to whether solute retention actually reaches a limiting value as alkyl surface coverage increases or whether these trends are an artifact of the retention parameter measured. In all of these studies the capacity factor,  $k'$ , was used to quantitate retention (partitioning mechanism was assumed). The  $k'$  is defined as  $K_{eq}$  (partition equilibrium constant) times the phase ratio. The following question was raised in Chapter I. What is phase ratio (especially the stationary phase volume)? As stated before, stationary phase volume increases as chain length increases. Do we count the volume of the adsorbed molecules on the surface as a part of mobile phase or the stationary phase? Therefore, it is unclear whether solute retention increases because of increasing partition equilibrium constant or merely because of the phase ratio increase.

Sentell and Dorsey [140] also studied the effect of bonding density on RPLC retention. They actually calculated phase ratio and expressed their results in terms of  $K_{eq}$  since they knew the phase ratio and the capacity factor. Their conclusion was that the retention levels off or plateaus beyond bonding density of  $3.1 \mu\text{mole}/\text{m}^2$ . Since adsorption will show an increase in retention as bonding density is increased, they concluded that this is evident of partitioning mechanism in RPLC. Closely examining their procedure of determining the mobile phase volume ( $V_m$ ) and stationary phase volume ( $V_s$ ) reveals that they did not take solvent adsorption into the account when calculating  $V_m$  or  $V_s$ . They determined mobile phase volume by solvent disturbance peak, which is dependent on the eluent composition (refer to Figure 3-1). Their calculation of stationary phase volume does not account for the adsorbed volume either. So, the validity of their conclusion can also be questioned as well as their conclusion about the retention mechanism. Most of all, in all of the studies sited here, partition mechanism was thought to be taking place. But as pointed out in Chapter I, neither the partitioning nor adsorption alone cannot describe the retention in RPLC.

#### **Effect of mobile phase composition on RPLC retention.**

While the fundamental mechanism or mechanisms of RPLC are still unresolved, a number of useful empirical observations of great practical significance have been established. One of the most important of these is the relationship between retention and mobile phase composition [213]. The dependence of reversed-phase retention ( $k'$ ) on organic modifier composition (%B in binary solvent system) is of interest for several reasons. First, the study of this relationship for a wide range of solutes and separation conditions might provide

insight into the fundamental basis of analyte retention in RPLC; i.e., the retention mechanism. Second, reversed-phase retention data are widely used to estimate octanol-water partition coefficient ( $\log P_{o/w}$ ). These procedures typically require extrapolation of values of  $k'$  as a function of %B to pure water (0 %B); hence a knowledge of how  $k'$  depends on %B is relevant to this application. Third, changes in %B often result in significant changes in relative retention or selectivity [214]; a better understanding of the  $k'$ -%B relationship should lead to a more effective use of solvent strength (%B) as a means of optimizing HPLC separation.

Based on various models of the retention process, many such relationships have been proposed. Due to its simplicity, one of the most useful, however approximate, of these is the logarithmic-linear relationship given below:

$$\ln k' = \ln k'_w - S\varphi \quad (3-11)$$

where  $k'$  is the solute retention factor at a specific mobile phase composition ( $\varphi$ ) and  $k'_w$  is the extrapolated  $k'$  for pure water ( $\varphi=0$ ).  $\ln k'_w$  is the intercept of the relationship defined by equation 3-11 and  $S$  is the slope of the plot of  $\ln k'$  vs.  $\varphi$  where  $\varphi$  is the volume fraction of organic modifier. In fact equation 3-11 is not particularly accurate. It has been shown that a quadratic form, refer to Equation 3-12, is generally better, at least from the point of view of statistical goodness of fit [215].

$$\ln k' = \ln k'_w + S_1\varphi + S_2\varphi^2 \quad (3-12)$$

Equation 3-12 has the additional virtue of being derivable based on regular solution theory [25, 50] and simple lattice model [28]. However, for practical work, equation 3-11 is usually

preferred and over a sufficiently narrow range in mobile phase composition it is usually quite satisfactory.

The experimental dependence of retention on solvent composition  $\phi$  in RPLC has received considerable attention [215, 216]. Numerous studies [215, 216] and references therein] have been reported which purport to show the validity of equation 3-11, usually by means of correlation coefficients;  $R^2 = 1$  for various solutes and a range in values of  $\phi$ . It has been shown [217, 218] that depending on the solvent used, the best fitting equation could be different. For example, for one analyte studied on methanol and acetonitrile, equation 3-11 might fit best to methanol and equation 3-12 fits best to acetonitrile. Most data suggest that [215, 216] equation 3-11 is generally a good approximation for methanol and THF as solvents, while acetonitrile generally gives some-what curved plots of  $\log k'$  vs.  $\phi$ .

The relative curvature of plots of  $\log k'$  vs.  $\phi$  is also affected by the value of the column dead volume assumed for a given data set. Because there is considerable controversy over the best way of measuring  $V_o$ , this represents another uncertainty in the evaluation of different equations as predictors of  $k'$  vs.  $\phi$ .

Several other authors [219, 220] have compared the applicability of various fitting equations for  $k'$  vs.  $\phi$  in the case of a smaller number of different data sets. The results are in some cases contradictory and no compelling conclusions can be reached as to the superiority of a particular fitting equation. The data reviewed by Valko et al. [215] suggested that no single equation will provide the best fit of  $k'$  vs.  $\phi$  for all data sets (values of  $k'$  vs.  $\phi$  for a given solute, solvent and other conditions).

It is not the intend of the current study to find a solution to the above problem. The retention equation (Equation 2-28) derived in Chapter II on the basis of the proposed partition/ adsorption model may provide the solution of the problem stated above.

$$V_R = V_0 + (K_P - 1)V_s + SK_p K_H \quad (2-28)$$

The above equation can be rearranged as follows to measure  $k'$ :

$$\frac{V_R - V_0}{V_0} = k' = \frac{(K_P - 1)V_s}{V_0} + \frac{SK_p K_H}{V_0} \quad (3-13)$$

Equation 3-13 shows the complex dependence of the  $k'$  vs. eluent composition, which is dependent on the analyte distribution constant ( $K_P$ ) and adsorbed layer ( $V_s$ ). Due to this complex relationship, whether we find a linear correlation or not, it is irrelevant in this study since both, the predicted and experimental data sets will be compared using the same analysis (*ln k' vs.  $\phi$* ).

For the current study, the effect of bonded alkyl chain length ( $C_1$ ,  $C_4$ ,  $C_8$ ,  $C_{12}$  and  $C_{18}$ ) and acetonitrile-water binary mixture as mobiles phase (10% increment throughout the concentration range of acetonitrile) are studied using two different homologue series: alkyl benzenes (non-polar) and alkyl ketones (polar). Temperature is another variable in HPLC, so it was held constant at 30°C.



## **Experimental**

### **Adsorbents and Columns**

Same as described earlier in this chapter.

### **Solvents and Chemicals**

All solvents used were high purity HPLC grade (Sigma-Aldrich, Allentown, PA). All of the analytes used were at least 98% pure (Fluka - Sigma-Aldrich, Allentown, PA).

### **HPLC system and conditions**

All experimental retention volumes of all analytes were measured on the following HPLC system: PE model 200LC pump, autosampler model ISS200 and diode array detector model 235C (Perkin-Elmer, Norwalk, CT). The column temperature was thermostated at 30.0 °C with a water jacket (Alltech, Chicago, IL) and controlled by a circulating water-bath (Brinkmann Model RC6, Lauda-Konigshofen, Germany). The thermocouple (type K) was inserted into the water jacket and wrapped around the column. The temperature was measured using a thermometer (Control Company, Houston, TX). The thermometer accuracy is  $\pm 0.1^\circ\text{C}$  and the temperature in the water jacket were found to be within  $0.2^\circ\text{C}$ . All eluents were degassed with a degasser unit (Phenomenex, Torrance, CA).

All HPLC systems were equipped with Turbochrom-4 data acquisition system (Perkin-Elmer, Norwalk, CT). In order to get at least 10 points across a peak, the sampling rate was chosen depending upon the expected retention time (from 2 Hz to 10 Hz).

Extra-column volume (between injector and detector cell) of the system was measured by removing the column and connecting the injector line directly to the detector (this included about 1 m long 1/16" ID tubing before the column inside the water jacket). The average retention volume of a 1  $\mu\text{L}$  injection of 100 ppm benzene solution at 5 different flow rates was used. The measured extra-column volume was found to be 85  $\mu\text{L}$ .

All of the retention volumes were measured using flow rate of 1.00 mL/min. The flow rate was measured, before each run (each automated run was programmed for not more than 3 days), with pure water into a 5.0 mL TC volumetric flask and was timed with a stopwatch (Control Company, Houston, TX). In order to obtain an accurate flow rate each time, the flow rate was programmed in the pump in such a way that the measured flow rate, not the programmed one, was always 1.00 mL/min ( $\pm 0.02\text{mL/min}$ ).

Two homologous series were used: Alkyl benzenes (Benzene, Toluene, Ethyl benzene and propyl benzene) and ketones (Acetone, 2-Butanone, 2-Pentanone, 2-Hexanone and 2-Heptanone). All analytes were prepared in the appropriate acetonitrile-water mixture (same as the mobile phase) in the concentration range of 100 ppm to 300 ppm. Injection volume for analytes was varied from 1  $\mu\text{L}$  to 3  $\mu\text{L}$ . Alkyl benzenes were monitored at 254nm and ketones were monitored at 330nm.

The mobile phase composition was varied from 100 % acetonitrile (0 % water) to 0 % acetonitrile (100% water) at 10 % increment. When a composition of the mobile phase was changed, at least 25 column volumes ( $\sim 45$  min) of the new mobile phase were passed through the column before making injections. Acetonitrile and water were placed individually in their respective solvent reservoir and the pump was programmed to get the required mobile phase composition.

The reproducibility of the measured retention volumes (for each analyte at each composition for every column) was obtained by injecting each analyte three times for a given set of conditions. But injections were not made repetitively, rather they were made in three cycles. For example, for a given column, an injection of each analyte was made at each mobile phase composition starting from 100 % acetonitrile down to 0% acetonitrile. Then the whole cycle was repeated twice to get total of three injections. All analytes were injected individually at a given mobile phase composition. Depending upon the obtained retention time for each analyte at each mobile phase composition, the obtained standard deviation was found to be different. Table 3-IX summarizes the largest standard deviation ( $\sigma$ ) found for both homologous series at each mobile phase composition on all studied columns.

For all chromatograms generated, the individual peaks were found to be symmetrical, so the peak maximum was considered an adequate point for measuring retention time.

### **Results and Discussion**

Tables 3-X to 3-XIV list experimentally measured retention volumes (corrected for system volume) of each analyte at studied acetonitrile-water composition on C<sub>18</sub>, C<sub>12</sub>, C<sub>8</sub>, C<sub>4</sub> and C<sub>1</sub> column, respectively. Figures 3-5 to 3-9 gives graphical representation of the experimentally measured data on all five columns for ketone homologue series (from Acetone to Heptanone, respectively). Figures 3-10 to 3-13 gives graphical representation of the experimentally measured data on all five columns for alkyl benzene homologue series (from Benzene to Propyl Benzene, respectively).  $\log k'$  was calculated using equation 3-1. The data for  $V_r$  are taken from Tables 3-X to 3-XIV and the data for  $V_o$  are taken from Table 3-III.

**Table 3-IX:** The largest standard deviation ( $\sigma$ ), in mL, found for the retention volume from the five columns studied for each analyte at given mobile phase composition.

% Acetonitrile	100	90	80	70	60	50	40	30	20	10	0
Acetone	0.085	0.053	0.015	0.013	0.015	0.016	0.018	0.036	0.023	0.042	0.033
2-Butanone	0.056	0.052	0.015	0.012	0.015	0.016	0.020	0.018	0.033	0.135	0.540
2-Pentanone	0.044	0.051	0.018	0.008	0.008	0.017	0.018	0.043	0.069	0.189	-----
2-Hexanone	0.042	0.020	0.014	0.011	0.011	0.225	0.018	0.094	0.140	0.293	-----
2-Heptanone	0.032	0.047	0.017	0.019	0.021	0.031	0.084	0.198	0.853	-----	-----
Benzene	0.033	0.052	0.016	0.014	0.052	0.036	0.037	0.017	0.155	-----	-----
Toluene	0.014	0.049	0.017	0.018	0.028	0.060	0.055	0.003	0.156	-----	-----
Ethyl Benzene	0.040	0.049	0.013	0.021	0.041	0.103	0.142	0.267	-----	-----	-----
Propyl Benzene	0.039	0.056	0.016	0.030	0.076	0.201	0.667	-----	-----	-----	-----

----- The standard deviation was not obtained since there was no retention volume measured for that analyte at that mobile phase composition on a given column.

**Table 3-X:** Experimentally measured retention volume, in mL, (corrected for system volume) of each analyte, on a C<sub>18</sub> column, at a given acetonitrile-water composition.

% Acetonitrile	100	90	80	70	60	50	40	30	20	10	0
Acetone	1.864	1.788	1.807	1.853	1.928	2.026	2.195	2.384	2.677	3.408	11.521
Butanone	1.854	1.848	1.918	2.044	2.222	2.468	2.927	3.462	4.363	6.628	33.773
Pentanone	1.895	1.933	2.068	2.297	2.631	3.142	4.250	5.765	8.668	16.328	-----
Hexanone	1.958	2.050	2.274	2.644	3.231	4.199	6.691	10.853	20.276	47.765	-----
Heptanone	2.043	2.201	2.558	3.144	4.143	5.938	11.273	22.434	53.090	-----	-----
Benzene	1.895	2.077	2.436	3.016	3.985	5.735	10.618	18.932	34.402	-----	-----
Toluene	1.982	2.247	2.760	3.620	5.133	8.083	17.661	37.423	83.936	-----	-----
Ethyl Benzene	2.054	2.416	3.126	4.343	6.616	11.430	29.326	73.464	-----	-----	-----
Propyl Benzene	2.169	2.686	3.702	5.529	9.096	17.337	52.360	-----	-----	-----	-----

----- Not determined.

**Table 3-XI:** Experimentally measured retention volumes, in mL, (corrected for system volume) of each analyte, on a C<sub>12</sub> column, at a given acetonitrile-water composition.

% Acetonitrile	100	90	80	70	60	50	40	30	20	10	0
Acetone	1.893	1.814	1.831	1.878	1.946	2.046	2.219	2.402	2.684	3.340	9.249
Butanone	1.869	1.855	1.927	2.041	2.213	2.446	2.890	3.393	4.220	6.169	24.724
Pentanone	1.895	1.918	2.045	2.250	2.564	3.030	4.052	5.418	7.972	14.315	-----
Hexanone	1.934	2.002	2.200	2.526	3.046	3.907	6.104	9.689	17.630	39.749	-----
Heptanone	1.994	2.112	2.409	2.904	3.754	5.282	9.864	19.017	43.468	-----	-----
Benzene	1.875	2.022	2.319	2.814	3.658	5.151	9.318	16.183	28.604	-----	-----
Toluene	1.932	2.133	2.544	3.234	4.482	6.868	14.575	30.164	66.040	-----	-----
Ethyl Benzene	1.979	2.247	2.789	3.747	5.553	9.272	23.287	56.829	-----	-----	-----
Propyl Benzene	2.047	2.413	3.158	4.519	7.232	13.346	39.735	-----	-----	-----	-----

----- Not determined.

**Table 3-XII:** Experimentally measured retention volumes, in mL, (corrected for system volume) of each analyte, on a C<sub>8</sub> column, at a given acetonitrile-water composition.

% Acetonitrile	100	90	80	70	60	50	40	30	20	10	0
Acetone	1.942	1.864	1.877	1.920	1.986	2.090	2.249	2.406	2.654	3.192	6.900
Butanone	1.903	1.893	1.937	2.050	2.212	2.429	2.800	3.231	3.888	5.274	15.790
Pentanone	1.916	1.928	2.025	2.200	2.482	2.892	3.726	4.810	6.705	11.015	43.832
Hexanone	1.931	1.961	2.121	2.398	2.837	3.434	5.245	7.943	13.487	27.756	-----
Heptanone	1.962	2.044	2.253	2.651	3.322	4.524	7.860	14.282	30.428	-----	-----
Benzene	1.873	1.982	2.197	2.600	3.280	4.468	7.508	12.352	20.285	-----	-----
Toluene	1.903	2.047	2.333	2.861	3.820	5.604	10.942	21.171	42.637	-----	-----
Ethyl Benzene	1.933	2.110	2.481	3.179	4.496	7.169	16.332	37.463	-----	-----	-----
Propyl Benzene	1.969	2.203	2.691	3.628	5.493	9.611	25.911	-----	-----	-----	-----

----- Not determined.

**Table 3-XIII:** Experimentally measured retention volumes, in mL, (corrected for system volume) of each analyte, on a C<sub>4</sub> column, at a given acetonitrile-water composition.

% Acetonitrile	100	90	80	70	60	50	40	30	20	10	0
Acetone	1.948	1.868	1.884	1.923	1.988	2.066	2.196	2.337	2.479	2.747	4.050
Butanone	1.890	1.867	1.974	1.993	2.131	2.300	2.582	2.859	3.212	3.782	6.707
Pentanone	1.882	1.874	1.945	2.082	2.295	2.601	3.164	3.795	4.691	6.159	14.407
Hexanone	1.886	1.892	1.994	2.186	2.501	2.991	4.065	5.493	7.900	12.313	-----
Heptanone	1.894	1.910	2.050	2.310	2.754	3.517	5.447	8.591	14.956	-----	-----
Benzene	1.833	1.874	2.021	2.290	2.747	3.504	5.255	7.542	10.408	-----	-----
Toluene	1.842	1.902	2.076	2.410	3.000	4.062	6.876	11.405	18.818	-----	-----
Ethyl Benzene	1.852	1.923	2.135	2.548	3.314	4.805	9.340	18.087	-----	-----	-----
Propyl Benzene	1.863	1.952	2.212	2.729	3.737	5.844	13.321	-----	-----	-----	-----

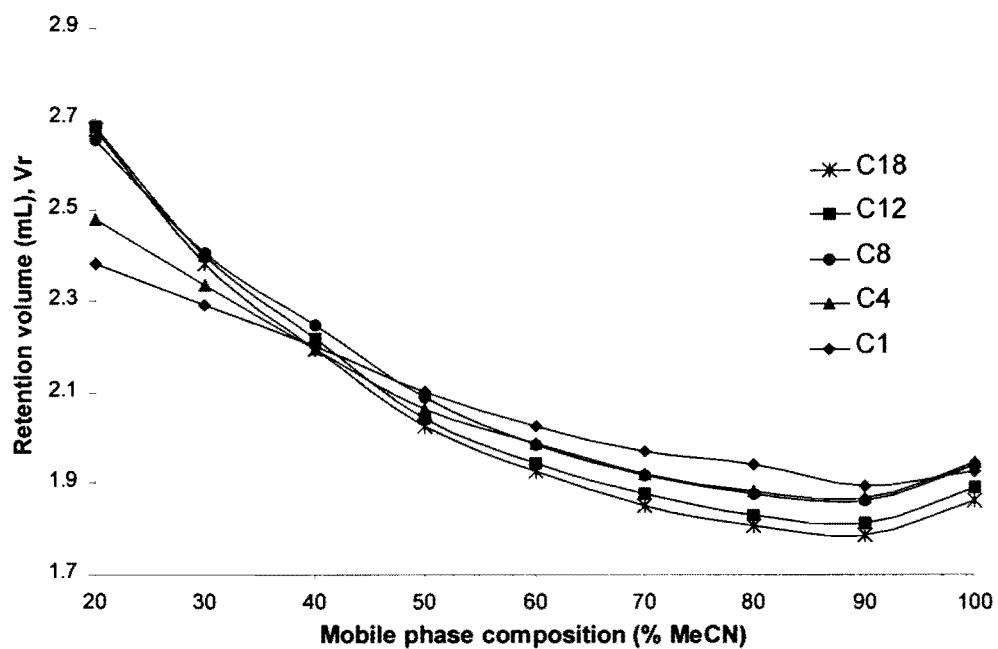
----- Not determined.



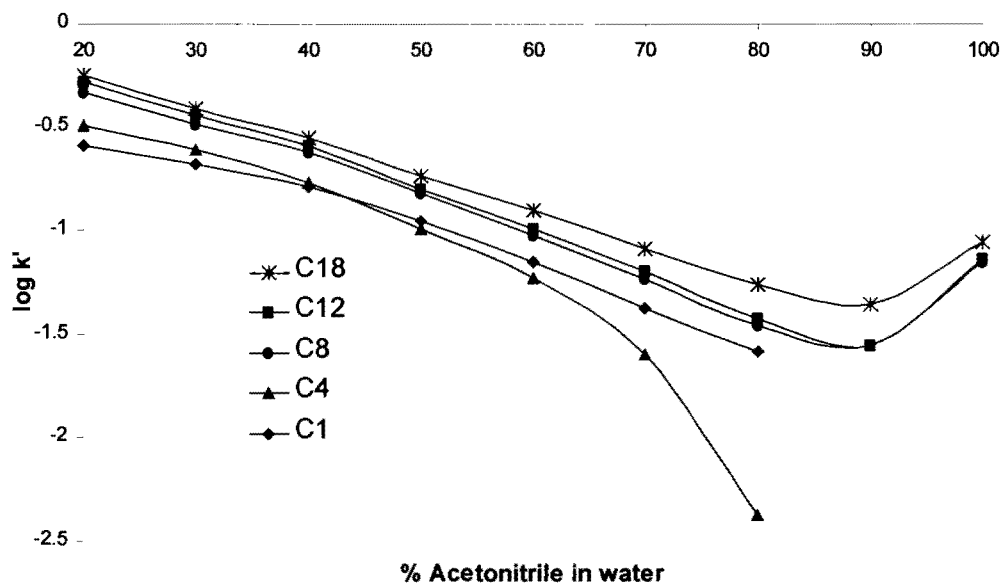
**Table 3-XIV:** Experimentally measured retention volumes, in mL, (corrected for system volume) of each analyte, on a C<sub>1</sub> column, at a given acetonitrile-water composition.

% Acetonitrile	100	90	80	70	60	50	40	30	20	10	0
Acetone	1.928	1.894	1.942	1.972	2.028	2.103	2.203	2.293	2.383	2.515	4.046
Butanone	1.911	1.910	1.940	2.014	2.124	2.271	2.472	2.642	2.823	3.018	6.114
Pentanone	1.905	1.890	1.950	2.054	2.230	2.468	2.837	3.187	3.567	3.926	10.396
Hexanone	1.896	1.893	1.957	2.108	2.347	2.619	3.357	4.066	4.962	5.797	-----
Heptanone	1.897	1.889	1.978	2.157	2.491	3.020	4.078	5.469	7.611	-----	-----
Benzene	1.866	1.867	1.961	2.151	2.518	3.006	3.961	4.904	5.808	-----	-----
Toluene	1.867	1.872	1.979	2.208	2.617	3.316	4.731	6.450	6.851	-----	-----
Ethyl Benzene	1.867	1.874	2.000	2.272	2.763	3.693	5.605	8.834	-----	-----	-----
Propyl Benzene	1.867	1.880	2.028	2.356	2.958	4.181	5.947	-----	-----	-----	-----

----- Not determined.



(A)



(B)

**Figure 3-5:** Experimentally measured retention data for Acetone on all five columns.  
 A. Retention volume, in mL, versus mobile phase composition.  
 B.  $\log k'$  versus mobile phase composition.

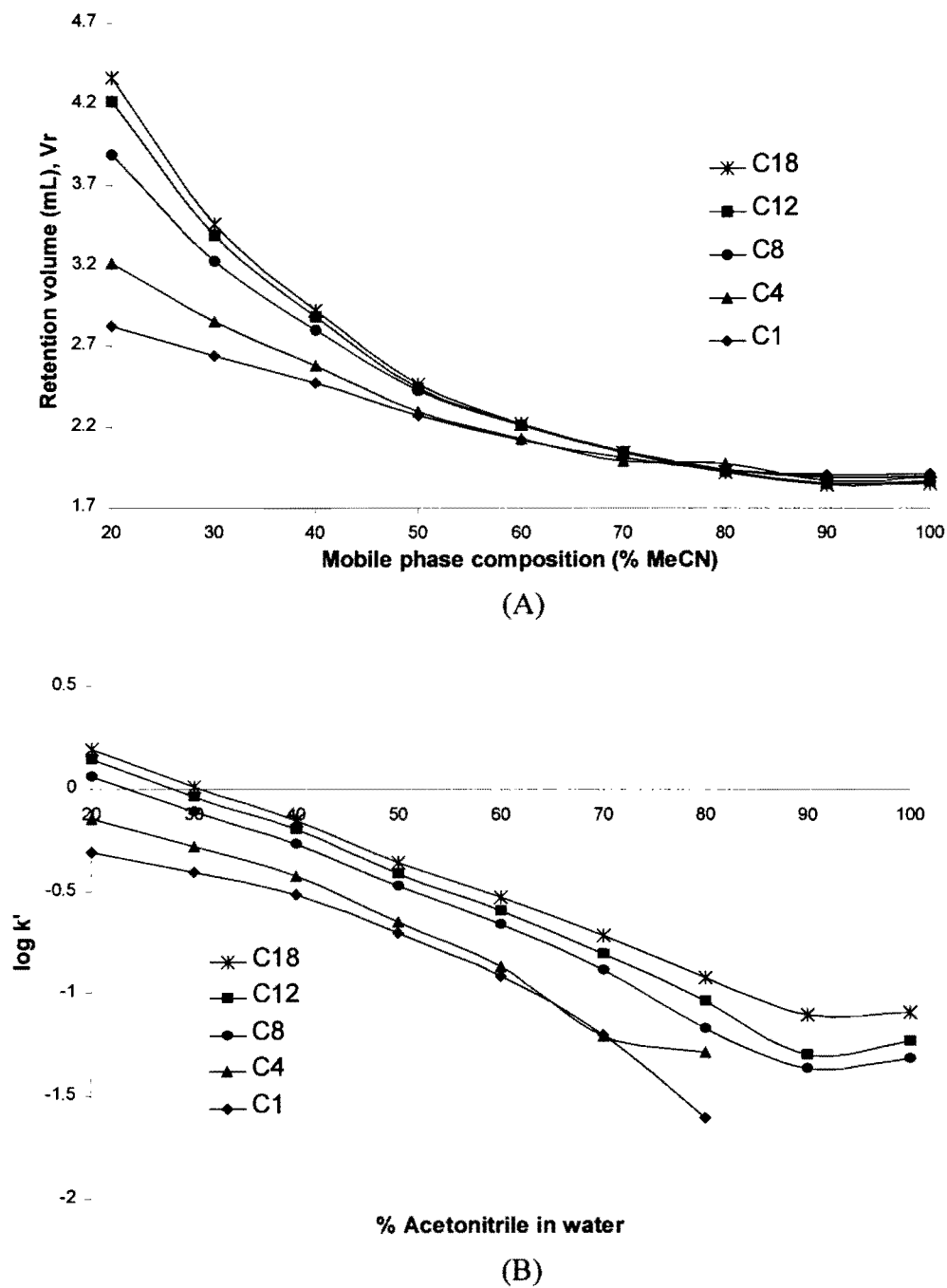
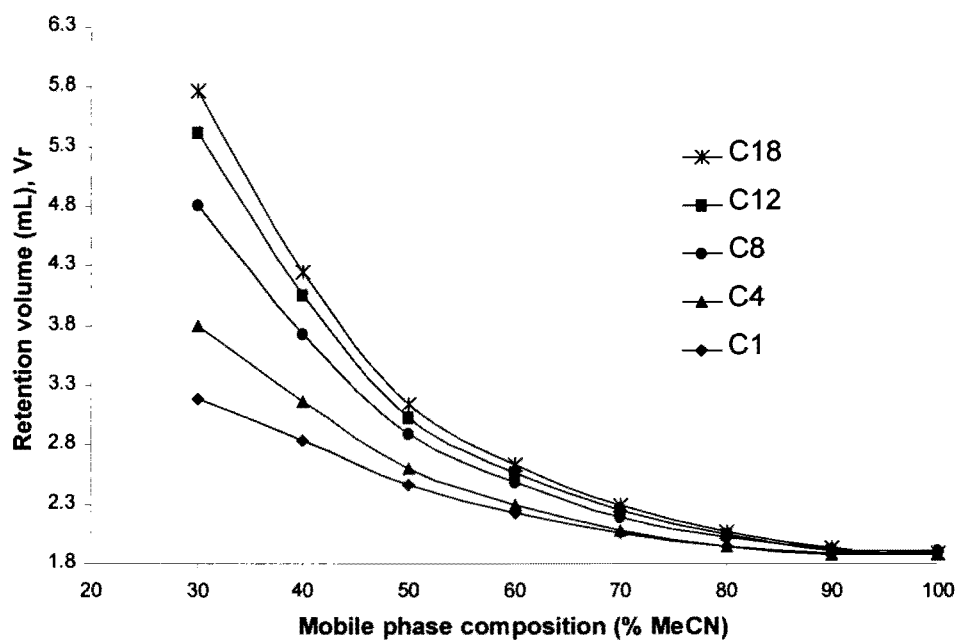
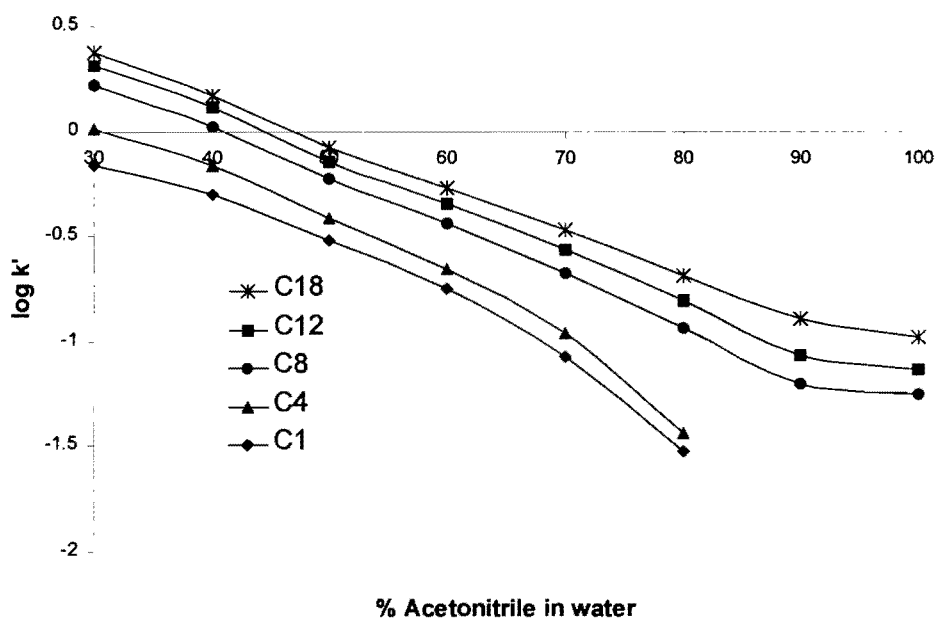


**Figure 3-6:** Experimentally measured retention data for Butanone on all five columns.  
 A. Retention volume, in mL, versus mobile phase composition.  
 B.  $\log k'$  versus mobile phase composition.

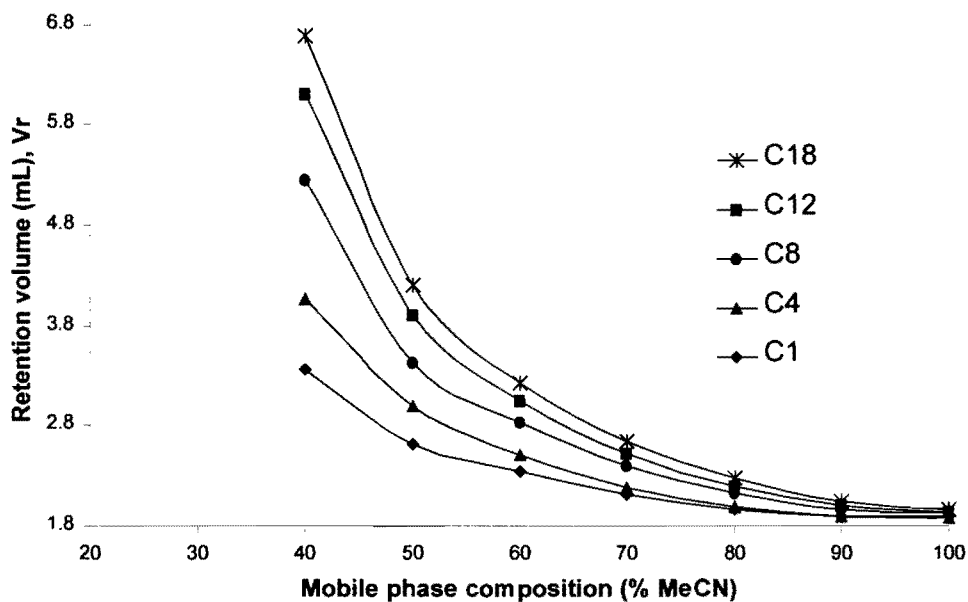


(A)

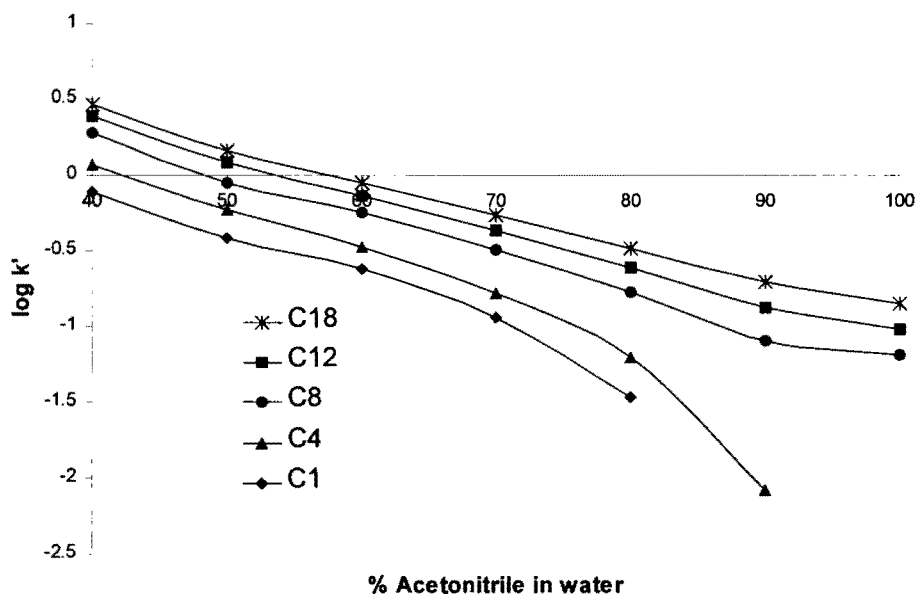


(B)

**Figure 3-7:** Experimentally measured retention data for Pentanone on all five columns.  
 A. Retention volume, in mL, versus mobile phase composition.  
 B.  $\log k'$  versus mobile phase composition.

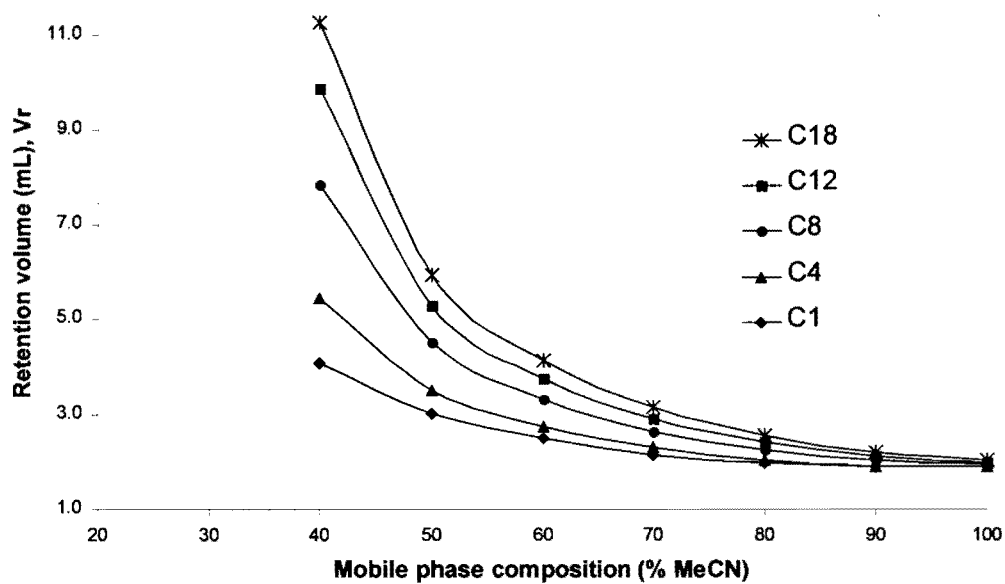


(A)

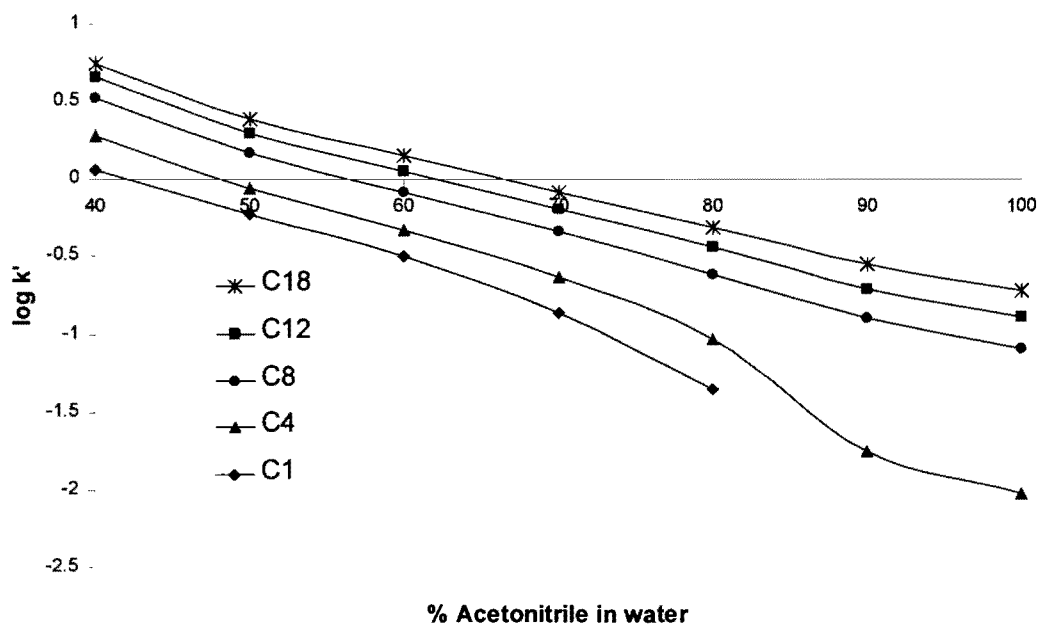


(B)

**Figure 3-8:** Experimentally measured retention data for Hexanone on all five columns.  
 A. Retention volume, in mL, versus mobile phase composition.  
 B.  $\log k'$  versus mobile phase composition.

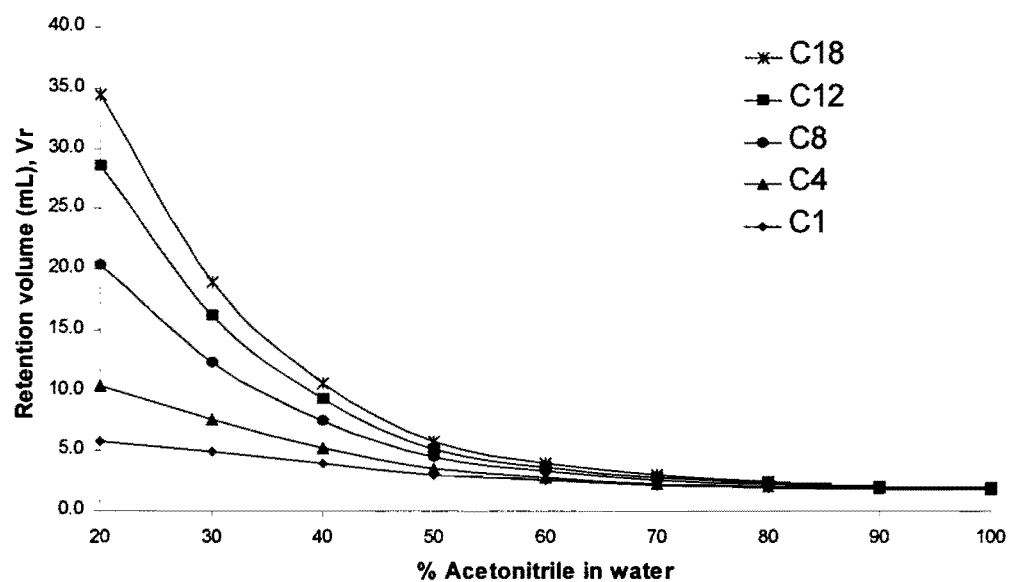


(A)

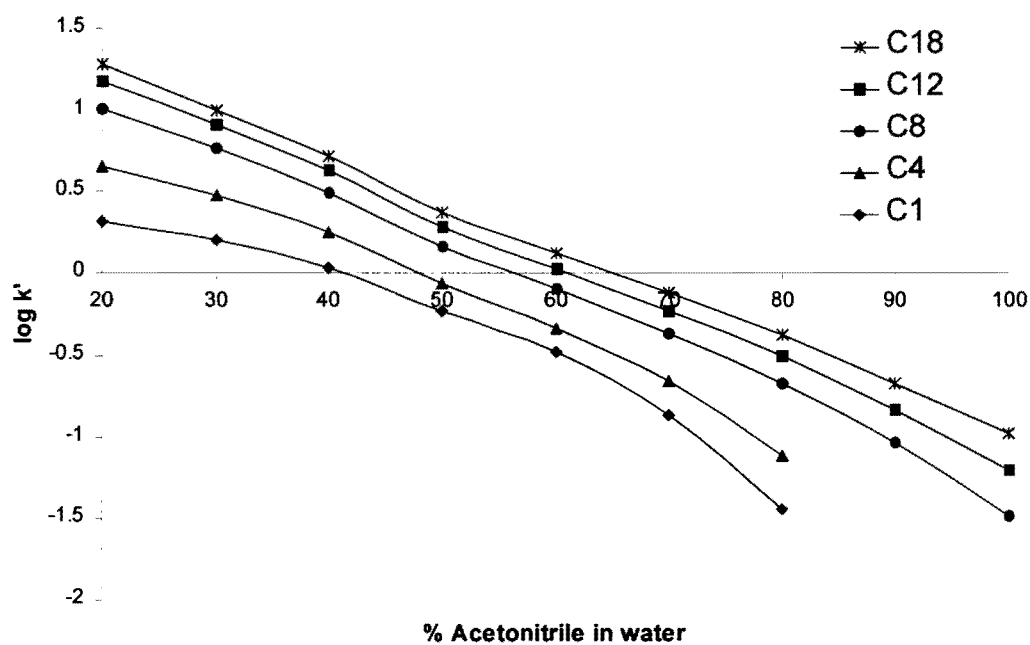


(B)

**Figure 3-9:** Experimentally measured retention data for Heptanone on all five columns.  
 A. Retention volume, in mL, versus mobile phase composition.  
 B.  $\log k'$  versus mobile phase composition.



(A)

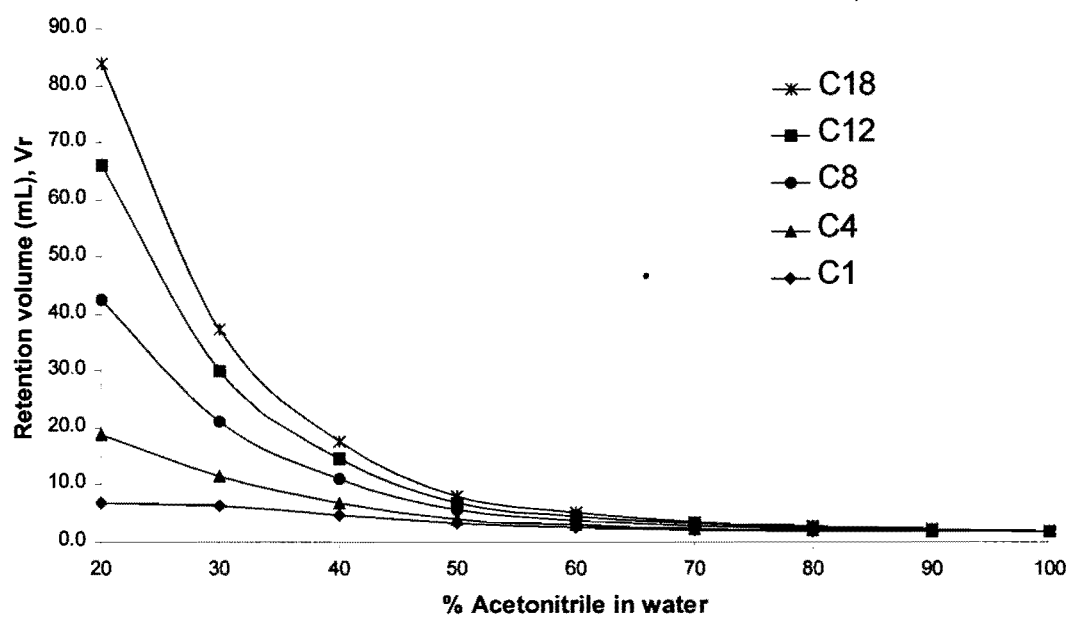


(B)

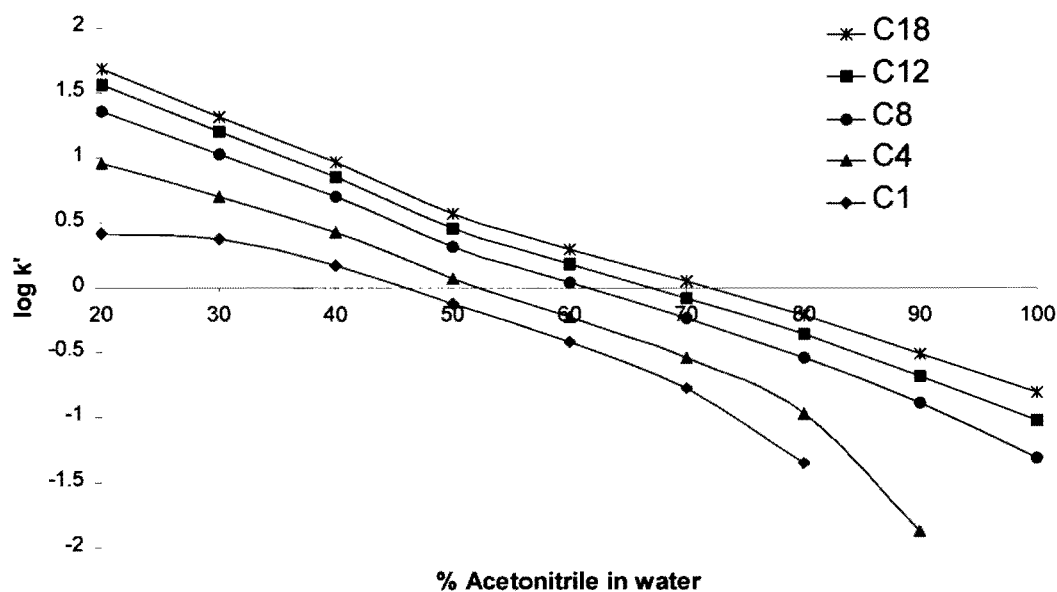
**Figure 3-10:** Experimentally measured retention data for Benzene on all five columns.

A. Retention volume, in mL, versus mobile phase composition.

B.  $\log k'$  versus mobile phase composition.



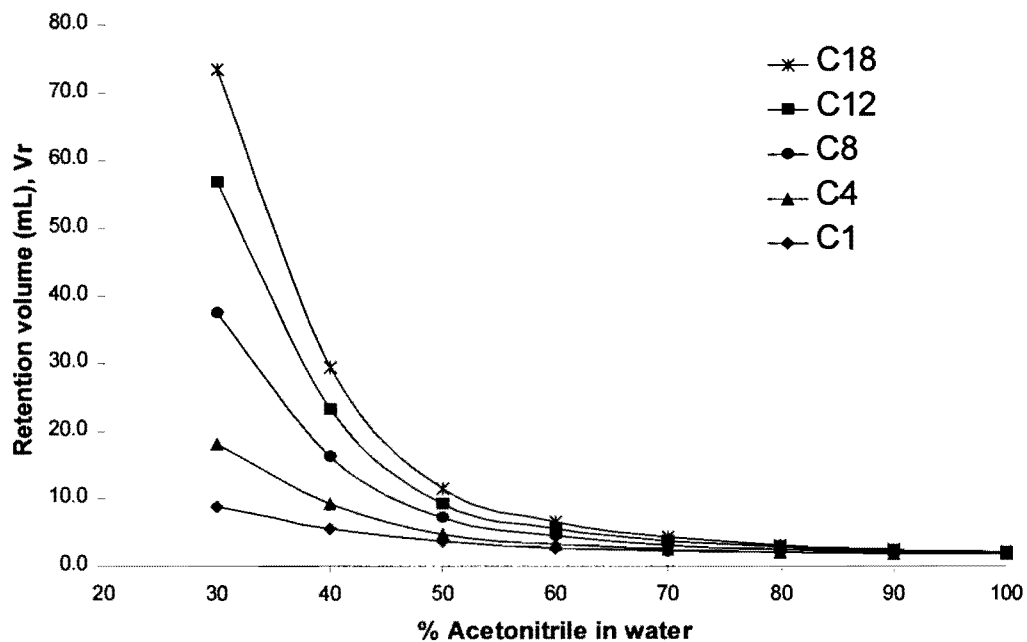
(A)



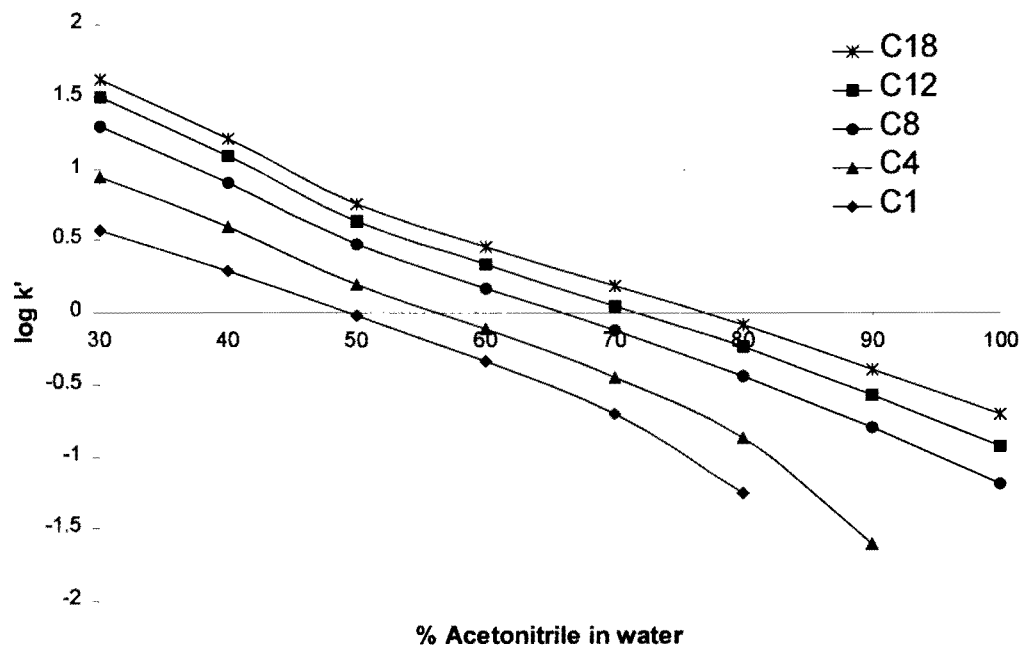
(B)

**Figure 3-11:** Experimentally measured retention data for Toluene on all five columns.  
 A. Retention volume, in mL, versus mobile phase composition.  
 B.  $\log k'$  versus mobile phase composition.



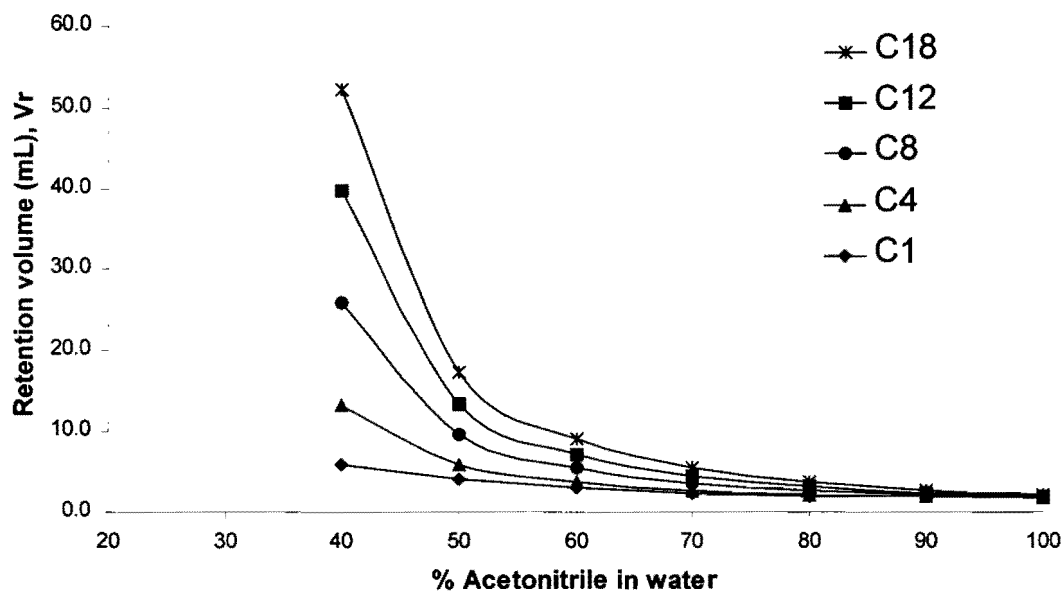


(A)

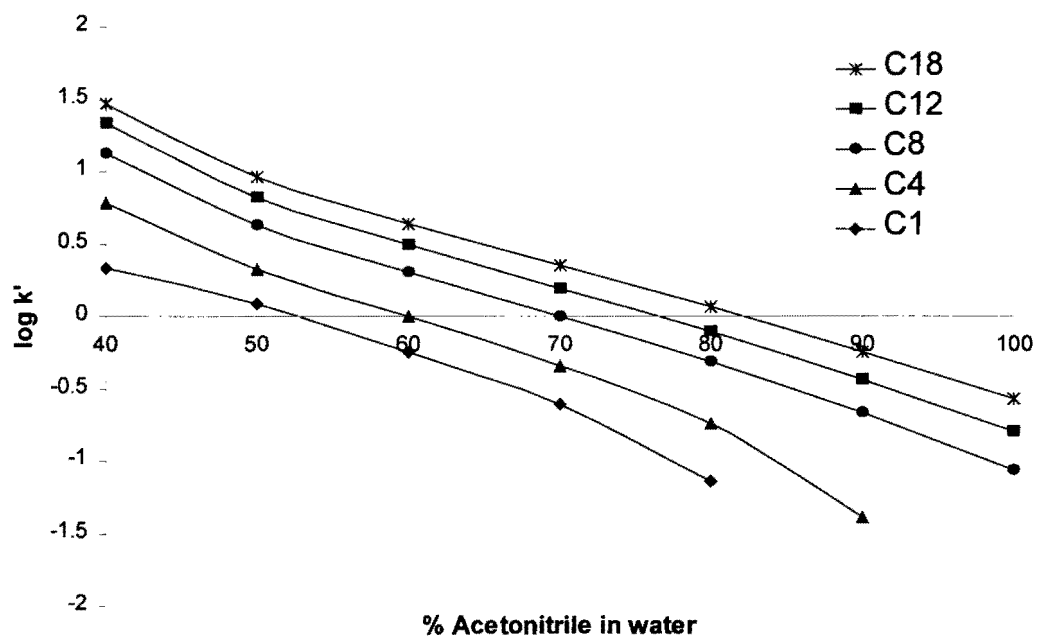


(B)

**Figure 3-12:** Experimentally measured retention data for Ethyl Benzene on all five columns.  
 A. Retention volume, in mL, versus mobile phase composition.  
 B.  $\log k'$  versus mobile phase composition.



(A)



(B)

**Figure 3-13:** Experimentally measured retention data for Propyl Benzene on all five columns.  
 A. Retention volume, in mL, versus mobile phase composition.  
 B.  $\log k'$  versus mobile phase composition.

The three general trends listed below are usually expected for a given set of RPLC data. (i) A retention volume of a given analyte increases as the water content in the mobile phase increases (for a given column). (ii) A retention volume of a given analyte, at a certain acetonitrile-water, decreases as a bonded alkyl chain length decreases. (iii) For a given column and mobile phase composition, retention volume of an analyte increases as the polarity (e.g., from Acetone to Heptanone and Benzene to Ethyl benzene) of the analyte decreases. Some of these trends are noticed in the data given in Tables 3-X to 3-XV. However, some exceptions to the general trends listed above are also observed.

For each column studied the experimentally measured retention volume of Acetone and Butanone decreases as the acetonitrile-water composition changes from pure acetonitrile to 90% acetonitrile. This is opposite of what should happen; as the mobile phase strength decreases the retention volume should increase.

Acetone is the most polar analyte studied here and should show the lowest retention volume on a given column at a given mobile phase composition. The retention volume for Butanone is found to be lower than Acetone on all of the columns studied (pure acetonitrile as the mobile phase). The trend becomes unusual as the bonded alkyl chain length decreases. On a C<sub>8</sub> column, for pure acetonitrile as the mobile phase, the following order of retention volume is observed: Pentanone < Butanone < Acetone < Hexanone < Heptanone. On C<sub>4</sub> and C<sub>1</sub> columns, the retention volume of Acetone is found to be the highest for ketone homologue series. The most unusual result is found on the C<sub>1</sub> column where the retention volume of Acetone is found to be higher than all analytes studied (including alkyl benzenes) for pure acetonitrile as the mobile phase. This is totally unexpected since the other analytes are more non-polar than acetone.

The last trend can be seen better in the next section where the data for the Henry constant,  $K_H$ , are measured for each analyte on all columns studied.

### Henry constant, $K_H$

Henry constant,  $K_H$ , is a slope of the excess adsorption isotherm at low analyte concentration;  $K_H = \lim_{c \rightarrow 0} \frac{d\Gamma}{dc}$ . For the studied analytes, the retention volume for their elution from pure acetonitrile is needed to calculate  $K_H$  as described in Equation 2-30 (page 76). Table 3-XV lists  $K_H$  for each analyte on every column studied. The retention volumes, in mL, for each analyte in pure acetonitrile as the mobile phase are taken from Tables 3-X to 3-XIV (for columns C<sub>18</sub>, C<sub>12</sub>, C<sub>8</sub>, C<sub>4</sub> and C<sub>1</sub>, respectively) and values for  $V_0$ , in mL, are taken from Table 3-III. Figure 3-14 shows the measured  $K_H$  of all analytes versus the carbon number of the bonded alkyl chain length.

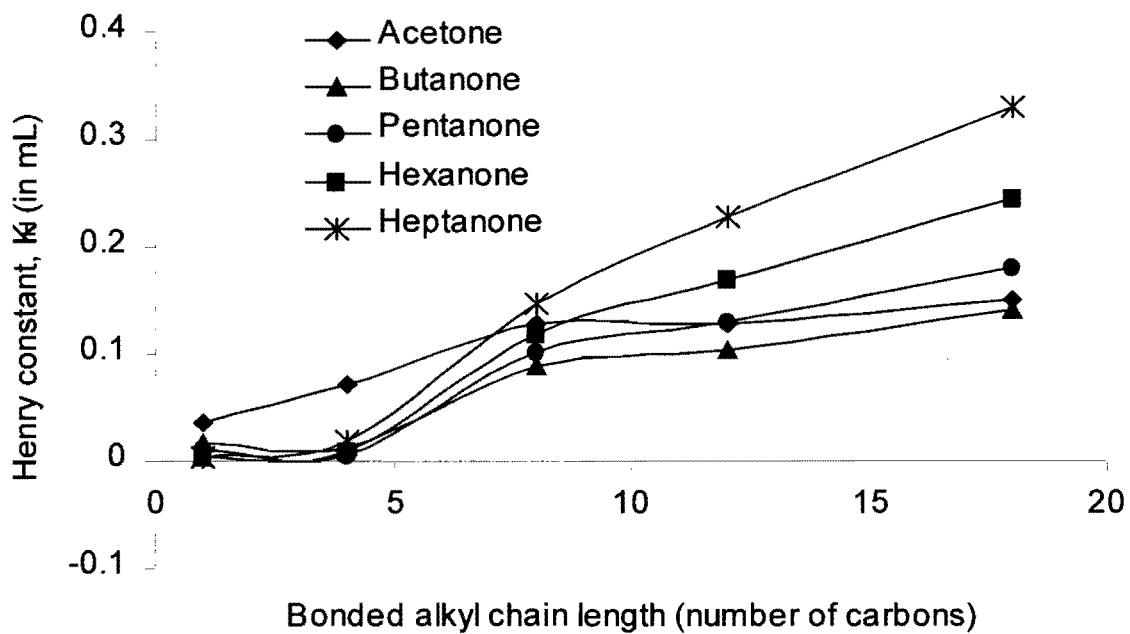
The Henry constant reflects an analyte interaction with the surface (bonded alkyl chains, in this case). The observed trend for Henry constant is that as the carbon number of the bonded alkyl chain length decreases (C<sub>18</sub> to C<sub>8</sub> only), their values decrease. For C<sub>4</sub> and C<sub>1</sub>, we have an unusual trend for all analytes studied. Acetone shows a very unusual trend since it shows that on C<sub>4</sub> and C<sub>1</sub> column, it was adsorbed much higher than all other analytes (giving higher  $K_H$  values). This is unusual, as stated in the last section, since other analytes are more non-polar than Acetone. Alkyl benzenes have negative  $k'$  values on C<sub>4</sub> and C<sub>1</sub> columns indicating that they were not adsorbed on the surface, rather, they were repelled giving  $V_r$  less than  $V_0$ .

The explanation of the trend observed here could be attributed to the specific effects of the surface, especially residual silanols. The effect of residual silanols is greater on the

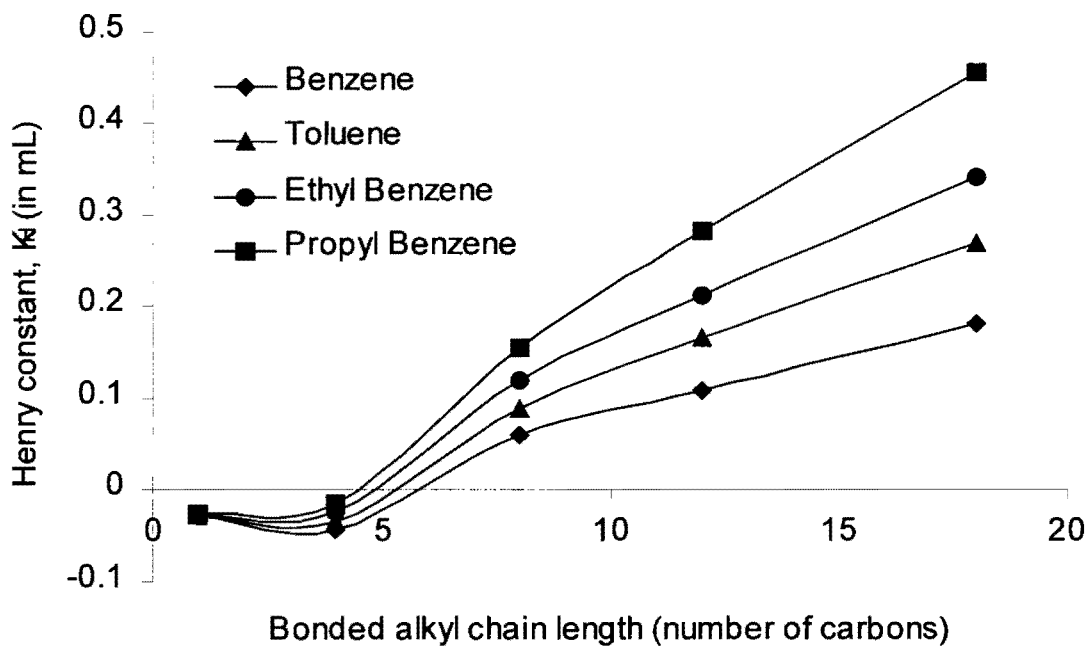
**Table 3-XV:** Measured Henry constant,  $K_H$ , (in mL) for all analytes studied on every column.

Analyte	C <sub>18</sub>	C <sub>12</sub>	C <sub>8</sub>	C <sub>4</sub>	C <sub>1</sub>
Acetone	0.151 ± 0.021	0.128 ± 0.025	0.128 ± 0.044	0.072 ± 0.011	0.035 ± 0.091
Butanone	0.141 ± 0.020	0.104 ± 0.024	0.089 ± 0.046	0.013 ± 0.012	0.017 ± 0.064
Pentanone	0.182 ± 0.021	0.130 ± 0.024	0.102 ± 0.053	0.006 ± 0.011	0.011 ± 0.054
Hexanone	0.245 ± 0.020	0.169 ± 0.025	0.118 ± 0.044	0.010 ± 0.012	0.003 ± 0.052
Heptanone	0.330 ± 0.020	0.228 ± 0.024	0.148 ± 0.051	0.018 ± 0.012	0.003 ± 0.045
Benzene	0.182 ± 0.020	0.109 ± 0.023	0.060 ± 0.044	-0.043 ± 0.012	-0.027 ± 0.034
Toluene	0.269 ± 0.020	0.167 ± 0.024	0.089 ± 0.043	-0.035 ± 0.012	-0.027 ± 0.034
Ethyl Benzene	0.341 ± 0.020	0.213 ± 0.023	0.119 ± 0.049	-0.024 ± 0.012	-0.027 ± 0.035
Propyl Benzene	0.456 ± 0.020	0.282 ± 0.023	0.155 ± 0.049	-0.014 ± 0.013	-0.026 ± 0.035

The errors were calculated by performing propagation of error using the standard deviation of the column's dead volume and retention volume of an analyte at 100% acetonitrile composition.



(A)



(B)

**Figure 3-14:** Measured Henry constant (in mL),  $K_H$ , of all analytes (A-Ketones and B-Alkyl Benzenes) versus carbon number of bonded alkyl chain length for all five columns.

shorter bonded alkyl chains since the distance between the residual silanols and analyte is greatly reduced, thus giving higher electrostatic interactions. The more polar the analyte, higher the interactions and this leads to longer retention for polar analytes on shorter bonded alkyl chains.

When the explanation presented above is applied to the generated data, it makes sense since acetone was retained the longest on the shorter bonded alkyl chains. In addition, all of the non-polar analytes were repelled from the stationary phase, thus giving retention volumes less than  $V_o$ .

## Conclusions

In this chapter, three of the four independent variables ( $V_o$ ,  $V_s$  and  $K_H$ ) of Equation 2-28 were measured using RPLC. All three variables were measured independently in a binary system (e.g., acetonitrile-water or acetonitrile-analyte). All of these parameters will be used in Chapter V to calculate the theoretically predicted retention volume,  $V_R$ , of an analyte at given conditions (e.g., acetonitrile-water composition, column etc.).

The experimentally measured retention volumes,  $V_r$ , given in this chapter for all analytes at each acetonitrile-water composition on all five columns will be compared to the theoretical predicted retention volume,  $V_R$ , under identical conditions to see the validity of the model presented in Chapter II.

We still need one more parameter to predict the retention volume using Equation 2-28. This parameter is  $K_P$  and this was measured using headspace gas chromatography. The next chapter discusses the measurement of  $K_P$ .

## **Chapter IV: Measurement of $K_p$ by Headspace Gas Chromatography (HS-GC)**

### **Summary**

An isochoric headspace system is introduced. This system is known to work at atmospheric pressure. The principles of the isochoric headspace system are also discussed. Two different methods (Isochoric vapor extraction and Isochoric vapor loading) are introduced for vapor transfer and measurement processes. Step-by-step procedures followed by theories for both of the isochoric methods are then described. A procedure is described to calibrate different volumes of the isochoric headspace system.

For the current study, measuring gas-liquid distribution constants followed by the liquid-liquid partition coefficient, more emphasis is placed on the vapor loading method. Step-by-step calculation of a gas-liquid distribution constant using the vapor loading method is given followed by a discussion on the precision and accuracy of the given vapor loading method using the isochoric headspace system. Finally, the results for gas-liquid distribution constants and liquid-liquid partition coefficients for all analytes in given acetonitrile-water mixture are given and discussed.

### **Introduction**

The study of the thermodynamic vapor-liquid phase equilibrium (VLE) of solutions has many practical applications, such as designing cost-effective industrial separation processes, estimating the emissions of volatile hazardous chemicals from wastewater streams into the atmosphere, and providing guidance in the selection of solvents for chemical reactors in which kinetics solvent effects are important. The measurement of the limiting activity



coefficient of the solute under infinite dilution or the vapor-liquid partitioning Henry's constant or gas-liquid distribution constant (inverse of vapor-liquid partitioning Henry's constant) can provide a better understanding of the mechanism of solute-solvent molecular interactions, for the development of theoretical thermodynamic models.

There are many techniques available for VLE studies. Comprehensive reviews on the measurement techniques and detailed comparisons of the data obtained using these methods have been conducted [222-224]. The usual conditions for studying the distribution between the gas- and the liquid phase are at equilibrium (static) conditions with very low analyte concentration. It is assumed that at these conditions the analyte-analyte interactions in both phases are negligible and analyte-solvent interactions exists only in the liquid phase. These conditions are considered to be ideal (components activity coefficients are equal to 1) and the ratio of the analyte concentration in the liquid phase to the analyte concentration in the gas phase is constant. The definition of the gas-liquid distribution constant,  $K$ , assuming ideal analyte conditions, is given in Equation 4-1.

$$K = \frac{C_e^L}{C_e^G} \quad (4-1)$$

where  $C_e^L$  is the concentration of the analyte in the liquid phase at equilibrium, and  $C_e^G$  is the concentration of the analyte in the gas phase at equilibrium.

Headspace gas chromatography (HSGC) gives a direct quantitative analysis of the vapor over liquid sample matrix and, therefore, is very suitable for VLE studies. The traditional HSGC methods [225-227] for VLE studies require quantitative determination of the equilibrium solute concentration both in the vapor and in the liquid phases through direct measurements, using error-producing calibration procedures. Kolb et al. [228] developed

another direct measurement technique, the vapor-phase calibration method, which simplifies the calibration procedure but requires that, the solute concentration in the original sample is known. To obtain experimental simplicity and high accuracy for practical applications, automated indirect HSGC methods will be desirable. The methods of McAuliffe [229] and others [230, 231] indirectly calculate the VLE partitioning from two separate headspace measurements. The first headspace analysis is conducted under equilibrium. The system equilibrium is then altered by mechanically venting part of the vapor. The second headspace analysis is conducted after the system reestablishes its equilibrium. With this type of indirect method, it is impossible to achieve measurement simplicity, automation and consistency, due to mechanical difficulty [228]. The multiple headspace extraction (MHE) method [232] was developed using the same concept. However, the method described in the literature [232] has many practical variants that could cause large experimental uncertainties.

The inverse of  $K$ , is equal to the dimensionless Henry's constant,  $H_C$ , if the solute is under infinite dilution, i.e,  $1/K = H_C$  [233]. Two independent measurements are required to obtain the  $K$  value of a VLE problem. Both liquid and vapor phases are directly analyzed in traditional methods, while two independent headspace measurements were made using the indirect headspace methods discussed above. From the physics of a VLE problem, an analyte is distributed into two unknown phases from its initial state to the equilibrium state, and the mass of the analyte is conserved during the distribution. In mathematical terms, the problem at phase equilibrium involves two unknown variables and can be solved with two equations. Therefore, it is sufficient and necessary to make two and only two independent measurements to solve a VLE problem using any indirect HSGC method.

Lincoff and Gossett [234-235] developed an indirect HSGC method to determine Henry's constants using EPICS (equilibrium partitioning in closed systems) and solute mass conservation. In their method, two sample vials were used and the volume ratio of the two testing solutions was arbitrarily taken to be ten [234] and four [235]. The mass of the solute in the two solutions was equal [234], or the mass ratio was measured [235]. It was assumed that the solute in two solutions was under infinite dilution, therefore, the VLE partitioning coefficients of the solute in these two solutions are equal to the dimensionless Henry's constant at a given temperature. The advantages of the EPICS method are that no special apparatus is required and it can be easily automated. Henry's constant can be obtained by measuring the vapor concentration ratios from a pair of sealed vials with different solution volumes and solute concentrations through HSGC. However, the EPICS method has the following limitations:

- (1) it requires that one know the ratio of the amount of solute in the two solutions or the concentrations;
- (2) because the concentrations of the solutions in the two testing vials were different, according to the experimental procedure proposed in paper [234], the measurements were only valid when the method was based on the assumption that the solute was under infinite dilution. Therefore, the procedure according to that described in their experiments is only applicable to measure the Henry's constant of the solute.
- (3) it requires standard addition to the original sample to obtain two testing solutions with different concentrations when applying the method to the analysis of an industrial or environmental sample of unknown concentration. So, one must know the solute mass or concentration of the original solution in order to obtain the mass ratio of the two testing

solutions. Therefore, the experimental procedures proposed by Lincoff [234] are not applicable to solutions of unknown concentration.

- (4) The measurement error is very high when the Henry's constant is less than 0.1 (or  $K > 10$ ), as indicated by the precision analysis of Gossett [235].

Ettre et al. [231] developed another indirect HSGC method, phase ratio variation (PRV), to measure the VLE partitioning coefficient  $K$  based on solute mass conservation and equilibrium headspace (EHS). The authors derived a linear equation whose slope is related to  $K$  as a function of the vapor phase concentration,  $C_G$ , at equilibrium (measured by GC), solute concentration in the original solution  $C_L^0$  (constant), and a volume ratio parameter,  $\beta$  (known constant), which was called the phase (volume) ratio in the paper [233]. They then used four vials filled with the same solution but with different volumes. They conducted a headspace measurement for each vial at equilibrium to derive the slope of the linear equation, in order to determine the solute partitioning coefficient,  $K$ . The method requires at least four independent measurements to determine the slope or  $K$ . Again, the method is not accurate when large partitioning coefficients of  $K$  ( $>144$ ) are to be measured, as indicated by Ettre et al. [233].

Practically all headspace techniques [225-235] employ the analyte equilibration in closed vial containing a known volume of the liquid phase with known starting concentration of the analyte. After achieving the equilibrium an aliquot of the vapor phase is transferred into GC for analysis. The resulting analyte peak area is proportional to the analyte concentration in the vial gas phase.

All equilibrium (static) headspace methods [225-235] are based on the following relationships

$$n_0 = c_0^L V_0^L \quad (4-2)$$

$n_0$  is the number of moles of analyte introduced into the headspace vial in the form of the solution with initial concentration  $c_0^L$  and volume  $V_0^L$ . Vial is closed and set into the HS system at chosen temperature for equilibration [230].

After achieving the equilibrium (at temperature  $T$ ), analyte is distributed between the vapor phase and the liquid phase, which could be written in the form

$$n_0 = c_e^L V^L + c_e^G V^G \quad (4-3)$$

where  $c_e^L$  and  $c_e^G$  are the corresponding analyte concentrations in the liquid and in the gas phase at equilibrium,  $V^L$  and  $V^G$  are the volumes of liquid and gas phases, respectively.

The sum of these two volumes is equal to the volume of the vial used and is constant.

The individual volumes in general are not the same as they were at starting conditions.

Solvent evaporation may play noticeable role in the change of these volumes during equilibration. This is especially true at large  $\beta$  (ratio of  $V^G/V^L$ ) values.

Combining equations 4-1 to 4-3, equation 4-4 is obtained:

$$c_0^L V_0^L = c_e^G (K V^L + V^G) \quad (4-4)$$

This is the main equation for gas-liquid distribution constant determination using static headspace methods. All proposed methods [225-235] for HSGC determination of  $K$  are based on this equation.

It is useful to perform some simple analysis of Equation 4-4. By dividing both sides by  $c_e^G V_0^L$  (assuming that this product is not equal to zero):

$$\frac{c_0^L}{c_e^G} = K \frac{V^L}{V_0^L} + \frac{V^G}{V_0^L} \quad (4-5)$$

The constant volume of the introduced liquid phase is assumed, then  $V^L/V_0^L=1$  and Equation 4-5 simplifies to:

$$\frac{c_0^L}{c_e^G} = K + \frac{V^G}{V_0^L} \quad (4-6)$$

If analyte concentration in the original solution is known then  $K$  could be calculated directly from Equation 4-6 ( $c_e^G$  is measured by GC;  $c_0^L$ ,  $V^G$ , and  $V_0^L$  are known from experimental set up). If the original analyte concentration is unknown, then either phase ratio variation (PRV) [228, 229, 233, 235-237], or multiple headspace extraction (MHE) [232, 238, 239] methods could be used. Several publications were devoted to the introduction of new methods for GC-HS measurements of analyte distribution constants [43, 240, 241], at closer look they are but slight variations of basic PRV method first described in [228, 229, 233, 235-237].

It is essential to mention that for both PRV and MHE methods, the phase ratio in the HS vial should be on the same order of magnitude as the distribution constant. If, for example,  $K$  is on the order of 1000 and for PRV method the sample phase ratio was set below 10 in all vials. The difference in HSGC measured data for these vials will be well within the experimental error, which is on the level of 1% for most GC experiments. Detailed analysis or the experimental errors arising from this limitation is given in [242]. This effect leads to the necessity of introducing a very small volume (5 – 50  $\mu$ L) of liquid sample into the HS vial with the vial volume usually on the level of 20 mL. In this case solvent evaporation during the equilibration step will introduce a significant error. To correct this problem the

volume ratio change due to the solvent evaporation should be accounted and Equation 4-5 should be used in all calculations, which significantly complicates the procedure for calculating the  $K$ .

Another significant problem with conventional HS technique arises from the commonly employed method of headspace sample introduction into GC system [239]. In HSGC, the sample vial is pressurized with inert gas (usually GC carrier gas) to the pressure equal or above the GC column head-pressure. This excessive vial pressure drives the headspace gas phase from the vial into the GC inlet. This means that the headspace system has to do work for the sample to be transferred. This work performed by the system immediately destroys the equilibrium achieved in the vial. So, the transferred amount generally does not represent an equilibrium condition in the headspace vial.

If all operational conditions of HSGC system are maintained constant throughout a series of analysis, quantitative results with calibration performed at the same conditions are valid for typical HSGC experiments [239]. However, any thermodynamic measurements (e.g., partition coefficient) performed on HSGC system require the maintenance of true equilibrium since no calibration is possible for this type of measurements.

Vapor expansion work may result in the local and fast temperature changes in the vial. According to Clausius-Clayperon equation

$$\ln\left(\frac{p}{p_0}\right) = \frac{\Delta H_{evap}}{RT} \left(\frac{1}{T} - \frac{1}{T_0}\right) \quad (4-7)$$

the pressure drop in the HS system leads to the decrease of the temperature, which cause the condensation of saturated vapor and formation of the fog droplets in the vial vapor phase.

Vapor phase in the vial is saturated with the solvent vapor (whichever solvent is used).

Solvent condensation will happen first close to the point of sample transfer in to GC (at HS needle entrance) and consecutively will cause local changes in the analyte amount in the vapor (analyte could be trapped (dissolved) in the solvent droplets). This effect may introduce significant error in the determination of the analyte distribution constants.

Equilibration kinetics is usually an exponential process. Because the highest rate of the concentration change is at the beginning of the equilibrium disturbance, we have to expect significant influence of the equilibrium disturbance during the sample introduction from the HS vial into the GC system.

Here, an isochoric headspace system is introduced that allows analyte vapors to be equilibrated without the vial pressurization and the transfer of the analyte vapors (aliquot of HS gas volume) into the GC without equilibrium disturbance. A method is also introduced, which allows one to measure the gas-liquid distribution constant or the partition coefficient from a single experiment.

### **Experimental (for Isochoric Headspace System)**

A homemade headspace system was constructed based on headspace autosampler model M-150 (Asist Inc., Cleveland, OH) and was connected to Hewlett-Packard (Agilent Corp., Little Falls, DE) model 5890 GC with DB-5 (Agilent Corp., Little Falls, DE) capillary column (30 m length and 0.25 mm I.D., 0.25  $\mu\text{m}$  film thickness). Figures 4-1 and 4-2 show the schematic of the Isochoric headspace system. Figures 4-3 to 4-6 show the actual photographs of the Isochoric headspace system and its different components. All of the connections were made using tubing having I.D. of 0.02" and material used to make the tubing was PEEK (PolyEther Ether Ketone).



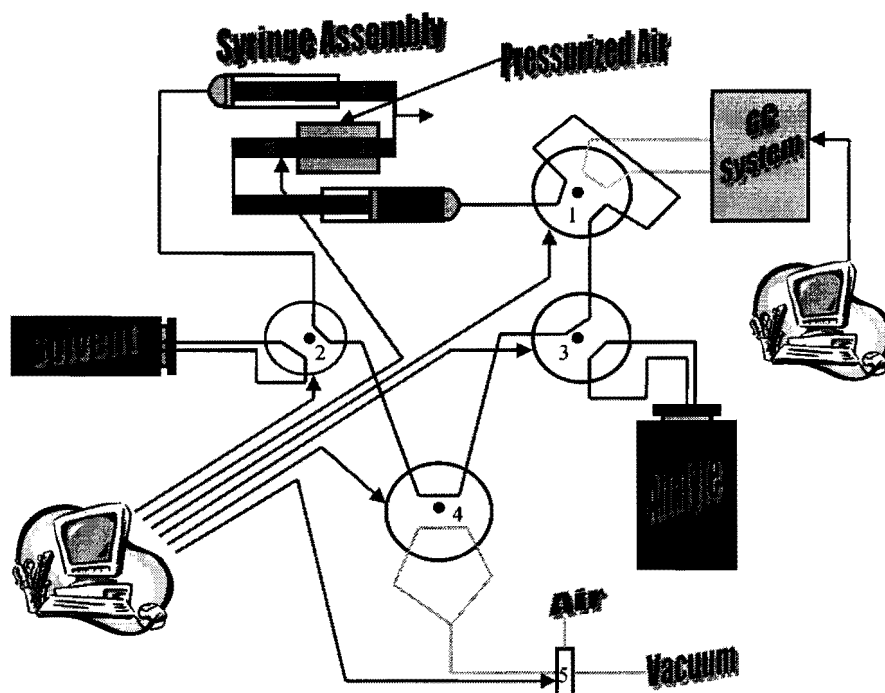


**Figure 4-1:** Principle schematic of the isochoric headspace system. Valve 1 is a 6-port valve equipped with injection loop of 14  $\mu\text{L}$  volume; valves 2 and 3 are 4-port; valves 4 and 5 are optional for cleaning purpose.

One-computer controls the syringe assembly as well as all five valves and the other computer collects the data generated by the GC.

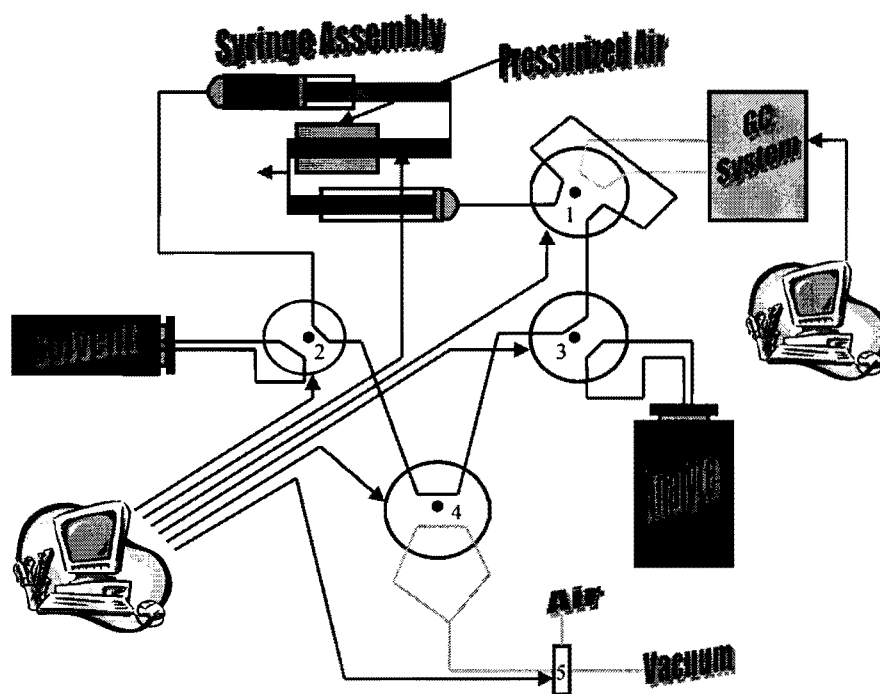


**Figure 4-2:** Same as Figure 4-1 except showing movement of syringes in the opposite direction.

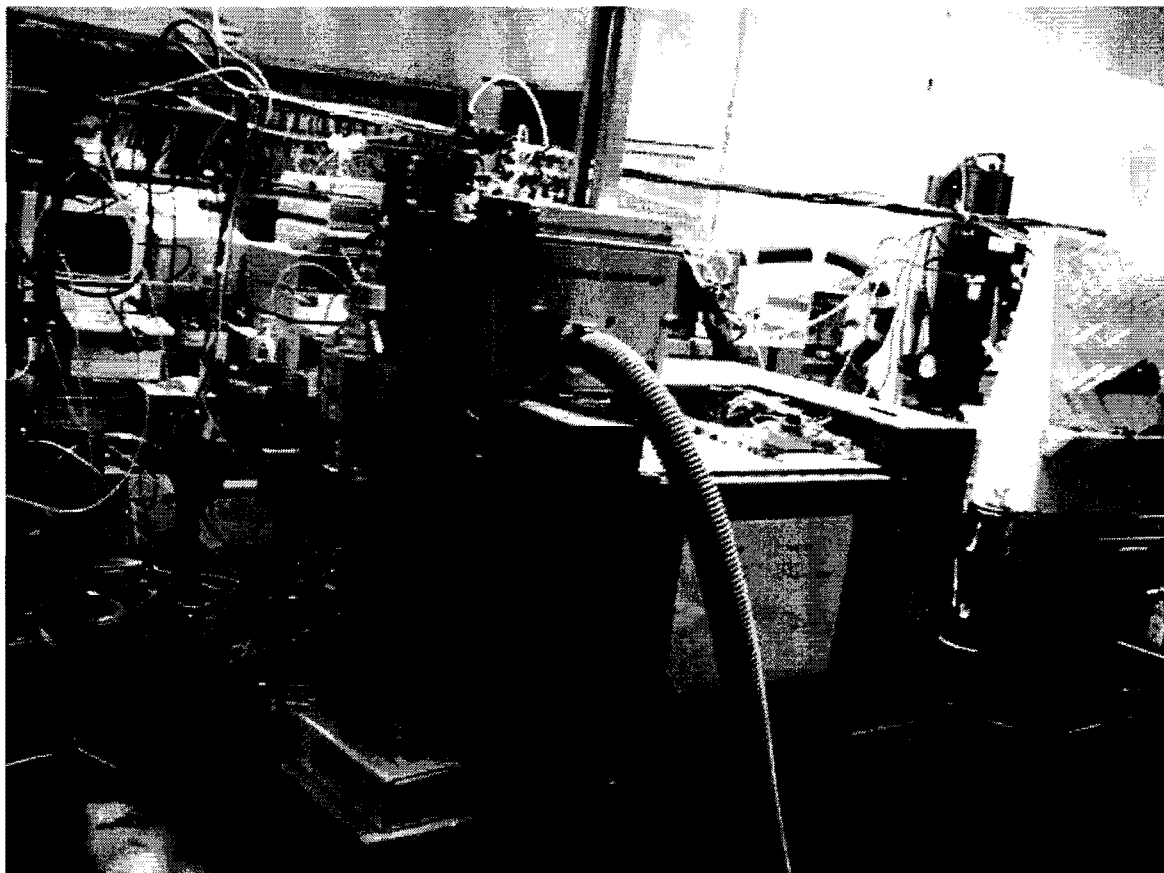


**Figure 4-3:** Photograph of the Isochoric headspace system installed on top of HP 5890 GC.

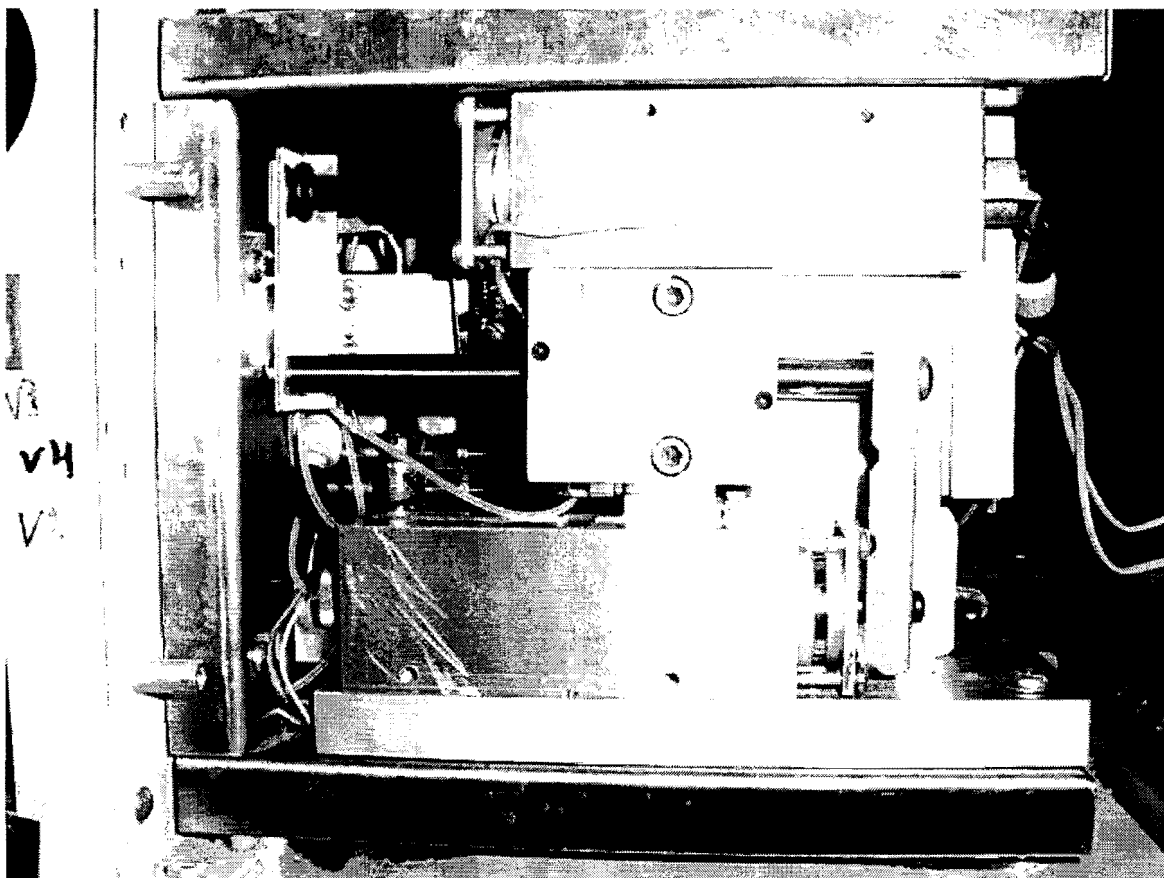


**Figure 4-4:** Photograph of the syringe assembly inside the Isochoric headspace system.

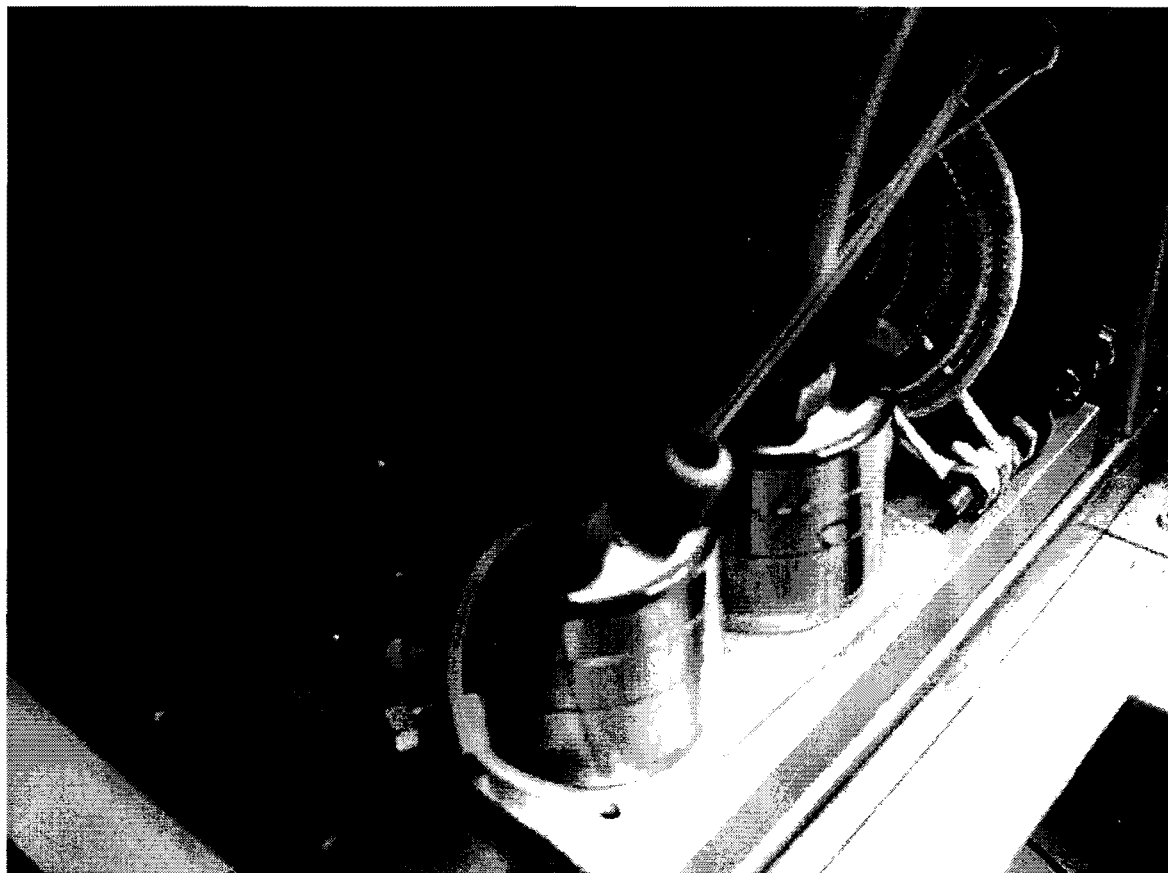


**Figure 4-5:** Photograph of the valves inside the Isochoric headspace system.

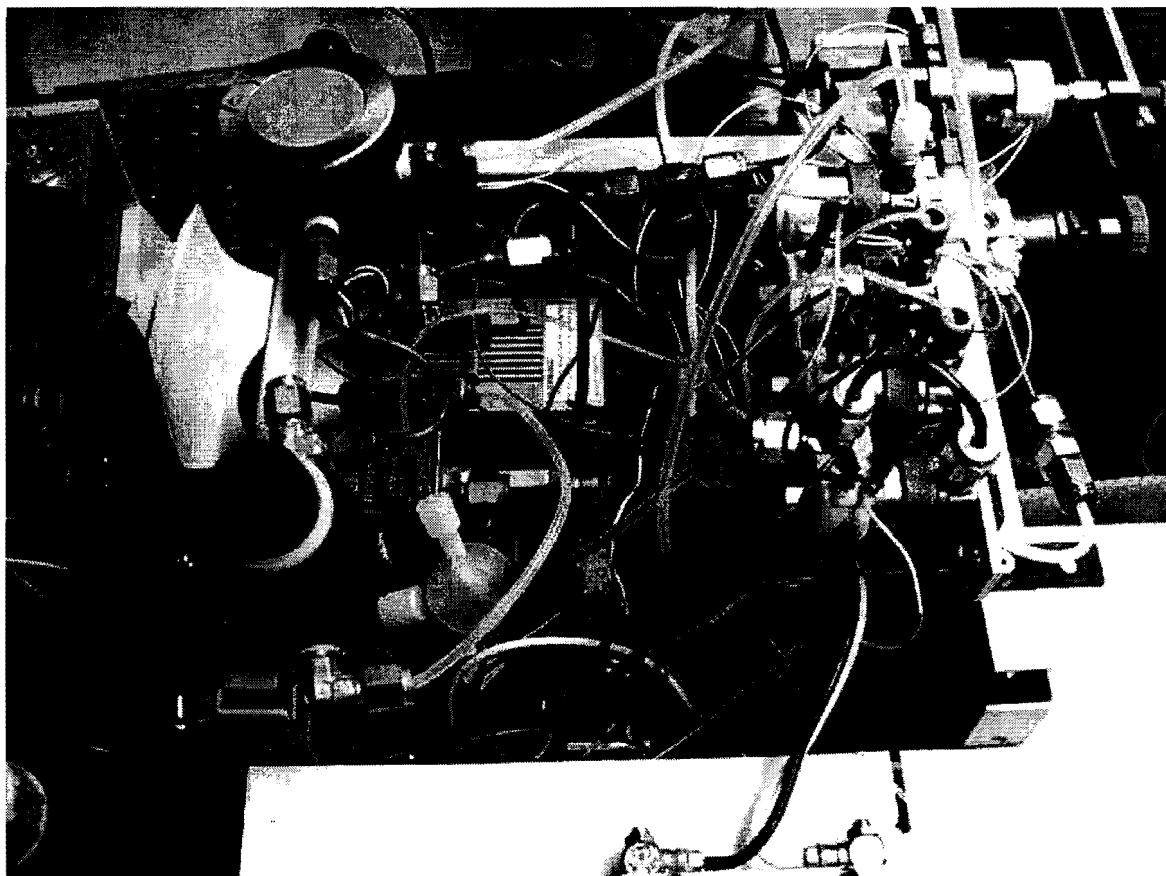


**Figure 4-6:** Photograph of the backside of the Isochoric headspace system where all of the electronic connections are located.

The headspace system was controlled by computer software (Asist Inc., Cleveland, OH). The data generated by GC were collected by Turbochrom Navigator software version 4.1 (Perkin-Elmer Corp.).

Temperature of the headspace system was monitored on-line with Dual Thermometer (serial # M111680, next calibration due Jan 2002, accuracy of 0.1°C) equipped with RS-232 output cable (Control Company, Houston, TX). The on-line temperatures were recorded every 30 minutes with Traceable Data Acquisition System Software version 2.0 (Control Company, Houston, TX).

Two computers were setup to control the Isochoric headspace system and to collect the data generated from the GC.

All other parameters to setup either the headspace system or the GC are analyte dependent and they will be discussed later.

### **Principles of Isochoric Headspace System**

The general principle of the isochoric headspace system is illustrated in Figures 4-1 and 4-2. For the actual photographs, refer to Figure 4-3 for the Isochoric headspace system and refer to Figures 4-4 to 4-6 for different components of the system.

The system consists of three main valves (1-3) and optional valves 4 and 5, HS vial (solvent vial), analyte bottle (sample bottle) and syringe assembly. The HS vial (labeled solvent in Figures 4-1 and 4-2) and the analyte bottle (labeled analyte in Figures 4-1 and 4-2) have two connecting lines each. The syringe assembly (includes the connecting capillary tubes connecting one syringe to the other going through valves 1, 2 and 3) consists of two gas-tight syringes and a pneumatic motion actuating system. The plungers of both syringes

have the same diameter and are fixed together in a way that aspirating action of one syringe corresponds to the simultaneous displacement action of another. The aspirated and displaced volumes are equal. Reciprocating movement of syringe plungers causes a corresponding movement of the vapor phase in the syringe assembly loop. Depending on the position of the valves either the HS vial (valve 2) or the analyte bottle (valve 3) may be included into the syringe assembly loop. The pressurized air controls the syringe speed. The higher the pressure applied the faster the movement of the syringes. HS vial, all valves, and syringe assembly are placed in the thermostated oven (6'x6'x6') made of aluminum blocks. Temperature stability measured at different points of the system was within 1°C. Valves 4 and 5 are used for the connection of the syringe assembly to the vacuum or to cleaning air.

### **Vapor Transfer and Measurement Processes**

This system allows two different types of headspace experiments:

- 1) The equilibration and analysis of the vapor over the liquid sample with analyte already dissolved in (similar to MHE - Multiple Headspace Extraction) and
- 2) The sequential transfer of the pure analyte vapor from the analyte bottle into to the HS vial containing pure solvent (or any other matrix), equilibration of the analyte with the liquid phase and analysis of the equilibrated vapor. This method is called the vapor loading method and is separated into two parts: (i) analyte is present inside the HS vial before loading and (ii) no analyte present inside the HS vial before loading.



## Isochoric Vapor Extraction Method

### Experimental Procedure

- a. A known volume of analyte solution is placed into the HS vial (refer to Figure 4-7). Note that the analyte bottle attached to valve 3 and valve 3 (as shown in Figure 4-1) are not required for this method.
- b. Valve 2 is actuated, connecting the HS vial to the syringe assembly and the injection loop (refer to Figure 4-8).
- c. Slow reciprocation motions of the syringes allow the equilibration of the whole system vapor phase (including the injection loop).
- d. After achieving equilibrium, valve 1 (injection valve) is actuated for ~2 sec allowing the displacement of the vapor phase from the injection loop into GC column for analysis (refer to Figure 4-9). Once the injection has been made, the valve returns to its neutral position.
- e. The sample vial is disconnected from the syringe assembly. Valve 5 is actuated connecting the vacuum line to valve 4. Then valve 4 is actuated connecting vacuum line to the syringe assembly (refer to Figure 4-10). After several reciprocating piston strokes, valve 1 is actuated to see if any analyte vapors are still present inside the syringe assembly loop. Then, if cleaned, valve 5 is brought back to its neutral position. This connects inert gas (or air) line to the syringes to fill them with inert gas (or air) with selected pressure, usually atmospheric (Figure 4-11).

- f. After the syringes have been filled with atmospheric pressured inert gas (or air), the system is back to its original position for the next cycle (Figure 4-12). Return to step *b* to start the next cycle.

The total volume of the gas phase in the whole system is on the level of 26 mL (volume of HS vial plus volume of the syringe assembly). So, the withdrawal of 20  $\mu\text{L}$  (volume based on the geometric calculation of the capillary tube used for the injection loop) of the vapor phase (0.08% of the whole volume) does not introduce any noticeable error. Because of this, it is possible to perform sequential injections of the analyte vapor during the equilibration and determine when the equilibrium is actually established. In principle, if required, the withdrawn analyte, although very small, could be accounted for.

Solvent and analyte vapors remaining in the syringe assembly (includes the connecting lines) at the end of the first cycle are removed (cleaned) in step *e*. The removed amount is known since the vapor phase concentration was measured after the equilibration was established. The volume of the syringe assembly is calibrated or calculated (will be discussed later) before this method is applied.

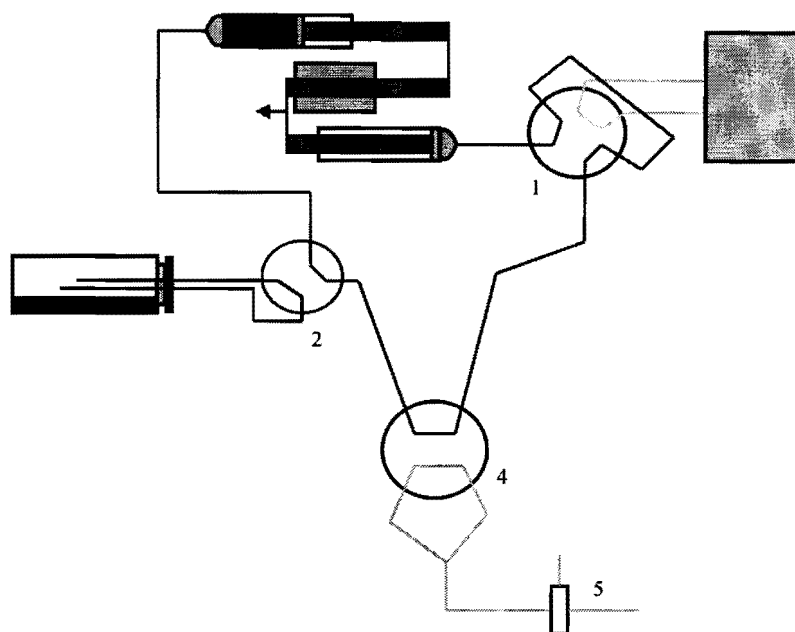


**Figure 4-7:** Schematic of an Isochoric headspace system for the use of vapor extraction method. Refer to Figure 4-1 for individual listing of the components used. Same as Figure 4-1 except valve 3 and analyte bottle are not shown since they are not required for this method. Shown system is in its neutral position at the start of the vapor extraction method.

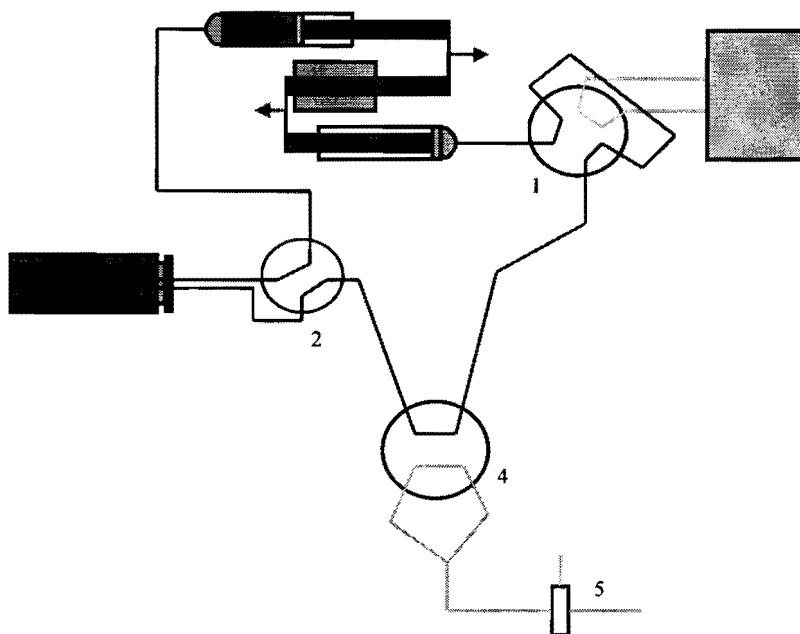


**Figure 4-8:** Same as Figure 4-7 except valve 2 is actuated to equilibrate the analyte vapor present in the solvent with the syringe assembly and the injection loop.

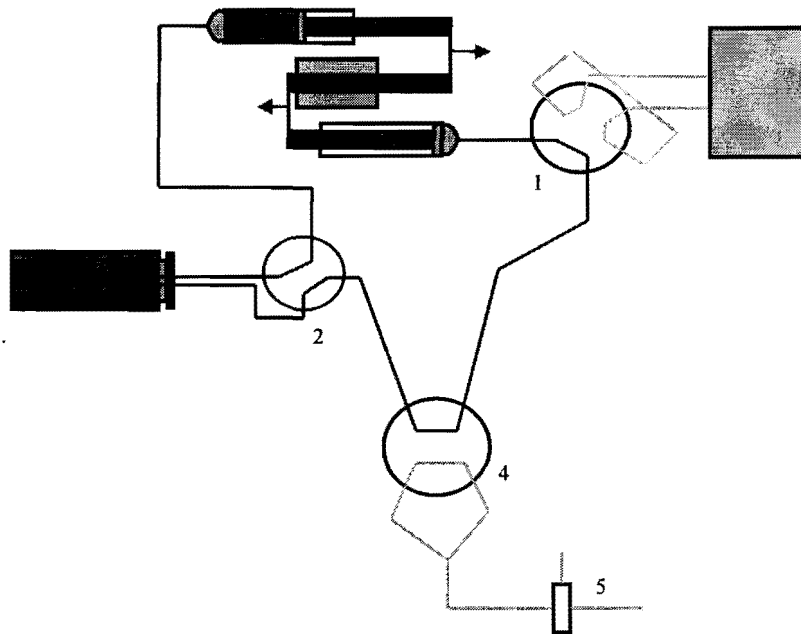


**Figure 4-9:** Same as Figure 4-8 except, in addition to valve 2, valve 1 is actuated to inject the equilibrated analyte vapors into the GC system for analysis.

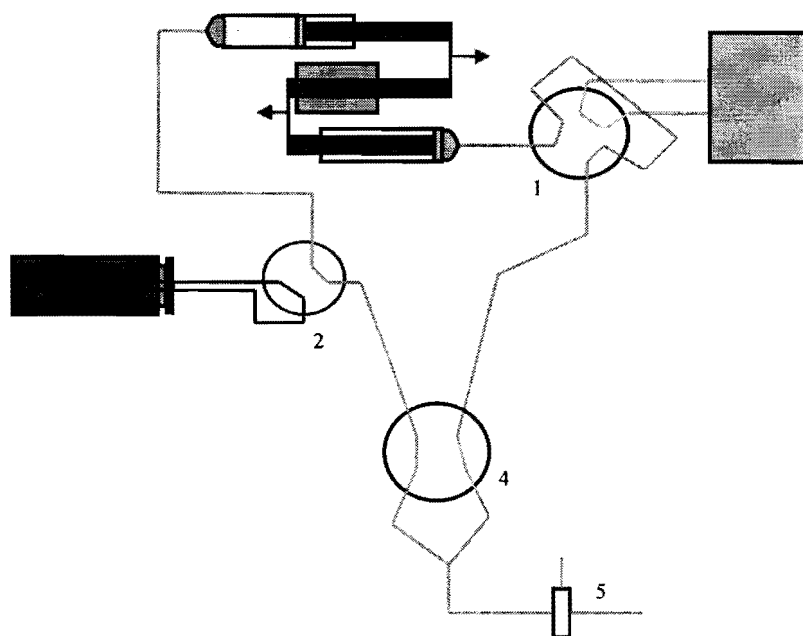


**Figure 4-10:** Same as Figure 4-9 except only valves 4 and 5 are actuated to start the vacuum to clean the analyte and solvent vapors from the syringe assembly.

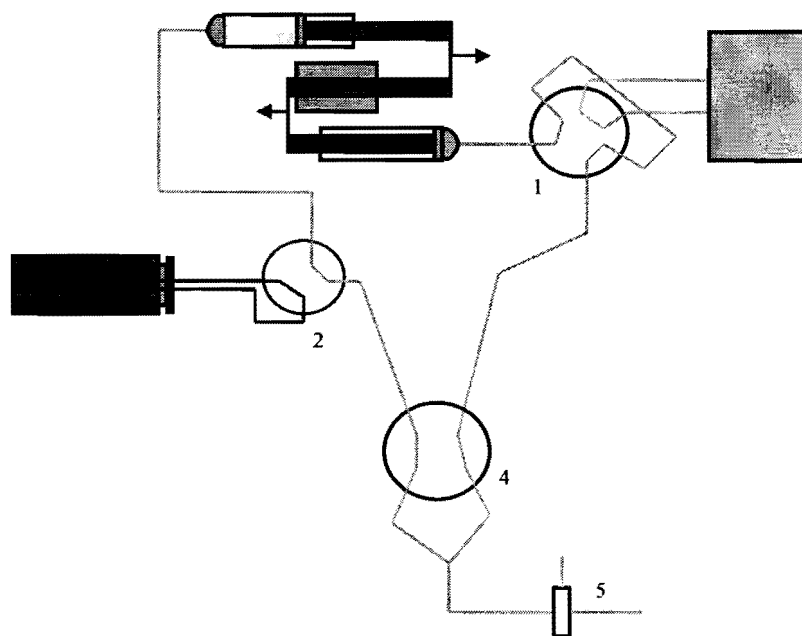


**Figure 4-11:** Same as Figure 4-10 except valves 5 is brought back to its neutral position to fill the syringe assembly with inert gas (or air) at atmospheric pressure.

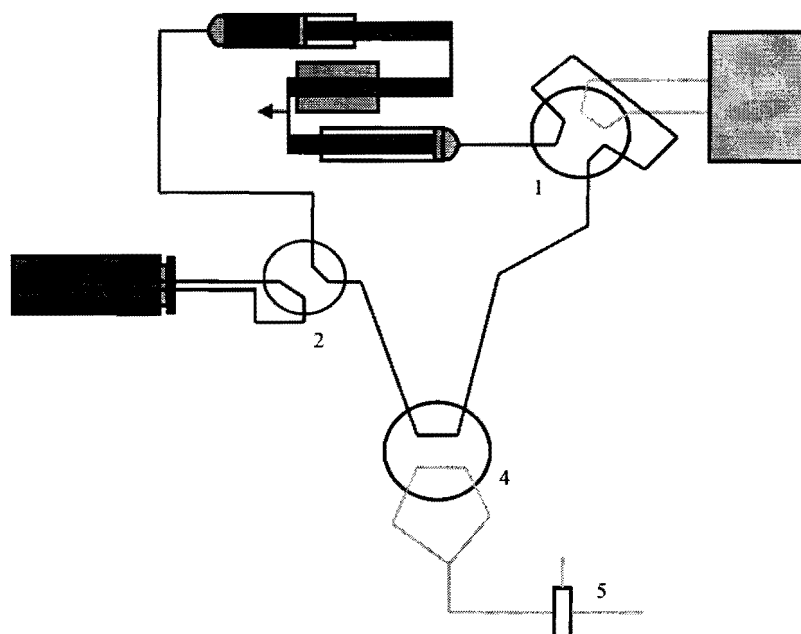


**Figure 4-12:** Same as Figure 4-7 except HS vial has less amount of analyte vapor present compared to the previous cycle. The cycle can start again (go back to Figure 4-7) for the Isochoric vapor extraction method.



### Theory of Sequential (discontinuous) Withdrawal of the Analyte Vapor in the Isochoric System.

The original amount of the analyte ( $n_0$ ) in the sample solution (present inside the HS vial) is

$$n_0 = c_0^L V_L \quad (4-8)$$

where  $c_0^L$  is the starting analyte concentration in the liquid phase and  $V_L$  is the volume of the liquid phase placed in the HS vial. It is assumed that the liquid phase volume does not change during multiple extraction process.

After first equilibration of the vapor phase with connected syringes (step *d*), or the syringe assembly, the analyte will be distributed between the vapor and the liquid phase.

$$n_0 = c_0^L V_L = c_1^L V_L + c_1^G (V_V + V_S - V_L) \quad (4-9)$$

where  $V_V$  is the volume of the vial;  $V_S$  is the volume of the syringe assembly (with connecting lines),  $c_1^L$  is the equilibrium concentration in the liquid phase, and  $c_1^G$  is the equilibrium concentration in the vapor (gas) phase. Using Equation 4-1, unknown equilibrium concentration in the liquid phase with  $Kc_1^G$  can be substituted:

$$c_0^L = c_1^G \left[ K - 1 + \frac{V_V + V_S}{V_L} \right] \quad (4-10)$$

In the step *e* of the first cycle the  $c_1^G V_S$  analyte amount is discarded. The amount of analyte left in the system is equal to  $n_1 = c_1^L V_L + c_1^G (V_V - V_L)$  or using the same substitution from Equation 4-1, we can write  $n_1 = c_1^G [V_V + V_L (K - 1)]$ . This amount of the analyte will be

redistributed between the liquid and the gas phase again in the second cycle. The second distribution equilibrium by the analogy with Equation 4-9 could be written in the form

$$c_1^G [V_V + V_L (K - 1)] = c_2^G [V_V + V_S + V_L (K - 1)] \quad (4-11)$$

or as the ratio of two consecutive equilibrium concentrations in our process which is equal to

$$\frac{c_1^G}{c_2^G} = 1 + \frac{V_S}{V_V + V_L (K - 1)} \quad (4-12)$$

the distribution constant from any two consecutive measurements in our multiple extraction process can be calculated:

$$K = 1 - \frac{V_V}{V_L} + \frac{c_i^G}{c_{i-1}^G - c_i^G} \frac{V_S}{V_L} \quad (4-13)$$

This is an advantage over the MHE process described by Ettre and Kolb [239] where the discarded amount was not known and correctness of the determination of the distribution constant and analyte concentration was dependent on the precision of the first measurement.

This method allows significant decrease of the measurement errors since it is possible to eliminate statistical errors of chromatographic concentration measurements by averaging consecutive concentration ratios. To maintain sufficient measurement accuracy, the last term in the Equation 4-12 should not be less than 0.05 (selecting 5% difference between consecutive measurements). If the total volume of the syringe assembly is 2 mL and the volume of the HS vial is 20 mL, then  $V_L(K-1)$  should be less than 20. This means that if expected gas-liquid distribution constant is on the level of 1000, then the volume of the liquid phase should not be more than 20  $\mu\text{L}$ .

This difficulty can be overcome in the second method (described below) of analyte vapor loading into the HS vial. This method also allows measurement of the whole distribution isotherm (as well as adsorption isotherm on the solid samples).

### **Isochoric Vapor Loading Method**

This method allows sequential transfer of the analyte (or mixture of analytes) vapor (from the analyte bottle) into the HS vial (which contains any solvent or matrix). A known volume of solvent (or any other matrix) is placed into the HS vial and the analyte (or the mixture of analytes) into the analyte bottle (refer to Figure 4-13). Then, the following operational sequence is performed:

- a. Valve 3 is actuated to connect the analyte bottle to the syringe assembly and the injection loop.
- b. Slow reciprocation motions of the syringes allow the equilibration of the analyte vapor between the analyte bottle and the syringe assembly (including the injection loop) (refer to Figure 4-14).
- c. After achieving the equilibrium, injection valve 1 is actuated for ~2 sec (making an injection) allowing the displacement of the gas phase from the injection loop into the GC column for chromatographic analysis. This is the measurement of the amount of the analyte transferred from the analyte bottle into the syringe assembly (refer to Figure 4-15).
- d. Valve 3 is deactivated and valve 2 is activated. This connects the syringe assembly to the HS vial.

- e. Slow reciprocation motions of the syringes allow the equilibration of the solvent present inside the HS vial with the analyte vapor from the syringe assembly (including the injection loop) (refer to Figure 4-16).
- f. After achieving equilibrium, valve 1 is actuated for ~2 sec (making an injection) allowing the displacement of the gas phase from the injection loop into the GC column for chromatographic analysis (refer to Figure 4-17). This is the measurement of the amount of the analyte left in the gas phase (total gas phase volume = volume of the vial - volume of the liquid phase + volume of the syringe assembly) after equilibration with the solvent or any other matrix.
- g. The HS vial is disconnected from the syringe assembly by deactivating valve 2. Valve 5 is actuated to start the vacuum between valve 5 and valve 4 (refer to Figure 4-18). After several reciprocating syringe movement valve 5 is actuated. This connects the vacuum line to the syringe assembly to clean out the solvent and analyte vapors from the syringe assembly (refer to Figure 4-19). After certain number of reciprocating movement of the syringes, valve 1 is actuated to make an injection (refer to Figure 4-20). This shows us how clean the syringe assembly really is. Once it is cleaned, valve 5 is brought back to its neutral position, allowing atmospheric air into the syringe assembly (refer to Figure 4-21). This step is necessary since there was a vacuum inside the syringe assembly and now it is at atmospheric pressure. The last step is to bring valve 4 back to its neutral position (refer to Figure 4-22). The schematic in Figure 4-22 is similar to the one shown in Figure 4-13, except that the HS vial has equilibrated analyte vapor (less than the previous cycle) from the previous cycle. The next cycle can now begin starting from step **a**.

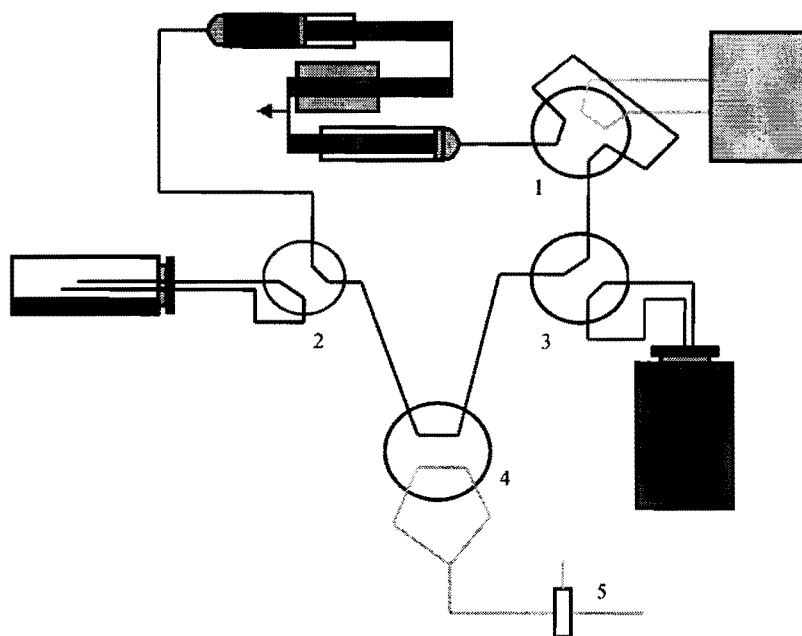


**Figure 4-13:** Refer to Figure 4-1 for the identity of each component of the illustrated system. All valves are in their neutral positions. This setup is necessary for the Isochoric vapor loading method. Valves 4 and 5 are optional for cleaning.

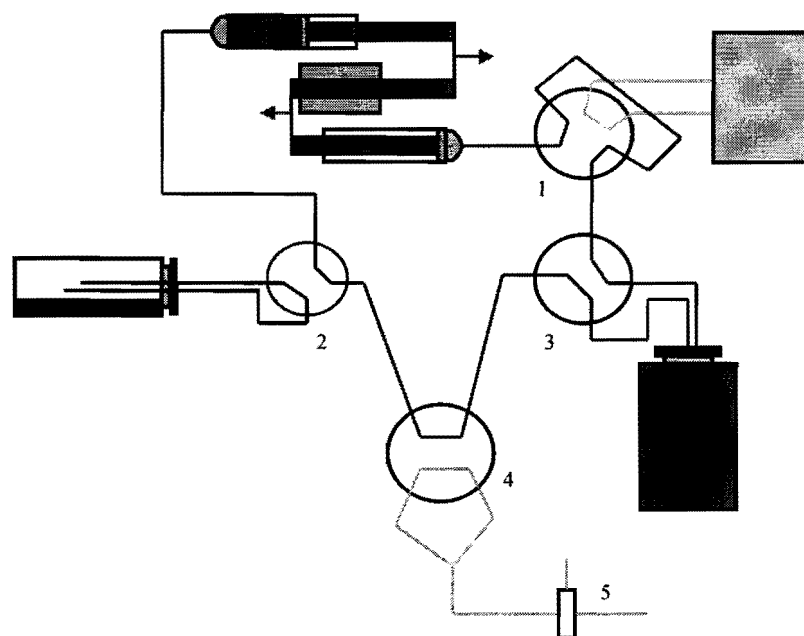


**Figure 4-14:** Same as Figure 4-13 except valve 3 is actuated for equilibration of the analyte vapors between the analyte bottle and the syringe assembly. The syringes are moved back and forth to drive the analyte vapors to equilibrium through the connected parts.

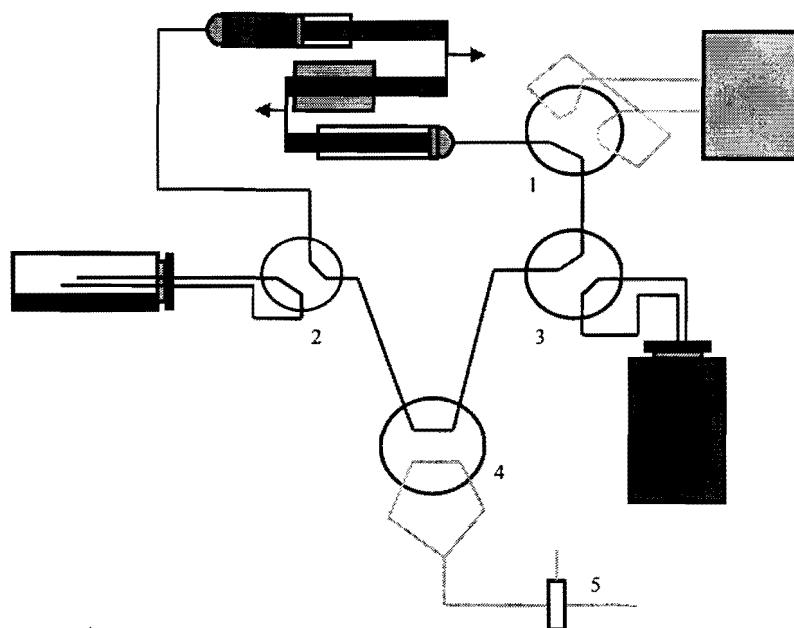


**Figure 4-15:** Same as Figure 4-14 except valve 3 is deactivated and valve 1 is actuated for injection of the equilibrated analyte vapor to quantitate the concentration of analyte in the syringe assembly.

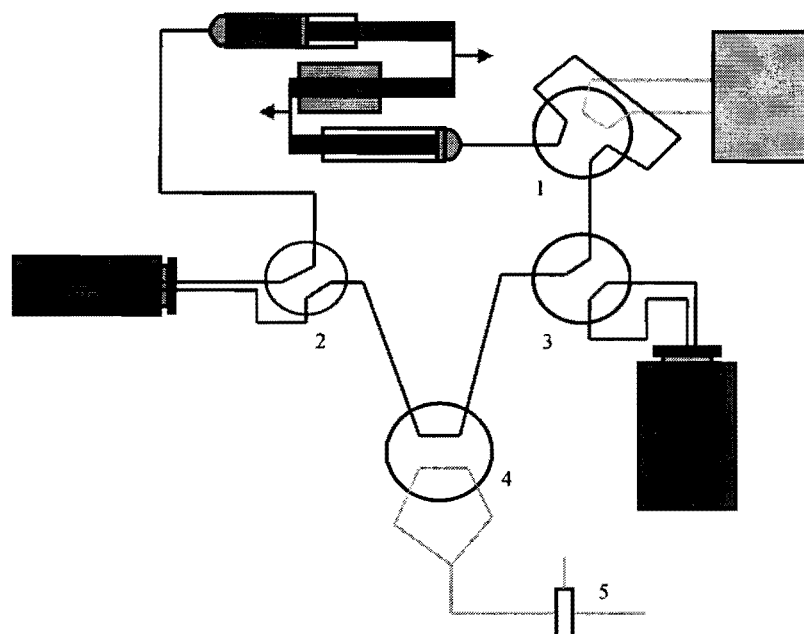


**Figure 4-16:** Same as Figure 4-15 except valve 2 is actuated for the equilibration of the analyte vapors between the syringe assembly and the solvent inside the vial. The syringes are moved back and forth to drive the analyte vapors to equilibrium through the connected parts.



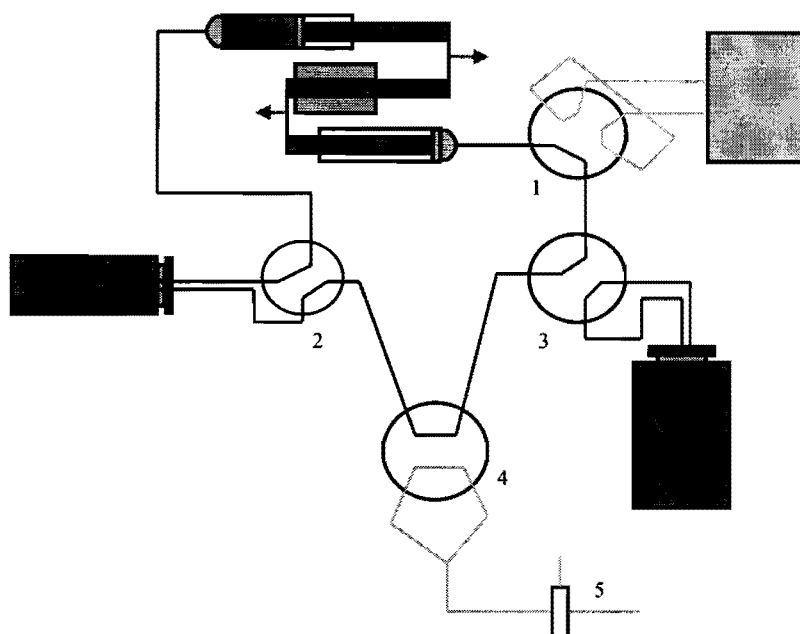


**Figure 4-17:** Same as Figure 4-16 except, in addition to valve 2, valve 1 is actuated for injection of the equilibrated analyte vapor to quantitate the concentration of analyte in the gas phase (HS vial plus syringe assembly).

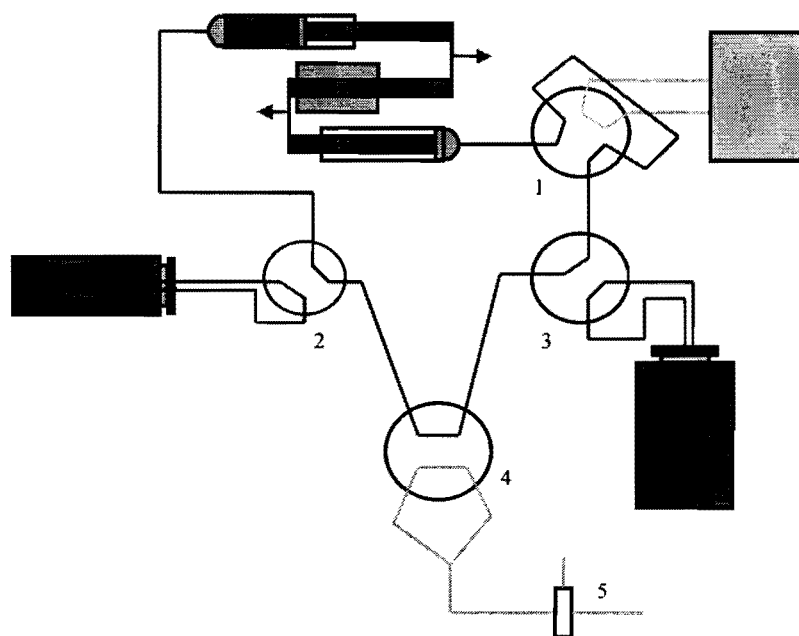


**Figure 4-18:** Same as Figure 4-17 except valve 5 is actuated (all others in neutral position) to start the vacuums between the valves 4 and 5. The equilibrated analyte vapors are still inside the vial (the concentration is already known) and inside the syringe assembly.

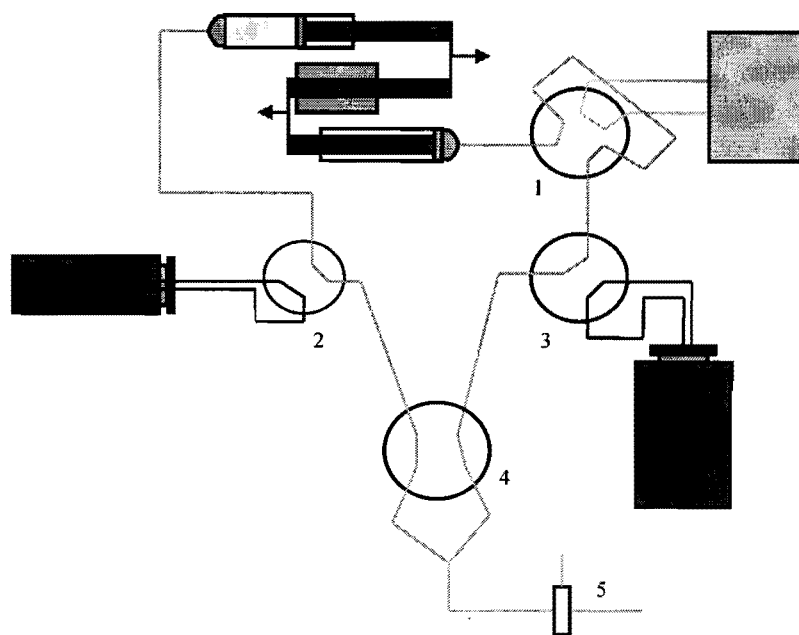


**Figure 4-19:** Same as Figure 4-18 except, in addition to valve 5, valve 4 is actuated to start the vacuum from both sides of the syringe assembly to clean the analyte and solvent vapors from the syringe assembly. The equilibrated analyte vapors are still inside the vial (the concentration is already known).

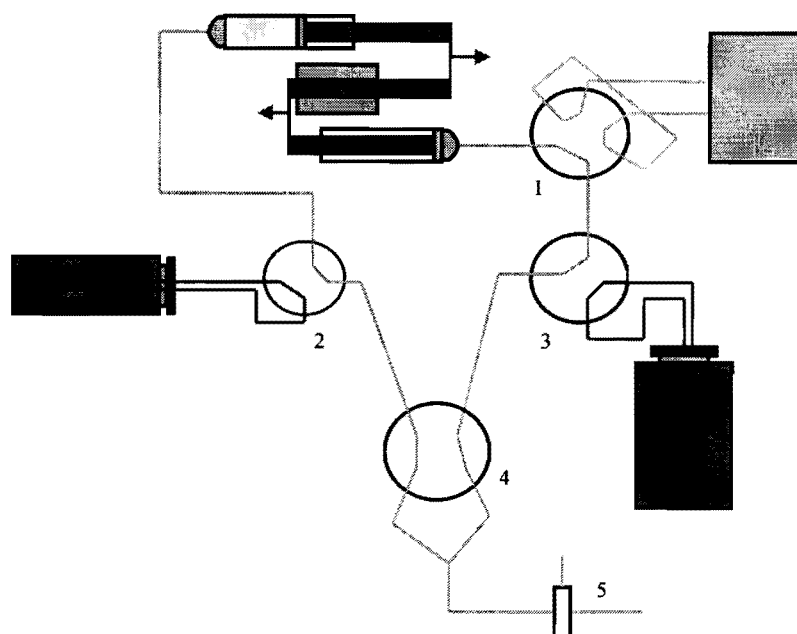


**Figure 4-20:** Same as Figure 4-19 except, in addition to valves 4 and 5, valve 1 is actuated for injection of the cleaned syringe assembly to see if the analyte and solvent vapors are cleaned or not. The equilibrated analyte vapors are still inside the vial (the concentration is already known).

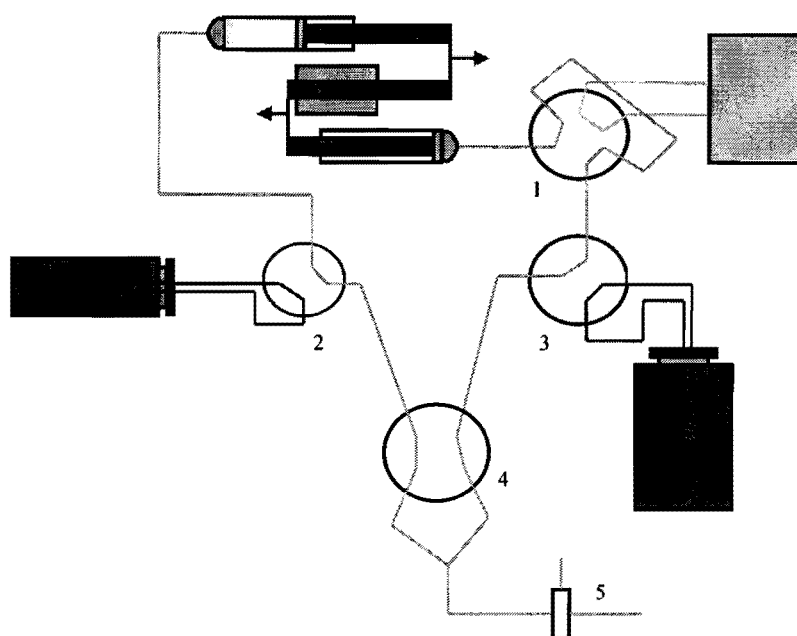


**Figure 4-21:** Same as Figure 4-20 except, in addition to valve 4, valve 1 and 5 are brought back to its neutral position to pressurize the syringe assembly with atmospheric air. The equilibrated analyte vapors are still inside the vial (the concentration is already known).

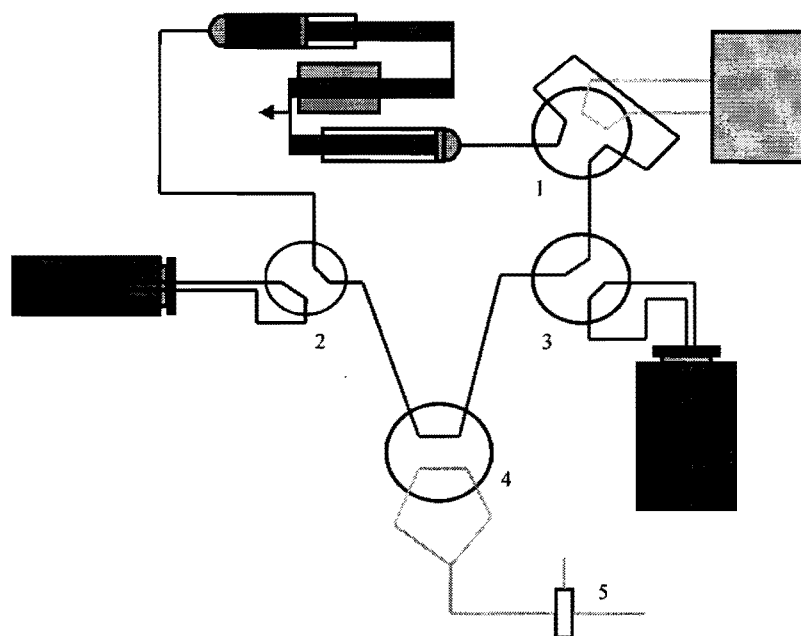


**Figure 4-22:** Same as Figure 4-21 except all valves are in their neutral positions. This figure is identical to figure 4-13, except the equilibrated analyte vapors from the previous cycle are inside the HS vial (the concentration is already known) to which the vapors from the next cycle (Figures 4-13 to 4-21) will be added.

The amount of analyte placed into the analyte bottle ( $n_0$ ) should be small enough to be completely evaporated. The initial analyte vapor concentration could be calculated as  $n_0/V_B$ .

The amount of analyte transferred from the analyte bottle into the volume of syringe assembly (step *b*) is calculated as

$$n_s = n_0 \frac{V_S}{V_S + V_B} \quad (4-14)$$

where  $V_S$  is the syringe assembly volume and  $V_B$  is the volume of the analyte bottle. In step *d*, analyte vapor is distributed between the volume of syringe assembly and the gas phase volume inside the HS vial. If the HS vial is empty, then equilibrium analyte concentration in the gas phase can be calculated as follows:

$$c_v^0 = \frac{n_s}{V_v + V_S} \quad (4-15)$$

If the HS vial contains solvent (or any other matrix), the total amount of analyte present inside the syringe assembly will now be distributed between the liquid (volume of solvent inside the sample vial) and the gas phase ( $V_v + V_S$  - volume of the liquid phase ( $V_L$ )). The difference between the initial analyte amount in the syringe assembly ( $n_s$ ) and chromatographically measured amount  $n_e = c_{chr}(V_v + V_S - V_L)$  represents the amount of analyte absorbed by the liquid inside the HS vial (at equilibrium).

Since the concentration, at equilibrium, of the analyte present in both phases (liquid and gas) is known, the distribution constant can be calculated by equation 4-1.

The total volume of the gas phase in the system is about 25 mL and withdrawal of 20  $\mu$ L of the gas phase (0.08% of the total gas phase volume) does not introduce any noticeable

error. Because of that, it is possible to perform sequential injections of the analyte vapor during the equilibration (step *f*) and determine when the equilibrium is actually established. In principle, if required the withdrawn analyte, although very small, could be accounted for.

As indicated above, this method allows an on-line equilibration check. Consecutive injections during equilibration of the analyte with the solvent (step *f*) usually show exponential decay of the analyte amount in the gas phase. Equilibrium is reached when two or more consecutive injections show similar peak areas in respective chromatograms obtained from the GC.

The process described above could be repeated several times allowing a sequential transfer of the analyte from the analyte bottle into the solvent present inside the HS vial.

#### **Theory of Isochoric Vapor Transfer where the Analyte is Not Added to the Solvent Before the 1<sup>st</sup> Loading.**

The theoretical description of the isochoric vapor loading method can be done in a stepwise consideration from the sequential transfer of the analyte from the analyte bottle to the solvent present inside the HS vial.

It is assumed that the analyte concentration in the bottle does not show any noticeable change during the sequential vapor transfer from the analyte bottle to the syringe assembly. This assumption is correct if saturated analyte vapor is used or if the volume of the bottle is significantly larger than the volume of the syringe assembly. Another assumption made for simplicity of theoretical description is that the solvent vapor pressure is low and the solvent loss during sequential vapor transfer could be avoided. The analyte molecules in the gas phase are assumed to behave ideally (no analyte-analyte interactions in the gas phase).



In the first cycle, the amount of analyte in the sample vial is 0. The transferred amount, from the syringe assembly to the HS vial, is equal to

$$n_s^1 = V_S c_B \quad (4-16)$$

where  $V_S$  is the volume of the syringe assembly,  $c_B$  is the analyte concentration in the analyte bottle and accordingly in the syringe assembly after its equilibration with the analyte bottle.

After connection of the syringe assembly to the HS vial and equilibration (step *f*), the transferred amount of the analyte will be distributed between the gas and the liquid phase, so we can write

$$n_s^1 = c_1^L V_L + c_1^G (V_S + V_V - V_L) \quad (4-17)$$

where  $c_1^L$  is the equilibrium concentration of the analyte in the liquid phase,  $V_L$  is the volume of the liquid phase,  $c_1^G$  is the equilibrium concentration in the gas phase. Substituting Equation 4-1 we get

$$V_S c_B = c_1^G [(K - 1)V_L + V_S + V_V] \quad (4-18)$$

or the equilibrium analyte concentration in the gas phase after the first cycle could be expressed as

$$c_1^G = \frac{V_S c_B}{(K - 1)V_L + V_S + V_V} \quad (4-19)$$

In the second transfer cycle, the amount of the transferred analyte will be the same as in the first step. The total amount of the analyte in the HS vial and in the syringe assembly will be the sum of the analyte amount left in the HS vial after the first cycle and the new transferred amount, which is equal to

$$c_1^G [(K-1)V_L + V_V] + V_S c_B \quad (4-20)$$

After equilibration, this amount will be redistributed between the gas and the liquid phase.

For the second equilibrium:

$$c_1^G [(K-1)V_L + V_V] + V_S c_B = c_2^G [(K-1)V_L + V_S + V_V] \quad (4-21)$$

where  $c_2^G$  is the analyte equilibrium concentration in the second step. Substitution of  $c_1^G$  from the Equation 4-19 gives:

$$c_2^G = c_B V_S \frac{2(K-1)V_L + 2V_V + V_S}{[(K-1)V_L + V_S + V_V]^2} \quad (4-22)$$

A similar procedure could be applied for  $i$  number of cycles. The analyte equilibrium concentration in any cycle  $i$  could be easily expressed from its concentration in the previous cycle

$$c_i^G [(K-1)V_L + V_S + V_V] = c_{i-1}^G [(K-1)V_L + V_V] + V_S c_B \quad (4-23)$$

The expression  $[(K-1)V_L + V_S + V_V]$  is in terms of volume in which the total amount of the analyte would occupy in the gas phase. We denote this as  $\Phi$  and Equation 4-23 could be written in the following form:

$$c_i^G = c_{i-1}^G \frac{\Phi - V_S}{\Phi} + \frac{V_S c_B}{\Phi} \quad (4-24)$$

Consecutive substitution backwards up to  $i = 0$ , gives:

$$c_n^G = c_B \frac{V_S}{\Phi} \left[ \left(1 - \frac{V_S}{\Phi}\right)^{n-1} + \dots + \left(1 - \frac{V_S}{\Phi}\right) + 1 \right] = c_B \frac{V_S}{\Phi} \sum_{i=0}^{n-1} \left(1 - \frac{V_S}{\Phi}\right)^i \quad (4-25)$$

This is a geometrical progression and its sum could be written in the form

$$c_B^G = c_B^G \left\{ 1 - \left( 1 - \frac{V_S}{\Phi} \right)^n \right\} \quad (4-26)$$

Since  $V_S$  is a fraction of  $\Phi$ , the limit of this expression at  $n \rightarrow \infty$  is equal to  $c_b$ . The rate of the convergence is dependent mainly on the value  $K$ .

Although the process described above is incremental, it can be described as continuous, assuming small transfer increments performed without time variations so the time for each cycle is  $\Delta t$ . It is also assumed that the equilibration process is fast. The change of the analyte concentration in the HS vial is proportional to the difference between the analyte concentration in the analyte bottle ( $c_B$ ) and the actual ( $c$ ) concentration in the HS vial.

$$\frac{dc}{dt} = k(c_B - c) \quad (4-27)$$

Simple transformation and integration gives

$$-\ln(c_B - c) = kt + A \quad (4-28)$$

where  $A$  is an integration constant. Concentration in the HS vial before the first transfer is equal to zero, so the integration constant  $A$ , at  $t=0$ , is equal to  $-\ln(c_B)$ .

The time scale is set according to the transfer steps and the first transfer is at  $t = 1$ . The equilibrium concentration could be expressed from Equation 4-19. Substituting this concentration in Equation 4-28, at  $t = 1$  gives:

$$-\ln\left(c_B - \frac{V_S}{\Phi}c_B\right) = k - \ln(c_B) \quad \text{or} \quad k = -\ln\left(1 - \frac{V_S}{\Phi}\right) \quad (4-29)$$

Substituting expressions for  $A$  and  $k$  into Equation 4-28 gives:

$$-\ln(c_B - c(t)) = -t \cdot \ln\left(1 - \frac{V_S}{\Phi}\right) - \ln(c_B) \quad (4-30)$$

After simple rearrangement

$$c(t) = \left[1 - \left(1 - \frac{V_S}{\Phi}\right)^t\right] c_B \quad (4-31)$$

This expression is same as Equation 4-26, which was also obtained using stepwise derivation. This confirms the applicability of a continuous description of the process.

Substituting the expression for  $\Phi$  in Equation 4-31 and using the transfer number  $n$  instead of  $t$ , a final form is obtained:

$$c_n = \left[1 - \left(1 - \frac{V_S}{(K-1)V_L + V_S + V_V}\right)^n\right] c_B \quad (4-32)$$

This equation shows that the analyte equilibrium concentration in the gas phase, in each loading cycle, is a function of the distribution constant  $K$ , analyte concentration in the analyte bottle and all operational volumes ( $V_L$ ,  $V_S$ , and  $V_V$ ). This allows the calculation of  $K$  from any equilibrium step of our process. An important condition is that all previous steps should have been performed at the same conditions and reached the equilibrium.

Equation for the calculation of the distribution constant  $K$  from the analyte vapor concentration in the  $n^{\text{th}}$  step could be obtained from Equation 4-32 and has the following final form:

$$K = 1 - \frac{V_S + V_V}{V_L} + \frac{V_S}{V_L} \cdot \frac{1}{1 - \left(1 - \frac{c_n}{c_B}\right)^{1/n}} \quad (4-33)$$

### Theory of Isochoric Vapor Transfer Where the Analyte is Added to the Solvent in the Beginning.

Using the approach from the last section, it is possible to derive a general equation for the incremental analyte loading into the vial, which already contains analyte in the liquid sample. For this case, the analyte concentration in the gas phase in the HS vial, at equilibrium before the first transfer is denoted as  $c_0$ . The analyte concentration in the analyte bottle is  $c_B$  (it is better to have  $c_B > c_0$ , although it is not necessary). Derivation in continuous form is simpler so this procedure is used.

The change in the analyte concentration is still proportional to the difference between the concentrations in the analyte bottle and in the HS vial gas phase, so Equation 4-28 can be used as the starting point. Before the first transfer the analyte concentration in the vial is  $c_0$ , so at  $t=0$

$$A = -\ln(c_B - c_0) \quad (4-34)$$

is obtained. At  $t=1$ , the amount of the analyte in the HS vial after the first transfer is expressed as

$$c_0(\Phi - V_S) + c_B V_S = c_1 \Phi \quad (4-35)$$

Substituting  $A$  from Equation 4-34 and  $c_1$  from Equation 4-35 into the Equation 4-28 gives

$$k = -\ln\left(1 - \frac{V_S}{\Phi}\right) \quad (4-36)$$

The final form of the transfer equation after all transformations is

$$\frac{c_B - c(t)}{c_B - c_0} = \left(1 - \frac{V_S}{\Phi}\right)^t \quad (4-37)$$

In this expression there are two unknowns ( $K$  and  $c_0$ ), so at least two measurements are needed to obtain both. In the discontinuous form of the process, it is convenient to use two consecutive measurements,  $n-1$  and  $n$ . Equation 4-37 for cycle  $n$  divided by the same expression for cycle  $n-1$  leading to

$$\frac{c_B - c_n}{c_B - c_{n-1}} = 1 - \frac{V_S}{\Phi} \quad (4-38)$$

Substituting  $\Phi$  in the Equation 4-38 for its corresponding expression, a direct equation for the distribution constant  $K$  when using this method is obtained.

$$K = 1 + \frac{c_B - c_n}{c_n - c_{n-1}} \frac{V_S}{V_L} - \frac{V_V}{V_L} \quad (4-39)$$

Since  $\Phi = (K - 1)V_L + V_S + V_V$  and substituting  $K$  from Equation 4-39 back into the Equation 4-38 giving,

$$\Phi = \frac{c_B - c_{n-1}}{c_n - c_{n-1}} V_S \quad (4-40)$$

Using Equation 4-40, an equation for  $c_0$  with only measurable values is written:

$$c_0 = c_B - \frac{(c_B - c_{n-1})^n}{(c_B - c_n)^{n-1}} \quad (4-41)$$

$c_0$  is the equilibrium analyte concentration in the gas phase in the HS vial before the first transfer step. This analyte gas concentration represents the evaporated concentration from the original sample solution placed into the HS vial. The original analyte concentration,  $c_{org}$ , in the liquid sample can now be calculated.

$$c_{org} = c_0 \left( \frac{V_V}{V_L} + K - 1 \right) \quad (4-42)$$

Substituting  $c_0$  from Equation 4-41 and  $K$  from Equations 4-39 in Equation 4-42, a final expression for  $c_{org}$  is obtained:

$$c_{org} = \frac{c_B - c_n}{c_n - c_{n-1}} \cdot \frac{V_S}{V_L} \left[ c_B - \frac{(c_B - c_{n-1})^n}{(c_B - c_n)^{n-1}} \right] \quad (4-43)$$

This method is equivalent to the well-known method of standard addition [248]. The difference being that the additions of known amount of analyte vapor are made automatically in the same HS vial. This significantly decreases sample preparation errors and extends the method's applicability to the sample with high gas-liquid distribution constants.

To measure the gas-liquid distribution constant,  $K$ , for the current study, the vapor loading method is preferred. In particular, the method in which there is no analyte present in the HS vial before the first load. The schematics of this method have been shown in Figures 4-13 to 4-22. Since two different mathematical derivations have been suggested, the continuous process derivation will be used since it is easy to derive, as shown before.

### Calibration of System Volumes

Accurate measurements of the system volumes are essential for correct application of the MHE and the vapor loading methods.

The volume of the analyte bottle (attached to valve 3 in Figure 4-1) is not necessary since the concentration in the syringe assembly and the analyte bottle (at equilibrium) is identical. Since the syringe assembly volume will be measured and the concentration of the

analyte inside the syringe assembly is known, the mass of the analyte being transferred from the syringe assembly to the HS vial (containing solvent) is also known. This is the only amount that is needed, so the volume of the analyte bottle does not need to be measured.

The volume of the HS vial was measured by filling the HS vial with HPLC grade water at room temperature (25°C) and weighing it. Fifteen HS vials were measured (5 times each). The average error of the measurements of the volume of a single vial was less than 0.2%. The average volume of the HS vial from 15 vials is found to be 24.3 mL with 0.7% relative standard deviation.

The volume of the syringe assembly (with connecting capillary lines) can be determined using vapor transfer of any volatile analyte from the analyte bottle (attached to valve 3) into the empty HS vial (attached to valve 2) (refer to Figure 4-1). Since an empty HS vial is being used, the volume of the liquid phase is 0 and expression for  $\Phi$  reduces to  $V_S + V_V$ . Equations 4-26 and 4-32 are reduced to the following:

$$c_n = c_B \left[ 1 - \left( \frac{V_V}{V_S + V_V} \right)^n \right] \quad (4-44)$$

Rearrangement of Equation 4-44 leads to the following:

$$\ln(c_B - c_n) = n \ln \left( \frac{V_V}{V_S + V_V} \right) + \ln(c_B) \quad (4-45)$$

Using the results from the measurement of several consecutive points for analyte vapor transfer from the analyte bottle with concentration  $c_B$  into the originally empty HS vial, the volume of the syringe assembly can be calculated using Equation 4-45. The volume of the HS vial has been measured independently, as stated before, and found to be 24.3 mL. The dependence of the  $\ln(c_B - c_n)$  versus the cycle number,  $n$ , (transfer number) should be



linear according to the Equation 4-45. The logarithm of the slope of this dependence is equal to  $\frac{V_v}{V_s + V_v}$ . The volume of the syringe assembly (with the connecting capillary lines) can be expressed as

$$V_s = V_v \left( \frac{1}{\exp(\text{Slope})} - 1 \right) \quad (4-46)$$

The volume of the syringe assembly was found to be 2.32mL with 3.2% relative standard deviation (average of four determinations). Two different analytes (acetone and 1, 4 Dioxane) were used and four consecutive transfers each analyte were made in separate HS vial.

The volume of the injection loop was found to be  $\approx 20 \mu\text{L}$  (from geometric calculation of the 0.02 inch I.D. PEEK tubing,  $\approx 4$  inches in length). Note that the injection loop volume is negligible (0.08%) when compared to the volume of the HS vial (24.3 mL) plus the volume of the syringe assembly (2.32 mL).

### **The speed of the syringe piston**

The speed of the syringe piston strokes and the total number of reciprocal piston actions required are essential for the achievement of uniform distribution of the analyte vapor between different parts of the isochoric headspace system. Pneumatic actuation system was used and the variation in pressure of the air was needed for setting the speed of the syringe movement. The higher the pressure applied faster the speed of the syringe piston. The pressurized air was controlled through a pressure gauge (maximum limit 50 psi).

The dependence of the GC peak areas on the number of syringe strokes has been measured at different speed of the syringe piston movement. These experiments were done

for the step *b* of the isochoric vapor loading method, from the analyte bottle to the syringe assembly, with consecutive injections into GC after every five completed syringe strokes. The syringe pistons were set for a certain speed fixed for each experiment. The measured dependence is shown in Figure 4-23. The relative standard deviation of the experimental peak areas on the plateau (Figure 4-23, last six points) at 5.1 ml/min syringe speed is 0.4%.

Vapor equilibration is faster at greater piston speed. This is because the faster the flow the more turbulent it is. Fast syringe speed also produces a noticeable pressure drop along the connecting capillaries (this is important for valve 2 – when it is actuated, the right side of the piston movement forces the vapor through three valves and the injection loop; refer to Figure 4-1). Generation of the pressure drop should be avoided for the purpose of achievement of true thermodynamic equilibrium. Measurements of the pressure drop generation across two valves consecutively connected with PEEK capillaries (15 cm long) with 0.5 mm I.D. have been performed using a calibrated syringe pump (with 50 mL gas-tight syringe) and electronic pressure gauge (1 Torr accuracy). Results are shown in Table 4-I.

The volume change required to achieve pressure drop of 10 Torr inside the syringe assembly (2.32 mL volume) is only 60  $\mu$ L. The energy introduced into the system with this action is only 0.0061 Joule, but it can generate a temperature change of about 3°C in the syringe assembly volume. Since the syringe assembly is always connected to the HS vial (24.3 mL) or the analyte bottle (1 L), the actual temperature change in the total gas phase volume does not exceed 0.3°C. This was the reason for limiting the piston speed of maximum of 5 mL/min. Average piston speed used in all of our experiments was 3 mL/min. 8 psi of pressurized air was necessary to achieve the speed of 3 mL/min. The pressure gauge

**Table 4-I.** Dependence of the pressure drop on the gas flow rate.

Flow rate [ml/min]	0.5	1	2	3	4	5	7	10
Pressure drop [Torr]	0	1	2	3	6	11	26	57

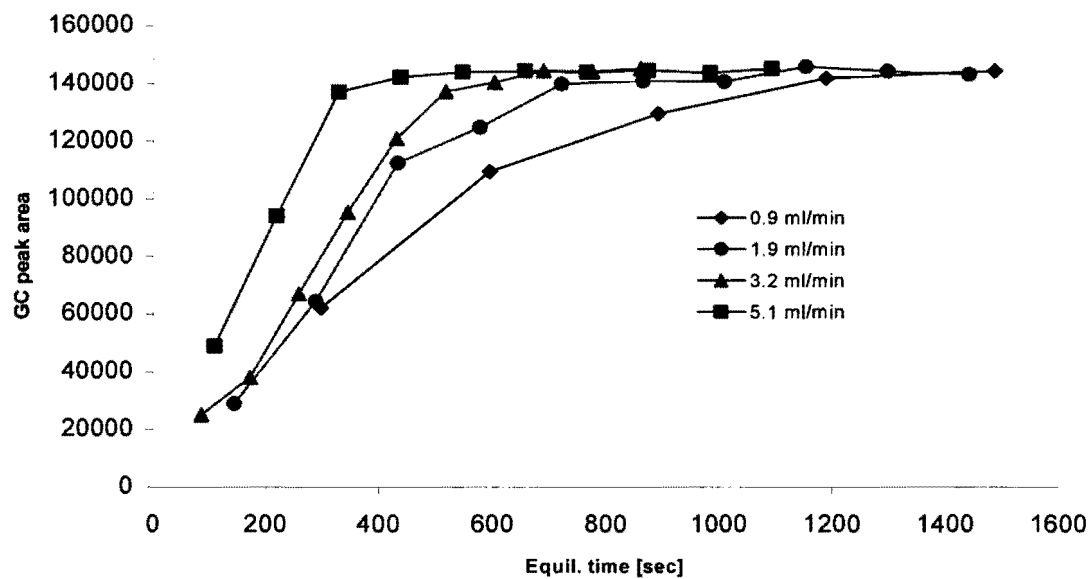


**Figure 4-23.** Vapor composition equilibration between the analyte bottle and the syringe assembly measured at different syringe piston speeds.

maintained the pressure very accurately since the air coming into the pressure gauge was house air that was always kept above 60 psi.

### **Experimental (for the measurement of $K_p$ )**

All analytes (Ketones – Acetone, Butanone, Pentanone, Hexanone and Heptanone & Alkyl Benzenes – Benzene, Toluene, Ethyl Benzene and Propyl Benzene) were at least 98% pure. All solvents (Acetonitrile and Water) were HPLC grade and all chemicals listed above were obtained from Sigma-Aldrich (Sigma-Aldrich, St. Louis, MO).

All solvents were transferred into the headspace vial (part # HSV-150, Asist Inc., Cleveland, OH) via auto-pipettes (adjustable 100 and 1000  $\mu\text{L}$  – Eppendorf). Analytes were transferred into the analyte bottle via 10 or 50  $\mu\text{L}$  gas-tight syringes (Hamilton, Morristown, NJ).

A Gas Chromatograph model 5890 from Agilent (Little Falls, DE) with DB-1701 capillary column (15m length and 0.25 mm I.D., 0.25  $\mu\text{m}$  film thickness) was used. Detector was FID and the detector temperature was set at 300°C. The injector and oven temperature were varied from one analyte to the other. The reason for the injector temperature to be varied was that it should be kept as low as possible (since headspace system is placed right on top of it, so the extra heat can change the temperature at the bottom of the headspace system), but at least as high as the oven temperature so that the analyte does not condense upon entering the column. The column was inserted into a capillary tube and connected directly to valve 1 with finger tight ferrule. The injection is made directly onto the column.

The carrier gas was Helium. The flow of the carrier gas was controlled through the pressure gauge. The pressure reading used for each analyte is outlined in Table 4-II.

**Table 4-II:** List of GC conditions used for all analytes in order to separate Acetonitrile (solvent) and the Analyte.

Analyte	Oven Temperature (°C)	Pressure reading for Helium (psi)	Injector Temperature (°C)
Acetone	60	10.0	60
Butanone	60	10.0	60
Pentanone	90	12.0	90
Hexanone	120	12.0	120
Heptanone	150	13.0	150
Benzene	70	8.0	110
Toluene	110	10.0	110
Ethyl Benzene	140	10.0	140
Propyl Benzene	160	11.0	160

Some conditions that were varied to achieve the separation of the solvent and the analyte peaks are also outlined in Table 4-II. All separations were achieved isothermally. The solvent used was a mixture of acetonitrile-water. Since the detector used was FID, it will detect acetonitrile and give a peak in the chromatogram along with the analyte. So, the conditions stated (oven temperature and flow rate of Helium) above were varied in such a way that a baseline separation was achieved between the two peaks in a chromatogram.

Once the GC conditions were finalized for an analyte, the next step was to calibrate the response of the FID detector. This was performed by placing known volume of analyte in the analyte bottle and let it completely evaporate in the bottle.

{The analyte volume was calculated using the ideal gas law equation ( $PV = nRT$ ). The volume of the bottle is found to be 1.20 L. The saturated vapor pressure of all analytes at room temperature was obtained from the handbook of Chemistry and Physics. The gas constant is a known constant (0.0821 L-atm/mol-K) and the temperature was taken as 25°C since the bottle is sitting at room temperature. The number of moles is the quantity we are trying to determine. The number of moles is transferred to weight by multiplying it with molecular weight of an analyte. The weight can be transferred to the volume by dividing it with the analyte density at 25°C. The volume calculated here is the maximum volume that can be place inside the 1.20 L bottle at 25°C. Any volume lower than the calculated one will be completely evaporated (saturated) inside the bottle.}

The analyte vapor was equilibrated with the syringe assembly and the injection was made after the equilibration. Each calibration curve, for an analyte, had at least three points. This was performed to calculate the “true” concentration found in the gas phase and the liquid phase. If this calibration was not performed, then the distribution constant would have been

the same, but the concentrations would have been wrong. Since the distribution constant is composed of two concentrations, the units cancel each other and the final value is identical whether the system was calibrated or not. The experimentally measured calibration values are not given here for this reason.

There are three more variables that need to be measured before the measurements of the gas-liquid distribution constants can be measured.

1. The number of reciprocating syringe strokes to measure the equilibration time of analyte vapors between the analyte bottle and the syringe assembly (step *a* of the isochoric vapor loading method).

This was measured by placing the calculated volume of an analyte in the analyte bottle and starting the reciprocating syringe movement right away. Actuating valve 3 connected the analyte bottle and the syringe assembly. After every 5 syringe strokes, an injection was made to measure the peak area of an analyte. The equilibration was achieved when two or more consecutive peak areas were found to be similar. The plateau of the exponential growth curve (peak area versus number of syringe strokes) was chosen as the equilibration time. The number found for that equilibration was programmed into the software for step *a* of the isochoric vapor loading method for that analyte. The obtained results are summarized in Table 4-III.

2. The number of reciprocating syringe strokes to measure the equilibration time of analyte vapors between the analyte vapor and the solvent (step *e* of the isochoric vapor loading method).



**Table 4-III:** The number of syringe strokes required, for each analyte, for the listed steps of the vapor loading method to determine the *K*.

Analyte	step a*	step e*	step g*
Acetone	20	20	20
Butanone	20	20	20
Pentanone	25	25	20
Hexanone	25	25	20
Heptanone	30	30	20
Benzene	20	35	20
Toluene	25	40	20
Ethyl Benzene	30	45	20
Propyl Benzene	35	50	20

\* Refer to text for complete description.

Once the analyte vapor was equilibrated with syringe assembly from the analyte bottle, as described above in 1, valve 3 was brought back to its neutral position. The HS vial containing 400  $\mu\text{L}$  of acetonitrile was loaded into the headspace system before.

After every 5 syringe strokes, an injection was made to measure the peak area of an analyte. The equilibration was achieved when two or more consecutive peak areas were found to be similar. The plateau of the exponential decay curve (peak area versus number of syringe strokes) was chosen as the equilibration time. The number found for that equilibration was programmed into the software for step *e* of the isochoric vapor loading method for that analyte. The obtained results are also summarized in Table 4-III.

3. Once the vacuum has been turned on (step *g* of the isochoric vapor loading method), the number of reciprocating syringe strokes to clean out the analyte- and the solvent vapors from the syringe assembly before the next cycle begins.

This is to measure the number of syringe strokes needed, when the vacuum is turned on, to clean the syringe assembly. Once the vacuum starts, every 5 syringe strokes an injection was made to see if the analyte and the solvent vapors are gone. The cleaning of this kind takes an exponential decay approach. For this reason, the syringe assembly is not completely cleaned (keeping time in perspective). The syringe assembly is said to be clean, when two or more consecutive injections show similar peak area counts. The results are given in Table 4-III.

{The cleaning is actually not necessary in the current study since the bottle is kept at 25°C (room temperature) and the HS system is kept at 30°C. There was no condensation in the bottle since the temperature difference was only 5°C. But, at high temperature differences,

when HS temperature is raised to 50°C or higher, the vapors may condense and this presents a problem. This was observed when  $K$  was measured at 50°C or higher.}

### **Step by Step Calculation of Gas-Liquid Distribution Constant Using the Isochoric Vapor Loading Method.**

The step-by-step description of the Isochoric vapor loading method was described earlier in this Chapter (pages 158 to 171). The representative schematics of each step are illustrated in Figures 4-13 to 4-22. A step-by-step calculation of the gas-liquid distribution constant using the isochoric vapor loading method is shown here.

The volumes of components inside the HS system are already known: 2.32mL for syringe assembly ( $V_{syr}$ ), 24.3mL for HS vial ( $V_V$ ) and 0.4mL of liquid (solvent) phase ( $V_L$ ). The volume of the gas phase inside the HS vial ( $V_H$ ) is 23.9mL and the total volume ( $V_T$ ) of the gas phase (when the syringe assembly and the HS vial are connected) is 26.22mL.

The concentration of analyte in the analyte bottle is  $C_B$ . The movement of the syringe assembly drives the equilibration of the analyte between the analyte bottle and the syringe assembly loop (refer to Figure 4-14). Once equilibrated, the concentration inside the syringe assembly loop is same as it was inside the bottle. For the 1<sup>st</sup> cycle, the gas phase concentration of the analyte inside the bottle,  $C_{B,G}^I$ , is measured by GC when valve 1 is actuated for 2 seconds (refer to Figure 4-15). Then, valve 3 is closed and valve 2 is open (refer to Figure 4-16). The analyte vapors are then equilibrated between the gas phase and the liquid phase inside the HS vial (refer to Figure 4-17) and after they have been equilibrated, valve 1 is actuated for 2 seconds to measure the equilibrium concentration of the analyte in the gas phase,  $C_{eq,G}^I$ , by GC (refer to Figure 4-18). From the two

concentrations measured by GC and known volumes of the system, the gas-liquid distribution constant is calculated as follows:

For the 1<sup>st</sup> loading cycle, the amount of analyte in the HS vial is 0. The transferred amount, from the syringe assembly to the HS vial,  $M_{syr}^1$  is equal to

$$M_{syr}^1 = C_{B,G}^1 V_{syr} \quad (4-47)$$

After connection of the syringe assembly to the HS vial and equilibration, the transferred amount of the analyte will be distributed between the gas and the liquid phase giving

$$M_{syr}^1 = C_{eq,L}^1 V_L + C_{eq,G}^1 (V_{syr} + V_V - V_L) \quad (4-48)$$

where  $C_{eq,L}^1$  is the equilibrium concentration of the analyte in the liquid phase after the 1<sup>st</sup> loading cycle. Since all of the other variables in the Equation 4-48 are known, we can calculate the  $C_{eq,L}^1$  for the 1<sup>st</sup> loading cycle. Since the concentration of the analyte in the gas phase and liquid phase, at equilibrium is known,  $K$  can be calculated using Equation 4-1 for the 1<sup>st</sup> loading cycle. At the end of 1st loading cycle, valve 2 was closed and vacuum was applied to the syringe assembly loop to clean the solvent and analyte vapors from the syringe assembly loop. Then the second loading cycle can start from the beginning in the same HS vial.

For the 2<sup>nd</sup> loading cycle the  $C_{B,G}^2$  and  $C_{eq,G}^2$  are measured as discussed for loading cycle number 1, but the superscripts 2 are used instead of 1, indicating loading cycle number. The transferred amount, from the syringe assembly to the HS vial, for the 2<sup>nd</sup> loading cycle is equal to

$$M_{syr}^2 = C_{B,G}^2 V_{syr} \quad (4-49)$$

After connection of the syringe assembly to the HS vial and equilibration, the transferred amount of the analyte will be distributed between the gas and the liquid phase. However, there is certain amount of analyte present in the gas and liquid phase inside the HS vial from the 1<sup>st</sup> loading cycle. The amount of analyte present inside the gas phase and liquid phase inside the HS vial is equal to  $C_{eq,G}^1(V_V - V_L)$  and  $C_{eq,L}^1 V_L$ , respectively. So, the following mass balance equation can be written for the 2<sup>nd</sup> loading cycle.

$$M_{syr}^2 + C_{eq,G}^1(V_V - V_L) + C_{eq,L}^1 V_L = C_{eq,L}^2 V_L + C_{eq,G}^2(V_{syr} + V_V - V_L) \quad (4-50)$$

where  $C_{eq,L}^2$  is the equilibrium concentration of the analyte in the liquid phase after 2<sup>nd</sup> loading cycle. Since all of the other variables in the Equation 4-50 are known,  $C_{eq,L}^2$  for the 2<sup>nd</sup> loading cycle can be calculated. Now, for the 2<sup>nd</sup> loading cycle, the equilibrium concentration of the analyte in the gas phase and the liquid phase are known, so  $K$  is calculated using Equation 4-1.

The cumulative addition of the mass of the analyte, in the liquid phase, at loading cycle number  $i$  ( $i \neq 1$ ), can be calculated by combining Equation 4-49 and Equation 4-50 gives

$$C_{eq,L}^i V_L = C_{B,G}^i V_{syr} + C_{eq,G}^{i-1}(V_V - V_L) + C_{eq,L}^{i-1} V_L - C_{eq,G}^i(V_{syr} + V_V - V_L) \quad (4-51)$$

Then the following equation can be used to determine  $K$  at loading cycle number  $i$  ( $i \neq 1$ ).

$$K^i = \left( \frac{1}{C_{B,G}^i} \right) \left( \frac{C_{B,G}^i V_{syr} + C_{eq,G}^{i-1}(V_V - V_L) + C_{eq,L}^{i-1} V_L - C_{eq,G}^i(V_{syr} + V_V - V_L)}{V_L} \right) \quad (4-52)$$

Every concentration in Equation 4-52 can either be the peak area taken from a chromatogram of the analyte or the actual concentration in ppm by converting peak area to

ppm using a calibration curve generated ahead of time. It really does not matter what kind of concentration (peak area or ppm) is used, since it will not change the calculated value for  $K$ .

For an illustration of this calculation,  $K$  is calculated for Benzene in the presence of 0.4 mL of acetonitrile/ water (90:10, v/v). The GC detector was calibrated before and the found relationship between the peak area of Benzene (Y axis) and the concentration of Benzene (in ppm) (X axis) was found to be

$$Y = (6745)(X) \quad (4-53)$$

The calculation is shown in Table 4-IV. Eight loading cycles were performed to measure the gas-liquid distribution constant of Benzene in 90% acetonitrile / 10% water (solvent). Two concentrations,  $C_{B,G}^i$  and  $C_{eq,G}^i$ , of Benzene were measured during each loading cycle of the isochoric vapor loading method as described earlier. The measured peak areas for the two concentrations are listed in Row 2 and Row 13 of Table 4-IV and Row 3 and Row 14 of Table 4-IV, respectively. Both of these concentrations were converted to ppm using Equation 4-52 and the obtained values are given in Row 4 and 5 for cycle number 1 and in Row 15 and 16 for cycle number  $i$  ( $i \neq 1$ ) in Table 4-IV. Column B of Table 4-IV indicates how each concentration (units are ppm) or amount (units are  $\mu\text{g}$ ) was calculated for each loading cycle. The equations used for 1<sup>st</sup> loading cycle are different than rest of the loading cycles, so they were separated accordingly in Table 4-IV.

The calculated equilibrium liquid phase concentrations were plotted against the measured equilibrium gas phase concentrations, at each loading cycle, to calculate the gas-liquid distribution constant. The slope of the line is the gas-liquid distribution constant. Using the values obtained from Table 4-IV, a graph was generated to determine the gas-

**Table 4-IV:** An Excel spreadsheet showing the step-by-step calculation of the gas-liquid distribution constant of Benzene in acetonitrile: water mixture (90:10, v/v) as a solvent at 30°C.

A	B	C	D	E	F	G	H	I
1	cycle number	1						
2	$C'_{B,G}$ (peak area)	482026						
3	$C'_{eq,G}$ (peak area)	10032				$V_{syr}$	2.32 mL	
4	Row 2 converted to ppm using Equation 4-53.	71.5				$V_V$	24.3 mL	
5	Row 3 converted to ppm using Equation 4-53.	1.5				$V_L$	0.4 mL	
6	$C'_{B,G} \times V_{syr}$ (Equation 4-47)	166				$V_H$	23.9 mL	
7	$C'_{eq,G} \times V_H$	39				$V_T$	26.22 mL	
8	$M'_{eq,L}$ (Equation 4-48) (Row 6 - Row 7)	127			slope of calibration curve		6745	
9	$C'_{eq,L}$ (Row 8 / Row 16)	317						
10	$K'$	213						
11								
12	Cycle number	2	3	4	5	6	7	8
13	$C'_{B,G}$ (peak area)	476964	475492	475885	477249	475747	472868	471289
14	$C'_{eq,G}$ (peak area)	16168	23224	31354	39038	46163	52810	59894
15	Row 2 converted to ppm using Equation 4-53.	70.7	70.5	70.6	70.8	70.5	70.1	69.9
16	Row 3 converted to ppm using Equation 4-53.	2.4	3.4	4.6	5.8	6.8	7.8	8.9
17	$C'_{B,G} \times V_{syr}$	164	164	164	164	164	163	162
18	$C'^{T'}_{eq,G} \times V_H$	35.5	57.3	82.3	111.1	138.3	163.6	187.1
19	$M'^{T'}_{eq,L}$	127	264	394	518	642	764	885
20	$C'_{eq,G} \times V_T$	63	90	122	152	179	205	233
21	$M'_{eq,L}$ (Equation 4-51) (Row 6 + Row 7 + Row 8 - Row 9)	264	394	518	642	764	885	1002
22	$C'_{eq,L}$	659	985	1296	1604	1911	2213	2504

liquid distribution constant for Benzene in presence of 90% acetonitrile in water, v/v. Refer to Figure 4-24 for the graph, with the slope of the line,  $K$ , found to be 290.

**Precision and Accuracy of the Measured Gas-Liquid Distribution Constant(s) by the Isochoric Vapor Loading Method.**

Calculating the gas-liquid distribution constant from the slope (average of eight loading cycles, in the above example) of a linear line reduces or almost eliminates systematic errors since the whole experiment is performed in a single HS vial. However, there are always random errors. The imprecision in the obtained value for the gas-liquid distribution constant depends on many variables. The majority of the random error in the measured gas-liquid distribution constant is due to small changes in temperature and measured peak area of the analyte. The error introduced from the measurement of the concentration of an analyte is irrelevant since the final value (gas-liquid distribution constant) divides one concentration by the other and will cancel the error introduced. The measured peak area in the syringe assembly does not introduce big error since this concentration remains fairly stable throughout the experiment (the %RSD of the measured peak area given in row # 2 is 0.67%).

The effect of the measured peak area when the analyte is equilibrated with the solvent was studied for all measured gas-liquid distribution constants. The measured peak area should represent true equilibrium concentration. The only way to know this is to perform an experiment as described before (refer to Table 4-III) to determine the number of syringe strokes required to reach the equilibrium (e.g., 35 syringe strokes for Benzene). Since the number of syringe strokes is at the plateau of a decay profile, it is assumed that equilibrium is close. As long as this plateau is reached, from one loading cycle to another, the obtained



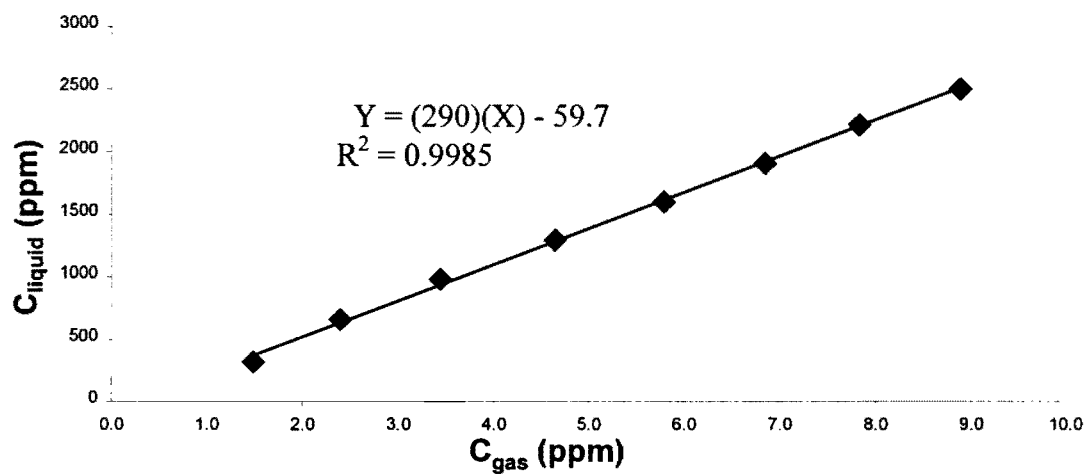


**Figure 4-24:** Linear regression using found concentrations of Benzene, at equilibrium for each cycle, in the liquid phase versus the gas phase. The slope of this line (290) represents the gas-liquid distribution constant of Benzene in 90:10 acetonitrile: water, v/v, at 30°C.

peak area is taken as the equilibrium concentration. To observe this during the experiment performed, three injections of an equilibrated analyte vapor with the solvents were measured by moving two full syringe strokes and then making an injection. In other words, using benzene as an example, three injections were made after 35, 37 and 39 syringe strokes, respectively. Since it is known that benzene should be in equilibrium after 35 syringe strokes, the measured peak area at 37 and 39 syringe strokes should provide a very similar peak area count. Table 4-V lists the obtained peak areas for the described experiment (Benzene in 90:10 acetonitrile: water, v/v). For each loading, it is seen that the peak area obtained after the 35 strokes is the highest of the three. The next two peak areas, after 37 and 39 syringe strokes, are very similar to each other. This indicates that the equilibrium was reached at this point. The difference between these two peak areas is less than 1.0% (0.8% being the highest).

When the highest difference in peak area is used as the error and  $K$  for the Benzene in 90:10 acetonitrile: water, v/v, is calculated again, the  $K$  is found to be 287 or 293, depending upon the positive or negative error. So, equal error, in %, is found from the difference in peak area. In this case, 1% difference in peak area gave 1% error in the measured value of  $K$ .

The last variable that can introduce error is the temperature. The temperature inside the HS system was programmed to be constant at 30°C. To see the exact temperature inside the HS system, two thermocouples were placed inside the HS system. One where the HS vial is sitting and the other where the syringe assembly is located. The HS vial is located in the center of the headspace system and the syringe assembly is located on the left side of the system. There is a small fan sitting inside the HS system to circulate the air to maintain constant temperature and to avoid sudden change in temperature. Two probes located inside

**Table 4-V:** Peak area of Benzene during equilibration process with the solvent (acetonitrile: water, 90:10, v/v).

	A	B	C	D	E	F	G	H	I
1	cycle number	1	2	3	4	5	6	7	8
2	Area count found in the gas phase inside the syringe assembly	482026	476964	475492	475885	477249	475747	472868	471289
3	Area count found in the gas phase at equilibration with the solvent after 35 syringe strokes	11165	16744	24070	32174	39483	46688	53846	60263
4	Area count found in the gas phase at equilibration with the solvent after 37 syringe strokes	10009	16278	23225	31234	38834	45952	52788	59411
5	Area count found in the gas phase at equilibration with the solvent after 39 syringe strokes	10032	16168	23224	31354	39038	46163	52810	59894

the HS system were programmed to take a temperature reading every 30 minutes. The time for an average experimental loading cycle took about 2 hours, so we had four temperature readings per cycle to observe the temperature drift. An example of the collected temperature reading is presented as a chart in Figure 4-25. For the example given in Figure 4-25, the average difference between the two probes during an experiment was found to be 0.6°C. As stated earlier, the temperature is controlled within 1°C. For air circulated heating system, this is as good as it got and the best we could do. In the next generation of the Isochoric HS system, currently working in our laboratory, the temperature is controlled through a water circulating bath and very tight temperature readings between the two probes (locations stated before) are found (within 0.2°C).

Temperature is the variable that introduces the largest error in measuring the gas-liquid distribution constant. This is because the temperature has an effect on the distribution constant,  $K$ , as per the following exponential relationship:

$$\log K = (B'/T) - C' \quad (4-54)$$

where  $B'$  and  $C'$  are constants.

This is an exponential relationship, so a slight change in the temperature will have a large effect on the measured gas-liquid distribution constant. The effect of a change in temperature (for example, 1°C) on the measured distribution constant for every analyte studied was not performed in the current study since the  $\log K = 1/T$  relationship is different depending on analyte and the matrix (solvent, for the current study).

However, the measurement of the gas-liquid distribution constant was performed in triplicate to calculate the average and to determine the standard deviation or the precision of

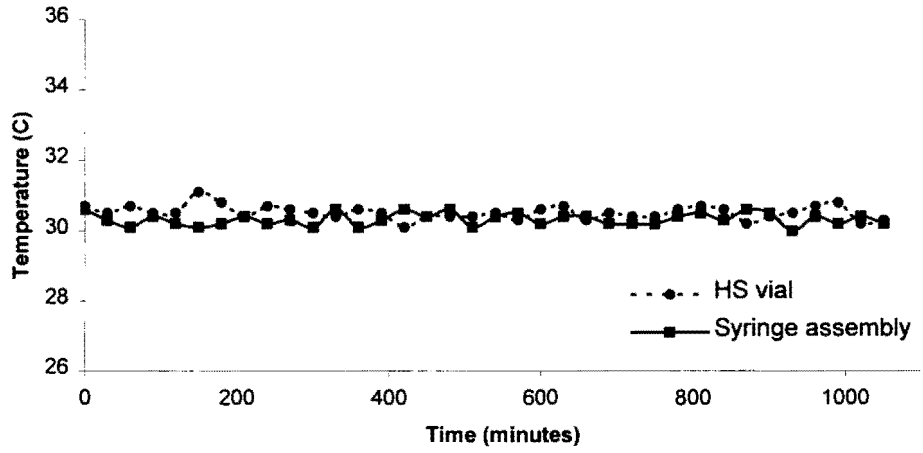


**Figure 4-25:** An example of the temperature readings found from within the HS system during typical HS experiment. A point was recorded every 30 minutes. The temperature was recorded at two different locations of the HS system: next to syringe assembly and next to HS vial.

the measured value for different analytes at different solvent composition. The gas-liquid distribution constant of methanol in water was measured three times at  $30 \pm 1^\circ\text{C}$ . The three values obtained are 2021, 2141 and 1940. The average of the three is 2034 and standard deviation is 101 (or %RSD is 5%). The gas-liquid distribution constant of propyl benzene in acetonitrile was also measured three times. The three values obtained were 5166, 4576 and 4880. The average of the three is 4874 and standard deviation is 295 (or %RSD is 6%). The gas-liquid distribution constant of Butanone in water was measured three times at  $30 \pm 1^\circ\text{C}$ . The three values obtained are 237, 243 and 235. The average of the three is 238 and standard deviation is 4 (or %RSD is 2%). The general trend observed, for analytes, was that higher water composition in the solvent gave lower %RSD ( $\approx 2\%$ ) than higher acetonitrile composition ( $\approx 6\%$ ) in the solvent. The three replicates of each set of data were performed within one week. The precision of the used method to measure the gas-liquid distribution constant is found in the range of 2 to 6 %RSD.

The next sets of experiments were performed to see the effect of mixing binary (e.g., acetonitrile-water) solvents (since there is a decrease in the volume after mixing), the effect of the solvent volume, the day to day variability as well as instrument to instrument variability on the measured gas-liquid distribution constants. The results obtained for all of these experiments using different analytes and different solvent compositions are summarized in Table 4-VI. The effect of mixing binary solvents was studied first. As seen from Table 4-VIA, the results found are different depending upon the composition of the binary mixture. When the collapse of the volume is high when two neat solvents are mixed, as in 90% acetonitrile: 10%water, the results is found to be very different (about 12%). When the collapse of the volume is low when two neat solvents are mixed, as in 90% water:

10% acetonitrile, the results are found to be somewhat similar (about 6% difference). Since all of the HPLC data were obtained by mixing the two individual solvents by the pump and not pre-mixing them, it was decided that the solvent must be added separately. For example, 0.4mL of 90% acetonitrile: 10% water was made in the HS vial by adding 0.36mL of acetonitrile and 0.04mL of water. The total volume of the solvent was taken as 0.4mL eventhough we know that there is a decrease in the final volume. This was also done to eliminate errors due to the measurement of solvent. If solvents were pre-mixed, then every time the solvents are pre-mixed, the composition may be different depending how long ago they were mixed. One of the solvent being acetonitrile, it is known that some acetonitrile will be evaporated if the mixed solvent is kept for a long time. All of the problems due to mixing are avoided when the solvents are added separately since every time the measured volumes will be accurate and the decrease in the final volume is a physical phenomenon and will not change from one experiment to another (e.g., analyte to analyte).

The effect of solvent volume on the measured gas-liquid distribution constants was also studied. The results are summarized in Table 4-VIB. All solvents were added separately in the HS vial to get the final volume. It is seen that the measured values are close to each other (about 6 % difference). The headspace sensitivity is increased with lower solvent volumes. The solvent volume of 0.4mL was found to be adequate to give enough HS sensitivity to measure most of the gas-liquid distribution constants.

The day to day and instrument to instrument variability were also measured and the obtained results are summarized in Table 4-VIC and Table 4-VID, respectively. The difference between the measured values at different time is found to be 4% and when using different instrument is found to be 1%, indicating that the measured values can be

**Table 4-VI:** Precision and accuracy of the measured gas-liquid distribution constants at  $30 \pm 1^\circ\text{C}$ .

A. The effect of mixing binary solvents on the measured values.

Analyte = Acetone	90% acetonitrile: 10% water	10% acetonitrile: 90% water
0.4mL added separately	1058	386
Two solvents were pre-mixed and then 0.4mL of volume taken	934	386
The percent difference between the two	11.7	0.0

B. The effect of the solvent volume on the measured values (solvent added separately).

Analyte = Acetone	90% acetonitrile: 10% water	10% acetonitrile: 90% water
0.4mL	1058	386
0.8mL	1033	360
The percent difference between the two	2.4	6.7

Analyte = Pentanone	100% acetonitrile
0.4mL	3079
0.3mL	2879
The percent difference between the two	6.5

C. The day to day variability on the measured values when using 0.4mL of solvent (added separately).

Analyte = Acetone	90% acetonitrile: 10% water
April 3, 2000	1058
April 13, 2000	1016
The percent difference between the two	4.0

D. The instrument to instrument variability on the measure values when using 0.4mL of solvent.

Analyte = Acetone	100% water
The instrument on which all of the gas-liquid distribution constants given in this chapter were measured.	385
Second instrument on which the one and only given gas-liquid distribution constant was measured.	389
The percent difference between the two	1.0



reproduced at different times and when using different instruments.

The accuracy of the measured data can be obtained when the found values are compared to the values found in the literature or when using different methods. Unfortunately, all of the data given in the literature were measured using a typical HS system where the HS vial is pressurized. The pressurization of the HS vial changes from one laboratory to the next depending upon the GC setup. This is because the pressure inside the HS vial is kept higher than the inlet pressure found in GC to drive the analyte vapor from high- to low pressure when making an injection. By performing an HS experiment using pressurized HS vials to measure a physical parameter, e.g. gas-liquid distribution constant is fundamentally wrong, as described earlier in this chapter. In any case, a comparison is made here to illustrate the point stated above. The distribution constant of methanol in water at 30°C, using the Isochoric headspace system, was found to be 2034 (average of three measurements). When this value is compared to the literature values (measured using typical HS system where the HS vial is pressurized), our measured value is found to be about half ( $K = 3867$ ) of those found in the literature [241]. This could be attributed to the reason stated before. Every HS experiment is performed differently where the pressurization of the HS vial is different giving very different values for any measured gas-liquid distribution constant. To avoid this, the isochoric headspace system can be used, which is known to work at atmospheric pressure and found results then can be compared from one laboratory to the other since the problem of pressurizing the HS vial has been eliminated.

The accuracy of the method has been studied in a different way. The well-known relationship of *log K versus 1/T* was used to demonstrate the accuracy. The results are given in the next section (Results and Discussion: Gas-Liquid Distribution Constants, page ).

The results are found to be accurate since a linear line was obtained when  $\log K$  was plotted against  $1/T$ . However, the obtained error on the extrapolated point is cumulative from the other points of the linear line. To illustrate this point, refer to Figure 4-26. A typical  $\log K$  versus  $1/T$  is plotted for an analyte, for example. The three points on the line (at 40, 50 and 60°C) had some error associated with it (indicated by the error bar). When linear regression is used to extrapolate the point at 30°C, it is shown that the error is accumulated from the three points. If the extremes of the error of the three points are taken as three points to draw the linear line (dashed line 1 or 2 in Figure 4-26), then the calculated point has accumulated error from the three points, as shown by the arrow in Figure 4-26.

It has been demonstrated that the method used is accurate and gives reproducible results. However, there are some practical things that need to be considered when evaluating the measured gas-liquid distribution constants and the next section highlights some of them.

### **Evaluation of the Data for the Gas-Liquid Distribution Constant(s) by the Isochoric Vapor Loading Method.**

From the experimental data, when the concentration of an analyte in the liquid phase is plotted against the concentration of an analyte in the gas phase at equilibrium, it was earlier in this chapter that the slope of the line (refer to figure 4-24) is the gas-liquid distribution constant. But, what about the intercept? It is interesting to note that the intercept can be used to give an approximate concentration of an analyte in the gas phase of the HS vial before the first loading cycle. For example, the intercept obtained from the linear line (refer to Figure 4-24) is 59.7. Let's say that  $Y = 0$ , or the concentration of an analyte

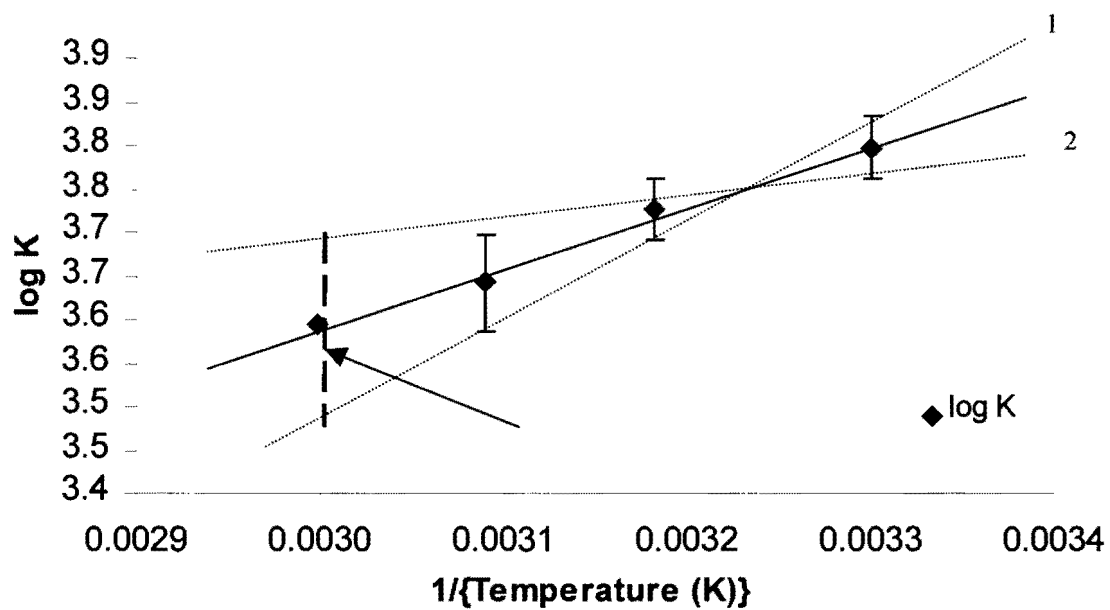


**Figure 4-26:** An illustration of the accumulation of the error on the extrapolated point from the linear regression. Dashed lines 1 and 2 are drawn from the three extreme points of the error bar of the three data points. The arrow indicated the accumulated error for the extrapolated point.

(Benzene, in this example) in the liquid phase is zero. This is only true before the first loading cycle. When  $Y = 0$ ,  $X = 0.21$  ppm since  $X$  axis has unit in ppm. It is known that the concentration in the gas phase inside the HS vial before the first cycle is zero since no analyte was present inside the HS vial. The only place where 0.21ppm concentration of analyte can reside is in the connection lines of the HS vial to valve 2 (refer to Figure 4-1). These two capillary tubing do not get cleaned in the vacuum cycle after each loading cycle. This means that when an experiment in a HS vial is finished (e.g., 100% acetonitrile as solvent) and next HS vial is loaded with 90% acetonitrile in water, as was the case above, the analyte vapors inside the two capillaries discussed above were not cleaned. These analyte vapors were then introduced in the HS vial where 90% acetonitrile in water was present. So, in reality, the analyte was not present in the gas phase of the HS vial before the experiment, but as described here there were some analyte vapors in the gas phase inside the HS vial. This is only estimation and the concentration found in the gas phase inside of one HS vial to another would vary depending upon the gas phase concentration of the analyte in the last cycle of a previous HS vial. In summary, this can be explained as a carryover of analyte vapors from one HS vial to another. Theoretically, if there were no carryover then we would have seen the line cross zero. For all of the measured gas-liquid distribution constants (approximately 200 of them), the sign for intercept found for each and every one was negative. This indicates strongly that for each and every measured gas-liquid distribution constant, there was a carryover of analyte vapor from one HS vial to the next. This makes sense because even when an analyte was switched, e.g. from Benzene to Toluene, the system was first calibrated with Toluene. During the calibration of the system, Toluene vapors were

introduced inside the connecting lines before the measurement of gas-liquid distribution constants even began.

What if the intercept of the graph (refer to Figure 4-24) has a positive intercept? This would indicate that when the gas phase concentration is zero,  $X = 0$ ;  $Y =$  positive number or the analyte is present in the liquid phase before the equilibration of the first cycle. This was not observed in this study since no analyte was ever introduced in the solvent.

When the concentration in the liquid phase versus the concentration in the gas phase is plotted, if the first loading gives a negative number for the concentration in the liquid phase then the following can be assumed. When the concentration in the liquid phase, after the first cycle, is found to be negative, this indicates that the equilibration of that analyte between the gas phase and the solvent was not reached. When this happens, the mass of analyte at equilibrium in the gas phase is found to be higher than the calculated. This only happens when the analyte vapors are not in equilibrium with the solvent. This gives a higher peak area count than the calculated one. Otherwise, physically, it would not make sense.

During the measurement of some of the gas-liquid distribution constants, especially when the solvent is made up of higher water content, the graph similar to the one shown in figure 4-27 was generated from the obtained experimental results. This is an effect of vapor saturation in the gas phase. This was observed for non-polar analytes, which are not soluble in water (all four alkyl benzenes, Hexanone and Heptanone). This indicates that the measured gas phase concentration, at equilibrium, is not changing much from one loading cycle to the next, or it is getting saturated. However, the concentration of the analyte in the liquid phase is calculated based on the measured concentration in the gas phase, so the calculated concentration of the analyte in the liquid phase is found to increase exponentially.

An example of this situation is illustrated in in Figure 4-27. This situation is easily avoided by loading less number of cycles in a given experiment or start with lower concentration of analyte in the analyte bottle.

All of the different parameters described above were considered when measuring the gas-liquid distribution constants for all of the studied analytes. The next section highlights the results obtained for all of the measured gas-liquid distribution constants using the Isochoric vapor loading method on the Isochoric headspace system.

### **Results and Discussion: Gas-Liquid Distribution Constants**

The gas-liquid distribution constants of ketones (acetone, butanone, pentanone, hexanone and heptanone) and alkyl benzenes (benzene, toluene, ethyl- and butyl benzene) were measured in acetonitrile: water mixture (every 10%, v/v, increment throughout the concentration range) at  $30 \pm 1^\circ\text{C}$ . The experimental parameters were described on page 184. The isochoric vapor loading method was used is described on page 158. The step-by-step calculation using the vapor loading method was also described on page 190.

The gas-liquid distribution constants of acetone, butanone and pentanone were measured directly at  $30 \pm 1^\circ\text{C}$ . The individual values obtained for all three ketones at different acetonitrile: water mixtures are listed in Table 4-VII. The measurement of the gas-liquid distribution constants for hexanone and heptanone were difficult since the vapor pressure of hexanone and heptanone is very low at  $30^\circ\text{C}$ , or both analytes are not volatile. This has a practical problem with very low gas phase concentration and detection of this concentration by the FID detector in GC.

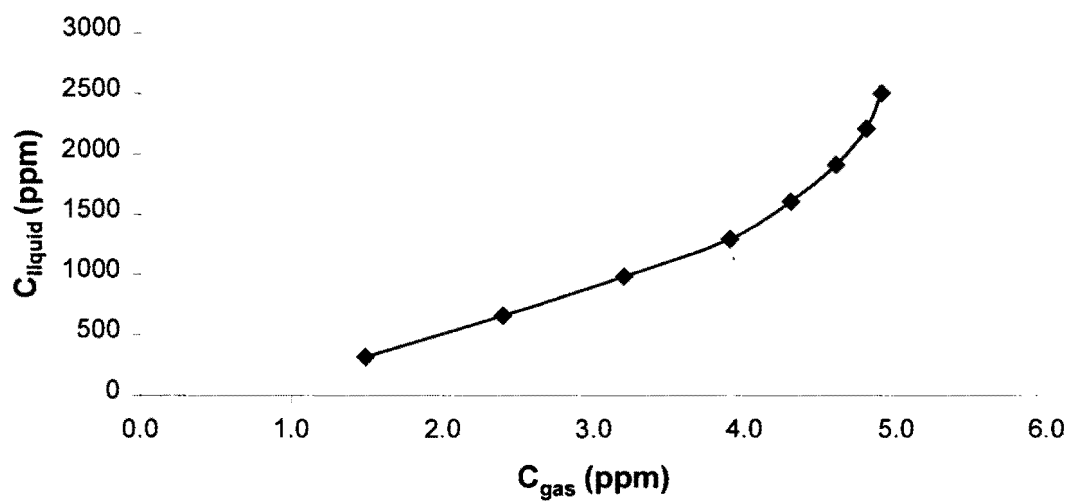


**Figure 4-27:** The graph representing the liquid phase concentration versus the gas phase concentration of an analyte, at equilibrium with some solvent at temperature  $T$ . The curvature of the line indicates that there is saturation of analyte vapors in the gas phase.

**Table 4-VII:** Measured gas-liquid distribution constants of acetone, butanone and pentanone in given acetonitrile: water mixtures at 30°C.

% acetonitrile in water, v/v	Acetone	Butanone	Pentanone
100	882 ± 60	1381 ± 83	3079 ± 188
90	1058 ± 76	1638 ± 99	2964 ± 179
80	1111 ± 73	1387 ± 71	2124 ± 107
70	1024 ± 54	1194 ± 61	1631 ± 82
60	873 ± 51	961 ± 49	1349 ± 69
50	766 ± 31	725 ± 29	884 ± 36
40	648 ± 26	546 ± 22	589 ± 24
30	522 ± 21	403 ± 16	355 ± 14
20	425 ± 13	316 ± 10	253 ± 8
10	386 ± 12	252 ± 8	196 ± 6
0	385 ± 8	234 ± 5	182 ± 4



To overcome this problem, the gas-liquid distribution constants for both analytes were measured at three temperatures higher than 30°C. The values obtained for hexanone at three different temperatures are given in Table 4-VIII. The linear relationship of  $\log K = 1/T$  was used to calculate the distribution constant at 30.0°C based on the values obtained at three given temperatures. As stated before in the accuracy and precision section that the obtained linear relationships are found to be very good for this relationship demonstrating the accuracy of the method. But, as stated in the same section before, the calculated values from this linear regression also has large error bar associated with it. The estimated errors on each calculated point are reported next to the calculated point in Table 4-VIII. The step-by-step calculation to obtain the gas-liquid distribution constant at 30.0°C from the given three temperature is given in Table 4-IX. The temperature reading given in Table 4-IX is the average temperature found inside the HS system during the experiment as described earlier. Similar results are given in Tables 4-X and 4-XI for heptanone.

The gas-liquid distribution constants obtained for all five studied ketones at 30°C are graphically represented in Figure 4-28. The most remarkable result shown in this figure is that for all studied ketones, the dependencies of  $K$  versus acetonitrile concentration intersect at the same point. This is because the transfer of acetone to pure water is more favorable than that of heptanone, and conversely the transfer of acetone to pure acetonitrile is less favorable than the transfer of heptanone, it follows that the various lines must cross. At this point, 40% acetonitrile in water, v/v, the distribution constants for all ketones are found to be equal to each other.

**Table 4-VIII:** Measured gas-liquid distribution constants of hexanone in given acetonitrile: water mixtures at three different temperatures.

% acetonitrile in water, v/v	60.5°C	50.7°C	41.2°C
100	3920 ± 464	4385 ± 334	5335 ± 427
90	3164 ± 211	3574 ± 396	4709 ± 284
80	1478 ± 143	1858 ± 126	2830 ± 143
70	626 ± 35	1016 ± 64	1549 ± 79
60	386 ± 25	689 ± 44	990 ± 50
50	192 ± 9	388 ± 24	597 ± 24
40	79.7 ± 3.7	197 ± 12	313 ± 13
30	39.9 ± 1.6	80.6 ± 4.9	153 ± 6
20	19.9 ± 0.6	34.6 ± 2.1	77.7 ± 2.3
10	9.50 ± 0.40	20.5 ± 1.2	50.0 ± 1.5

**Table 4-IX:** Step-by-step calculation of the gas-liquid distribution constant,  $K$ , of hexanone at 30.0°C in given acetonitrile: water mixtures.

Step A:  $\log K$  for each value from Table 4-VIII was calculated.

% acetonitrile in water, v/v	60.5°C	50.7°C	41.2°C
100	3.593	3.642	3.727
90	3.500	3.553	3.673
80	3.170	3.269	3.452
70	2.797	3.007	3.190
60	2.587	2.838	2.996
50	2.284	2.589	2.776
40	1.901	2.294	2.496
30	1.601	1.906	2.184
20	1.299	1.539	1.890
10	0.978	1.312	1.699

Step B: From the relationship of  $\log K$  versus  $1/T$  the following parameters were calculated.

% acetonitrile in water, v/v	slope	intercept	$R^2$
100	-0.0069	4.0060	0.973
90	-0.0089	4.0289	0.949
80	-0.0146	4.0380	0.968
70	-0.0204	4.0339	0.999
60	-0.0212	3.8836	0.985
50	-0.0255	3.8467	0.984
40	-0.0309	3.7982	0.970
30	-0.0302	3.4332	1.000
20	-0.0306	3.1316	0.986
10	-0.0374	3.2270	0.997

Step C:  $\log K$  at 30.0°C was calculated from the slope and intercept given above. Then,  $K$  at 30.0°C was calculated from inverse of  $\log K$ .

% acetonitrile in water, v/v	$\log K$ at 30.0°C	$K$ at 30.0°C
100	3.798	6284 ± 927
90	3.761	5769 ± 611
80	3.600	3984 ± 419
70	3.422	2642 ± 227
60	3.248	1769 ± 159
50	3.081	1204 ± 84
40	2.872	746 ± 52
30	2.526	336 ± 23
20	2.213	163 ± 9
10	2.106	128 ± 7

**Table 4-X:** Measured gas-liquid distribution constants of heptanone in given acetonitrile: water mixtures at three different temperatures.

% acetonitrile in water, v/v	51.1°C	55.5°C	60.2°C
100	5003 ± 321	4628 ± 463	3632 ± 335
90	4664 ± 326	3892 ± 454	3533 ± 255
80	1874 ± 95	1554 ± 320	1165 ± 99
70	1293 ± 133	937 ± 105	798 ± 74
60	876 ± 47	678 ± 64	552 ± 47
50	548 ± 23	488 ± 44	369 ± 43
40	253 ± 14	186 ± 9	168 ± 17
30	38.0 ± 1.5	27.4 ± 2.0	16.7 ± 1.5
20	23.0 ± 0.8	17.1 ± 1.0	11.9 ± 1.3
10	15.1 ± 1.5	11.3 ± 1.0	7.37 ± 0.58

**Table 4-XI:** Step-by-step calculation of the gas-liquid distribution constant,  $K$ , of heptanone at 30.0°C in given acetonitrile: water mixtures.

Step A:  $\log K$  of each value from Table 4-X was calculated.

% acetonitrile in water, v/v	51.1°C	55.5°C	60.2°C
100	3.699	3.665	3.560
90	3.669	3.590	3.548
80	3.273	3.191	3.066
70	3.112	2.972	2.902
60	2.943	2.831	2.742
50	2.739	2.688	2.567
40	2.403	2.270	2.226
30	1.580	1.438	1.221
20	1.362	1.233	1.074
10	1.179	1.053	0.867

Step B: From the relationship of  $\log K$  versus  $1/T$  the following parameters were calculated.

% acetonitrile in water, v/v	slope	intercept	$R^2$
100	-0.0154	4.4961	0.929
90	-0.0132	4.3369	0.964
80	-0.0227	4.4394	0.989
70	-0.0230	4.2721	0.957
60	-0.0221	4.0653	0.994
50	-0.0190	3.7200	0.956
40	-0.0193	3.3723	0.910
30	-0.0395	3.6068	0.990
20	-0.0317	2.9845	0.999
10	-0.0343	2.9398	0.992

Step C:  $\log K$  at 30.0°C was calculated from the slope and intercept given above. Then,  $K$  at 30.0°C was calculated from inverse of  $\log K$ .

% acetonitrile in water, v/v	$\log K$ at 30.0°C	$K$ at 30.0°C
100	4.035	10840 ± 1757
90	3.941	8721 ± 1298
80	3.758	5730 ± 825
70	3.583	3829 ± 813
60	3.403	2531 ± 360
50	3.151	1414 ± 240
40	2.794	622 ± 99
30	2.423	265 ± 36
20	2.034	108 ± 17
10	1.911	81.5 ± 15.6

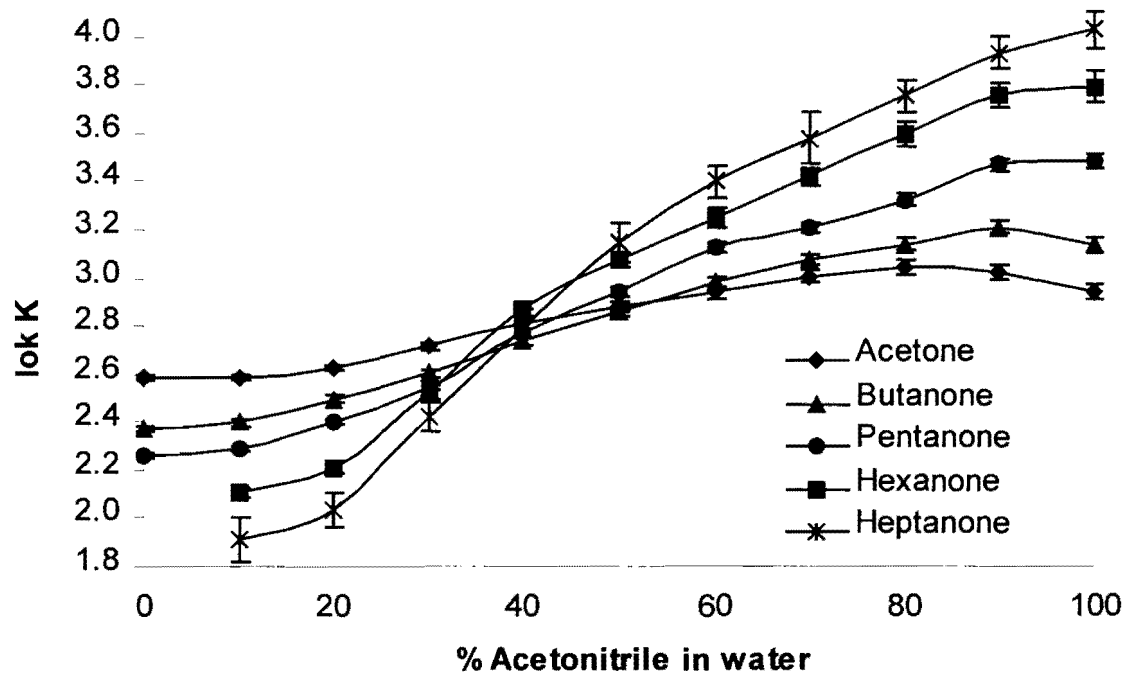


**Figure 4-28:** Plot of  $\log K$  of measured gas-liquid distribution constants at 30°C versus volume fraction of acetonitrile for all five ketones.

The error on each measured gas-liquid distribution constant was calculated by performing propagation of errors. Each of the following errors were included: (i) peak area from the analyte bottle, (ii) peak area when equilibrated with the solvent, (iii) a standard deviation base on solvent composition and, for hexanone and heptanone only (iv) accumulated error from the  $\log K$  vs.  $1/T$  regression line as described earlier in this chapter. Note that the gas-liquid distribution constant for every analyte at every acetonitrile-water composition was not performed in triplicate, so an estimation of standard deviation was used based on equivalent data from other analytes with similar conditions.

The gas-liquid distribution constants of the four alkyl benzenes (Benzene, Toluene, Ethyl Benzene and Propyl Benzene) were measured directly at  $30 \pm 1^\circ\text{C}$ . The individual values obtained for four alkyl benzenes at different acetonitrile: water mixtures are listed in Table 4-XII. The gas-liquid distribution constants obtained for four studied alkyl benzenes at  $30^\circ\text{C}$  are graphically represented in Figure 4-29. As discussed earlier for ketones, there is a very narrow range in acetonitrile: water composition at which the distribution constants of four alkyl benzenes are the same. This is because the transfer of benzene to pure water is more favorable than that of Propyl benzene, and conversely the transfer of benzene to pure acetonitrile is less favorable than the transfer of Propyl benzene, it follows that the various lines must cross. This composition for the five alkyl benzenes studied is around 35 % acetonitrile in water, v/v.

The measured gas-liquid distribution constants were used to calculate the liquid-liquid partition coefficient,  $K_P$ . The overall objective of the headspace study was to measure the  $K_P$  for all analytes at different acetonitrile-water composition and the next section outlines the obtained results.

**Table 4-XII:** Measured gas-liquid distribution constants of four alkyl benzenes in given acetonitrile: water mixtures at 30°C (----- Indicates that the values were not measured).

% acetonitrile in water, v/v	Benzene	Toluene	Ethyl Benzene	Propyl Benzene
100	409 ± 25	876 ± 53	1823 ± 142	4874 ± 308
90	290 ± 18	698 ± 44	1386 ± 84	3513 ± 236
80	213 ± 11	400 ± 20	793 ± 40	1732 ± 88
70	156 ± 8	299 ± 15	462 ± 24	913 ± 47
60	92.1 ± 4.7	153 ± 8	256 ± 13	456 ± 23
50	54.6 ± 2.5	94.2 ± 3.8	147 ± 6	247 ± 10
40	28.4 ± 1.8	39.3 ± 4.2	56.3 ± 2.5	77.3 ± 4.9
30	15.4 ± 1.7	16.5 ± 1.8	14.6 ± 0.6	10.0 ± 1.0
20	7.30 ± 0.62	-----	-----	-----
10	3.44 ± 0.36	-----	-----	-----



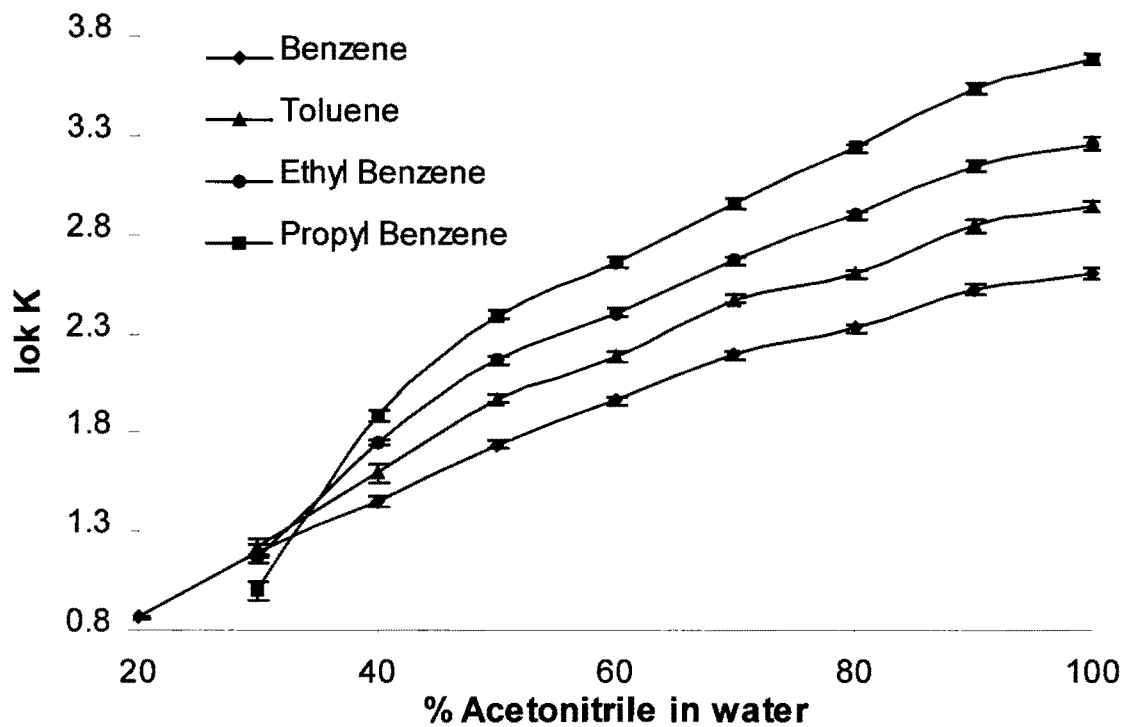


**Figure 4-29:** Plot of  $\log K$  of measured gas-liquid distribution constants at 30°C versus volume fraction of acetonitrile for all five alkyl benzenes.

## Results and Discussion: Liquid-Liquid Partition Coefficients ( $K_P$ )

So far, in this chapter, the gas-liquid distribution constants,  $K$ , were discussed. This is the constant that measures the distribution of the analyte between the gas phase and the liquid phase. The liquid-liquid partition coefficient,  $K_P$ , measures the partitioning of an analyte between two liquid phases. Going back to the retention model introduced in Chapter II, the analyte must partition itself between the mobile phase and the adsorbed layer, which is made up of the organic component of the mobile phase. This partition coefficient can be calculated using the measured gas-liquid distribution constants.

The definition of  $K_P$  was given in the model (refer to Equation 2-12) as the concentration of an analyte in the adsorbed layer (acetonitrile) divided by the concentration of an analyte in the mobile phase (acetonitrile-water mixture). If we divide the gas-liquid distribution constant obtained for an analyte in acetonitrile by the gas-liquid distribution constant obtained for the same analyte in the acetonitrile-water mixture, then the obtained value is the liquid-liquid partition coefficient,  $K_P$ , of that analyte between acetonitrile and acetonitrile-water mixture. The big assumption being, of course, is that the analyte behaves ideally in the gas phase.

The well known Henry's law:  $p_i = H x_i$ , where  $H$  is the Henry's law constant;  $x_i$  is the mole fraction of an analyte and  $p_i$  is the partial pressure of the analyte. According to this law, there is a general linearity between the partial vapor pressure and the mole concentration of the analyte under so-called ideal conditions. In an ideal condition, the activity coefficient of an analyte is said to equal to one and only solvent molecules surround each analyte molecule. Therefore only the intermolecular interaction forces between solute-solvent

molecules are effective, while the probability of additional solute-solute interaction increases with the concentration of the analyte.

The liquid-liquid partition coefficients of five ketones studied are given in Table 4-XIII. The gas-liquid distribution constants were taken from Table 4-VII, 4-IX and 4-XI. The graphical representation of the liquid-liquid partition coefficients versus the mobile phase composition is given in Figure 4-30.

The liquid-liquid partition coefficients of four alkyl benzenes studied are given in Table 4-XIV. The gas-liquid distribution constants were taken from Table 4-XII. The graphical representation of the liquid-liquid partition coefficients versus the mobile phase composition is given in Figure 4-31.

It is well known from the liquid-liquid partition theory that each methylene group of the analyte contributes equal amount of energy. So, if we plot the  $\ln K_p$  versus the number of methylene groups in the analyte, a linear line can be expected. If a linear line is obtained, that we can say that the measured values are found to be accurate. The calculated  $\ln K_p$  for ketones are given in Table 4-XV and for alkyl benzenes in Table 4-XVI. It is very interesting to note that, for both of the homologue series, a linear relationship is obtained for all of the analytes at each of the mobile phase composition studied ( $R^2$  of 0.94 or better), again, indicating the accuracy of the measured gas-liquid distribution constants.

**Table 4-XIII:** Calculated liquid-liquid partition coefficients of five ketones in given acetonitrile: water mixtures at 30°C.

% acetonitrile in water, v/v	Acetone	Butanone	Pentanone
100	1.000	1.000	1.000
90	0.833 ± 0.083	0.843 ± 0.072	1.039 ± 0.089
80	0.794 ± 0.075	0.995 ± 0.079	1.450 ± 0.115
70	0.861 ± 0.075	1.156 ± 0.091	1.888 ± 0.149
60	1.010 ± 0.091	1.436 ± 0.113	2.283 ± 0.182
50	1.152 ± 0.092	1.904 ± 0.138	3.483 ± 0.255
40	1.360 ± 0.108	2.527 ± 0.183	5.231 ± 0.383
30	1.690 ± 0.135	3.428 ± 0.248	8.677 ± 0.633
20	2.075 ± 0.155	4.369 ± 0.294	12.15 ± 0.83
10	2.282 ± 0.172	5.489 ± 0.370	15.75 ± 1.07
0	2.291 ± 0.164	5.912 ± 0.376	16.91 ± 1.09

% acetonitrile in water, v/v	Hexanone	Heptanone
100	1.000	1.000
90	1.089 ± 0.198	1.243 ± 0.274
80	1.577 ± 0.286	1.892 ± 0.410
70	2.378 ± 0.406	2.831 ± 0.756
60	3.552 ± 0.614	4.282 ± 0.924
50	5.217 ± 0.851	7.665 ± 1.798
40	8.428 ± 1.375	17.44 ± 3.96
30	18.71 ± 3.04	40.92 ± 8.69
20	38.48 ± 6.03	100.2 ± 22.4
10	49.18 ± 7.78	133.0 ± 33.3

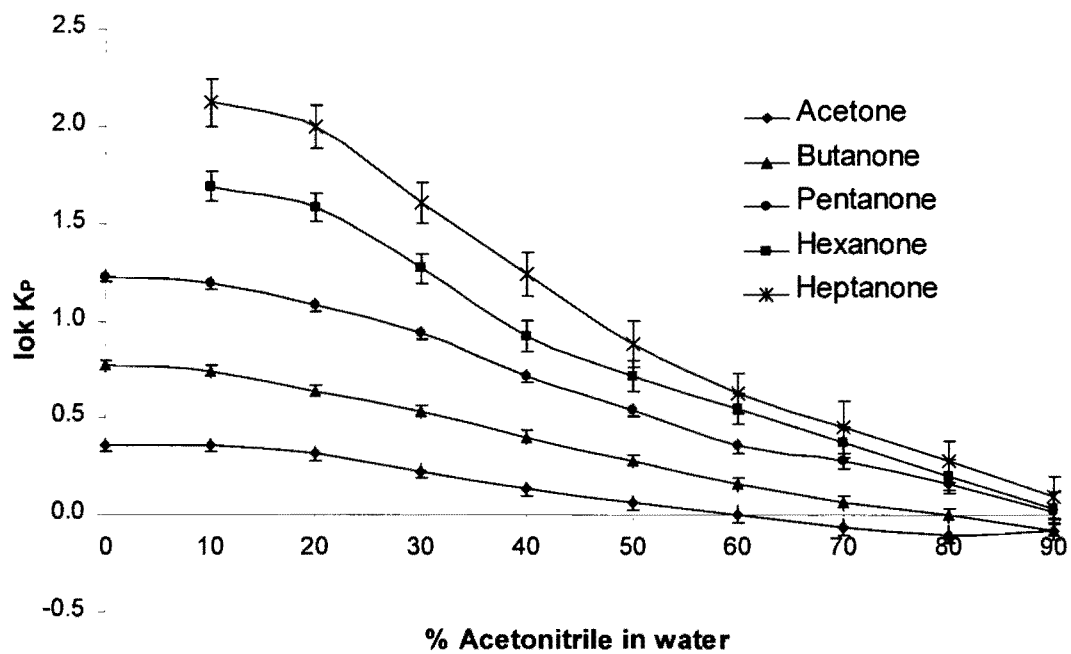


**Figure 4-30:** Plot of  $\log K_P$  of calculated liquid-liquid partition coefficients at 30°C versus mobile phase composition (in acetonitrile-water) for all five ketones studied.

**Table 4-XIV:** Calculated liquid-liquid partition coefficients of four alkyl benzenes in given acetonitrile: water mixtures at 30°C (----- Indicates that the values were not calculated).

% acetonitrile in water, v/v	Benzene	Toluene
100	1.000	1.000
90	1.232 ± 0.121	1.256 ± 0.110
80	1.920 ± 0.151	2.192 ± 0.172
70	2.622 ± 0.205	2.928 ± 0.233
60	4.441 ± 0.353	5.718 ± 0.451
50	7.491 ± 0.572	9.299 ± 0.679
40	14.40 ± 1.28	22.29 ± 2.76
30	26.56 ± 3.56	53.09 ± 6.56
20	56.03 ± 6.20	-----
10	119.0 ± 15.5	-----

% acetonitrile in water, v/v	Ethyl Benzene	Propyl Benzene
100	1.000	1.000
90	1.315 ± 0.130	1.387 ± 0.128
80	2.298 ± 0.214	2.814 ± 0.229
70	3.898 ± 0.368	5.338 ± 0.434
60	7.118 ± 0.664	10.69 ± 0.87
50	12.44 ± 1.10	19.72 ± 1.49
40	32.38 ± 2.91	63.05 ± 5.68
30	124.9 ± 11.0	487.4 ± 57.1

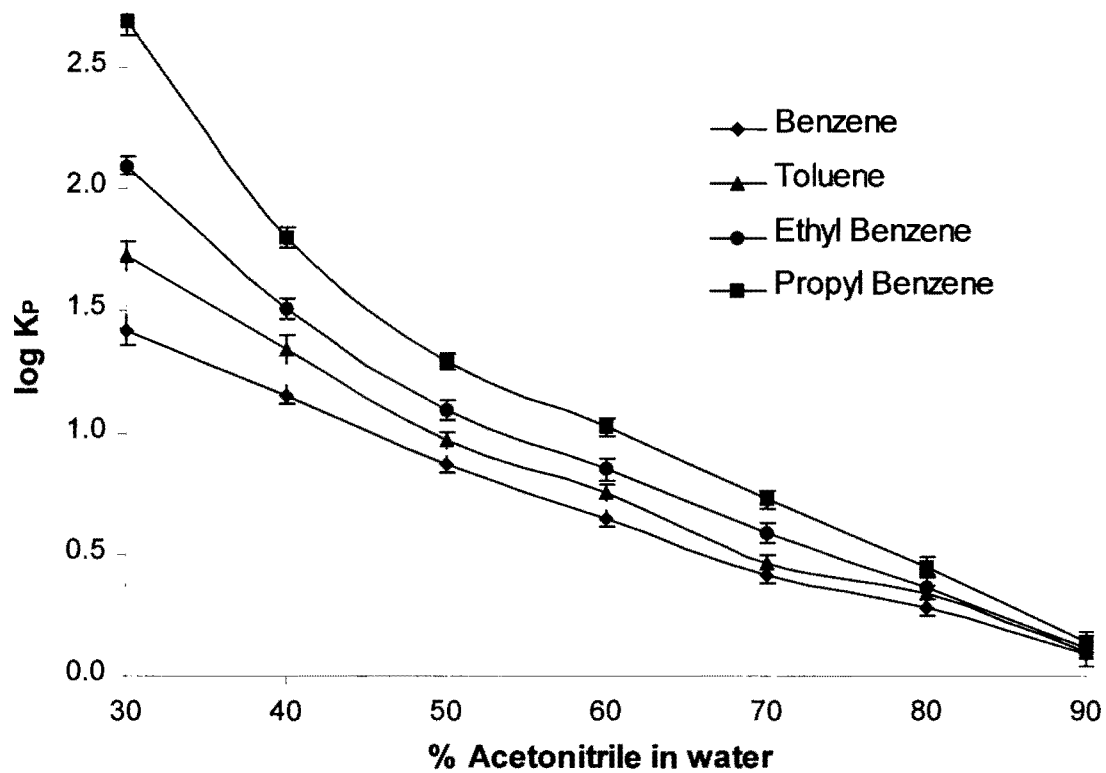


**Figure 4-31:** Plot of  $\log K_P$  of calculated liquid-liquid partition coefficients at 30°C versus mobile phase composition (in acetonitrile-water) for all four alkyl benzenes studied.

**Table 4-XV:** The transfer of methylene groups from the studied ketones from the mobile phase to the adsorbed layer.

A. Calculated  $\ln K_p$  of five ketones in given mobile phase composition at 30°C.

(----- Indicates that the values were not calculated).

% acetonitrile in water, v/v	Acetone	Butanone	Pentanone	Hexanone	Heptanone
100	0	0	0	0	0
90	-0.183	-0.171	0.038	0.085	0.218
80	-0.231	-0.005	0.372	0.456	0.637
70	-0.150	0.145	0.636	0.866	1.041
60	0.010	0.362	0.826	1.267	1.454
50	0.141	0.644	1.248	1.652	2.037
40	0.307	0.927	1.655	2.132	2.859
30	0.525	1.232	2.161	2.929	3.712
20	0.730	1.474	2.497	3.650	4.607
10	0.825	1.703	2.757	3.895	4.891
0	0.829	1.777	2.828	-----	-----

B. Calculated slopes, intercepts and  $R^2$  values.

(----- Indicates that the values were not calculated).

% acetonitrile in water, v/v	slope	intercept	$R^2$
100	-----	-----	-----
90	0.1057	-0.3197	0.941
80	0.2197	-0.4133	0.959
70	0.3102	-0.4231	0.969
60	0.3795	-0.3546	0.985
50	0.4799	-0.2953	0.992
40	0.6307	-0.3162	0.997
30	0.8071	-0.3098	0.999
20	0.9930	-0.3871	0.995
10	1.0324	-0.2831	0.998
0	0.9994	-0.1874	0.999



**Table 4-XVI:** The transfer of methylene groups from the studied alkyl benzenes from the mobile phase to the adsorbed layer.

A. Calculated  $\ln K_P$  of four alkyl benzenes in given mobile phase composition at 30°C.

(----- Indicates that the values were not calculated).

% acetonitrile in water, v/v	Benzene	Toluene	Ethyl Benzene	Propyl Benzene
100	0	0	0	0
90	0.209	0.228	0.274	0.327
80	0.652	0.785	0.832	1.035
70	0.964	1.074	1.360	1.675
60	1.491	1.744	1.963	2.369
50	2.014	2.230	2.521	2.982
40	2.667	3.104	3.478	4.144
30	3.279	3.972	4.827	6.189

B. Calculated slopes, intercepts and  $R^2$  values.

(----- Indicates that the values were not calculated).

% acetonitrile in water, v/v	slope	Intercept	$R^2$
100	-----	-----	-----
90	0.0403	0.1587	0.963
80	0.1194	0.5276	0.945
70	0.2419	0.6635	0.962
60	0.2854	1.1781	0.980
50	0.3195	1.6377	0.971
40	0.4803	2.1474	0.983
30	0.9584	2.1708	0.975

## Conclusions

An isochoric headspace system that is introduced can measure the gas-liquid distribution constants at atmospheric pressure. This system has a big advantage over the conventional HS system where the HS vials are pressurized in order to make an injection. The pressurization of the HS vial destroys the equilibrium inside the HS vial. This may be the reason for the reproducibility problems noticed in the literature for the obtained values of  $K$  between different research groups. The introduced headspace system can give better reproducibility since it operates at atmospheric pressure.

Using the isochoric headspace system, a vapor loading method was described, in which the analyte vapor is being added from analyte bottle to the HS vial containing the solvent. This has a big advantage over the known headspace methods in the literature in that only one experiment is needed to measure the gas-liquid distribution constant. This avoids lot of unnecessary errors (e.g., sample preparation) introduced in the measured values.

The gas-liquid distribution constants,  $K$ , of five ketones and four alkyl benzenes were measured using the vapor loading method on the isochoric headspace system. The obtained results were shown to be accurate with very good reproducibility. The calculated liquid-liquid partition coefficient,  $K_p$ , from the measured  $K$  is evidence of this since both homologue series showed linear dependence ( $R^2$  better than 0.96) of  $K_p$  against the carbon number of the side chain in a particular homologue series. This proves that the measured values of  $K$  are accurate since each methylene group contributed equivalent amount of the Gibbs free energy when distributed between the mobile phase and the adsorbed layer.

## Chapter V: Comparison of Calculated Retention Volumes ( $V_R$ ) Versus Experimentally Measured Retention Volumes ( $V_r$ ) of all Analytes.

### Summary

The independently measured variables from Chapter III ( $V_o$ ,  $V_s$  and  $K_H$ ) and Chapter IV ( $K_p$ ) were used to predict the retention of a given analyte under various acetonitrile-water compositions on a given column using Equation 2-28. The predicted  $V_R$  was compared to the experimentally measured  $V_r$  (refer to Chapter III) of the same analyte under same conditions. The comparison was performed for both homologous series (ketones and alkyl benzenes) studied. Based on the comparison, some conclusions are made towards the validity of the partition/ adsorption model presented in Chapter II.

### Introduction

The partition/ adsorption model presented in Chapter II describes RPLC retention as a sum of two processes: (i) partitioning between the mobile phase and the adsorbed layer that is made up of the organic modifier from the mobile phase followed by (ii) analyte adsorption on the hydrophobic surface. The following equation (same as Equation 2-28) was derived using the proposed model.

$$V_R = V_o + (K_p - 1)V_s + SK_p K_H \quad (5-1)$$

where  $V_R$  = retention volume of an analyte,  
 $V_o$  = total liquid volume inside the column,  
 $K_p$  = distribution coefficient of an analyte between the mobile phase and the adsorbed layer,  
 $V_s$  = total adsorbed layer volume,  
 $S$  = the total surface area of the adsorbent per column and  
 $d\Gamma(c_s)/dc_s = K_H$  = Henry adsorption constant.

Since all of the parameters in Equation 5-1 are measured independently, this model can be experimentally verified. Equation 5-1 has four unknowns ( $V_o$ ,  $V_s$ ,  $K_H$  and  $K_P$ ). In order to predict the retention of an analyte under certain LC conditions, these four unknowns must be measured. Dead volume ( $V_o$ ), and adsorbed layer volume ( $V_s$ ) of the organic modifier (acetonitrile for the current study) are functions of a given chromatographic column and were measured independently in a binary system (acetonitrile and water) as shown in Chapter III. The Henry constant ( $K_H$ ) of the analyte is the slope of its adsorption from pure organic component and was measured in a binary system (acetonitrile and the analyte) as described in Chapter III. The liquid-liquid partition coefficient ( $K_P$ ) of an analyte between the mobile phase and the adsorbed layer of acetonitrile was measured (refer to Chapter IV) by headspace gas chromatography (HS-GC). By gathering data for the four unknowns and placing them in Equation 5-1, the retention volume of an analyte for given chromatographic conditions (this is a ternary system – acetonitrile, water and analyte) can be predicted. By comparing the theoretically predicted  $V_R$  (all parameters were measured in a binary system) using Equation 5-1 to the experimentally measured  $V_r$  (this is a ternary system), the validity of the partition/ adsorption model presented here can be tested.

## Results

The experimentally measured retention volumes,  $V_r$ , are taken from Tables 3-X to 3-XIV. The dead volumes,  $V_o$ , of the columns are taken from Table 3-IV. The measured Henry's constants,  $K_H$ , are taken from Table 3-XV. The measured adsorbed layer

volumes,  $V_s$ , are taken from Tables 3-IV to 3-VIII. The measured liquid-liquid partition coefficients,  $K_P$ , are taken from Tables 4-XIII and 4-XIV.

### **Comparison of $V_R$ versus $V_f$**

First, using Equation 5-1,  $V_R$  of all nine analytes at each acetonitrile: water mobile phase composition studied on all five columns ( $C_{18}$ ,  $C_{12}$ ,  $C_8$ ,  $C_4$  and  $C_1$ ) were calculated. The calculated  $V_R$  for all analytes under given acetonitrile-water composition are given in Tables 5-I to 5-V when using columns having different bonded alkyl chains,  $C_{18}$  to  $C_1$  respectively. The theoretical predicted values were compared to the experimentally measured values using two different graphical representation: 1) retention volume versus mobile phase composition and 2)  $\ln k'$  versus mobile phase composition. The obtained graphs for five studied ketones are given in Figures 5-1 to 5-5 when using columns having different bonded alkyl chains,  $C_{18}$  to  $C_1$ . The obtained graphs for five studied alkyl benzenes are given in Figures 5-6 to 5-10 when using columns having different bonded alkyl chains,  $C_{18}$  to  $C_1$ .

**Table 5-I:** Calculated retention volumes (in mL),  $V_R$ , of all analytes on a  $C_{18}$  column. ---  
 -- Indicates that the value was not calculated.

% acetonitrile in water, v/v	100	90	80	70	60	50	40	30	20
Acetone	1.864	1.784	1.765	1.797	1.869	1.938	2.037	2.168	2.263
Butanone	1.854	1.780	1.852	1.927	2.063	2.289	2.573	2.900	3.069
Pentanone	1.895	1.914	2.125	2.349	2.564	3.189	4.058	5.514	-----
Hexanone	1.958	2.010	2.290	2.751	3.452	4.426	6.231	-----	-----
Heptanone	2.043	2.203	2.631	3.251	4.241	6.506	12.89	-----	-----
Benzene	1.895	2.013	2.365	2.724	3.689	5.279	8.749	13.95	23.99
Toluene	1.982	2.135	2.697	3.137	4.857	7.039	14.74	31.11	-----
Ethyl Benzene	2.054	2.266	2.926	3.999	6.222	9.844	23.12	80.24	-----
Propyl Benzene	2.169	2.473	3.593	5.576	9.876	17.06	50.91	-----	-----

**Table 5-II:** Calculated retention volumes (in mL),  $V_R$ , of all analytes on a C<sub>12</sub> column. --  
 --- Indicates that the value was not calculated.

% acetonitrile in water, v/v	100	90	80	70	60	50	40	30	20
Acetone	1.893	1.813	1.797	1.828	1.898	1.967	2.062	2.189	2.278
Butanone	1.869	1.798	1.867	1.938	2.067	2.289	2.547	2.850	2.994
Pentanone	1.895	1.914	2.107	2.313	2.511	3.111	3.883	5.196	-----
Hexanone	1.934	1.981	2.228	2.636	3.259	4.166	5.717	-----	-----
Heptanone	1.994	2.134	2.500	3.035	3.892	5.916	11.34	-----	-----
Benzene	1.875	1.981	2.288	2.603	3.456	4.922	7.898	12.34	20.56
Toluene	1.932	2.064	2.536	2.909	4.371	6.306	12.73	26.26	-----
Ethyl Benzene	1.979	2.156	2.697	3.582	5.426	8.537	19.35	65.58	-----
Propyl Benzene	2.047	2.292	3.176	4.747	8.173	14.07	40.66	-----	-----

**Table 5-III:** Calculated retention volumes (in mL),  $V_R$ , of all analytes on a  $C_8$  column. --  
 --- Indicates that the value was not calculated.

% acetonitrile in water, v/v	100	90	80	70	60	50	40	30	20
Acetone	1.942	1.865	1.850	1.878	1.947	2.013	2.103	2.224	2.306
Butanone	1.903	1.837	1.901	1.968	2.089	2.290	2.527	2.798	2.909
Pentanone	1.916	1.933	2.106	2.300	2.484	3.014	3.703	4.851	-----
Hexanone	1.931	1.971	2.184	2.548	3.099	3.861	5.181	-----	-----
Heptanone	1.962	2.078	2.380	2.838	3.565	5.216	9.660	-----	-----
Benzene	1.873	1.964	2.222	2.505	3.247	4.465	6.956	10.54	16.69
Toluene	1.903	2.010	2.391	2.711	3.927	5.463	10.611	21.13	-----
Ethyl Benzene	1.933	2.075	2.503	3.234	4.741	7.182	15.71	51.35	-----
Propyl Benzene	1.969	2.157	2.830	4.072	6.762	11.23	31.43	-----	-----



**Table 5-IV:** Calculated retention volumes (in mL),  $V_R$ , of all analytes on a C<sub>4</sub> column. --  
 --- Indicates that the value was not calculated.

% acetonitrile in water, v/v	100	90	80	70	60	50	40	30	20
Acetone	1.948	1.879	1.861	1.888	1.953	2.012	2.086	2.157	2.187
Butanone	1.890	1.834	1.888	1.948	2.053	2.219	2.384	2.481	2.441
Pentanone	1.882	1.896	2.043	2.208	2.352	2.767	3.220	3.696	-----
Hexanone	1.886	1.917	2.094	2.396	2.830	3.404	4.263	-----	-----
Heptanone	1.894	1.981	2.222	2.586	3.135	4.347	7.286	-----	-----
Benzene	1.833	1.908	2.131	2.358	2.947	3.935	6.174	10.11	19.66
Toluene	1.842	1.927	2.238	2.482	3.410	4.600	8.918	19.16	-----
Ethyl Benzene	1.852	1.960	2.298	2.847	3.952	5.776	12.62	44.36	-----
Propyl Benzene	1.863	2.000	2.504	3.397	5.289	8.485	23.81	-----	-----

**Table 5-V:** Calculated retention volumes (in mL),  $V_R$ , of all analytes on a  $C_1$  column. ---  
 -- Indicates that the value was not calculated.

% acetonitrile in water, v/v	100	90	80	70	60	50	40	30	20
Acetone	1.928	1.879	1.869	1.887	1.931	1.974	2.031	2.097	2.127
Butanone	1.911	1.867	1.909	1.954	2.036	2.171	2.319	2.463	2.475
Pentanone	1.905	1.915	2.023	2.146	2.266	2.604	3.012	3.607	-----
Hexanone	1.896	1.919	2.042	2.258	2.593	3.047	3.775	-----	-----
Heptanone	1.897	1.961	2.123	2.379	2.794	3.719	6.063	-----	-----
Benzene	1.866	1.920	2.071	2.244	2.702	3.443	4.555	5.619	6.353
Toluene	1.867	1.926	2.132	2.316	3.013	3.884	6.616	11.40	-----
Ethyl Benzene	1.867	1.940	2.157	2.543	3.356	4.650	8.875	24.58	-----
Propyl Benzene	1.867	1.958	2.273	2.882	4.230	6.433	15.76	-----	-----

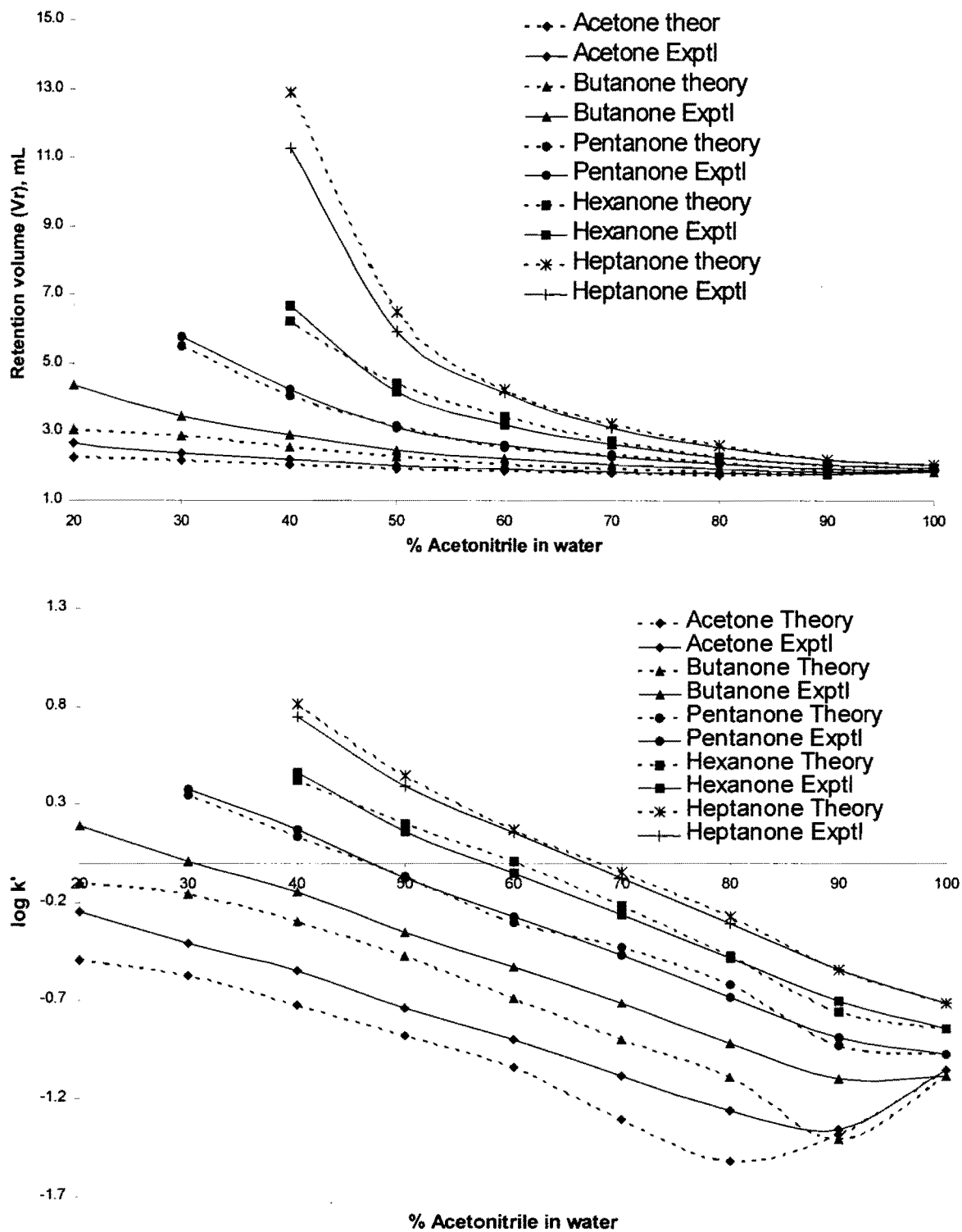


**Figure 5-1:** Comparison of theoretical versus experimentally measured values for all studied ketones on a C<sub>18</sub> column. Top graph presents in terms of retention volume and the bottom in terms of  $\log k'$ .

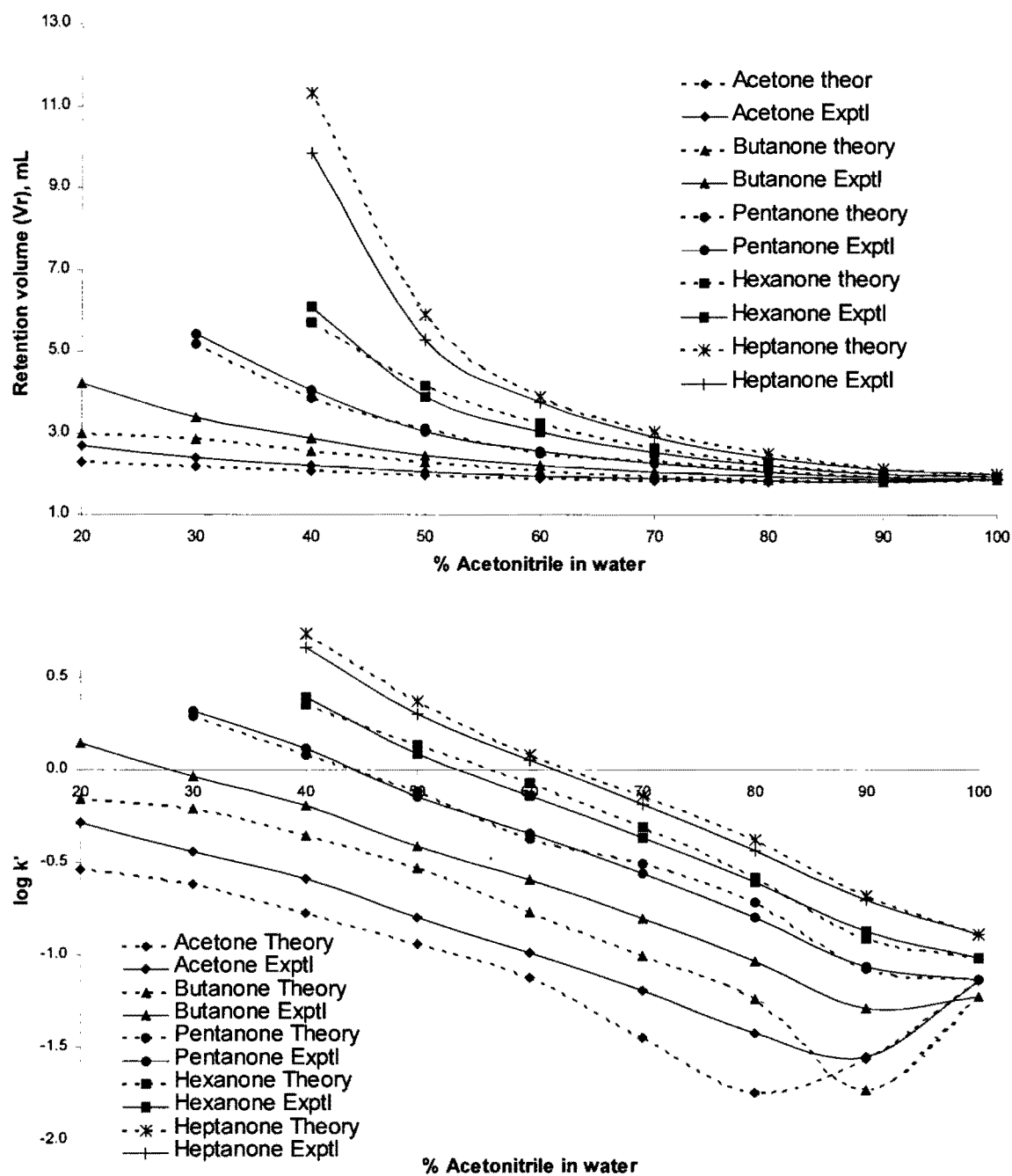


**Figure 5-2:** Comparison of theoretical versus experimentally measured values for all studied ketones on a  $C_{12}$  column. Top graph presents in terms of retention volume and the bottom in terms of  $\log k'$ .

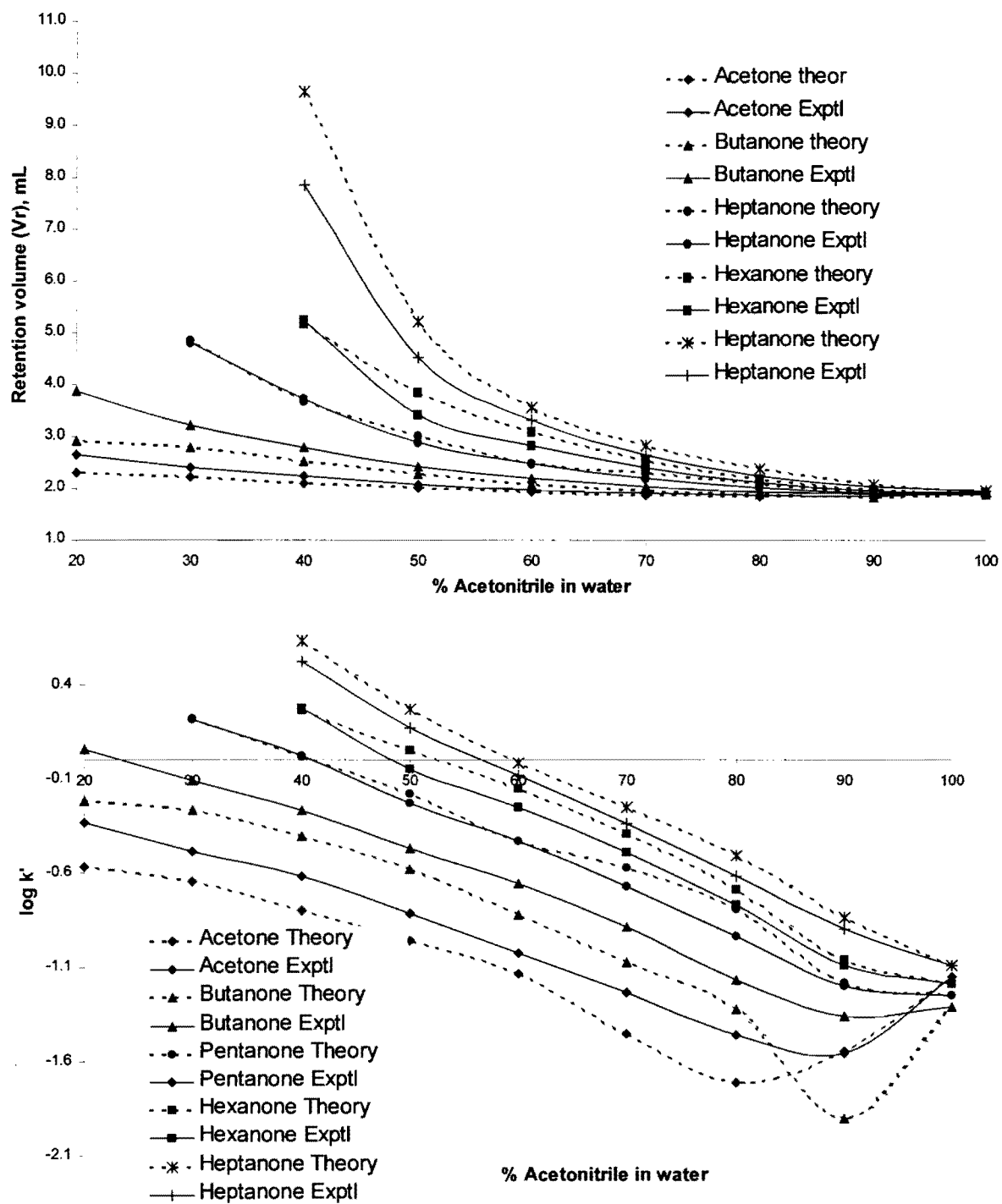


**Figure 5-3:** Comparison of theoretical versus experimentally measured values for all studied ketones on a C<sub>8</sub> column. Top graph presents in terms of retention volume and the bottom in terms of  $\log k'$ .

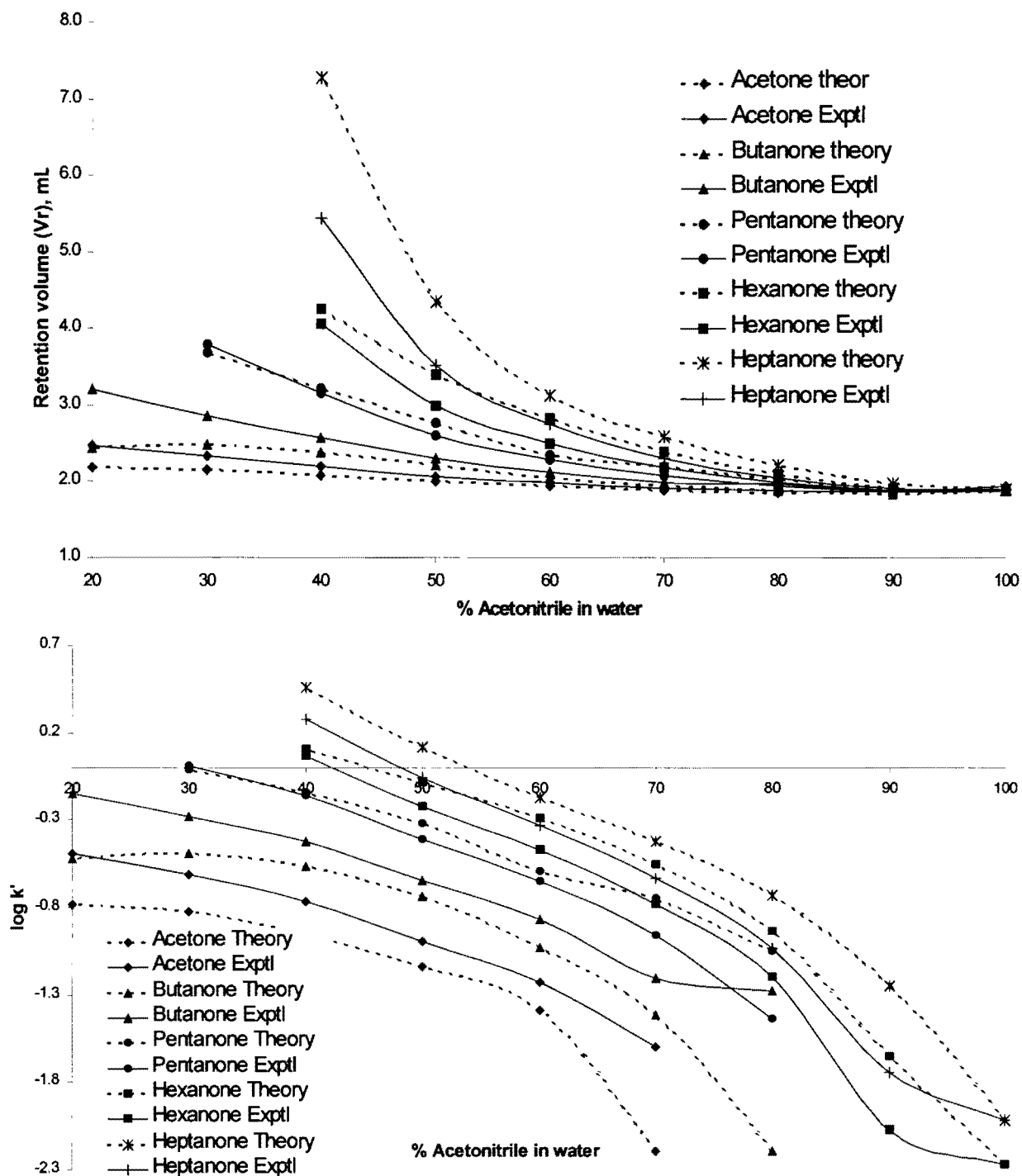


**Figure 5-4:** Comparison of theoretical versus experimentally measured values for all studied ketones on a C<sub>4</sub> column. Top graph presents in terms of retention volume and the bottom in terms of  $\log k'$ .

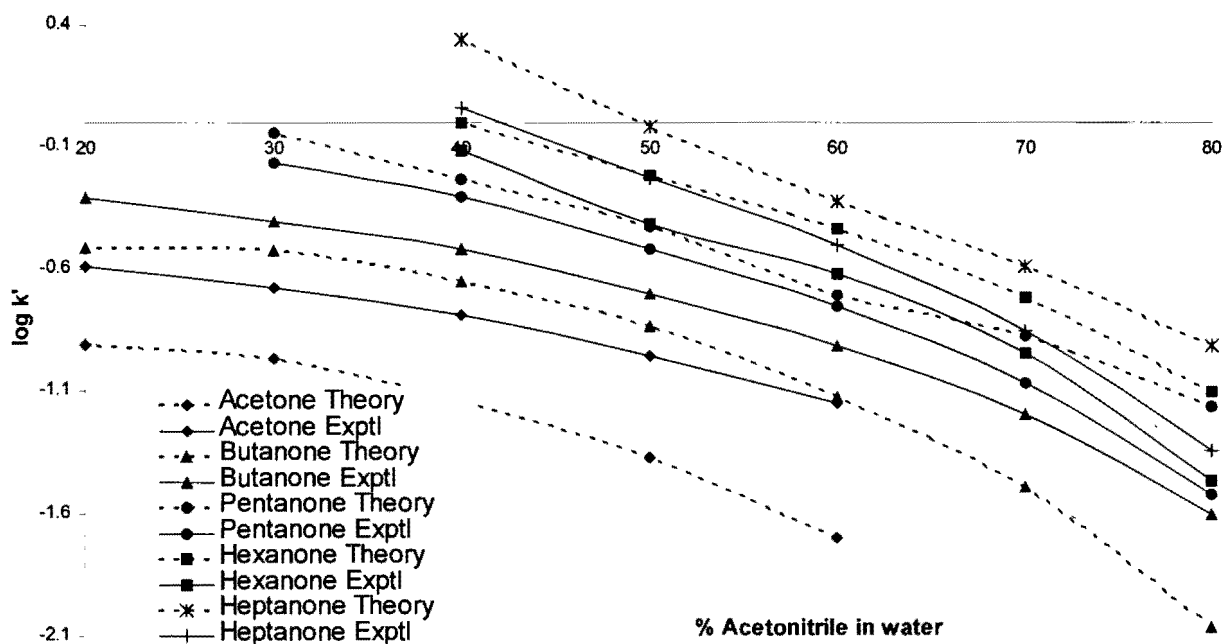
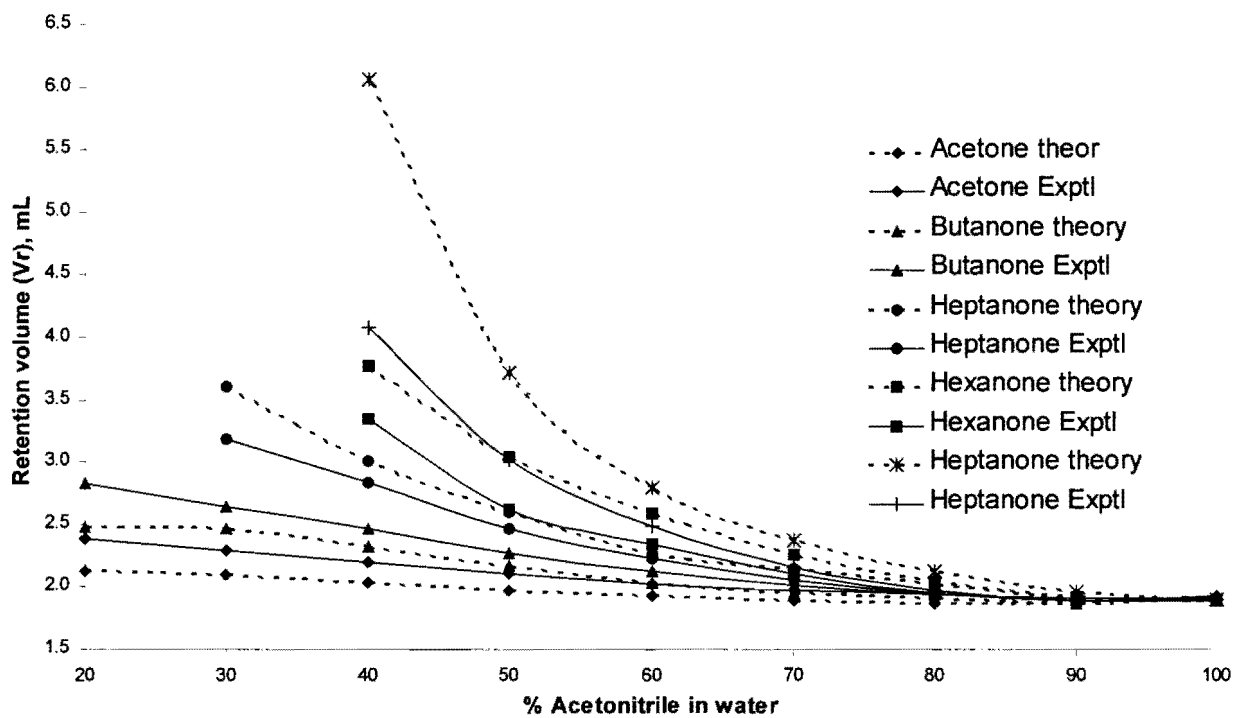


**Figure 5-5:** Comparison of theoretical versus experimentally measured values for all studied ketones on a  $C_1$  column. Top graph presents in terms of retention volume and the bottom in terms of  $\log k'$ .

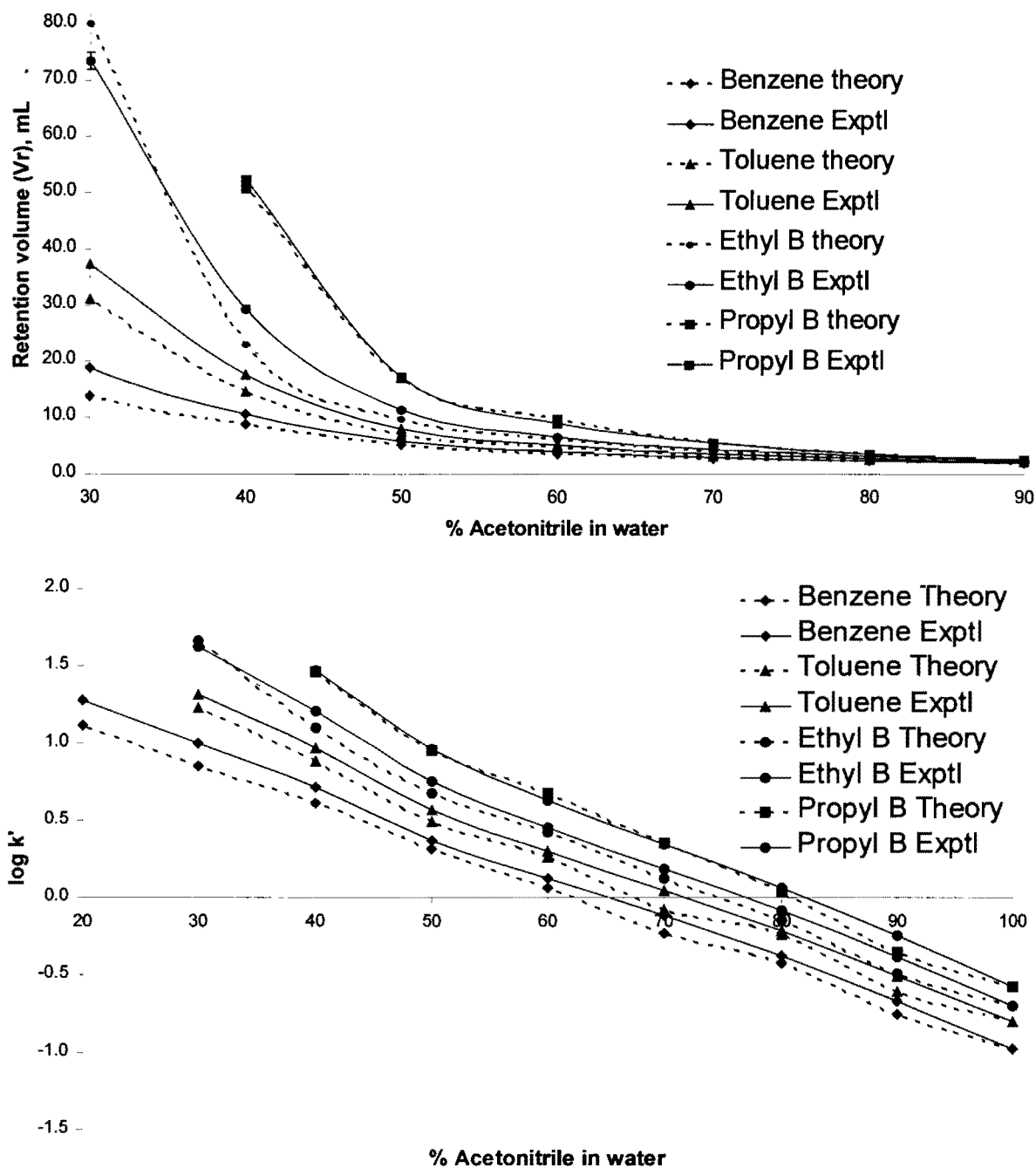


**Figure 5-6:** Comparison of theoretical versus experimentally measured values for all studied alkyl benzenes on a C<sub>18</sub> column. Top graph presents in terms of retention volume and the bottom in terms of  $\log k'$ .



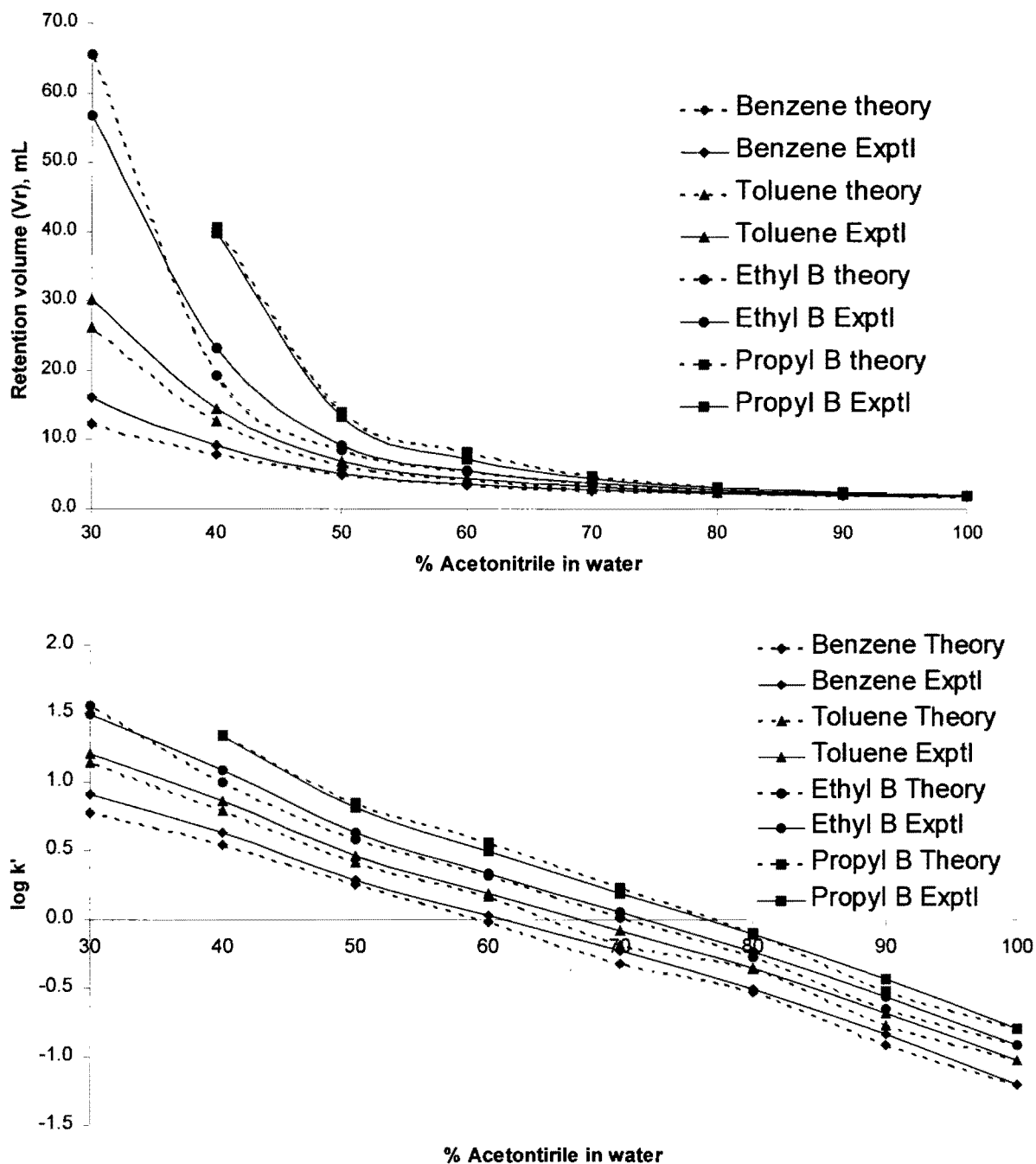


**Figure 5-7:** Comparison of theoretical versus experimentally measured values for all studied alkyl benzenes on a C<sub>12</sub> column. Top graph presents in terms of retention volume and the bottom in terms of  $\log k'$ .

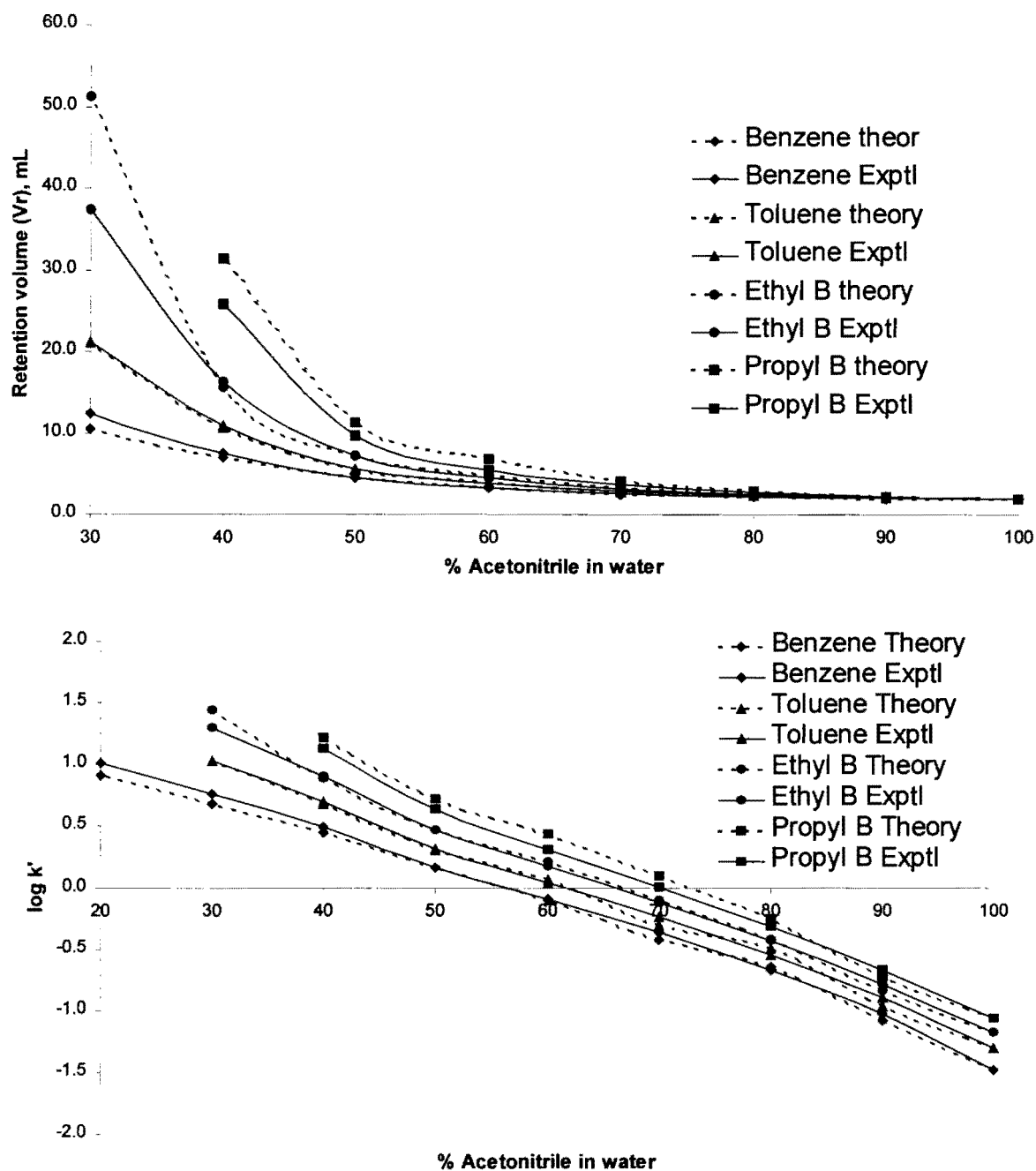


**Figure 5-8:** Comparison of theoretical versus experimentally measured values for all studied alkyl benzenes on a  $C_8$  column. Top graph presents in terms of retention volume and the bottom in terms of  $\log k'$ .

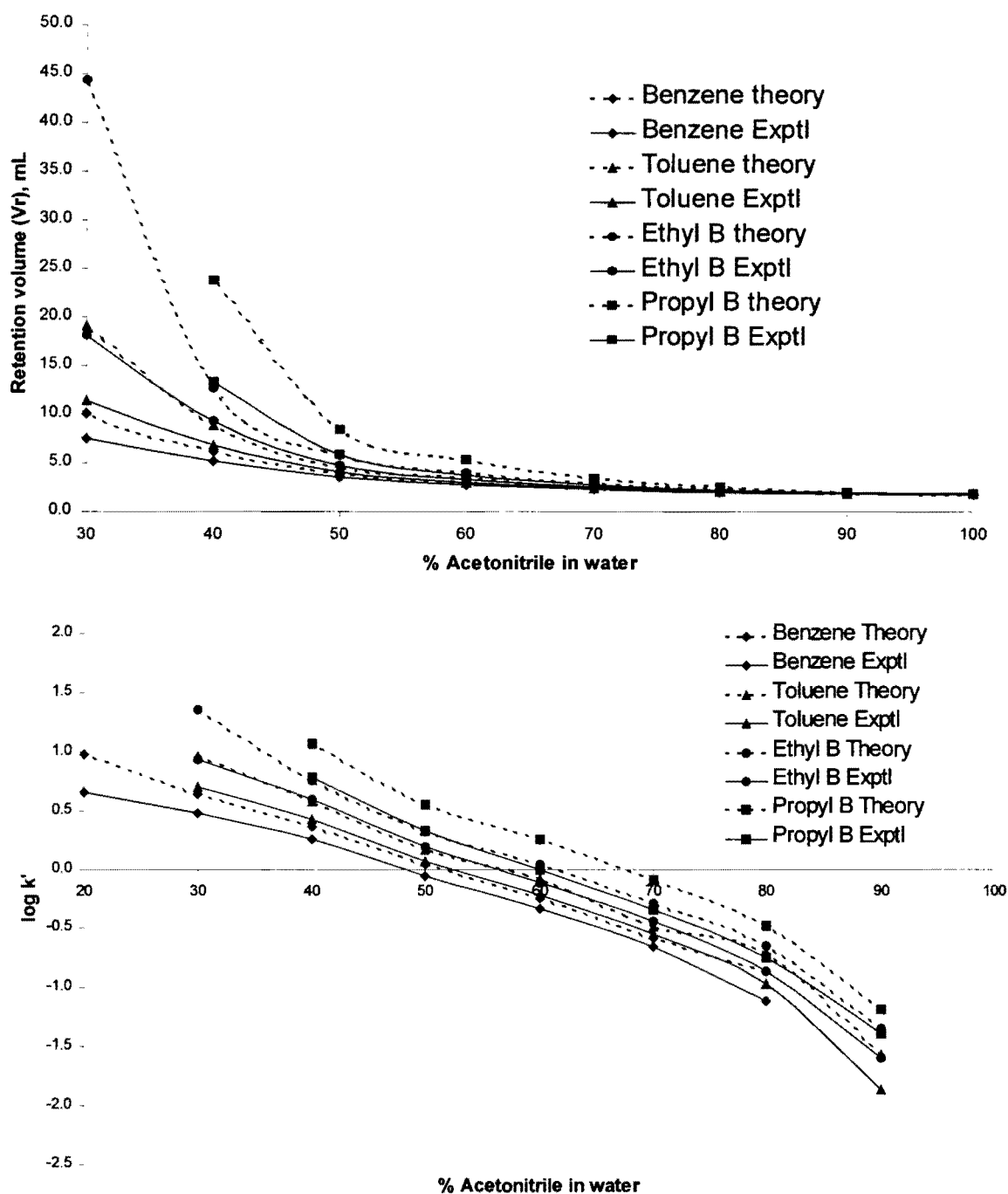


**Figure 5-9:** Comparison of theoretical versus experimentally measured values for all studied alkyl benzenes on a C<sub>4</sub> column. Top graph presents in terms of retention volume and the bottom in terms of  $\log k'$ .

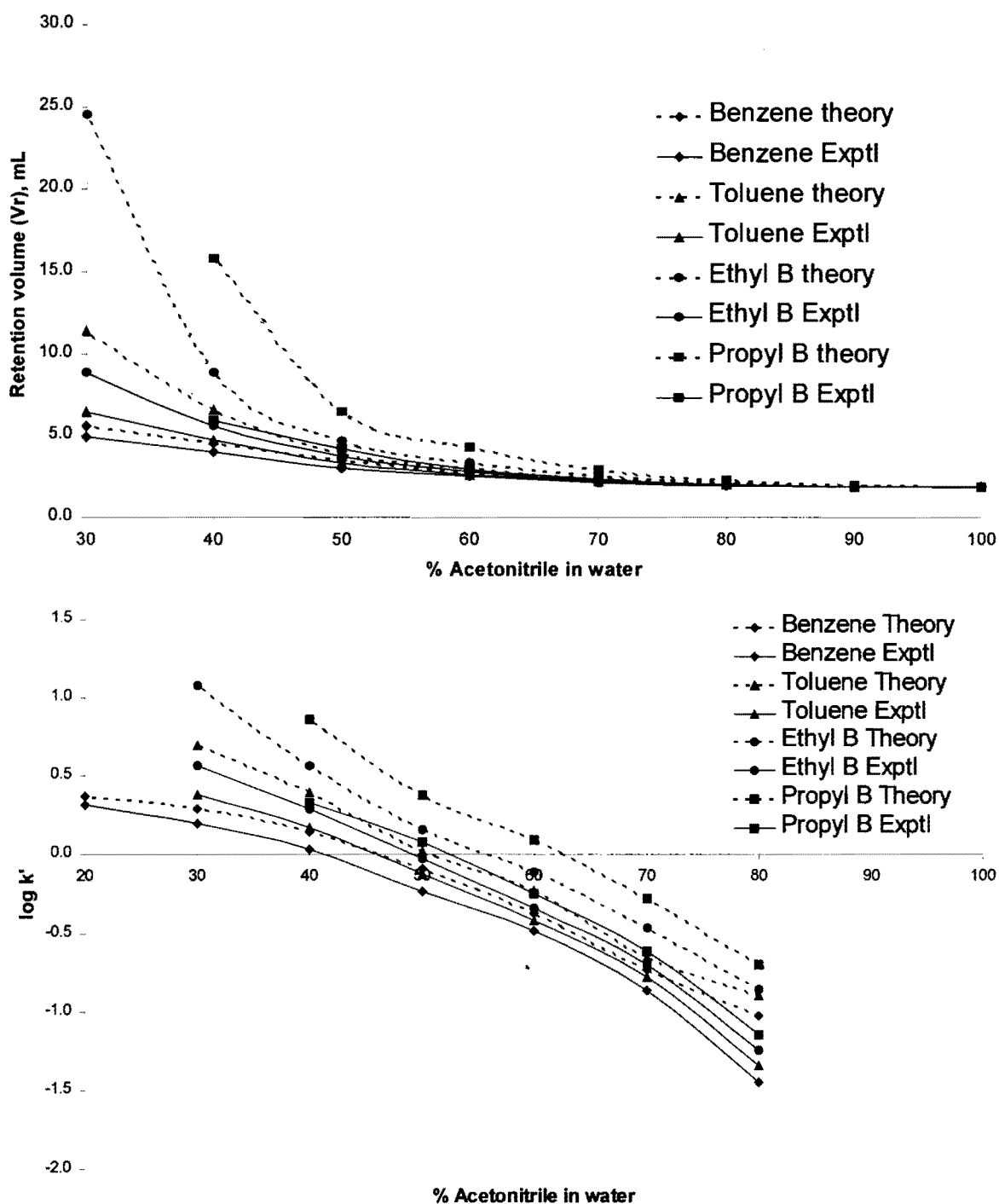


**Figure 5-10:** Comparison of theoretical versus experimentally measured values for all studied alkyl benzenes on a  $C_1$  column. Top graph presents in terms of retention volume and the bottom in terms of  $\log k'$ .

## Discussion

It can be seen for all of the ketones studied from the Figures 5-1 to 5-5 that the theoretically predicted retention using the described model gave comparable retention volumes when using different bonded alkyl chain length ( $C_{18}$ ,  $C_{12}$ ,  $C_8$ ). However, when using  $C_4$  and  $C_1$ , the relatively non-polar analytes (hexanone and heptanone) started to deviate from the experimental values, especially at higher water content in the mobile phase. The same trends are observed for alkyl benzenes in Figures 5-6 to 5-10. The model gave comparable retention volumes (for all four alkyl benzenes studied) when using  $C_{18}$ ,  $C_{12}$  and  $C_8$  columns, but started to predict higher retention values (for very non-polar analytes – ethyl and butyl benzene) for columns  $C_4$  and  $C_1$  and when using higher water content in the mobile phase.

The deviation seen in both homologous series is the same and may be attributed to the adsorbed layer not fully formed at these mobile phase compositions and to the additional surface effects (e.g., residual silanols) on shorter bonded alkyl chains. As shown in Chapter III, the adsorbed layer is fully formed at about 40% acetonitrile in water, v/v. Any mobile phase composition below this does not have a stable adsorbed layer formed. Since all alkyl bonded length chains studied showed similar thickness or the volume of this adsorbed layer, it is obvious that the surface effects (e.g., residual silanols) are more pronounced when shorter bonded alkyl chains are used. As the length of the bonded alkyl chain is increased, the residual silanol effect starts to diminish and its effect on experimentally measured retention volumes is not observed. Since residual silanols are polar, their largest contributions are seen on the non-polar analytes, which

have shown to elute much faster on experimentally measured than predicted retention volumes.

In Chapter III, the same reason was given for the found Henry's constants when using shorter bonded alkyl chains as the stationary phase. Acetone was shown to give the highest Henry's constant on a C<sub>1</sub> column when compared to all other analytes. This means that acetone was retained the longest even though it was the most polar and the smallest analyte being studied. Acetone had high affinity for the polar environment provided by the residual silanols, so it was retained longer than all of other studied analytes. Most of the other analytes studied gave retention volume lower than the dead volume of the column, indicating that they were repelled from the stationary phase and were eluted off the column much faster.

If the assumptions given above are correct, then it would make sense from the results in that the predicted retention volumes for same analytes on shorter bonded alkyl chain columns are found to be higher since the presented retention model does not take specific surface effects into account (e.g., residual silanols). In addition, the experimentally measured retention volumes are found to have the residual silanol effect (especially when the adsorbed layer is not fully formed). This means that the model fails to explain the retention on shorter bonded alkyl chains, especially when the composition of the mobile phase is highly aqueous where it is known that a stable adsorbed layer is not formed. There is no term in the Equation 5-1 that would account for this effect because the equation to predict the retention of an analyte using the partition/ adsorption model was derived based on how the analyte is distributed in different phases

(partitioning between the mobile phase and the solvated layer and then adsorption on the bonded phase) inside the column.

Even though the model presented does not describe the retention on shorter bonded alkyl chains when using high aqueous mobile phase, there is one interesting observation made that is explained by the model. This observation is made with the experimentally measured retention volume of acetone and butanone, for example on  $C_{18}$  column, in which they both elute off the column faster in 90% acetonitrile in water than 100% acetonitrile. This is very interesting since in RPLC, the analytes show a trend of retaining longer when strength of the mobile phase is decreased. When the experimentally measured retention volumes for both were compared to the predicted retention volumes, they were very comparable. The model predicted that the retention of both analytes would decrease upon increasing the water content by 10%. This is mainly due to the liquid-liquid partition coefficient of those analytes in 90% acetonitrile in water. The  $K_P$  for both is found to be smaller than 1.00, indicating that both analytes prefer to be in 90% acetonitrile in water than 100% acetonitrile. This directly correlates to the analytes eluting off the column faster in 90% acetonitrile than 100% acetonitrile. This also indicates that the retention of acetone is mobile phase dependent and should not be used to measure the dead volume of the column.

### **Comparison of $V_R$ versus $V_r$ in terms of statistics**

All measured values in Chapter III and IV have an error associated with it, so it is possible to calculate the propagation of error for the predicted  $V_R$  using Equation 5-1.

Two examples are used to calculate the propagation of error using the rules of

propagation of error (refer to Table 5-VI for step-wise calculation). First one is Benzene in 50% acetonitrile in water mobile phase on a C<sub>18</sub> column. The calculated  $V_R$  using Equation 5-1 is found to be 5.283 mL. The error on this value is found to be 0.566 mL. The measured  $V_r$  value is 5.735 mL. The error on this value is found to be 0.115 mL. So, the two values are statistically equivalent. Second example is ethyl benzene in 30% acetonitrile in water mobile phase on a C<sub>8</sub> column. The calculated  $V_R$  using Equation 5-1 is found to be 51.37 mL. The error on the value is found to be 12.45 mL. The measured  $V_r$  value is 37.46 mL and the error on this value is found to be 0.75 mL. So, the two values are not statistically equivalent.

Similar comparisons for each analyte on every column using different acetonitrile-water composition were calculated. However, an easier method was applied to see if the two values are similar or not. If the % difference between the predicted  $V_R$  using Equation 5-1 and experimentally measured  $V_r$  were found to be less than 15%, then the values were said to be equivalent. This is because the added error from each of the four variables is found to about 15% (dead volume – 2%, Henry's constant – 4%, liquid-liquid distribution constant – 4 to 10% and adsorbed layer volume – unknown error).

## Conclusions

The proposed model is found to be valid when applied to different bonded alkyl chains and with different analytes (polar and non-polar). However, the model predicted greater retention volumes when compared to experimentally measured retention volumes of non-polar analytes on short bonded alkyl chains (C<sub>4</sub> and C<sub>1</sub>) in presence of high water content (more than 60% water) in the mobile phase. This could be attributed to the



**Table 5-VI:** Calculation of propagation of error.

A. analyte – Benzene, mobile phase - 50% acetonitrile in water, column - C<sub>18</sub>

**Predicted V<sub>R</sub>** using equation 5-1.

$$\text{Equation 5-1} \Rightarrow V_R = V_o + (K_P - 1)V_S + SK_P K_H$$

$$V_R = 1.713 \pm 0.036 + (7.491 \pm 0.572 - 1)(0.34 \pm 0.01) + (7.491 \pm 0.572)(0.182 \pm 0.02)$$

$$V_R = 1.713 \pm 0.036 + (2.207 \pm 0.265) + (1.363 \pm 0.265)$$

$$V_R = 5.283 \text{ mL} \pm 0.566 \Rightarrow \text{or} \Rightarrow 4.717 \text{ mL} - 5.850 \text{ mL}$$

**Experimental V<sub>r</sub>**

$$V_r = 5.735 \pm 0.02 \text{ mL/min}$$

$$V_r = 5.735 \pm 0.115 \Rightarrow \text{or} \Rightarrow 5.620 \text{ mL} - 5.850 \text{ mL}$$

*Predicted V<sub>R</sub> and experimental V<sub>r</sub> are found to be statistically equivalent.*

B. analyte – Ethyl Benzene, mobile phase – 30% acetonitrile in water, column – C<sub>8</sub>

**Predicted V<sub>R</sub>** using equation 5-1.

$$\text{Equation 5-1} \Rightarrow V_R = V_o + (K_P - 1)V_S + SK_P K_H$$

$$V_R = 1.814 \pm 0.053 + (124.9 \pm 11.0 - 1)(0.28 \pm 0.01) + (124.9 \pm 11.0)(0.119 \pm 0.049)$$

$$V_R = 1.814 \pm 0.053 + (34.69 \pm 4.43) + (14.86 \pm 7.97)$$

$$V_R = 51.37 \text{ mL} \pm 12.45 \Rightarrow \text{or} \Rightarrow 38.92 \text{ mL} - 63.82 \text{ mL}$$

**Experimental V<sub>r</sub>**

$$V_r = 37.46 \pm 0.02 \text{ mL/min}$$

$$V_r = 37.46 \pm 0.75 \Rightarrow \text{or} \Rightarrow 36.71 \text{ mL} - 38.21 \text{ mL}$$

*Predicted V<sub>R</sub> and experimental V<sub>r</sub> are found not to be statistically equivalent.*

adsorbed layer not fully formed at these mobile phase compositions and the surface effects (e.g., residual silanols) on shorter bonded alkyl chains. The proposed model does not take surface effects (e.g., residual silanols) into the account, thus giving higher retention values than measured retention values when stated experimental conditions were used.

## Chapter VI: Overall Conclusions

This dissertation has outlined several studies that positively contribute to the growing research on understanding of the retention mechanism of reversed-phase liquid chromatography. Some important contributions of the current study are summarized below.

1. It was shown that stationary phase plays a major role in retention and it is not a passive receptor. A discussion of the structure of the bonded phase was presented and it was concluded that the bonded alkyl chains are in their least energy state or “collapsed” phase.
2. It was shown that there is preferential adsorption of the organic component of the mobile phase on the surface and, due to this adsorption, the physical/ chemical environment near the surface is changed. In other words, the adsorbed layer is somewhat different in composition than the mobile phase.
3. Based on excess adsorption isotherm studies, it was shown that the adsorbed layer is a multilayer when acetonitrile is used as the organic modifier.
4. It was also shown that this multilayer adsorption is on top of the collapsed bonded layer.
5. A partition/ adsorption model was presented which describes the RPLC retention as a sum of two processes: partitioning into the organic adsorbed layer followed by analyte adsorption on the hydrophobic surface.

6. The following equation was derived using the proposed model, which can predict the analyte retention under RPLC conditions.

$$V_R = V_0 + (K_P - 1)V_s + SK_P K_H \quad (6-1)$$

where  $V_R$  = retention volume of an analyte,  
 $V_0$  = total liquid volume inside the column,  
 $K_P$  = distribution coefficient of an analyte between the mobile phase and the adsorbed layer,  
 $V_s$  = total adsorbed layer volume,  
 $S$  = the total surface area of the adsorbent per column and  
 $d\Gamma(c_s)/dc_s = K_H$  = Henry adsorption constant.

7. Since all of involved parameters in Equation 6-1 were measured independently, this model was experimentally verified using two homologue series (ketones and alkyl benzenes) as analytes using acetonitrile-water mixture as the mobile phase. The effect of bonded alkyl chain length ( $C_{18}$ ,  $C_{12}$ ,  $C_8$ ,  $C_4$  and  $C_1$ ) was also studied, but the temperature was held constant at 30°C. The  $V_0$  and  $V_s$  are function of a given chromatographic column and were measured independently in a binary system (acetonitrile and water). The  $K_H$  of the analyte is the slope of its adsorption from pure organic component and was also measured in a binary system (acetonitrile and the analyte). The  $K_P$  of an analyte between the mobile phase and the adsorbed layer was measured by headspace gas chromatography (HS-GC). From the four independently measured variables and using Equation 7-1, we were able to predict the retention of an analyte for a given chromatographic conditions (this is a ternary system – acetonitrile, water and analyte).
8. It was shown that the model predicted very good retention volumes for all analytes under given set of conditions (longer bonded alkyl chains –  $C_{18}$ ,  $C_{12}$  and  $C_8$  and when stable

adsorbed layer is formed – more than 40% acetonitrile in the mobile phase). The retention volumes of non-polar analytes on shorter bonded alkyl chains ( $C_4$  and  $C_1$ ) when using high water content in the mobile phase were predicted to be higher than the measured retention volumes. This effect could be attributed to the adsorbed layer not fully formed and to the specific effects of silica surface (e.g., residual silanols) on shorter bonded alkyl chains.

9. The limitations of the model are that it does not predict comparable retention volumes for non-polar analytes at high water content using shorter bonded alkyl chain ligands. The studied analytes must be semi-volatile to volatile and should not ionize under given mobile phase compositions. The volatility of the analytes is important in order to measure their gas-liquid distribution constants by HSGC. Since we are trying to solve one equilibrium (between mobile phase and adsorbed layer), an ionization of an analyte will introduce more equilibria in the solution and will complicate the described model.
  
10. An Isochoric headspace system was introduced. This system is known to work at atmospheric pressure. The principles of the Isochoric headspace system were discussed. Two different methods (Isochoric vapor extraction and Isochoric vapor loading) were introduced for vapor transfer and measurement processes. Step-by-step procedures followed by theories for both of the isochoric methods were then described. A procedure was described to calibrate different volumes of the isochoric headspace system.

11. The gas-liquid distribution constants were measured using the vapor loading method on the isochoric headspace system. The presented method and the headspace system were shown to give accurate and reproducible gas-liquid distribution constants. From the measured gas-liquid distribution constants, the liquid-liquid partition coefficients were calculated and were shown to contribute equivalent amount of Gibbs free energy per methylene group for the transfer between the mobile phase and the adsorbed layer.

## Appendix I – Derivation of the mass-balance equation for a two component system.

The derivation of equation 2-6 from equation 2-5 is given on pages 57 and 58.

The focus here is on the derivation of equation 2-7 from equation 2-6 that was not given on page 58.

$$-F\left(\frac{\partial c_e}{\partial x}\right)_t dt dx = \left(\frac{\partial}{\partial t} \Psi(c_e)\right)_x dt dx \quad (2-5)$$

$$\Psi(c_e) = v_0 c_e + s\Gamma^{(v)}(c_e) \quad (2-6)$$

When equation 2-6 is plugged in equation 2-5, the following is obtained:

$$-F\left(\frac{\partial c_e}{\partial x}\right)_t dt dx = \left(\frac{\partial}{\partial t} (v_0 c_e + s\Gamma^{(v)}(c_e))\right)_x dt dx \quad (2-6A)$$

or equation partial derivatives,

$$-F\left(\frac{\partial c_e}{\partial x}\right)_t = (v_0)\left(\frac{\partial c_e}{\partial t}\right)_x + s\left(\frac{\partial \Gamma^{(v)}(c_e)}{\partial t}\right)_x \quad (2-6B)$$

Since the concentration of the analyte is measured by the detection in the liquid phase we have to substitute the surface excess by the concentration in the mobile phase according to the following expression:

$$\left(\frac{\partial \Gamma^{(v)}(c_e)}{\partial t}\right)_x = \left(\frac{\partial \Gamma^{(v)}(c_e)}{\partial c_e}\right)_x \left(\frac{\partial c_e}{\partial t}\right)_x \quad (2-6C)$$

When equations 2-6B and 2-6C are combined, the following equation is obtained.

$$-F\left(\frac{\partial c_e}{\partial x}\right)_t = \left(v_0 + s\frac{d\Gamma^{(v)}(c_e)}{dc_e}\right)\left(\frac{\partial c_e}{\partial t}\right)_x \quad (2-6D)$$

Since the concentration of the analyte is a function of both  $x$  and  $t$ , its full derivative is

$$dc_e = \left( \frac{\partial c_e}{\partial x} \right) dx + \left( \frac{\partial c_e}{\partial t} \right) dt \quad (2-6E)$$

Dividing this expression by  $dt$  at constant  $c_e$  ( $dc_e=0$ ) we obtain an equation relating partial derivatives:

$$\left( \frac{\partial c_e}{\partial t} \right)_x = - \left( \frac{\partial c_e}{\partial x} \right)_t \left( \frac{\partial x}{\partial t} \right)_c \quad (2-6F)$$

Substituting into the Equation 2-6D, the following expression is obtained:

$$-F \left( \frac{\partial c_e}{\partial x} \right)_t = \left( v_0 + s \frac{d\Gamma^v(c_e)}{dc_e} \right) \left( - \frac{\partial c_e}{\partial x} \right)_t \left( \frac{\partial x}{\partial t} \right)_c \quad (2-6G)$$

Dividing both parts by  $-\left(\partial c_e / \partial x\right)_t$  the following expression is obtained:

$$F = \left( v_0 + s \frac{d\Gamma^v(c_e)}{dc_e} \right) \left( \frac{\partial x}{\partial t} \right)_c \quad (2-6H)$$

Where  $\left(\partial x / \partial t\right)_c = u_c$  (the linear velocity of the chromatographic band at a certain concentration of the analyte) is substituted.

$$F = \left( v_0 + s \frac{d\Gamma^v(c_e)}{dc_e} \right) u_c \quad (2-6I)$$

Divide both parts of the equation by  $u_c$  and substitute  $F/u_c = v_r$ . To go from the reduced amounts (area  $dx$ ) to total amounts (column length), both parts of the equation are multiplied by  $L$  (the column length). The final expression is equation 2-7.

$$V_R(c_e) = V_0 + S \frac{d\Gamma^{(v)}(c_e)}{dc_e} \quad (2-7)$$



## References

1. Horvath, C.; Melander, M. *J. Chromatogr. Sci.* **1977**, *15*, 393.
2. Majors, R. E. *Anal. Chem.* **1972**, *44*, 1722.
3. Melander, W. R.; Horvath, C. In *High-Performance Liquid Chromatography – Advances and perspectives*; Horvath, C., Ed.; Academic Press: New York, 1980; p. 113.
4. Jaroniec, M. *J. Chromatogr. A* **1993**, *656*, 37.
5. Scott, R. P. W.; Kucera, P. *Anal. Chem.* **1973**, *45*, 749.
6. Snyder, R. *Principles of Adsorption Chromatography*; Marcel Dekker: New York, 1968.
7. Snyder, R. *Anal. Chem.* **1974**, *46*, 1384.
8. Soczewinski, E. *Anal. Chem.* **1969**, *41*, 179.
9. Lodke, D. C. *J. Chromatogr. Sci.* **1974**, *12*, 433.
10. Kirkland, J. J. *J. Chromatogr. Sci.* **1975**, *9*, 171.
11. Colin, H.; Ward, N.; Guiochon, G. *J. Chromatogr.* **1978**, *149*, 169.
12. Poppe, H. *J. Chromatogr. A* **1993**, *656*, 19.
13. Knox, J. H.; Pryde, A. *J. Chromatogr.* **1975**, *112*, 171.
14. Scott, R. P. W.; Kucera, P. *J. Chromatogr.* **1977**, *142*, 213.
15. Horvath, C.; Melander, W.; Molnar, I. *J. Chromatogr.* **1976**, *125*, 129.
16. Schoenmakers, P. J.; Billet, H. A. H.; Galan, L. de *J. Chromatogr.* **1976**, *122*, 185.
17. Schoenmakers, P. J.; Billet, H. A. H.; Galan, L. de *Chromatographia* **1982**, *15*, 205.
18. Karger, B. L.; Gant, J. R.; Hartkopf, A.; Weiner, P. H. *J. Chromatogr.* **1976**, *128*, 65.
19. Wang, H. L.; Duda, J. L.; Radke, C. S. *J. of Colloid and Interface Sci.* **1978**, *66*, 153.
20. Lochmuller, C. H.; Wilder, D. R. *J. Chromatogr. Sci.* **1979**, *17*, 574.
21. Sokolowski, A.; Wahlund, K. G. *J. Chromatogr.* **1980**, *189*, 299.

22. Korosi, G. Ph. D. Dissertation, Universite de Lausanne, Lausanne, 1980.
23. Nahun, A.; Horvath, C. *J. Chromatogr.* **1981**, *203*, 53 & 65.
24. Gilpin, R. K.; Squires, J. A. *J. Chromatog. Sci.* **1981**, *19*, 195.
25. Colin, H.; Guichon, G.; Jandera, P. *Anal. Chem.* **1982**, *54*, 435.
26. Colin, H.; Guichon, G.; Jandera, P. *Anal. Chem.* **1983**, *55*, 442.
27. Colin, H.; Guichon, G.; Jandera, P. *Chromatographia* **1983**, *17*, 83.
28. Martire, D. E.; Boehm, R. E. *J. Phys. Chem.* **1983**, *87*, 1045.
29. Katz, E. D.; Ogan, K.; Scott, R. P. W. *J. Chromatogr.* **1986**, *352*, 67.
30. Dill, K. A. *J. Phys. Chem.* **1987**, *91*, 1980.
31. Dorsey, J. G.; Dill, K. A. *Chem. Rev.* **1989**, *89*, 331.
32. Ying, P. T.; Dorsey, J. G.; Dill, K. A. *Anal. Chem.* **1989**, *61*, 2540.
33. Gilpin, R. K.; Jaroniec, M.; Lin, S. *Chromatographia* **1990**, *30*, 393.
34. Kowalska, T.; Kus, P. *Chromatographia* **1990**, *29*, 583.
35. Buszewski, B.; Suprynowicz, Z.; Staszczuk, P.; Albert, K.; Pfeleiderer, B.; Bayer, E. *J. Chromatogr.* **1990**, *499*, 305.
36. Kowalska, T. *Chromatographia* **1991**, *31*, 119.
37. Park, J. H.; Jang, M. D.; Chae, J. J.; Kim, H. C.; Suh, J. K. *J. Chromatogr. A* **1993**, *656*, 69.
38. Lochmuller, C. H.; Resse, C.; Aschman, A. J.; Breiner, S. J. *J. Chromatogr. A* **1993**, *656*, 3.
39. Guillaume, Y. C.; Guinchard, C. *Anal. Chem.* **1996**, *68*, 2869.
40. Tan, L. C.; Carr, P. W. *J. Chromatogr. A* **1998**, *799*, 1.
41. Kaczmarski, K.; Prus, W.; Kowalska, T. *J. Chromatogr. A* **2000**, *869*, 57.

42. Sinanoglu, O. In *Advances in Chemical Physics*; Hirschfelder, J. O., Ed.; Wiley: New York, 1967, Vol. 12, p. 283.
43. Sinanoglu, O. In *Molecular Association in Biology*; Pullman B., Ed.; Academic Press: New York, 1968, p. 427.
44. Park, J. H.; Lee, J. E.; Jang, M. D.; Li, J.; Carr, P. W. *J. Chromatogr.* **1991**, *586*, 1.
45. Carr, P. W.; Li, J.; Dallas, A. J.; Eikens, D. I.; Tan, L. C. *J. Chromatogr. A* **1993**, *656*, 113.
46. Tijssen, R.; Schoenmakers, P. J.; Bohmer, M. R.; Koopal, L. K.; Billet, H. A. H. *J. Chromatogr. A* **1993**, *656*, 135.
47. Park, J. H.; Lee, Y. K.; Weon, Y. C.; Tan, L. C.; Li, J.; Li, L.; Evans, J. F.; Carr, P. W. *J. Chromatogr. A* **1997**, *767*, 1.
48. Cheong, W. J.; Carr, P. W. *J. Chromatogr.* **1990**, *499*, 373.
49. Alvarez-Zepeda, A.; Barman, B. N.; Martire, D. E. *Anal. Chem.* **1992**, *64*, 1978.
50. Jandera, P. *J. Chromatogr.* **1984**, *314*, 13.
51. Wise, S. A.; Bonnett, W. J.; Guenther, F. R.; May, W. E. *J. Chromatogr. Sci.* **1981**, *19*, 457.
52. Wise, S. A.; Sander, L. C. *J. High Resolut. Chromatogr.; Chromatogr. Commun.* **1985**, *8*, 248.
53. Krstulovic, A. M.; Colin, H.; Tchaplal, A.; Guichon, G. *Chromatographia* **1983**, *17*, 228.
54. Melander, W.; Horvath, C. *Chromatographia* **1982**, *15*, 86.
55. Jinno, K.; Kawasaki, K. *Chromatographia* **1984**, *18*, 499.
56. Tanaka, N.; Sakagami, K.; Araki, T. *J. Chromatogr.* **1980**, *199*, 327.
57. Berendsen, G. E.; Galan, de L. *J. Chromatogr.* **1980**, *196*, 21.

58. Lochmullar, C. H.; Hangac, H. H.; Wilder, P. R. *J. Chromatogr. Sci.* **1981**, *19*, 130.
59. Sentell, K. B.; Dorsey, J. G. *J. Chromatogr.* **1989**, *461*, 193.
60. Sander, L. C.; Wise, S. A. *Anal. Chem.* **1987**, *59*, 2309.
61. Sander, L. C.; Wise, S. A. *CRC Crit. Rev. Anal. Chem.* **1987**, *18*, 299.
62. Sander, L. C.; Wise, S. A. *Anal. Chem.* **1989**, *61*, 1749.
63. Rodecki, A.; Lamparczyk, H.; Kaliszan, R. *Chromatographia* **1979**, *12*, 595.
64. Issaq, H. J.; Fox, S. D.; Lindsey, K.; McConnell, J. H.; Weiss, D. E. *J. Liq. Chromatogr.* **1987**, *10*, 49.
65. Grushka, E.; Colin, H.; Guichon, G. *J. Chromatogr.* **1982**, *248*, 325.
66. Dufek, P. J. *J. Chromatogr.* **1984**, *299*, 109.
67. Chmielowiec, J.; Sawatzky, H. *J. Chromatogr. Sci.* **1979**, *17*, 245.
68. Snyder, L. R. *J. Chromatogr.* **1979**, *179*, 167.
69. Scott R. P. W.; Simpson, C. F. *Faraday Symp. Chem. Soc.* **1980**, *15*, 69.
70. Jaroniec, M.; Martire, D. E.; Borowko, M. *Adv. Colloid Interface Sci.* **1985**, *22*, 177.
71. Everett, D. H.; Ottewill, R. H.; Rochester, C. H. In *Adsorption from solutions*; Smith A. L., Ed., Academic Press: New York, 1983.
72. Hammers, W. E.; Meurs, G. J.; Delingny, C. L. *J. Chromatogr.* **1982**, *246*, 169.
73. Jaroniec, M.; Martire, D. E.; Borowko, M. *J. Chromatogr.* **1986**, *351*, 1.
74. Schantz, M. M.; Martire, D. E. *J. Chromatogr.* **1987**, *391*, 35.
75. Butte, W.; Fookan, C.; Klusmann, R.; Schuller, D. *J. Chromatogr.* **1981**, *214*, 59.
76. Unger, S. H.; Chiang, G. H. *J. Med. Chem.* **1981**, *24*, 262.
77. Colin, H.; Krstulovic, A. M.; Guichon, G. *J. Chromatogr.* **1983**, *255*, 295.
78. Miyake, K.; Terada, H. *J. Chromatogr.* **1978**, *157*, 386.

79. Nahum, A.; Horvath, C. *J. Chromatogr.* **1980**, *192*, 315.
80. Mirrless, M. S.; Moulton, S. J.; Murphy, C. T.; Taylor, P. J. *J. Med. Chem.* **1976**, *19*, 615.
81. Baker, J. K. *Anal. Chem.* **1979**, *51*, 1693.
82. Molnar, I.; Horvath, C. *J. Chromatogr.* **1977**, *142*, 623.
83. Claudy, P.; Letoffe, J. M.; Gaget, C.; Morel, D.; Serpinet, J. *J. Chromatogr.* **1985**, *329*, 331.
84. Tchaplá, A.; Colin, H.; Guichon, G. *Anal. Chem.* **1984**, *56*, 621.
85. Colin, H.; Krstulovic, A. M.; Gonnord, M. F.; Guichon, G.; Yun, Z.; Jandera, P. *Chromatographia* **1983**, *17*, 9.
86. Mockel, H. J.; Weller, G.; Meltzer, H. *J. Chromatogr.* **1987**, *388*, 255, 267, 275, 285.
87. Bohmer, M. R.; Koopal, L. K.; Tijssen, R. *J. Phys. Chem.* **1991**, *95*, 6285.
88. Karch, K.; Sebastian, I.; Halasz, I. *J. Chromatogr.* **1976**, *122*, 3.
89. Colin, H.; Guichon, G. *J. Chromatogr.* **1977**, *141*, 289.
90. Berendsen, G. E.; Pikaart, K. A.; Galan, de L. *J. Liq. Chromatogr.* **1980**, *3*, 1437.
91. Hemetsberger, H.; Behrensmeyer, P.; Henning, J.; Ricken, H. *Chromatographia* **1979**, *12*, 71.
92. Sander, L. C.; Callis, J. B.; Field, L. R. *Anal. Chem.* **1983**, *55*, 1068.
93. Riedo, F.; Czencz, M.; Liardon, O.; Kovats, E. *Helv. Chim. Acta* **1978**, *61*, 1912.
94. Korosi, G.; Kovats, E. *Colloids Surfaces* **1981**, *2*, 315.
95. Folay, P. J. *J. Am. Chem. Soc.* **1962**, *84*, 2857
96. Gangoda, M. E.; Gilpin, R. K.; Figueirinhas, J. *J. Phys. Chem.* **1989**, *93*, 4815.
97. McCormick, R. M.; Karger, B. L. *Anal. Chem.* **1980**, *52*, 2249.
98. McCormick, R. M.; Karger, B. L. *J. Chromatogr.* **1980**, *199*, 259.

99. Slaats, E. H.; Markovski, W.; Fekete, J.; Poppe, H. *J. Chromatogr.* **1981**, *207*, 299.
100. Yonker, C. R.; Zwier, T. A.; Burke, M. F. *J. Chromatogr.* **1982**, *241*, 257.
101. Yonker, C. R.; Zwier, T. A.; Burke, M. F. *J. Chromatogr.* **1982**, *241*, 269.
102. Sander, L. C.; Wise, S. A. *Anal. Chem.* **1984**, *56*, 504.
103. Marcus, Y.; Migron, Y. *J. Phys. Chem.* **1991**, *95*, 400.
104. Migron, Y.; Marcus, Y. *J. Chem. Soc. Faraday Trans.* **1991**, *87*, 1339.
105. Marcus, Y. *J. Chem. Soc. Faraday Trans I* **1989**, *85*, 381.
106. Marcus, Y. *J. Chem. Soc. Faraday Trans I* **1990**, *86*, 2251.
107. Munk, P. *Intorduction to Macromoleculare Science*; Wiley: New York, 1989.
108. Flory, P. J. *Statistical Mechanics of Chain Molecule*; Wiley-Interscience: New York, 1969.
109. Fadeev, A. Y.; Staroverov, S. M. *J. Chromatogr.* **1989**, *447*, 103.
110. Fadeev, A. Y.; Lisichkin, G. V.; Runov, V. K.; Staroverov, S. M. *J. Chromatogr.* **1991**, *558*, 31.
111. Iler, R. K. *The Colloid Chemistry of Silicas and Silicanes*; Cornell University Press: Ithaca, New York, 1955.
112. Lowen, W. K.; Broge, E. C. *J. Phys. Chem.* **1961**, *65*, 16.
113. Nawrocki, J.; Buszewski, B. *J. Chromatogr.* **1988**, *449*, 1.
114. Kimata, K.; Iwaguchi, K.; Onishi, S.; Jinno, K.; Eksteen, R.; Hosoya, K.; Araki, M.; Tanaka, N. *J. Chromatogr. Sci.* **1989**, *27*, 721.
115. Kimata, K.; Tanaka, N.; Araki, T. *J. Chromatogr.* **1992**, *594*, 87.
116. Alvarez-Zepeda, A.; Martire, D. E. *J. Chromatogr.* **1991**, *550*, 285.
117. Tilly-Melin, A.; Askemark, Y.; Wahlund, K. G.; Schill, G. *Anal. Chem.* **1979**, *51*, 76.

118. Koch, C. S.; Koster, F.; Findenegg, G. H. *J. Chromatogr.* **1987**, *406*, 257.
119. Lochmuller, H.; Marshall, D. B.; Wilder, D. R. *Anal. Chim. Acta* **1981**, *130*, 31.
120. Stahlberg, J.; Almgren, M. *Anal. Chem.* **1985**, *57*, 817.
121. Carr, J. W.; Harris, J. M. *Anal. Chem.* **1986**, *58*, 626.
122. Carr, J. W.; Harris, J. M. *Anal. Chem.* **1987**, *59*, 2546.
123. Jones, J. L.; Rutan, S. C. *Anal. Chem.* **1991**, *63*, 1318.
124. Hayashi, Y.; Helburn, R. S.; Rutan, S. C. In *Proceedings of the 4<sup>th</sup> Symposium on Computer-Enhanced Analytical Spectroscopy*; Wilkins, C. L., Ed., Plenum: New York, 1992.
125. Rutan, S. C.; Harris, J. M. *J. Chromatogr. A* **1993**, *656*, 197.
126. Albert, K.; Bayer, E. *J. Chromatogr.* **1991**, *544*, 345.
127. Iler, R. K. *The Chemistry of Silica*; Wiley: New York, 1979.
128. Schunk, T. C.; Burke, M. F. *J. Chromatogr. A* **1993**, *656*, 289.
129. Gilpin, R. K.; Gangoda, M. E. *J. Chromatogr. Sci.* **1983**, *21*, 352.
130. Marqusee, J. A.; Dill, K. A. *J. Phys. Chem.* **1986**, *85*, 434.
131. Gilpin, R. K.; Gangoda, M. E. *Anal. Chem.* **1984**, *56*, 1470.
132. Albert, K.; Evers, B.; Bayer, E. *J. Magn. Res.* **1985**, *62*, 428.
133. Albert, K.; Pfeleiderer, B.; Bayer, E. In *Chemically Modified Surfaces in Science and Industry (Chemically Modified Surfaces)*; Leyden, D. E., Ed.; Gordon & Breach: New York, Vol. 2, 1988, p. 287.
134. Shah, P.; Rogers, L. B.; Fetzer, J. C. *J. Chromatogr.* **1987**, *388*, 411.
135. Zeigler, R. C.; Maciel, G. E. *J. Am. Chem. Soc.* **1991**, *113*, 6349.
136. Lochmuller, C. H.; Hunnicutt, M. L. *J. Phys. Chem.* **1986**, *90*, 4318.

137. Montgomery, M. E.; Green, M. A.; Wirth, M. J. *Anal. Chem.* **1992**, *64*, 1170.
138. McNally, M. E.; Rogers, L. B. *J. Chromatogr.* **1985**, *331*, 23.
139. Morel, D.; Serpinet, J. *J. Chromatogr.* **1982**, *248*, 231.
140. Sentell, K. B.; Dorsey, J. G. *Anal. Chem.* **1989**, *61*, 930.
141. Berendsen, G. E.; Galan, de L. *J. Liq. Chromatogr.* **1978**, *1*, 403.
142. Golding, R. D. Ph. D. Dissertation, University of Arizona, Tucson, AZ, 1988.
143. Scott, R. P. W. *J. Chromatogr. Sci.* **1980**, *18*, 297.
144. Golding, R. D.; Burke, M. F. *J. Chromatogr.* **1987**, *384*, 105.
145. Sander, L. C.; Wise, S. A. *J. Chromatogr.* **1984**, *316*, 163.
146. Sander, L. C.; Wise, S. A. *LC-GC* **1990**, *8*, 378.
147. Sentell, K. B.; Henderson, A. N. *Anal. Chim. Acta* **1991**, *246*, 139.
148. Suzuki, S.; Green, P. G.; Bmgarner, P. J.; Dasgupta, S.; Goddard III, W. A.; Blake, G. *A. Science* **1992**, *257*, 942.
149. Torrellas-Hidalgo, L. Masters Thesis, University of Arizona, Tucson, AZ, 1985.
150. Karch, K.; Sebastian, I.; Halasz, I. *J. Chromatogr.* **1991**, *550*, 285.
151. Gilpin, R. K.; Gangoda, M. E.; Krishen, A. E. *J. Chromatogr. Sci.* **1982**, *20*, 345.
152. Yang, S. S.; Gilpin, R. K. *J. Chromatogr.* **1988**, *449*, 115.
153. Cole, L. A.; Dorsey, J. G. *Anal. Chem.* **1992**, *64*, 1317.
154. Morel, D.; Tabar, K.; Serpinet, J.; Claudy, P. I.; LeToffe, J. M. *J. Chromatogr.* **1987**, *395*, 73.
155. Cole, L. A.; Dorsey, J. G. *Anal. Chem.* **1992**, *64*, 1324.
156. Zwier, T. A. Ph. D. Dissertation, University of Arizona, Tucson, AZ, 1982.
157. Dallas, A. J. Ph. D. Dissertation, University of Minnesota, Minneapolis, MN, 1994.



158. Men, Y-D.; Marshall, D. B. *Anal. Chem.* **1990**, *62*, 2606.
159. Schunk, T. C.; Burke, M. F. *Int. J. Environ. Anal. Chem.* **1986**, *25*, 81.
160. Beaufils, J. P.; Hennion, M. C.; Rosset, R. *Anal. Chem.* **1985**, *57*, 2593.
161. Doyle, C. A.; Vickers, T. J.; Mann, C. K.; Dorsey, J. G. *J. Chromatogr. A* **2000**, *877*, 25.
162. Doyle, C. A.; Vickers, T. J.; Mann, C. K.; Dorsey, J. G. *J. Chromatogr. A* **2000**, *877*, 41.
163. LoBrutto, R. Ph. D. Dissertation, Seton Hall University, South Orange, NJ, 2000.
164. Rustamov, I.; Farcas, T.; Ahmed, F.; Chan, F.; LoBrutto, R.; McNair, H. M.; Kazakevich, Y. V. *J. Chromatogr. A* **2001**, *913*, 49.
165. Koster, F.; Findenegg, G. H. *Chromatographia* **1982**, *15*, 743.
166. Jacobson, J.; Frenz, J.; Horvath, C. *J. Chromatogr.* **1984**, *316*, 53.
167. Eltekov, Yu. A.; Kazakevich, Yu. V.; Kiselev, A. V.; Zhuchkov, A. A. *Chromatographia* **1985**, *20*, 525.
168. Eltekov, Yu. A.; Kazakevich, Yu. V. *J. Chromatogr.* **1986**, *365*, 213.
169. Huang, J.; Horvath, C. *J. Chromatogr.* **1987**, *406*, 275.
170. Knox, J.; Kaliszan, R. *J. Chromatogr.* **1985**, *349*, 211.
171. Eltekov, Yu. A.; Kazakevich, Y. V. *J. Chromatogr.* **1987**, *395*, 473.
172. Kazakevich, Y. V.; McNair, H. M. *J. Chromatogr. Sci.* **1995**, *33*, 321.
173. Kazakevich, Y. V.; LoBrutto, R.; Chan, F.; Patel, T. *J. Chromatogr. A* **2001**, *913*, 75.
174. Everett, D. H. *J. Chem. Soc., Faraday Trans I*, **1964**, *60*, 1803.
175. Everett, D. H. *Pure & Appl. Chem.* **1981**, *51*, 2181.
176. Riedo, F.; Kovats, E. *J. Chromatogr.* **1982**, *239*, 1.

177. Rowlen, K. L.; Harris, J. M. *Anal. Chem.* **1991**, *63*, 964.
178. Slaats, E. N.; Kraak, J. C.; Burgman, W. J. T.; Poppe, H. *J. Chromatogr.* **1978**, *149*, 255.
179. Krstulovic, A. M.; Colin, H.; Guiochon, G. *Anal. Chem.* **1982**, *54*, 2438.
180. Berendsen, G. E.; Schoenmakers, P. J.; Galan, de L.; Vigh, G.; Varga-Puchony, Z.; Inczedy, J. *J. Liq. Chromatogr.* **1980**, *3*, 1669.
181. Wells, M. J. M.; Clark, C. R. *Anal. Chem.* **1981**, *53*, 1341.
182. Horvath, C.; Lin, H. *J. Chromatogr.* **1978**, *149*, 43.
183. Larman, J. P.; Stefano, de J. J.; Goldberg, A. P.; Stout, R. W.; Snyder, L. R.; Stadalius, M. A. *J. Chromatogr.* **1983**, *255*, 163.
184. Thus, J. L. G.; Kraak, J. C. *J. Chromatogr.* **1985**, *320*, 271.
185. Wainwright, M. S.; Nieass, C. S.; Haken, J. K.; Chaplin, R. P. *J. Chromatogr.* **1985**, *321*, 287.
186. Popl, I. V. M.; Fahrnich, J. *J. Chromatogr.* **1983**, *281*, 293.
187. Fini, O.; Brusa, F.; Chiesa, L. *J. Chromatogr.* **1981**, *210*, 326.
188. Billet, H. A. H.; Dalen, Van J.; Schoenmakers, P. J.; Galan, de L. *Anal. Chem.* **1983**, *55*, 847.
189. Hennion, M. C., Picard, C., Caude, M. *J. Chromatogr.* **1978**, *166*, 21.
190. Gant, J. R.; Dolan, J. W., Snyder, L. R. *J. Chromatogr.* **1979**, *185*, 153.
191. Colin, H.; Diez-Masa, J. C.; Guiochon, G.; Gzajkivaska, T.; Miedziak, I. *J. Chromatogr.* **1978**, *167*, 41.
192. Knox, J. H.; Kaliszan, R.; Kennedy, G. J. *Faraday symposia of Chem. Soc.* **1980**, *15*, 113.

193. Watzig, H.; Ebel, S. *Chromatographia* **1991**, *31*, 544.
194. Mockel, H. J.; Freyholdt, T.; *Chromatographia* **1983**, *17*, 215.
195. Vigh, G. Y.; Varga-Ruchony, Z. *J. Chromatogr.* **1980**, *196*, 1.
196. Gibbs, J. W. *Collected Works; Longmans: New York*, 1928, Vol. 1, pp. 55-353.
197. Kazakevich, Y. V.; McNair, H. M. *J. Chromatogr. Sci.* **1993**, *31*, 317.
198. Stewart, H. N. M.; Perry, S. G. *J. Chromatogr.* **1968**, *37*, 97.
199. Tchaplá, A.; Heron, S.; Colin, H.; Guiochon, G. *Anal. Chem.* **1988**, *60*, 1443.
200. Kazakevich, Y. V.; McNair, H. M. *J. Chromatogr. A* **2000**, *872*, 49.
201. Classens, H. A.; Van de Ven, L. J.; Haan, de J. W.; Cramers, C. A.; Vonk, N. *HRC CC; J. High Resolut. Chromatogr.; Chromatogr. Commun.* **1983**, *6*, 433.
202. Shalkh, B.; Tomaszewski, J. E. *Chromatographia* **1983**, *17*, 675.
203. Engelhardt, H.; Ahr, G. *Chromatographia* **1981**, *14*, 227.
204. Spacek, P.; Kubin, M.; Vozka, S.; Porsch, B. *J. Liq. Chromatogr.* **1980**, *3*, 1465.
205. Berendsen, G. E.; Galan, de L. *J. Liq. Chromatogr.* **1978**, *1*, 561.
206. Unger, K. K.; Becker, N.; Roumeliotis, P. J. *J. Chromatogr.* **1976**, *125*, 115.
207. Tomellini, S. A.; Shu, S. H.; Fazio, F. D.; Hartwick, R. A. *HRC CC, J. High Resolut. Chromatogr., Chromatogr. Commu.* **1985**, *8*, 337.
208. Miller, M. L.; Linton, R. W.; Bush, S. G.; Jorgenson, J. W. *Anal. Chem.* **1984**, *56*, 2204.
209. Colin, H.; Krstulovic, A.; Guiochon, G.; Yun, Z. *J. Chromatogr.* **1981**, *255*, 295.
210. Jinno, K. *Chromatographia* **1982**, *15*, 667.
211. Roumeliotis, P.; Unger, K. K. *J. Chromatogr.* **1978**, *149*, 211.

212. Hennion, M. C.; Picard, C.; Combellas, C.; Caude, M.; Rosset, R. *J. Chromatogr.* **1981**, *210*, 211.
213. Snyder, L. R.; Glajch, J. L.; Kirkland, J. J. *Practical HPLC Method Development - 2<sup>nd</sup> edition*; Wiley-Interscience: New York, 1997.
214. Snyder, L. R.; Quarry, M. A.; Glajch, J. L. *Chromatographia* **1987**, *24*, 33.
215. Valko, K.; Snyder, L. R.; Glajch, J. L. *J. Chromatogr. A* **1993**, *656*, 501.
216. Tan, L. C.; Carr, P. W. *J. Chromatogr. A* **1993**, *656*, 521.
217. Johnson, B. P.; Khaledi, M. G.; Dorsey, J. G. *Anal. Chem.* **1986**, *58*, 2354.
218. Baty, J. D.; Sharp, S. *J. Chromatogr.* **1988**, *437*, 13.
219. Melander, W. R.; Horvath, C. *Chromatographia* **1984**, *18*, 353.
220. Sadlej-Sosnowska, N.; Sledzinska, I. *J. Chromatogr.* **1992**, *595*, 53.
221. Geng, X. D.; Bian, L. J. *Sci. China* **1992**, *35B*, 262.
222. Mackay, D.; Shiu, W. Y. *J. Phys. Chem. Ref. Data* **1981**, *10*, 1175.
223. Turner, L. H.; Chiew, Y. C.; Ahlert, R. C.; Kosson, D. S. *AIChE J.* **1996**, *42*, 1772.
224. Sherman, S. R.; Trampe, D. B.; Bush, D. M.; Schiller, M.; Eckert, C. A.; Dallas, A. J.; Li, J.; Carr, P. W. *Ind. Eng. Chem. Res.* **1996**, *35*, 1044.
225. Kieckblusch, T. G.; King, C. J. *J. Chromatogr. Sci.* **1979**, *17*, 273.
226. Hassam, A.; Carr, P. W. *Anal. Chem.* **1985**, *57*, 793.
227. Jones, W.; Egoville, M. J.; Strolle, E. O.; Dellamonien, E. S. *J. Chromatogr.* **1988**, *455*, 45.
228. Kolb, B.; Welter, C.; Bichler, C. *Chromatographia* **1992**, *34*, 235.
229. McAuliffe, C. A. *Chem. Tech.* **1971**, *1*, 46.

230. Ioffe, B. V.; Vitenberg, A. G. *Head-Space Analysis and Related Methods in Gas Chromatography*; Wiley: New York, 1984.
231. Guitart, R.; Puigdemont, A.; Arboix, M. *J. Chromatogr.* **1989**, *491*, 271.
232. Kolb, B.; Ettre, L. S. *Chromatographia* **1991**, *32*, 505.
233. Ettre, L. S.; Welter, C.; Kolb, B. *Chromatographia* **1993**, *35*, 73.
234. Lincoff, A. H.; Gossett, J. M. In *Gas Transfer at Water Surfaces*; Brutsaert W. and Jirka G. H., Eds., Reidel: Kordrecht, 1984, p. 17.
235. Gossett, J. M. *Environ. Sci. Technol.* **1987**, *21*, 202.
236. Markelov, M.; Guzowski, J. P. *Analytica. Chimica. Acta* **1993**, *276*, 235.
237. Vittenberg, A. G.; Butaeva, I. L.; Dimitrova, Z. St.; *Chromatographia* **1975**, *8*, 693.
238. Kolb, B. *Chromatographia* **1982**, *15*, 587.
239. Kolb, B.; Ettre, L. S. *Static Headspace-Gas Chromatography*; Wiley-VCH: New York, 1997.
240. Robbins, G. A.; Wang, A.; Stuart, J. D. *Anal. Chem.* **1993**, *65*, 3113.
241. Chai, X. S.; Zhu, J. Y. *J. Chromatogr. A* **1998**, *799*, 207.
242. Ioffe, B. V.; Vittenberg, A. G. *Chromatographia* **1978**, *11*, 282.